Optimization of Polypropylene Cellular Films for Piezoelectric Applications

Thèse

Abolfazl Mohebbi

Doctorat en génie chimique
Philosophiae doctor (Ph.D.)

Québec, Canada

Optimization of Polypropylene Cellular Films for Piezoelectric Applications

Thèse

Abolfazl Mohebbi

Sous la direction de :

Denis Rodrigue, directeur de recherche

Frej Mighri, codirecteur de recherche

Abdellah Ajji, codirecteur de recherche

Résumé

Cette thèse comporte deux objectifs principaux: la production en continu de films de polypropylène (PP) moussés ayant une structure cellulaire de forme oculaire, suivie par la préparation de films PP ferroélectrets par décharge corona pour des applications piézoélectriques.

Dans la première partie de ce travail, une production en continu par extrusion-calandrage a été développée pour produire des films de PP moussés pour des applications piézoélectriques. Le système est basé sur un moussage physique en utilisant de l'azote supercritique (SC-N_2) et le carbonate de calcium ($CaCO_3$) comme agent de nucléation. Les paramètres de mise en œuvre (conception de vis, profil de température, agent gonflant et de nucléation ainsi que leur contenu, et la vitesse d'étirement) ont été optimisés pour obtenir une forme spécifique (oculaire) comme structure cellulaire avec une distribution uniforme de la taille des cellules. Les résultats ont montré qu'une structure cellulaire avec un plus grand rapport d'aspect (*AR*) des cellules possède un plus faible module de Young, ce qui est approprié pour les films cellulaires piézoélectriques.

Dans la deuxième partie, des films PP ferroélectrets ont été produits. Suite à l'optimisation du procédé de décharge corona (tension de charge, distance de l'aiguille, temps de charge), les propriétés piézoélectriques des films obtenus ont été caractérisées et le coefficient piézoélectrique quasi-statique d_{33} a produit une valeur de 550 pC/N. Afin de mieux caractériser le comportement du film, l'analyse mécanique dynamique (DMA) a été proposée comme une méthode simple pour relier les propriétés piézoélectriques des films PP cellulaires à leur morphologie (taille, géométrie et densité des cellules).

Finalement, grâce à un post-traitement basé sur la saturation du film PP moussé avec le SC-N_2, une procédure en température et pression a été développée afin d'améliorer la structure cellulaire (cellules plus allongées). Ce traitement a permis d'augmenter de 45% le coefficient d_{33} (800 pC/N).

Abstract

This thesis is composed of two main objectives: the continuous production of thin foamed polypropylene (PP) films having an eye-like cellular structure, followed by the preparation of ferroelectret PP films through corona discharge for piezoelectric applications.

In the first part of this work, a continuous extrusion-calendaring setup was developed to produce PP foamed films for piezoelectric applications. The setup is based on physical foaming using supercritical nitrogen (SC-N_2) and calcium carbonate ($CaCO_3$) as nucleating agent. The processing parameters (screw design, temperature profile, blowing agent and nucleating agent content, and stretching speed) were optimized to achieve a specific stretched eye-like cellular structure with a uniform cell size distribution. The results showed that a cellular structure with higher cell aspect ratio (*AR*) has lower Young's modulus, which is appropriate for piezoelectric cellular films.

In the second part, ferroelectret PP films were produced. After optimization of the corona discharge process (charging voltage, needle distance, charging time), the piezoelectric properties of the resulting films were characterized and the optimum quasi-static piezoelectric d_{33} coefficient value was 550 pC/N. To better characterize the film behavior, dynamic mechanical analysis (DMA) was proposed as a simple method to relate the piezoelectric properties of the cellular PP films to their morphology (cell size, geometry and density).

Finally, through a post-processing treatment based on the saturation of the foamed PP film with SC-N_2, a temperature-pressure procedure was developed to improve the cellular structure (more stretched eye-like cells). This treatment was shown to increase by 45% the d_{33} coefficient (800 pC/N).

Table of contents

List of Tables

List of Figures

Abbreviations

AC	Alternating current
CF	Carbon fibers
COP	Cyclo-olefins polymers
DBD	Dielectric barrier discharges
DC	Direct current
DMA	Dynamic mechanical analysis
DNA	DeoxyriboNucleic Acid
DSC	Differential scanning calorimetry
DTGA	Derivative of the thermogravimetric analysis
DVB	1,4-divinylbenzene
EOC	Ethylene-octene copolymer
GED	Gas diffusion expansion
HDPE	High density polyethylene
HMS	High-melt-strength
IXPP	Irradiated crosslinked PP
L-PP	Linear PP
PE	Polyethylene

PEN	Poly(ethylene naphthalate)
PEOc	Poly(ethylene-co-octene)
PET	Poly(ethylene terephthalate)
PM	Photomultiplier
PP	Polypropylene
PP-g-MA	Maleic anhydride grafted PP
PS	Polystyrene
PTFE	Poly(tetrafluoro ethylene)
PVDF	Poly(vinylidene fluoride)
SAOS	Small amplitude oscillatory shear
SC	Supercritical
SCF	Supercritical fluid
SD	Standard deviation
SEM	Scanning electron microscope
TGA	Thermogravimetric analysis
TPE	Thermoplastic elastomer
TPT	Thermal-pressure treatments
TR	Trouton ratio
VR	Viscosity ratio
XPP	Cross-linked polypropylene

Symbols

A	Area (cm^2)
a	Length of unit-cell (μm)
A_F	Area of ferroelectret sample (cm^2)
AMR	Anisotropic modulus ratio (-)
AR	Cell aspect ratio (-)
b	Width of unit-cell (μm)
C	Capacitance (pF)
C_F	Capacitance of ferroelectret sample (pF)
C_{loss}	Loss capacitance (pF)
C_0	Concentration of gas molecules (g/cm^3)
c_{33}	Elastic modulus or elastic stiffness (MPa)
$\tilde{C}(\omega)$	Complex capacitance (pF)
D	Average cell diameter (μm)
d_{33}	Piezoelectric coefficient (pC/N)
E_c	Critical breakdown electric field (V/m)
E_e	Effective Young's modulus (MPa)
E_s	Young's modulus of solid material (MPa)

E'	Tensile storage moduli (MPa)
E''	Tensile loss moduli (MPa)
F	Formability factor (-)
f_a	Anti-resonance frequency (Hz)
f_0	Frequency factor of gas molecules joining nucleus (Hz)
g	Gravity acceleration (m/s^2)
$G_{nucl.}$	Gibbs free energy (kJ)
G'	Shear storage moduli (MPa)
G''	Shear loss moduli (MPa)
$G(s)$	Relaxation modulus (MPa)
k	Boltzmann's constant (J/K)
k_t	Electromechanical coupling factor
m	mass (g)
M_p	Pressure sensitivity of microphone (V/Pa)
n	Number of cells (-)
N_f	Cell density ($cells/cm^3$)
$N_{nucl.}$	Cell nucleation rate ($cells/cm^3.s$)
N_0	Nucleation density ($cells/cm^3$)
p	Pressure (Pa)
$\tilde{p}$	Sound pressure acting on the microphone diaphragm (Pa)
P_C	Critical pressure (Pa)

Q	Charge (pC)
q	Volume fraction of solid part (-)
S	Electrode spacing (μm)
S	Thickness of the sample (μm)
$\tilde{S}$	Variable thickness (μm)
T	Temperature (°C)
T_C	Critical temperature (°C)
T_g	Glass transition temperature (°C)
T_m	Melting temperature (°C)
$T_{max.\ dec}$	Maximum decomposition temperature (°C)
T_{10}	Temperature of 10% mass loss (°C)
t^e	Cell-wall thickness of eye-like structure (μm)
t^t	Cell-wall thickness of truss-like structure (μm)
$tan\ \delta$	Damping factor (-)
V_0	Theoretical threshold voltage (V)
$\tilde{V}$	Open-circuit voltage (V)
w_f	Weight fraction of additives (-)
Y	Young's modulus (MPa)
Z	Impedance (Ω)

γ_{bp}	Surface energy of polymer-bubble interface (J/m^2)
ΔH_{exp}	Heat of fusion (J)
ΔH^*	Heat of fusion of pure sample (J)
ΔP	Pressure drop of the gas/polymer solution (Pa)
δ_{pp}	Solubility parameters (1/(J/m^3)$^{0.5}$
ε	Permittivity factor (F/m)
$\dot{\varepsilon}$	Unidirectional elongation rate (1/s)
ε_{gr}	Relative dielectric constant of gas (-)
ε_{pr}	Relative dielectric constant of polymer (-)
ε_r^s	Relative permittivity of sample under constant stain (-)
ε_0	Vacuum permittivity (F/m)
$\eta_E^+(t, \dot{\varepsilon})$	Elongational viscosity growth function (Pa.s)
η_0	Zero shear viscosity (Pa.s)
ρ	Density (g/cm^3)
ρ^b	Densities of bulk material (g/cm^3)
ρ^c	Densities of cellular material (g/cm^3)
ρ_f	Density of foamed sample (g/cm^3)
ρ_p	Density of polymer (g/cm^3)
ρ_s	Area density of sample (g/cm^2)

σ	Surface charge density (pC/cm^2)
σ_E	Extensional stress (MPa)
ϕ	Expansion ratio (-)
χ_C	Degree of crystallinity (-)

Dedication

To my Father and my mother

for their unique LOVE!

To get something you never had,

You have to do something you never did …

José N. Harris!

Acknowledgments

First, I would like to thank my supervisor Professor Denis Rodrigue, for his advises, great support, and availability in different aspects of this project. I am grateful for all his considerations, help and the time he spent regarding this doctorate. In this regard, I would like to thank my co-supervisors Professor Frej Mighri and Professor Abdellah Ajji for all their advices and time to revise the papers.

Then, I would like to thank Mr. Yann Giroux, our group technician, for his training and help on different equipment and also Mr. Jean Côté, and Mr. André Ferland for their technical support.

I would like also to thank Professor Xiaoqing Zhang and Dr. Hojjat Mahi Hassanabadi for all their kind and scientific help, my friends and my colleagues and staff in the chemical engineering department at Université Laval.

I acknowledge the financial support from the Natural Sciences and Engineering Research Council of Canada (NSERC), Fonds Québécois de la Recherche sur la Nature et les Technologies (FRQNT), and Center for Applied Research on Polymers and Composites (CREPEC).

Ultimately, I would like to highly specify my appreciation to all my family members especially my parents for their love, kind support and encouragement the whole period of my life during this long and difficult way.

Forewords

This thesis is divided into seven chapters. In the first chapter the general context, objectives and their related experimental strategies are briefly discussed.

Chapters 2-3 present critical literature reviews on both parts of the work (PP foaming process and ferroelectret properties) in the form of published journal papers as follows:

Chapter 2

A. Mohebbi, F. Mighri, A. Ajji, D. Rodrigue*, Current issues and challenges in polypropylene foaming: A Review, Cellular Polymers,* **34**, 6, 299-337 (2015).

Regarding the first part of this work (foaming), a complete and critical literature review related to the most important issues and challenges in polypropylene (PP) foaming are extensively discussed and analyzed in terms of morphological, mechanical, thermal, and rheological characterizations. Although PP is the main material used in this work, the advantages of foamed PP (low material cost, high service temperature, high melting point, high tensile modulus, low density, and excellent chemical resistance) and its foaming limitations (low melt strength, poor cell morphology, and cell rupture/coalescence) are extensively discussed. Furthermore, to improve PP melt strength the presence of nucleating agent, introduction of long chain branching, blending with high melt strength polymers and crosslinking have been presented.

Chapter 3

A. Mohebbi, F. Mighri, A. Ajji, D. Rodrigue*, Cellular polymer ferroelectret: A review on their development and their piezoelectric properties, Advances in Polymer Technology*, **DOI: 10.1002/adv.21686** (2016).

In this chapter, a critical literature review related to the second part of this work (piezoelectricity) as the recent developments associated to the piezoelectric behavior of cellular polymers are extensively compared and discussed. The related concepts of

piezoelectricity, its history, piezoelectric d_{33} coefficient, ferroelectric and ferroelectret are introduced. Moreover, different procedures to produce ferroelectret cellular polymers and also various methods to measure the d_{33} coefficient with their related equations and parameters are presented. Furthermore, the effects of different parameters such as pressure, electrical breakdown strength of the gas phase, presence of fillers, and service temperature on the d_{33} coefficient are studied.

Chapters 4-6 present the experimental results in the form of accepted journal papers as follow:

Chapter 4

A. Mohebbi, F. Mighri, A. Ajji, D. Rodrigue*, Effect of processing conditions on the cellular morphology of polypropylene foamed films for piezoelectric applications, Cellular Polymers,* **Accepted** (2016).

In this work, an extrusion-calendaring foaming process to produce an appropriate eye-like cellular structure PP film for piezoelectric applications was developed. The effect of nitrogen state (supercritical or not), precise control of its flow rate, and appropriate die design to obtain a uniform thin foamed PP film were investigated. Moreover, the presence of a narrow temperature window in foaming was shown. Then, the important and critical role of die temperature, calendaring speed and the presence of calcium carbonate ($CaCO_3$) as a nucleating agent on the morphology of the cellular PP structure was investigated. Finally, based on the morphological and mechanical characterization of the samples, the optimum cellular structures for piezoelectric application was determined.

Chapter 5

A. Mohebbi, F. Mighri, A. Ajji, D. Rodrigue*, Polymer ferroelectret based on polypropylene foam: Piezoelectric properties prediction using dynamic mechanical analysis, Polymers for Advanced Technologies,* DOI: 10.1002/pat.3908 (2016).

While in Chapter 4, an optimum eye-like cellular structure was obtained, in this chapter their piezoelectric properties were characterized using a quasi-static method. Furthermore, dynamic mechanical analysis (DMA) was used Two new parameters called AMR1 and

AMR2 (anisotropic modulus ratio) were proposed to predict the piezoelectric behavior of the samples having different cell aspect ratio (*AR*) and homogeneity. Hence, DMA was used as a simple method to predict the piezoelectric properties of the cellular PP obtained. Finally, the relationship between AMR1, Young's modulus (mechanical parameter), *AR* value (morphological parameter) and quasi-static piezoelectric d_{33} coefficient of the samples were compared and discussed. Through this work, the charging parameters of the corona process (charging voltage, needle distance, charging time) were optimized and the effects of N_2 and air as the ionizing gas were compared.

Chapter 6

A. Mohebbi, F. Mighri, A. Ajji, D. Rodrigue*, Polymer ferroelectret based on polypropylene foam: Piezoelectric properties improvement using post-processing thermal-pressure treatment, Journal of Applied Polymer Science*, 134 (10) 44577 (2017).

Considering the piezoelectric d_{33} coefficient obtained for the sample having the highest *AR* value in the previous chapter, this chapter improves its piezoelectric behavior through thermal-pressure treatments (TPT) as post-processing procedures. The idea of using these TPT was to obtain a more stretched eye-like cellular structure, which can result in better piezoelectric d_{33} coefficients. These TPT procedures were based on the saturation of the cellular structure with supercritical N_2 to create a more stretched eye-like cellular structure. Moreover, from the DMA results, the parameter AMR1 was again used to predict the piezoelectric behaviour of the treated samples. Finally, the relationships between AMR1, Young's modulus and *AR*, as introduced in the previous chapter, were confirmed.

Finally, chapter 7 presents a general conclusion on all the work performed followed by some recommendations for future investigations.

For all the articles (chapters 2-6), my contributions are related to performing the experimental works, collecting and analyzing the data, as well as writing the first draft of the manuscripts, which were revised by all co-authors.

Chapter 1

Introduction

1.1 Context

Thermoplastic foams or cellular thermoplastics are expanded polymers containing two or more phases: a solid polymer matrix as a continuous phase and a gaseous phase as dispersed bubbles. The bubbles are generated by the introduction a gas or a blend thereof, obtained from a chemical or a physical blowing agent. Physical blowing agents are generally inert gases, which are dissolved into the polymer matrix during a saturation process, usually at high pressure. Since physical blowing agents are inert gases, this method is more environmentally friendly compared to the chemical one and therefore is more interesting for academic and industrial applications. In some cases, a nucleating agent (particles) is added to control bubble nucleation and achieve a more uniform cellular structure.

Physical foaming of polymers was first developed by Martini and Suh at the Massachusetts Institute of Technology in the 1980s to reduce material consumption and improve toughness (Martini, 1981). Based on these objectives, they actually developed the field of microcellular foams, which is still nowadays very active. A microcellular foam is usually defined as a foam having cell sizes less than 10 micrometers (Martini, 1981) and cell density higher than 10^9 cells/cm^3 (Okamoto, 2003). Afterwards, Colton and Suh obtained a microcellular foam from semi-crystalline polymers (Colton, 1989; Colton and Suh, 1992) and Doroudiani et al. reported on batch foaming of these polymers where the morphology of the crystalline region was shown to have a direct effect on the solubility and diffusivity of the blowing agent and the final foaming properties (Doroudiani et al., 1996). Actually, in this case, the crystalline zones can act as nucleating sites inside a polymer matrix. Finally, the continuous processing of microcellular foams was developed by Dow (Imeokparia et al., 1997).

Extrusion is one of the best known melt processing methods to produce continuous products such as films, sheets and pipes. Figure 1.1 presents the extruder used in this work. Generally, the extruder is composed of a single screw rotating inside a barrel (cylinder). This machine, equipped with heaters, contains three main zones from the beginning to the end as: solid conveying, melting and pumping. Feeding the polymer into this machine results in polymer melts as output. By using different dies having various shapes, it is possible to produce a variety of polymer products. In addition to melt the polymers, it is also possible to mix/blend them with additive particles, blowing agents or even other polymers. In these cases, an extruder having two screws (twin-screw extruder) is better to obtain good mixing. A photo of the screws in a twin-screw extruder is presented in Figure 1.2.

Figure 0.1. Extruder equipped with a flat die to produce film/sheet.

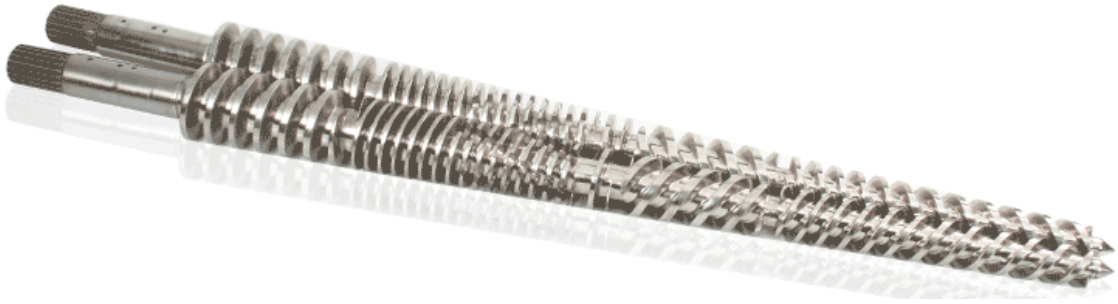

Figure 0.2. A photo of twin-screw (screwbarrels.wordpress.com).

The polymers fed into extruders are usually in two main forms: pellets (granules) or powder. It should be mentioned that the main parameter controlling the form is the polymerization technique used to produce the polymer. If the polymer was produced from emulsion or suspension polymerization, its final shape is usually a powder, while pellets are usually obtained from bulk polymerization. These two forms are shown in Figure 1.3.

Figure 0.3. (a,b) Polymer pellets and (c) powder.

Moreover, the dies, controlling the extruder output, control the final shape of the polymer product. Two main types of the die are usually encountered in extrusion: flat and annular/tubular dies. Polymer films and sheets can be obtained using a flat die, while tubular/annular dies can be used to produce polymer products such as pipes. A schematic representations and some examples of typical dies/products are presented in Figure 1.4.

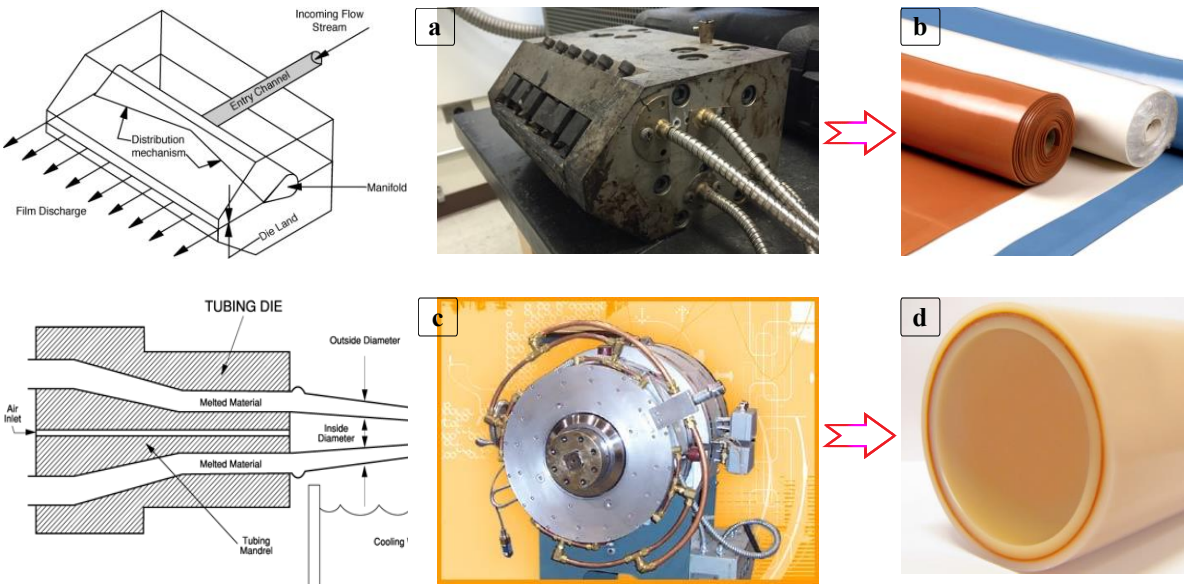

Figure 0.4. a) Flat die and its schematic representation (pslc.ws/macrog/process/restbar.htm), b) sheet product (bosspolymer.com.au), c) annular/tubular die and its schematic representation (extrapackaging.com/polyurethane/whatispolyurethane.php and foamtekcorp.com), and d) tubular product (mentor.com/products/mechanical/engineering-edge/volume5/issue1/layer-by-layer).

Experimentally, foamed polymer films can be produced by feeding a polymer (granule or powder) in a twin-screw extruder equipped with a flat die and injecting a high-pressure gas (physical blowing agent) in the melting zone of the machine. Through this process, the polymer is melted inside the machine and mixed with the blowing agent. Hence, a two-phase mixture of polymer and gas is obtained as it enters the die. At die exit, as a result of rapid pressure drop (from the high-pressure inside the die to the atmospheric pressure) the gas inside becomes supersaturated leading to the creation of several bubbles inside the polymer melt. Finally, after cooling of the obtained sheet at the die exit, a solid foamed polymer film is produced. Nitrogen (N_2) and carbon dioxide (CO_2) are the most common physical blowing agents in polymer foaming.

Thermoplastic foams have several advantages in comparison with unfoamed polymers such as lightweight, high strength to weight ratio, excellent insulation property (Klempner and Frisch, 1991), higher thermal stability and electrical insulation (Colton and Suh, 1987), high impact strength and toughness (Collais and Baird, 1995), and high fatigue life (Seeler and Kumar, 1993). Because of these unique properties, cellular plastics are used in various

industrial applications such as packaging, automotive, acoustic absorbents, and sporting equipment (Kumar, 1993; Nofar et al., 2012; Suh et al., 2000). Typical applications are presented in Figure 1.5.

Figure 0.5. Different applications of polymer foams.

Recently, cellular thermoplastic polymers have been investigated as good candidates for piezoelectric applications because of their low permittivity and low thermal conductivity, as well as high softness and flexibility. Furthermore, their impedance is closer to that of air and water than compact/solid materials, providing them the ability of charge storing as well.

Piezoelectric materials are able to convert electric or magnetic fields into mechanical displacement and vice versa. Since, “piezo” is a Greek word meaning “squeeze” or “pressure”, the word “piezoelectricity” was selected to indicate the relation between

"electricity" and "pressure". Piezoelectricity in materials was first discovered by Pierre and Jacque Curie in 1880 (Lin and Lin, 2012). This property is usually measured via the so-called piezoelectric d_{33} coefficient (Mellinger, 2003), and its values are reported with units of pC/N.

The first piezoelectric materials discovered were crystals such as quartz, topaz, special ceramics, as well as natural materials such as silk, bone, collagen, and DNA (a nucleic acid carrying the genetic information in cells) (Qaiss et al., 2012). Afterward, these materials were produced from polar polymers. For the first time, Kawai in 1969 found that when polar polymer films were drawn and polarized by heating at 90°C and cooled while a static electric field was imposed though their thickness (Kawai, 1969), they showed piezoelectric behavior. The most widely used polar polymer is poly(vinylidene fluoride) (PVDF) showing strong piezoelectric properties (Destruel et al., 1984; Kawai, 1969; Ohigashi, 1976). This group of polar polymers is also categorized as piezoelectric materials and their behavior is named "ferroelectric".

Recently, non-polar polymers were introduced with an obvious piezoelectric behaviour. About three decades ago, Kirjavainen and coworkers in Finland discovered a considerable piezoelectric d_{33} coefficient for charged cellular polypropylene (PP) (as a non-polar polymer) films (Kirjavainen, 1987; Savolainen and Kirjavainen, 1989). They found that after charging the voids of the cellular polymer by imposing a high external electric field, good piezoelectric-like property was obtained. Through this phenomenon, positive and negative electrical charges were created on the opposite faces of each cell surfaces (Qiu et al., 2013) and piezoelectric-like properties/electrical dipoles were obtained. Hence, a new group of piezoelectric materials was developed based on cellular polymers (Fang et al., 2008; Gilbert-Tremblay et al., 2012; Qaiss et al., 2012; Wegener, 2010; Wegener et al., 2005). Cellular non-polar polymer films, such as PP film, as a result of the macroscopic similarity in their polarization behavior, in comparison with typical ferroelectric polymers (such as ferroelectric PVDF), are often named "piezoelectret" and their behavior is called "ferroelectret" (Lindner et al., 2004; Tuncer, 2005).

The final physical and mechanical properties of foams depend on their cellular structure. Cell uniformity is the most important parameter. Moreover, foam morphology is mainly

characterized by parameters such as cell density and cell size distribution. It should be mentioned that for piezoelectric applications, in addition to the stated parameters, cell shape and orientation are also important (Li et al., 2012). It is reported that for piezoelectric properties, it is important to produce a film having an eye-shaped cellular structure having a proper cell aspect ratio (*AR*) defined as the ratio of length over width (Lindner et al., 2004; Tuncer, 2005; B.-X. Xu et al., 2013). Furthermore, to get good piezoelectric properties, an eye-shaped cell structure with $AR > 4$ should be obtained (Lindner et al., 2004; Tuncer, 2005; B.-X. Xu et al., 2013). Such structures can be obtained via biaxial or uniaxial stretching of foamed films.

Nowadays, ferroelectret materials are under investigation for new applications such as actuators, vibration control, ultrasonic transducers, tactile sensors, ferroelectret devices, energy conversion devices, speakers, microphones, keyboards, shock sensors, thermal and optical property measurement devices (Gerhard-Multhaupt, 2002; Lang and Muensit, 2006; Paajanen et al., 2000). Figure 1.6 presents some of these applications. Moreover, piezoelectric devices made from cellular polymer films (ferroelectrets) are very interesting because of their low material cost, ease of processing and the possibility to produce very thin and flexible films with low density (Qaiss et al., 2012).

Figure 0.6. Some important applications of ferroelectret materials.

By developing ferroelectret materials, it can be predicted that in the future:

- ✓ Someone is in a house, apartment, or office, and the living space (an object) can unobtrusively determine where everyone is.
- ✓ A poster or projection screen on a wall can play music.
- ✓ A pad on a desk can hear the person around and whatever happens.

These visions might soon come true with this novel class of internally charged cellular polymers (Bauer et al., 2004). A representative photo of these ideas is shown in Figure 1.7.

Figure 0.7. Predicted future applications of ferroelectret materials: poster or projection screen on the wall that can play music (pinterest.com and mockupworld.co).

1.2 Thesis objectives and experimental strategy

This Ph.D. work is composed of two main parts. The first part is devoted to the investigation of the effective parameters controlling the cellular morphology of polypropylene foamed films through a continuous extrusion-calendaring process. To address these issues, for the first time an experimental plan is designed to achieve the optimum processing of PP film having a uniform and thin eye-like cellular structure foamed PP film in a continuous process. Therefore, these objectives can be described as:

1. Investigate the effect of processing parameters (temperature profile, die temperature, calendaring temperature and speed) in continuous physical foaming to produce thin foamed PP film having an eye-like cellular structure.
2. Determine the best screw design to achieve a maximum gas saturation into PP.

3. Optimize the processing conditions related to the physical blowing agent such as gas flow rate and gas pressure to obtain a uniform thin foamed PP film via continuous extrusion.
4. Compare between the obtained cellular structure of foamed PP film with and without nucleating agent and optimize particle (nucleating agent) content in continuous extrusion.
5. Characterize thin foamed PP film from a morphological point of view (density, cell shape/dimension aspect ratio, cell size, cell density) and relate this information to mechanical properties (tension, dynamic mechanical analysis).

These objectives can be summarize as follows:

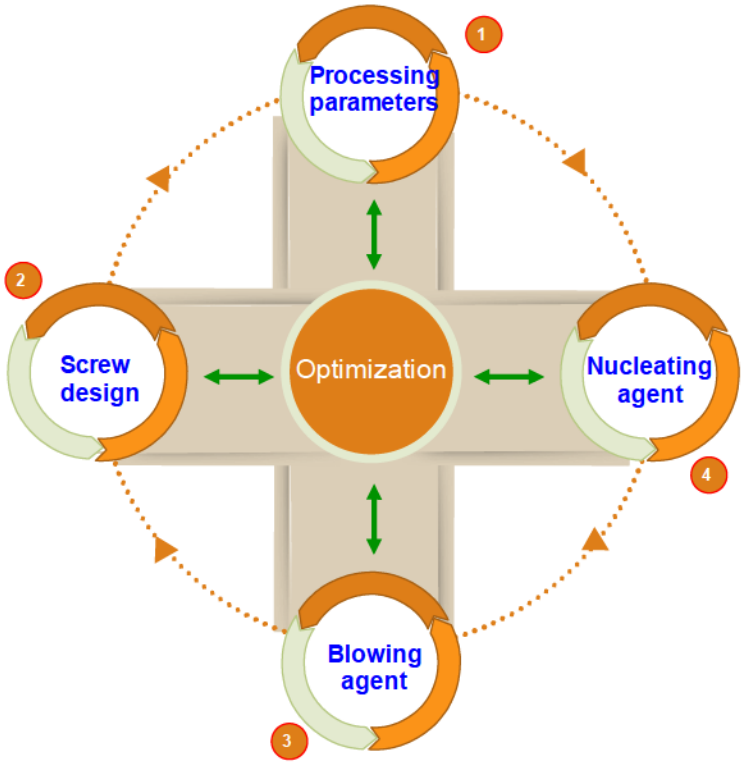

Figure 0.8. Schematic representation for the objectives of the first part.

In the second part of this investigation, the production of PP ferroelectret samples having good piezoelectric properties by applying corona charging and metallization on an optimized eye-like cellular PP film structure and study the parameters controlling their piezoelectric properties. Hence, the objectives of this part are as follow:

1. Investigate the charging parameters such as voltage, needle distance, and time in corona charging of PP film having an eye-like cellular structure.
2. Piezoelectric characterization of the samples and study the effect of morphological (cell shape, cell dimension aspect ratio, cell size) and mechanical (Young's modulus, storage and loss moduli) properties on the piezoelectric behavior of the samples.
3. Compare the final piezoelectric properties of the samples using air or nitrogen as ionizing gas through corona charging.

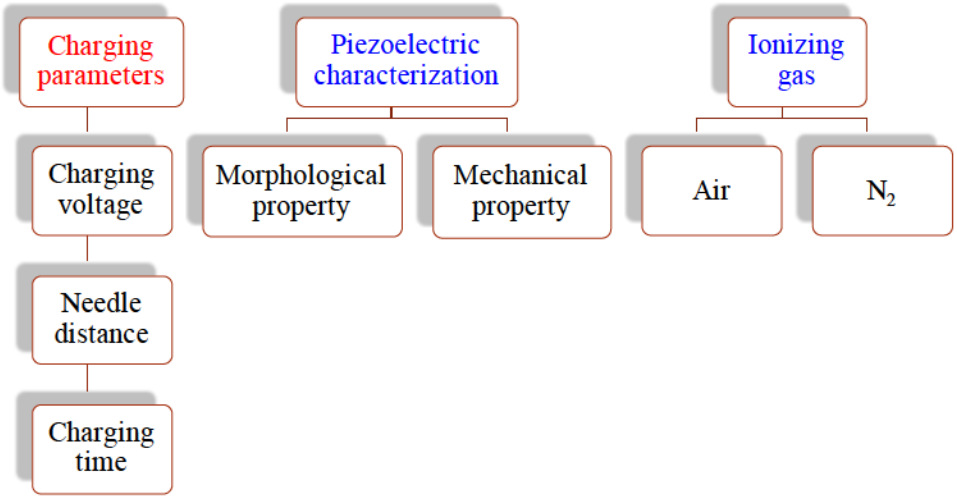

Figure 0.9. Schematic representation for the objectives the second part.

Finally, improve the piezoelectric properties of the samples through an effective post-processing thermal-pressure procedure.

Chapter 2

Literature review 1: Current issues and challenges in polypropylene foaming: A review

Abolfazl Mohebbi, Frej Mighri, Abdellah Ajji, Denis Rodrigue, *Cellular Polymers*, 34, 6, 299-337 (2015).

Résumé

Les mousses thermoplastiques présentent plusieurs avantages par rapport aux polymères non expansés tels que la légèreté, une grande résistance par unité de poids, des excellentes propriétés d'isolation, une stabilité thermique élevée, une grande résistance aux chocs et ductilité, ainsi qu'une résistance à la fatigue. Les propriétés exceptionnelles des plastiques cellulaires mènent à diverses applications industrielles comme l'emballage, les pièces automobiles, les absorbants et les équipements sportifs. De nos jours, le polypropylène (PP), en raison de ses caractéristiques exceptionnelles telles que le faible coût de la matière, la température de service élevée, un point de fusion élevé, un haut module de traction, une faible densité et une excellente résistance chimique, représente une résine majeure dans l'industrie de moussage. Cependant, la formation de mousse de PP classique est limitée par sa faible résistance à la fusion conduisant à une pauvre morphologie cellulaire, la rupture/coalescence des cellules et une réduction de densité limitée. Pour améliorer la résistance à l'état fondu du PP, plusieurs stratégies comprenant l'addition de particules comme agent de nucléation, l'introduction de ramifications à longue chaîne, le mélange à l'état fondu de polymères à haute résistance au fondu et la réticulation ont été proposés. Dans cette revue, ces questions sont discutées et analysées en termes de caractérisations mécaniques, thermiques et rhéologiques.

Abstract

Thermoplastic foams have several advantages in comparison with unfoamed polymers such as lightweight, high strength to weight ratio, excellent insulation property, high thermal stability, high impact strength and toughness, as well as high fatigue life. These outstanding properties lead cellular plastics to various industrial applications in packaging, automotive parts, absorbents, and sporting equipment. Nowadays, polypropylene (PP), because of its outstanding characteristics such as low material cost, high service temperature, high melting point, high tensile modulus, low density, and excellent chemical resistance, is a major resin in the foaming industry. However, foaming of conventional PP is limited by its low melt strength leading to poor cell morphology, cell rupture/coalescence and limited density reduction. To improve PP melt strength, several strategies including particle addition as nucleating agent, introduction of long chain branching, blending with high melt strength polymers and crosslinking have been proposed. In this review, these issues are discussed and analyzed in terms of mechanical, thermal, and rheological characterizations.

2.1 Introduction

Thermoplastic foams or cellular thermoplastics are expanded polymers containing two or more phases: a solid polymer matrix as a continuous phase and a gaseous phase as dispersed bubbles. Generally, such structure is produced by introducing a blowing agent in a polymer matrix. In addition, different types of particles can be added into the polymer matrix as nucleating agents.

Thermoplastic foams have several advantages in comparison with unfoamed polymers such as lightweight, high strength to weight ratio, excellent insulation property (Klempner and Frisch, 1991), higher thermal stability and electrical insulation (Colton and Suh, 1987), high impact strength and toughness (Collais and Baird, 1995), and high fatigue life (Seeler and Kumar, 1993). These unique properties endow cellular plastics with various industrial applications in packaging, automotive parts, acoustic absorbents, and sporting equipment (Kumar, 1993; Nofar et al., 2012; Suh et al., 2000).

The most common polymeric materials for thermoplastic foaming are polystyrene (PS) and polyethylene (PE). But PS and PE have limited physical properties. For example, they are not applicable at service temperatures higher than 100^{o}C. Also, foamed PE has a weak static load bearing capacity (Park and Cheung, 1997). On the other hand, polypropylene (PP), because of its outstanding characteristics such as low material cost, high service temperature (Antunes et al., 2010; Yu et al., 2011; Zhang et al., 2009), high melting point, high tensile modulus, low density, and excellent chemical resistance (Vasile and Seymour, 1993), is now being considered as a new candidate in foaming industries. In terms of mechanical properties, PP shows better stiffness for static load bearing in comparison with PE. PP is also a tough material showing better impact properties than PS (Park and Cheung, 1997). To date, several books have been published on foaming technologies and processing (Ferrigno, 1967; Gendron, 2004; Klempner and Frisch, 1991; Klempner and Sendijarevic, 2004; Lee, 2002; Lee et al., 2006; Lee and Ramesh, 2004; Lee and Scholz, 2008; Okamoto, 2003; Throne, 2004; Xu, 2011), with different applications of polymer foams (Exerowa and Kruglyakov, 1997; Schramm, 1994; Stevenson, 2012), polymer composite foams (Gupta et al., 2013; Mittal, 2013), and characterization of foam structures (Cantat et al., 2013).

The aim of this paper is to review the recent developments in PP foaming processes. First, the cellular foam concept, different classifications and applications are discussed. Then, the different stages of microcellular foaming will be defined and related concepts, such as supercritical fluids, will be discussed. Following, the different parameters to characterize/optimize a foam structure are presented and their equations/methods of calculation are reported. Finally, recent challenges/limitations about PP foaming processes are summarized. The latest information about the effect of different parameters/methods to improve PP foaming behavior are also reviewed.

2.2 Microcellular Foams

Polymeric foams are formed by the creation of gas bubbles through polymeric materials during a foaming process. Based on the cell type, the foams are categorized in two main groups: open-cell and closed-cell structures. While open-cell foams are commonly flexible, closed-cell foams are generally more rigid. Moreover, open-cell foams have several industrial applications, such as filters, separation membranes, sound insulators, battery electrode supports, battery separators, and tissue attachments (Huang et al., 2008).

The bubbles are formed by introducing a gas or a blend thereof, which is generated by using either a chemical or a physical blowing agent. In the case of chemical blowing agents, the gas is generated through a chemical reaction, usually the thermal decomposition of a powder. On the other hand, physical blowing agents are inert gases, which are dissolved into the polymer matrix during a saturation process, usually at high pressure. Since in physical processes an inert gas is used, this method is more environmentally friendly compared to the chemical one and therefore is more interesting from academic and industrial points of view. It is also used to produce lower density foams.

The final physical and mechanical properties of the foams depend on their cellular structure. The most important parameter in this context is the uniformity of the cellular structure. Foam morphology is mainly evaluated by parameters like cell density and cell size distribution. It should be mentioned that cell shape/orientation is also important for some special applications; e.g. where piezoelectric properties are required (Li et al., 2012).

2.3 Foam Classification

General classification of foams, as introduced by Lee (Lee, 2002), is based on cell density and cell size. In this context, foams are categorized in four main groups including conventional, fine-celled, microcellular and nanocellular foams. The specifications of these groups are summarized in Table 2.1.

Table 2.1. Foams classification (Lee, 2002; Leung et al., 2009).

Foam type	Cell size (μm)	Cell density (cells/cm^3)
Conventional	> 300	< 10^6
Fine-celled	10 - 300	10^6 - 10^9
Microcellular	0.1 - 10	10^9 - 10^{15}
Nanocellular	< 0.1	> 10^{15}

Nowadays, microcellular foams are more developed in the foaming industries. Microcellular foam is usually defined as a foam having cell sizes less than 10 micrometers (Martini, 1981) and cell density larger than 10^9 cells/cm^3 (Okamoto, 2003). This definition was first developed by Martini and Suh at the Massachusetts Institute of Technology in the 1980s to produce a material with low materials consumption and high toughness (Martini, 1981). Colton and Suh first obtained a microcellular foam from semi-crystalline polymers (Colton, 1989; Colton and Suh, 1992) and Doroudiani et al. found that in the batch foaming process of these polymers, the morphology of the crystalline region had an obvious effect on the solubility and diffusivity of the blowing agent and final foaming properties (Doroudiani et al., 1996). The continuous extrusion of microcellular foams was developed by Dow (Imeokparia et al., 1997).

Nanocellular foam is defined as a polymeric foam having cell sizes less than 0.1 μm and cell density higher than 10^{15} cells/cm^3. Some successful attempts to produce nanocellular foams using batch processes have been reported (Bao et al., 2013; Fujimoto et al., 2003; Krause et al., 2002; Li et al., 2004). A small amount of well-dispersed nanoparticles in the polymer may create enough nucleation sites to facilitate bubble nucleation (Lee et al., 2005).

Dey et al. (Dey et al., 1996) recommended another classification for polymeric foams based on their density. They categorized the foams into three groups: 1) high density foams (lower than 50% void), which are mostly used for structural applications; 2) medium density foams (between 50% and 90% void), which can be used in the automotive and packaging industries; and 3) low density foams (higher than 90% void), which are mainly used for heat or sound insulation purposes.

2.4 Microcellular foaming process

Microcellular foams are produced through saturating polymers by using a gas in its supercritical state and imposing a sudden thermodynamic instability (pressure drop). In this case, a large number of instantaneous nuclei are created (Mohebbi et al., 2011).

Generally, this foaming process consists of four steps:

(1) Saturation: a polymer matrix is saturated by dissolution of a gas at high pressure.
(2) Nucleation: Numerous nuclei are created through a thermodynamic instability. This thermodynamic instability can be in terms of pressure, temperature or both.
(3) Growth: The dissolved gas diffuses in the nuclei and several bubbles appear gradually by growth of successful (stable) nuclei.
(4) Stabilization: Depending on the type of process, foam growth is limited by imposing rapid cooling. In this situation, the foam is solidified and a stabilized foam structure is created.

It should be noted that nucleation in polymer systems occur by two different mechanisms: homogenous and heterogeneous nucleation (Porter and Easterling, 1992). Homogenous nucleation occurs due to the existence of a critical amount of a secondary component (such as gas bubbles) dissolved in a primary phase (polymer matrix) forming together a stable and uniform secondary phase under specific conditions. Heterogeneous nucleation occurs when, in addition to the above mentioned components, a particle/interface is used as a nucleating agent into the polymer matrix as well. Mohebbi et al. (Mohebbi et al., 2011) were able to monitor the effect of nano-aluminum oxide as a nucleating agent during heterogeneous

foaming. They investigated the effect of particle dispersion on final cell size. Moreover, it was shown that nucleation is the most effective step of the heterogeneous foaming process.

2.4.1 Supercritical Fluids

A supercritical fluid (SCF) is a substance at a temperature and pressure above its critical point (see Figure 2.1). Under these conditions, the material presents a behavior between gases and liquids; i.e. it can diffuse through solids like a gas and dissolve materials like a liquid. Moreover, close to the critical point, small changes in pressure or temperature lead to large changes in density (Eckert, 1996).

SCF have low viscosity and near zero surface tension. Hence, they have fast mass transfer into swollen polymers (Li et al., 2002). SCF are chemically inert, non-toxic, and non-flammable (Eckert, 1996; Zirkel et al., 2009).

Supercritical fluids are used as physical blowing agents in foaming processes. They also improve conventional manufacturing methods, in comparison with chemical blowing agents, especially in terms of environmental issues (Sauceau et al., 2007).

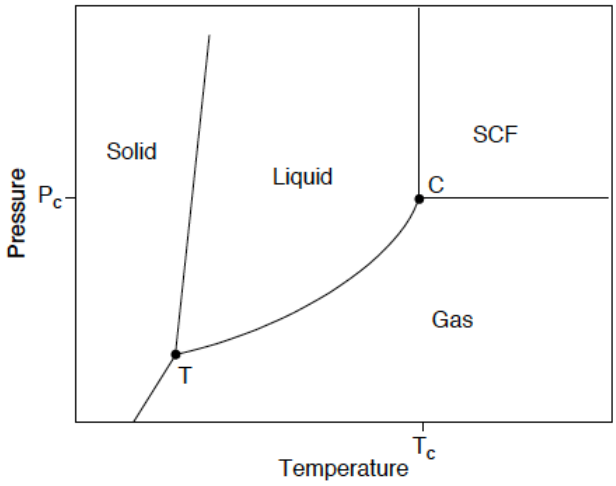

Figure 2.1. Phase diagram of fluids (T: triple point; C: critical point).

Carbon dioxide (CO_2) and nitrogen (N_2) are the most commonly used supercritical fluids. The critical conditions of CO_2 are $T_C = 304$ K and $P_C = 7.38$ MPa (Nalawade et al., 2006). Supercritical CO_2 (SC-CO_2) decreases the glass transition temperature (T_g) and the viscosity

of many polymers via plasticization (Sauceau et al., 2011). The critical conditions of N_2 are T_C = 126 K and P_C = 3.4 MPa (Zong and Yang, 2006). The most important characteristic of N_2 in comparison with CO_2 is that it is above its supercritical temperature at room condition. Hence, to create supercritical condition for N_2, it is only needed to increase the pressure above its supercritical pressure. Moreover, its supercritical pressure is much less than that of CO_2.

In batch foaming processes, the dissolution of blowing agents, such as CO_2 and N_2, leads to the formation of new crystallites (Yu et al., 2011). As N_2 molecules dissolve in PP, the mobility of the chains in the amorphous regions increases enough to rearrange and new crystalline regions can appear. On the other hand, since N_2 is not soluble in the crystalline region, by increasing the latter, more gas is available for foaming in the amorphous area from expelled N_2 molecules leading to lower foam density (Yu et al., 2011). Moreover, it is known that the interface between amorphous and crystalline regions can act as heterogeneous nucleation sites, which is related to the low energy barrier at crystalline/amorphous interfaces (Zhai et al., 2008).

2.5 Foaming characteristics and their calculation

2.5.1 Characterization of foam structure

Foam Density

Foam density can be determined from water displacement (ASTM D792) (Kuboki, 2013; Zhai and Park, 2011) or gas pycnometry (Gilbert-Tremblay et al., 2012).

Void Fraction

To calculate void fraction, the expansion ratio (∅), defined as the ratio between bulk density before foaming (polymer density) (ρ_p) and density of the foamed sample (ρ_f), is determined as:

$$\emptyset = \frac{\rho_p}{\rho_f} \tag{2.1}$$

Then, void fraction is determined as:

$$Void\ Fraction\ (\%) = \left(1 - \frac{1}{\emptyset}\right) \times 100 \tag{2.2}$$

Cell Density

Cell density (N_f) refers to the number of cells per unit volume of foam. On the other hand, nucleation density (N_o) represents the number of cell created per unit of unfoamed polymer matrix as:

$$N_0 = \left(\frac{n}{A}\right)^{3/2} \times \emptyset \tag{2.3}$$

where n is the number of cells in a micrograph of area A (in cm^2).

2.5.2 Characterization of thermal properties

Three main thermal properties, such as melting temperature (T_m), crystallization temperature (T_C), and heat of fusion (ΔH_{exp}), can be determined from thermal characterization using differential scanning calorimetry (DSC). Most of the time, the heating rate is set at 10°C/min for PP (Kuboki, 2013). From the curve, the degree of crystallinity (χ_C) can be determined as:

$$\chi_C = \frac{H_{exp}}{H^*} \times \frac{1}{w_f} \tag{2.4}$$

where ΔH_{exp} is the experimental heat of crystallization, ΔH^* is the enthalpy of the fully crystalline PP (290 J/g (Ferrigno, 1967)), and w_f is the weight fraction of PP in the composite/blend.

2.5.3 Characterization of rheological properties

The foam structure strongly depends on the rheological properties of the polymer matrix (Liao et al., 2010). Hence, characterization of the rheological properties is a useful method to predict the foaming behavior of polymers in the melt state. Several books were published to describe the relations between structure, properties and rheology of polymer melts and general non-Newtonian fluids (Dealy and Larson, 2006; Delay and Wissbrun, 1990; Doi, 1987; Doi and Edwards, 1986; Larson, 1999).

The general principle behind the use of rheology to understand the behavior of viscoelastic materials is very simple: to apply a deformation or stress to the structure of interest and track the response of the material. In this context, two types of deformation are very important in foam processing: shear and extensional deformations. As for the most of melt processing operations, shear is an important type of deformation and understanding the behavior of a material under shear not only provides information about the structure of the materials, but also provides how the material flow can be studied as well. Furthermore, since in polymer foaming the materials are expanded, information about the elasticity/extensibility of polymeric systems is very important. Therefore, studying the properties of polymers under extensional deformation is also a very important topic. Considering the importance of these deformations, some issues related to rheological properties of polymer melts are reviewed in the next two sections.

2.5.3.1 Shear rheology

In this case, a shear deformation is applied on the sample and the response is tracked. One of the simplest and widely used shear tests is small amplitude oscillatory shear (SAOS) where a small amplitude sinusoidal deformation is applied on the sample. First, a time sweep test should be performed to ensure that no degradation occurs during testing for the required time (fixed temperature). Then, a strain sweep test is performed to determine the limit of the linear viscoelastic region; moduli independent of strain amplitude. Finally, a frequency sweep test (fixed temperature and strain amplitude, which is chosen inside the linear viscoelastic region) is performed.

One useful parameter extracted from SAOS measurements is tan δ, calculated as:

$$\tan\delta = {}^{G''}/_{G'} \tag{2.5}$$

where G'' and G' are loss and storage moduli, respectively. The ratio of both moduli gives an idea about the viscoelastic behavior of the material; mostly elastic (tan δ<1) or mostly viscous (tan δ >1).

As mentioned before, high melt strength PP is suitable for foam processing. One of the methods to find a suitable PP grade is based on tan δ analysis (Suh et al., 2000). As illustrated in Figure 2.2, Park et al. showed that tan δ is inversely related to melt strength (Malone and Park, 1996). As can be seen, a PP sample with a lower tan δ value has higher melt strength and as a result, showed better foaming behavior.

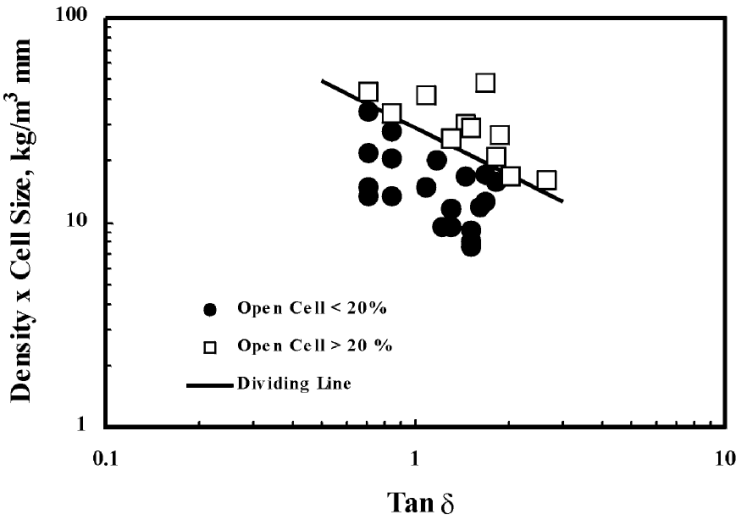

Figure 2.2. Effect of tan δ on PP foam density times cell size (Suh et al., 2000).

Based on this analysis, a formability factor (*F*) was proposed as (Malone and Park, 1996):

$$\mathrm{F} = \rho_f \, D \, (\tan\delta)^{0.75} \leq 1.8 \tag{2.6}$$

where ρ_f is foam density in pound per cubic foot, *D* is average cell diameter in millimeter and tan δ is the value from a rheological analysis using a 2.5 mm thick and 25 mm diameter

samples at 190 °C with a frequency 1 rad/s. *F* values less than or equal to 1.8 were shown to lead to foams having at least 80% closed-cells (Malone and Park, 1996).

It was shown that both the complex viscosity and storage modulus of the blends had obvious effect on the cellular morphology of the foamed samples (Huang and Wang, 2007). Moreover, cell size is controlled by cell growth and cell coalescence. On the other hand, these two parameters are strongly affected by the storage modulus of the matrix under the foaming conditions.

2.5.3.2 Extensional rheology

The most common extensional test is the uniaxial extension where the material (at time $t = 0$) is subjected to a constant unidirectional elongation rate ($\dot{\varepsilon}$). The elongational viscosity growth function, $\eta_E^+(t, \dot{\varepsilon})$, is usually reported and defined by:

$$\eta_E^+(t, \dot{\varepsilon}) = \frac{\sigma_E(t,\dot{\varepsilon})}{\dot{\varepsilon}} \tag{2.7}$$

where σ_E is the extensional stress (Dealy and Wissbrun, 1990). The extensional viscosity, in the linear viscoelastic regime, can be determined by:

$$\lim_{\dot{\varepsilon}\to 0} \eta_E^+(t, \dot{\varepsilon}) = \eta_E^+(t) = 3\eta^+(t) = 3\int_0^t G(s)\, ds \tag{2.8}$$

where *G(s)* is the relaxation modulus.

When the deformation is small or slow, the behavior of the material is linear and follows the theory of linear viscoelasticity where different relations between material's functions can be obtained. Thus, in linear viscoelasticity, the extensional properties can be calculated from shear data. On the other hand, when the deformation is large or fast due to the imposed nonlinearity, extensional properties cannot be predicted from shear data. However, extensional data are compared with shear data in order to obtain some information about nonlinear phenomena (Mahi Hassanabadi, 2013). Therefore, a plot of $\eta_E^+(t, \dot{\varepsilon})$ is presented with the value of $3\eta^+(\mathrm{t})$ to be compared. The ratio of $\eta_E^+(t, \dot{\varepsilon})/3\eta^+(t)$ is normally referred as the Trouton ratio (TR). In the linear viscoelasticity regime, TR = 1 and for materials

showing non-linear behaviour, the value is generally higher than 1; i.e. extensional thickening.

In the linear region, the extensional viscosity gradually increases with time and the viscosity is only a function of time ($\eta_E^+(t)$) as calculated from Equation (2.8). On the other hand, at longer times and for high extension rates, the extensional viscosity deviates from the linear behavior. In this region, the viscosity is a function of both time and strain rate ($\eta_E^+(t, \dot{\varepsilon})$) and increases rapidly with time. This fast increase in extensional viscosity is called strain-hardening. Different models have been developed to explain the nature of such hardening in polymeric systems (Marrucci and Ianniruberto, 2004; Wagner et al., 2006). This hardening behavior is very important in polymer foaming as it determines how much materials can be stretched before the breakup of the sample. This hardening also helps in stabilizing the foam structure during the cell growth stage. Different studies have been done to verify how this hardening behavior can be improved (Wagner et al., 2003; Wagner and Rolón-Garrido, 2008), but more work is still needed to completely understand the relations between the polymer molecular structure and its flow behavior. Especially, the effect of branching (long chain branching, short chain branching) is highlighted as such effect has been showed to have a substantial effect on the extensional properties of polymeric systems (Rolón-Garrido and Wagner, 2007; Wagner and Rolón-Garrido, 2008). For example, Xu et al. studied the relationships between foaming behavior and extensional properties of different types of PP (Xu et al., 2013), which will be reviewed in a following section.

2.6 Challenges about polypropylene in the foaming process

PP is a semi-crystalline polymer and in comparison with amorphous polymers, such as PS, it is difficult to obtain a uniform foam structure through a batch process, since gas diffusion in the crystalline region is much lower than in the amorphous region (Doroudiani et al., 1996; Doroudiani et al., 1998; Rachtanapun et al., 2003). Furthermore, foaming conventional linear PP is limited by its low melt strength (Burt, 1978; Park and Cheung, 1997; Yu et al., 2011; Zhai et al., 2010), which always results in poor cell nucleation behavior (Zhai et al., 2008).

Moreover, low melt strength of linear PP leads to the formation of cells with walls not strong enough to bear the extensional forces resulting from the foaming process. As a result, cell coalescence and rupture occur and a foam structure with high open-cell content will be created, thus limiting the maximum expansion ratio (Zhai et al., 2008; Zheng et al., 2010). Hence, several attempts have been made to overcome the problems of weak melt strength and cell nucleation of PP (Ding et al., 2013; Huang et al., 2008; Huang and Wang, 2007; Jiang et al., 2009; Kuboki, 2013; Malone and Park, 1996; Naguib et al., 2003; Park and Cheung, 1997; Wang et al., 2013; Xu et al., 2013; Xu et al., 2007; Zhai and Park, 2011; Zhai et al., 2008; Zhai et al., 2008; Zheng et al., 2010).

It was reported that, polyolefin foams obtained from a polymer having a melt flow rate of about 2 g/10 min is a good choice for construction application, insulation and packaging industries (Suh et al., 2000). Foamed films of nonpolar polymers, such as PP, can exhibit piezoelectric properties via a charging process, and can be used as electromechanical transducers (Zirkel et al., 2009).

2.7 Different methods to improve the foaming behavior of PP

Foamed PP, as result of its weak melt strength, has cell walls that may not have enough strength and might rupture during cell growth (Naguib et al., 2003; Naguib et al., 2004; Wang et al., 2013). To improve the melt strength of linear PP and its nucleation behavior, four methods are generally used: 1) adding particles into the polymer matrix as nucleating agents (Ding et al., 2013; Huang et al., 2008; Huang and Wang, 2007; Jiang et al., 2009; Naguib et al., 2003; Nam et al., 2002; Wang et al., 2013; Zheng et al., 2010), 2) introducing long chain branching (Kuboki, 2013; Park and Cheung, 1997; Spitael and Macosko, 2004; Xu et al., 2013; Yu et al., 2011), 3) blending with a high melt strength polymer (Huang et al., 2008; Huang and Wang, 2007; Xu et al., 2013; Zhai and Park, 2011; Zhang et al., 2009), and 4) crosslinking (Nam et al., 2005; Xu et al., 2013; Zhai et al., 2008). Each method is discussed in the next sections.

2.7.1 Effect of particles as nucleating agents

The addition of particles, as nucleating agents, followed by a careful control of the foaming conditions, could result in the formation of polymer foams having specific mechanical properties even better than their unfoamed polymer. Moreover, by using particles with special characteristics, such as high conductive properties, could produce foams with improved mechanical and functional properties (Antunes et al., 2013).

It is now accepted that penetrating gases, such as CO_2, could only diffuse in amorphous phases, but in contrast the crystal lamellas could act as nucleating sites (Jiang et al., 2009). As a result, in homogenous foaming of PP, the morphology of the obtained foam is not as uniform as heterogeneous foaming in the presence of nucleating agents, such as clay. Some researchers showed that for neat PP, the cells are mainly created at the centers, boundaries, and inter-lamellar amorphous regions of PP-spherulites (Jiang et al., 2009). It is believed that the crystallinity of semi-crystalline polymers, such as PP, may decrease in the presence of nanoparticles (Huang et al., 2005; Lee et al., 2005) producing more uniform cell structure. Moreover, the presence of nucleating agent leads to higher melt viscosity and strength (Huang and Wang, 2007; Nam et al., 2002; Zhai et al., 2010), which results in more cell growth resistance and prevents cell coalescence (Huang et al., 2008).

The presence of particles in the polymer during foaming reduces the critical radius of the bubbles according to the classical nucleation theory (Gibbs, 1961) and also its energy barrier in cell nucleation (Zhai and Park, 2011). Moreover, well-dispersed particles can increase the melt strength of the sample, which is useful to achieve improved cell structures.

Kuboki was able to produce an improved foamed PP in the presence of micron-size cellulose fibers using N_2 as a blowing agent via injection molding (Kuboki, 2013). Taki et al. (Taki et al., 2004), in their visual observation of the foaming of PP-clay composite using CO_2 as blowing agent, found that bubble growth in the early stage can be considered as a diffusion-controlled system. Hence, when PP foams in the presence of particles, the viscosity of the matrix does not affect the bubble growth rate in the early stage of foaming. But in general, the bubble growth rate decreased as clay content increased. This means that in the last stage of cell growth, the growth rate is viscosity-controlled.

Wang et al. produced, through a batch process, improved PP foams structure using carbon fibers (CF) as a nucleating agent and SC-CO_2 as blowing agent (Wang et al., 2013). The average length of used carbon fibers was 6 mm. Three different PP/CF composites with CF contents of 5, 15 and 25% wt. were prepared. They found that the viscosity of composites increased significantly as CF content increased. Moreover, the shear viscosities of composites decreased when the shear rate increased. In addition, the modulus and melt strength of the composites increased as CF content increased. Furthermore, the PP/CFs composites showed higher melt strength in comparison with neat PP. Hence, the cell structure of PP/CF composites was improved in comparison with neat PP. On the other hand, they reported that the foaming behavior of the composite with 25% wt. CF was enhanced compared with the other two samples. As illustrated by Wang et al. (Wang et al., 2013), the sample with 25% wt. CF has a more uniform cell size distribution. Moreover, they showed that by increasing fiber content from 5 to 25% wt., cell diameter decreased from 38 to 28 μm and the sample with 25% wt. yielded a maximum cell density of $8x10^6$ cells/cm^3. Accordingly, it can be concluded that the melt strength of the PP was increased by the presence of CF and higher melt strength resulted in minimum cell size and maximum cell density. It can also be concluded that the presence of CF in PP led to a foam structure with mostly closed-cell and spherical shape cells.

Jiang et al., using Sc-CO_2 as blowing agent, intensively studied the foaming behavior of PP in the presence of nano-clay as a nucleating agent through a batch process (Jiang et al., 2009). Two types of clay (1.30P and 1.44P) with four different loadings (0.5, 1, 3 and 5% wt.) were used. Moreover, maleic anhydride grafted PP (PP-g-MA) with a concentration of 0.6% wt. of maleic anhydride was used as a compatibilizer. The PP-g-MA content of all samples was 15% wt. In this case, the effect of PP-g-MA, led to a more uniform cell structure in the PP/PP-g-MA blend in comparison with neat PP. Moreover, about 130% increase in cell density was observed for PP/PP-g-MA blends. But an interesting result is that the mean cell size of PP/PP-g-MA blends increased as well. As a consequence, PP-g-MA facilitated both cells nucleation and their growth. It is believed that in this situation, more CO_2 diffused in the PP/PP-g-MA blends. Hence, in comparison with neat PP, these blends had a more uniform cell structure, as well as higher cell density and cell size (Jiang et al., 2009).

On the other hand, Jiang et al. (Jiang et al., 2009) also reported that the composites at low clay contents (0.5% wt.) for two types of clay, had the lowest cell size and cell size increased with increasing clay content. Based on their results, it can also be concluded that composites with 0.5 wt.% clay content had maximum cell density for both types of clay ($1.62x10^8$ cells/cm^3 for 1.30P). Moreover, a uniform closed-cell structure with pentagonal or hexagonal faces was obtained by using nano-clay in PP. The same shape and cellular structure was achieved for another investigation on PP-clay foaming (Nofar et al., 2012).

In another study on the PP-clay system with 4% wt. clay loading, a uniform and closed-cell structure having pentagonal or hexagonal faces was obtained (Okamoto et al., 2001). The authors emphasized that in addition to higher cell density, clay also increased the strain-induced hardening behavior of the samples and led to higher cell wall thickness in PP-clay foams. This strain-induced hardening behavior was probably adequate to increase the extensional viscosity under biaxial flow and limited cell rupture at high temperature. Hence, it can be concluded that for the PP-clay system, the probability to create a uniform and closed-cell structure is higher.

Nam et al. also obtained similar cell structure characteristics in the presence of clay (Nam et al., 2002). In their case, PP foaming was also followed through a batch process using CO_2 as a blowing agent. Clay particles were used at three different loadings (2, 4, 7.5% wt.) and PP-g-MA with 0.2% wt. of maleic anhydride was used to obtain better conditions for the foaming process. It was found that the average cell size decreased as clay loading increased. Also, their results indicated that the effect of temperature was much less with increasing particle loading. The best foaming behavior was reported for the sample produced with 7.5% wt., which had a cell density of $3.42x10^8$ cells/cm^3 with an average cell size of 27.5 μm.

Zheng et al. tried, through continuous extrusion, to improve the foaming behavior of linear PP using nano-clay as a nucleating agent and CO_2 as a blowing agent (Zheng et al., 2010). The morphology of foams made from nano-composites containing different clay contents was compared to that of linear PP and is shown in Figure 2.3. It can be seen that the presence of only 0.2% wt. of clay led to smaller cell sizes compared to neat PP, but higher cell coalescence and open-cell content was obtained. By increasing clay loading to 0.5 and

1% wt., cell coalescence was suppressed, especially at 1% wt. where SEM indicates a completely closed-cell structure. But at 5% wt., some large cells and non-uniform morphology were produced. As reported in another study (Huang et al., 2006), this can be related to the non-uniform distribution of the particles in the polymer matrix. Hence, at high clay loading, clay exfoliation was not successful and those areas with intercalated clay led to large bubbles. The same result was reported for high loadings of nano-graphene as a nucleating agent in PP foaming using Sc-CO_2 (Antunes et al., 2013).

It was also reported that PP-based nano-composites were much less sensitive to the foaming temperature than neat PP (Zheng et al., 2010). This fact is illustrated in Figure 2.4. In this case, the optimum clay content was between 0.5 to 1% wt. and the maximum cell density was around 10^9 cells/cm^3.

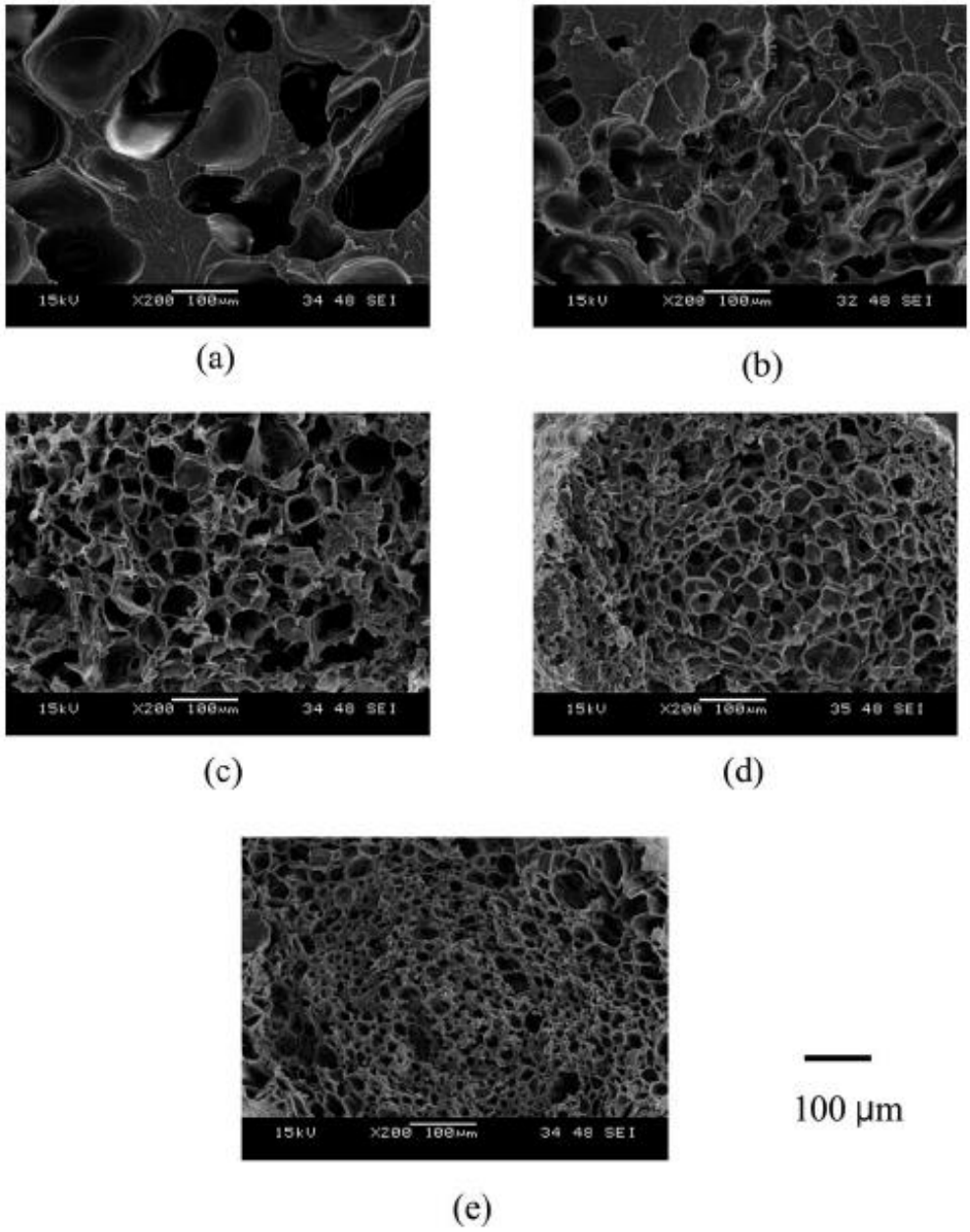

Figure 2.3. SEM micrographs of foamed PP nano-composites with (a) 0, (b) 0.2, (c) 0.5, (d) 1.0 and (e) 5.0% wt. clay loading foamed at 150 °C (Zheng et al., 2010).

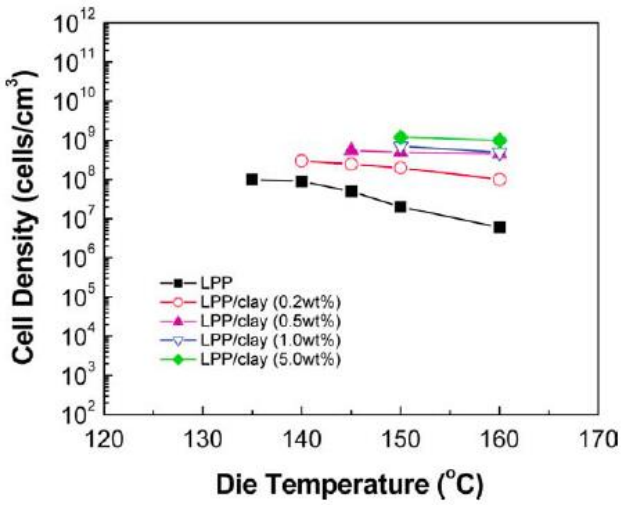

Figure 2.4. Effect of die temperature on cell density for neat PP and its nano-composites with different clay contents (Zheng et al., 2010).

The effect of nano-calcium carbonate, as a nucleating agent, on the foaming behavior of PP using Sc-CO_2 as blowing agent through a batch process was investigated (Ding et al., 2013). In this study, four different loadings (3, 5, 7 and 10% wt.) of calcium carbonate ($CaCO_3$) were used. Silane coupling agents were also used to modify the surface of nano-$CaCO_3$ which led to better particle dispersion through PP.

As illustrated in Figure 2.5 and Figure 2.6, PP nano-composites with 5% wt. $CaCO_3$ had the lowest cell size among all the samples. In fact, nano-particles had large surface areas and acted as heterogeneous nucleation sites. As a result, by increasing the nano-$CaCO_3$ loading, the nucleation rate was increased and led to enhanced cell density and lower cell sizes. On the other hand, it was found that using more than 5% wt. nano-$CaCO_3$ led to particle aggregation and decreasing surface area. Hence, larger cell sizes and lower cell density were achieved (Ding et al., 2013). It is clearly seen in Figure 2.5 that nano-$CaCO_3$ improved the cell structure of PP foams in comparison with the neat matrix, but for all the samples, a non-uniform cell structure and some unfoamed areas can be seen.

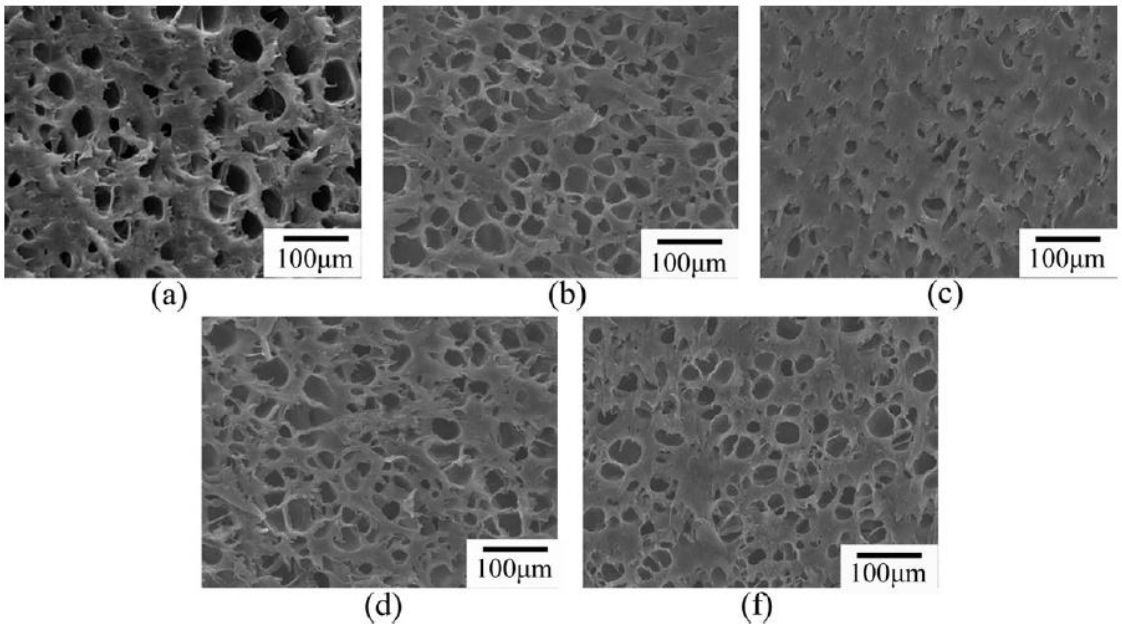

Figure 2.5. Cell morphology of foamed (a) neat PP, and PP/$CaCO_3$ composites with: (b) 3, (c) 5, (d) 7, and (e) 10% wt. $CaCO_3$ foamed at 150 °C (saturation conditions of all samples: 25 MPa and 80 °C) (Ding et al., 2013).

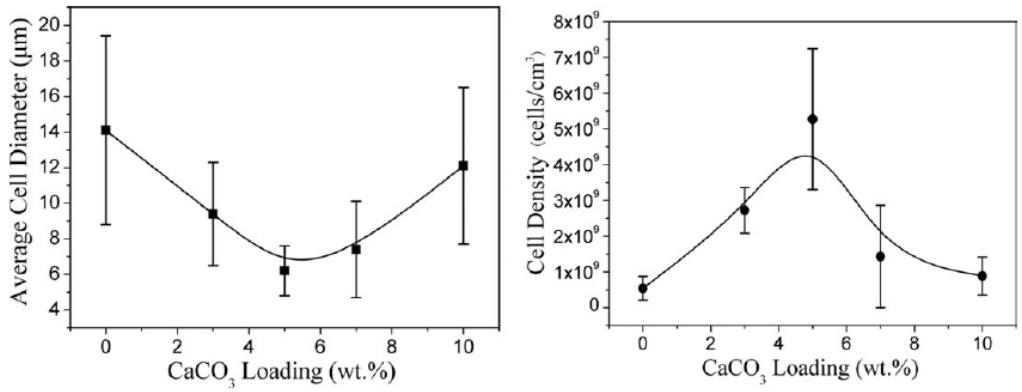

Figure 2.6. Variation of cell parameters of foamed PP composites as a function of $CaCO_3$ loading (saturation conditions of all samples: 25 MPa and 80 °C) (Ding et al., 2013).

In another study by Huang and Wang (Huang and Wang, 2007), comparison of the storage modulus and complex viscosity of PP and PP-$CaCO_3$ nano-composites were investigated and the results are presented in Figure 2.7. The composites showed higher complex viscosities over a wide frequency range with complex viscosity increasing with increasing nano-$CaCO_3$

loading. Both nano-composites showed higher storage modulus than neat PP at high frequencies, but exhibited lower storage modulus at low frequencies.

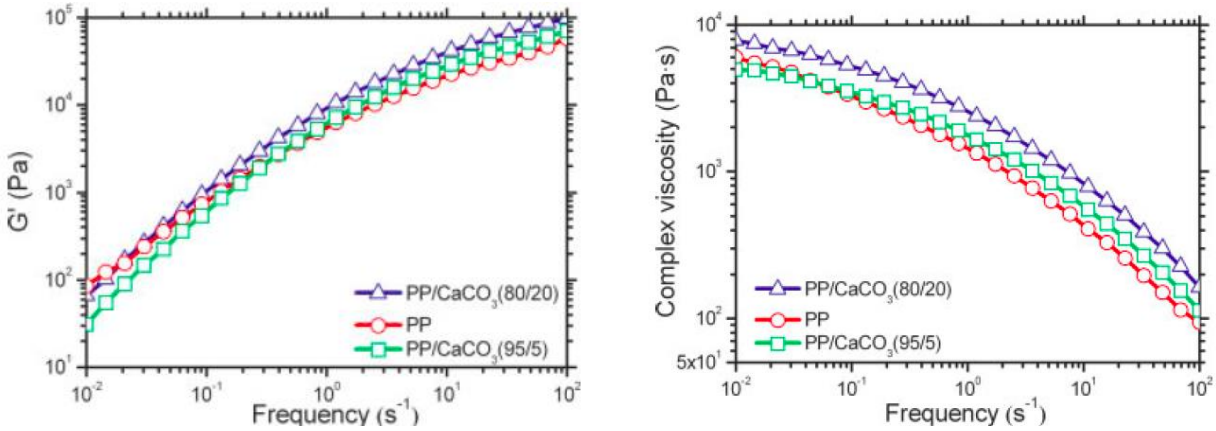

Figure 2.7. Storage modulus and complex viscosity as a function of frequency for PP and PP/$CaCO_3$ nano-composites (Huang and Wang, 2007).

As shown in Figure 2.8 (a,1), a microcellular structure with very fine cells was obtained for a PP-nano-composite with 5 wt.% $CaCO_3$. Cell size increased with increasing $CaCO_3$ loading from 5 to 20% wt. This is because at high $CaCO_3$ concentration, particle agglomeration occurs (Huang et al., 2006). Hence, larger bubbles around particle agglomerates were produced.

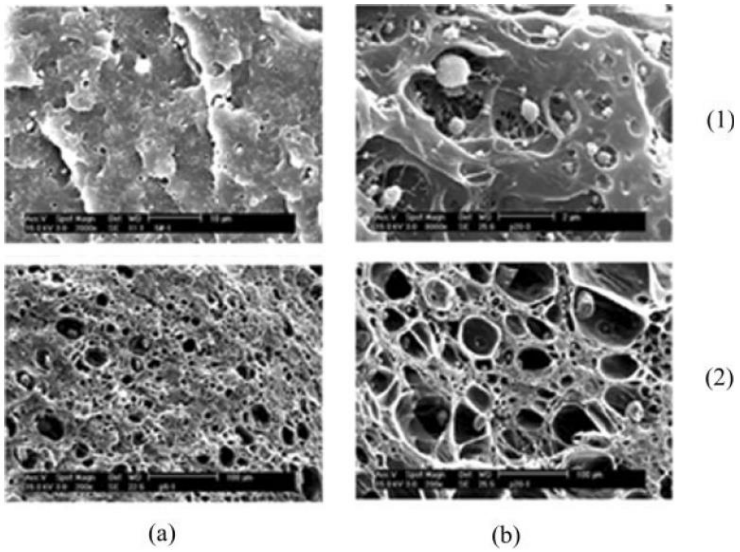

Figure 2.8. SEM micrographs of foamed PP nano-composites with (a) 5 and (b) 20% wt. $CaCO_3$ saturated at 15 MPa and foamed at: (1) 179 and (2) 182 °C (Huang and Wang, 2007).

As mentioned before, PP nano-composites showed lower storage modulus than neat PP at low frequency. This led to easier nucleation but limited the amount of gas held in the matrix during the foaming process. Hence, cell collapse occurred because there was not enough gas to diffuse to the cells and promote their growth (Huang and Wang, 2007). In this investigation, another interesting result about the structure of the nano-composites is the observation of non-uniform cellular shape composed of both ellipsoidal and spherical shapes. The authors believed that this was due to lower storage modulus of the nano-composites at low frequency. Hence, it can be concluded that the storage modulus had two different effects on foaming:

1- High storage modulus limits cell growth and inhibits cell coalescence.
2- Low storage modulus makes nucleation easier, but gas diffusion to the nuclei will be more difficult. Hence, the nucleated cells cannot overcome their critical radius and cell collapse can happen.

The maximum cell density achieved in this study was $8.4x10^{11}$ cells/cm^3 for nano-composites with 5% wt. $CaCO_3$.

In the studies of Naguib et al. (Naguib et al., 2003; Naguib et al., 2006), PP foams were produced from branched PP using n-butane as a blowing agent through continuous extrusion equipped with a filament die. They also used micron size talc as a nucleating agent with different loadings from 0.8 to 2.4% wt. It should be mentioned that the diffusion rate of a blowing agent small molecule, such as CO_2, is faster than higher molecular weight blowing agents, such as isopentane and butane (Park et al., 1998).

It is known that, because of the semi-crystalline behavior of PP, crystallization has an obvious effect on cell growth in foaming processes. The reason is that cell growth stops when crystallization starts (Naguib et al., 2000). Hence, from this point of view, one useful test to predict the foaming behavior of PP in the presence of particles or additives is to determine the effect of those additives on PP crystallization.

Naguib et al. found that even 0.2% wt. talc affected the crystallization behavior of PP (Naguib et al., 2003). They believe that talc particles decrease the mobility of the polymer chains. As a result, early crystallization happened and higher degree of crystallinity was obtained. On the other hand, by increasing talc loading above 0.2% wt., the degree of crystallinity of PP did not change much. These results illustrated that talc had significant effect on the cell density of branched PP. Moreover, the cell density increased with increasing talc content. It was possible to obtain PP foams with cell density of $6x10^7$ cells/cm^3 when 2.4% wt. talc was used.

Huang et al. studied the effect of two different nano-particles (nano-clay and nano-$CaCO_3$) on the foaming behavior of PP/high density polyethylene (HDPE) blends (Huang et al., 2008). They used three loadings (1, 3 and 5% wt.) and their results can be summarized as follow:

1- The effect of the interface between PP and HDPE phases, which is effective for cell nucleation of the blend, is gradually vanished by the presence of the nano-particles.
2- An obviously smaller cell size and more uniform cell distribution are obtained in the foamed nano-composite blends in comparison with the blends. This indicates that well dispersed nano-particles act as heterogeneous nucleating agents. Hence, providing more nucleation sites through the matrix, which results in the creation of more interfacial area between the particles and the matrix.
3- Increasing the nano-clay content from 1 to 3% wt. led to lower cell diameter and larger cell density.
4- Increasing the nano-particles content for both nano-clay and nano-$CaCO_3$ from 3 to 5% wt., led to a slight increase in cell diameter and decrease in cell density. Higher nano-particle content may produce less dispersed structure for nano-$CaCO_3$ (Huang et al., 2005, 2006) and also create intercalated structure for nano-clay (Jiang et al., 2009; Lee et al., 2005; Wang et al., 2004), which can result in lower interfacial contact area and less cell nucleation.
5- The minimum cell size and maximum cell density obtained were 1.4 μm and $5.1x10^{11}$ cells/cm^3 for the foamed blends of nano-$CaCO_3$, and 1.0 μm and $9.4x10^{11}$ cells/cm^3 for the foamed blends of nano-clay, respectively.

2.7.2 Effect of branching

It is known that the introduction of long-chain branching onto the PP backbone is one method to improve its melt strength, which is useful to improve foamability (Gotsis et al., 2004; Li et al., 2012; Liao et al., 2010; Naguib et al., 2002; Nam et al., 2005; Spitael and Macosko, 2004; Stange and Münstedt, 2006; Wang et al., 1996; Zhai et al., 2008). Hence, branched PP, also called high-melt-strength (HMS) PP, was proposed as an appropriate PP grade to produce good foamed products (Gaylord et al., 1992). Moreover, it was reported that blending of even small amounts (10%) of branched PP with linear polypropylene results in strain-hardening enhancement. As a result, cell coalescence can be prevented, leading to improve foaming behavior (Naguib et al., 2002; Spitael and Macosko, 2004). On the other hand, it is believed that a very large number of branches per chain may decrease the strain at break of the polymer melt, which results in lower foamability (Gotsis et al., 2004).

Based on thermodynamics principles, while foaming a given polymer/gas solution, production of larger cells is more favorable than smaller cells (Klempner and Frisch, 1991). Moreover, cell coalescence is also favorable (Ostwald ripening (Alemán et al., 2007)) and can occur very rapidly in foaming linear PP. As a result, for linear PP, high open cell contents was obtained as reported by Park and Cheung (Park and Cheung, 1997), as well as Nam et al. (Nam et al., 2005).

Park and Cheung studied the cell nucleation and initial growth behavior for a linear and a branched PP (Park and Cheung, 1997). They performed this study via continuous extrusion without any nucleation agent and using two different blowing agents (CO_2 and isopentane). As shown in Figure 2.9, it was observed that, in contrast with linear PP, the number of open-cells for the branched PP was significantly reduced. It was also reported that, for both linear and branched PP, higher cell density was achieved by increasing CO_2 or isopentane concentration from 10 to 20% wt. (Park and Cheung, 1997). It is believed that the presence of large amount of blowing agent in the polymer matrix has a reverse effect on the foaming behavior. This leads to the formation of large bubbles and lower cell density (Park et al., 1994). In this case, the optimum gas amount, which can also result in the creation of a single-phase polymer/gas solution, decreases the dependence of nuclei density to pressure drop rate

in the die (Park et al., 1995). Hence, in order to achieve uniform cell structures in continuous processes, the amount of blowing agent must be optimized with respect to gas solubility/diffusion under the processing conditions used. Finally, cell density of the branched PP was higher than for linear PP with a maximum obtained at 10^8 cells/cm^3.

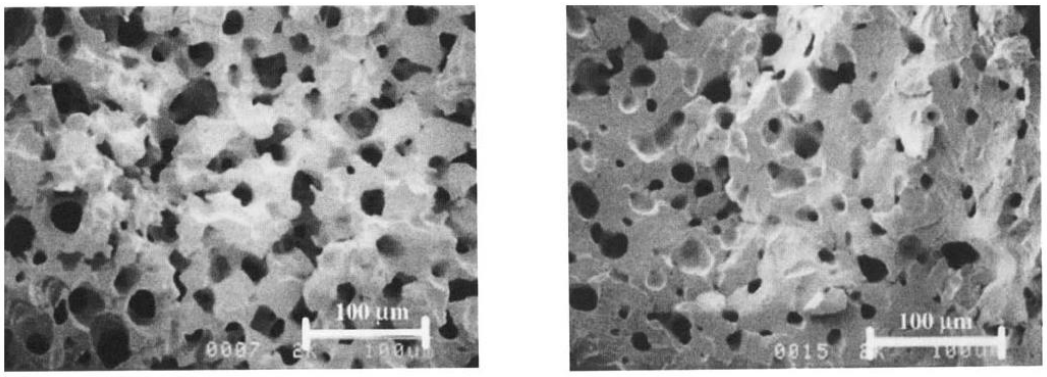

Figure 2.9. Cell morphology of (left) linear and (right) branched PP foamed at: P = 27.6 MPa, CO_2 = 4% (Park and Cheung, 1997).

Kuboki compared the thermal characteristics and foaming behavior of linear and branched PP in the presence of micron-size cellulose fibers using CO_2 as blowing agent through continuous extrusion equipped with a filament die (Kuboki, 2013). This work was performed with high cellulose fiber loading (20 and 40% wt.) and using 3% wt. PP-g-MA as a compatibilizer to improve fiber dispersion.

In the context of crystallization temperature, several papers reported that branched PP has higher T_C than linear PP (DeNicola et al., 1992; Kuboki, 2013; Naguib et al., 2005; Wang et al., 1996). By introducing branches in PP, the crystallization temperature can increase by up to 30°C. However, crystallization temperature decreases as the supercritical fluid (such as nitrogen or carbon dioxide) dissolves in branched PP (Naguib et al., 2005). It was found that linear PP showed slightly more crystallinity in comparison with branched PP. But addition of cellulose fibers led to crystallinity decrease for both linear and branched PP (Kuboki, 2013). Actually, the interface between PP and cellulose fibers can limit the crystallization process since the macromolecules have less freedom to move around and rearrange themselves into crystals.

The presence of PP-g-MA resulted in an increase in foam density for both linear and branched PP. But in general, the foam density of branched PP is higher than that of linear PP (Kuboki, 2013). Also, PP-g-MA led to foamed PP with better cell uniformity in comparison with samples without PP-g-MA. Nevertheless, it was found that in the presence of cellulose, PP type (linear or branched) and cellulose loading have a negligible effect on foam density (Kuboki, 2013). This means that by increasing the cellulose content from 20 to 40% wt., no significant change in foam density was observed.

Yu et al. compared the foaming behavior of linear and branched PP using N_2 as blowing agent in a batch process (Yu et al., 2011). They found that branched PP had better formability than linear PP. Moreover, branched PP was insensitive to foaming temperature and produced foams with smaller cell sizes (114 μm) in comparison with linear PP (147 μm) (Yu et al., 2011).

2.7.3 Effect of blending with high melt strength polymer

Polymer blending is a useful method to combine the properties of different polymers to obtain materials having superior properties, compared to the base materials (Zhai et al., 2008). Cell morphology and cell density of the blends depend strongly on the extensional strength of the polymer blend under the foaming conditions (Rachtanapun et al., 2004). Hence, blend composition must be optimized to obtain a good cell structure. From a rheological point of view, the melt shear viscosity ratio (VR) of the dispersed to the continuous phase (which should be obtained in the same conditions for both polymers) is an important parameter to predict the foaming behavior. For the same screw configuration and speed, a higher VR can result in the formation of larger dispersed phase domains (Huang, 2005; Huang et al., 2005; Potente et al., 2001). Some studies showed that VR close to unity is more favorable for the production of a uniform and small dispersed phase in polymer blends (Huang et al., 2008; Huang et al., 2005; Karami and Balke, 2000; Min et al., 1984; Yang, Lee et al., 1999).

Several papers reported that PP foamability is significantly enhanced by blending with HDPE (Doroudiani et al., 1998; Huang et al., 2008; Huang and Wang, 2007; Rachtanapun et al., 2004; Rachtanapun et al., 2004; Zhang et al., 2009), PS (Zhai et al., 2008), polytetrafluoroethylene (PTFE) (Wang et al., 2013), waste rubber powder (Xin et al., 2009), and ethylene-octene copolymer (EOC) (Gunkel et al., 2008). It was also found that blending

HDPE with PP facilitated the formation of microcellular structures because of the poorly bonded interfaces between immiscible PP and HDPE, which decreased the bubble nucleation energy and increased heterogeneous nucleation (Doroudiani et al., 1998; Huang and Wang, 2007; Rachtanapun et al., 2004).

Huang et al. showed the effect of VR by blending PP with two HDPEs (HDPE1 and HDPE2) of different viscosities (Huang et al., 2008). The VR of PP/HDPE1 was about 2, while the value for PP/HDPE2 is about unity. PP/HDPE2 had a uniform and well-developed structure in comparison with PP/HDPE1, which had a non-uniform cell structure and presented some cell rupture. It is believed that higher blend viscosity ratio leads to larger size of the dispersed phase (Han et al., 2007). Hence, PP/HDPE2, which has a lower viscosity ratio, could create smaller size HDPE2 dispersed phase in the continuous PP phase. As a result, the interfacial area between both phases increased, leading to a higher number of smaller cells in this foamed blend.

In the foaming process of the blends, most of the cell formation takes place at the interface between two phases, which is due to lower activation energy (Huang et al., 2008). Furthermore, due to the lower melting temperature of HDPE compared to PP, the cell nuclei are formed earlier in the HDPE phase and grow more easily compared with those in the PP phase (Huang et al., 2008).

In another experiment, the effect of HDPE1 content on the foaming behavior of the blends was compared. The results showed that increasing HDPE1 content from 25 to 75% wt. led to smaller unfoamed areas (Huang et al., 2008). It is believed that by increasing HDPE1 content, the size of the PP domains in the blends decreased and cells growth proceeded more easily in the HDPE1 domains. Hence, a more uniform structure was gradually obtained. Moreover, increasing HDPE1 content increased cell sizes and decreased cell densities of the foamed blends.

Improving the foaming behavior of PP was investigated through blending with HDPE using nano-calcium carbonate ($CaCO_3$) as nucleating agent at two different loadings (5 and 20% wt.) (Huang and Wang, 2007). In this study, three HDPE grades with different viscosities were used with CO_2 as the blowing agent and stearic acid as a coupling agent for batch foaming. As reported, the shear viscosities are as follows: HDPE1 < HDPE2 < PP < HDPE3.

It was concluded that blending PP with HDPE1, which had higher shear viscosity than PP, produced higher complex viscosity than neat PP, but PP/HDPE2 and PP/HDPE3 had lower complex viscosity than neat PP. On the other hand, PP/HDPE1 and PP/HDPE2 showed higher storage modulus than PP at low frequency. It should be mentioned that, since the foams were produced by batch foaming, the behavior at low frequencies was more important (Huang and Wang, 2007). Moreover, the results showed that both PP/HDPE1 and PP/HDPE2 blends had homogeneous and microcellular structures (Huang and Wang, 2007). This is because these two blends had higher storage modulus at low frequencies leading to limited cells growth and cell-coalescence. Because PP/HDPE3 had the lowest storage modulus, high and non-uniform cell growth and cell coalescence occurred and no homogeneous microcellular structure was produced.

Foaming behavior of PP/HDPE blend was also investigated by Zhang et al. using CO_2 as a blowing agent (Zhang et al., 2009). They found that, by imposing the sample to dynamic shear, increasing frequency should increase the melt strength. Hence, cell density increased and cell sizes decreased. Moreover, the cell structure changed from an elliptical shape to more spherical ones.

The foaming behavior of PP blended with poly(ethylene-co-octene) (PEOc) as an elastomeric material to produce a thermoplastic elastomer (TPE) was investigated by Zhai and Park (Zhai and Park, 2011). They also used two different nano-clay contents (0.5 and 2% wt.) as a nucleating agent, PP-g-MA (maleic anhydride level of 0.5% wt.) as a compatibilizer, and CO_2 as a blowing agent. The PP foams produced had a low expansion ratio (1.5-2.5), but the addition of PEOc improved foam expansion with values up to 3.5-4.2 (Zhai and Park, 2011). Blending of a thermoplastic polymer with an elastomeric phase increased the level of gas diffusion because of the existence of high free volume in the elastomers (Neway et al., 2004; Zhai et al., 2010). Hence, the amount of gas lost from the matrix during the foaming process increased, resulting in lower foaming expansion ratio.

Zhai and Park prepared different nano-composite samples from PP/PEOc blend (TPO) and nano-clay and coded them as TPOC n/m where n and m are nano-clay and PEOc contents, respectively (Zhai and Park, 2011). Even for samples TPOC0.5/0 and TPOC2.0/0, which did not contain PEOc, the XRD curves showed partial clay-exfoliation, which was due to PP-g-

MA (Zhai and Park, 2011). The presence of 5 and 10% wt. of PEOc led to further increase in nano-clay exfoliation degree. But increasing PEOc content for both clay loadings led to a weak and broad peak at $2\theta = 2.5\text{-}3.5°$, indicating the formation of intercalated structures. It was also found that the presence of PEOc in PP decreased its crystallinity. On the other hand, no apparent effect on crystallinity was observed by the addition of nano-clay (Zhai et al., 2010; Zhai and Park, 2011).

As illustrated in Figure 2.10, samples TPOC0.5/0 and TPOC2.0/0, which did not contain PEOc, had lower viscosity compared to other samples. But the introduction of 5% wt. PEOc increased the viscosity. Moreover, by comparison of Figure 2.10 (a) and (b), it can be concluded that increasing clay loading had a slight effect on viscosity, but led to a stronger frequency dependence of the viscosity. Also, the materials showed a more shear-thinning behavior. Generally, in blends, the creation of heterogeneous phases leads to improved cell nucleation at the interface as a result of its lower energy barrier for cell nucleation (Zhai and Park, 2011). But because of low compatibility between PP and PEOc, the increase of cell nucleation was not obvious. The presence of PEOc had a positive effect on nano-clay dispersion. The maximum cell density obtained was about $1x10^7$ cell/cm^3 for TPOC02.0/20.

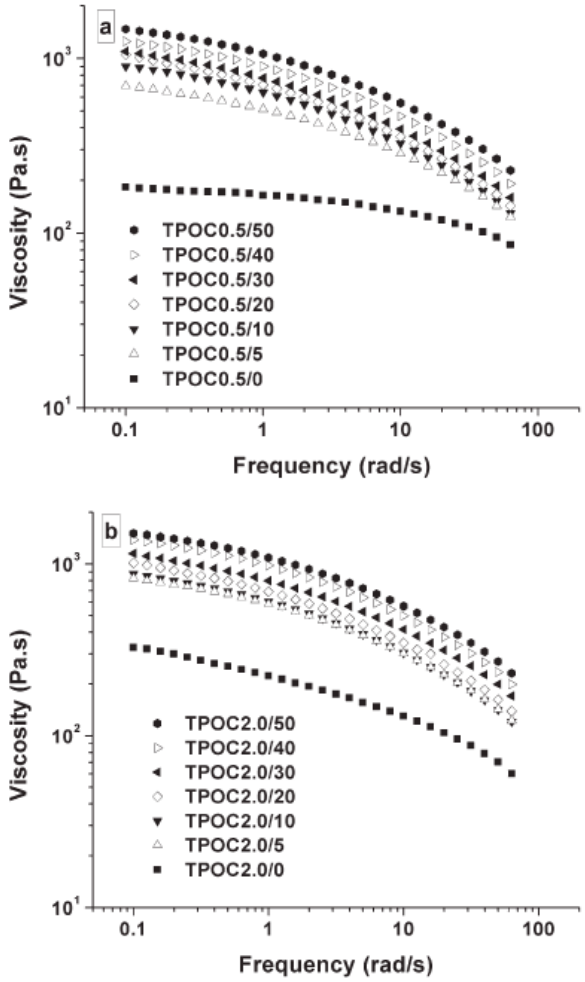

Figure 2.10. Complex viscosity of (a) TPOC0.5/m and (b) TPOC2.0/m nano-composites (Zhai and Park, 2011).

2.7.4 Effect of Crosslinking

Several attempts have been made to modify the foaming behavior of PP by creating crosslink points through the PP structure (Han et al., 2006; Liu et al., 2006; Nam et al., 2005; Zhai et al., 2008). The effect of crosslinking on PP foaming behavior using CO_2 as a blowing agent was investigated (Zhai et al., 2008). Four types of samples with different crosslinking degrees (PP-C1 to PP-C4) were prepared and their foaming structures were compared with neat PP. The crosslinked materials were prepared through a copolymerization reaction of propylene and 1,4-divinylbenzene (DVB) using a Ziegler-Natta catalyst (Zhai et al., 2008).

Figure 2.11 presents the variation of the complex viscosity as a function of frequency where the crosslinking degree increased gradually. It can be seen that the Newtonian plateau at low frequency was not observed in the crosslinked materials. Moreover, by increasing the crosslinking degree from PP-C1 to PP-C4, the complex viscosity increased gradually.

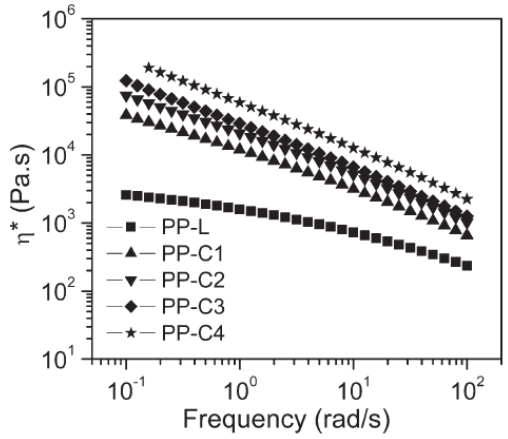

Figure 2.11. Complex viscosity as a function of frequency for PP and PP-C at 230 °C (Zhai et al., 2008).

The morphologies of all the foamed samples are shown in Figure 2.12. Neat PP, which has low melt strength (Figure 2.12a), showed a non-uniform and open-cell structure with large unfoamed areas. By introducing some degree of crosslinking for PP-C1 (Figure 2.12b), cell coalescence was efficiently decreased. Moreover, the open-cell structure was obviously reduced. Also, by increasing the crosslinking degree from PP-C1 to PP-C4, more uniform cell structures were produced.

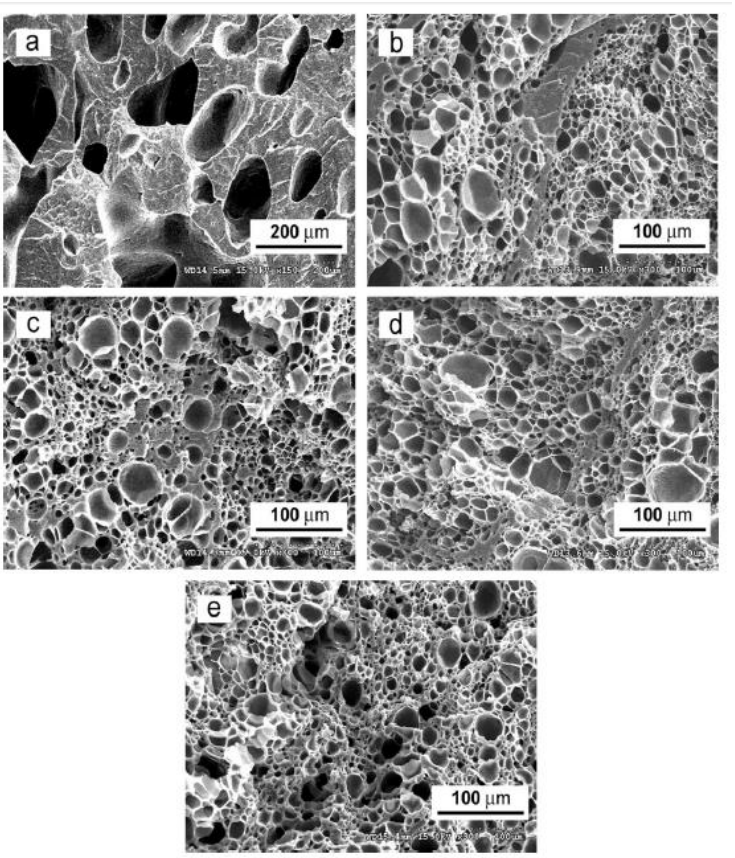

Figure 2.12. SEM micrographs of the foams: (a) PP, (b) PP-C1, (c) PP-C2, (d) PP-C3, and (e) PP-C4. Foaming conditions are 190 °C for 30 s (Zhai et al., 2008).

Xu et al. studied the relation between the foaming behavior and rheological parameters for different types of PP (Xu et al., 2013). Those PP types were: linear PP (L-PP), linear PP with HDPE (HMC-PP), long-chain branched PP (LCB-PP), and crosslinked PP (C-PP). Their results showed that at low frequencies, L-PP showed a Newtonian plateau, but the others are still in the transition region; i.e. below the zero shear viscosity (η_0). Moreover, HMC-PP showed the highest shear viscosity over all the frequency range. Higher shear viscosity provides higher melt strength, which makes the samples able to sustain higher stresses, lower gas diffusion rate in the polymer, and also less gas loss to the environment (Xu et al., 2013). They also examined the rheological behavior of the samples through extensional tests (Xu et al., 2013). No strain-hardening behavior was observed for linear PP. The HMC-PP showed strain-hardening only at low strain rate (0.01 s^{-1}). In contrast, LCB-PP showed strain-hardening at higher strain rates (0.1 and 1.0 s^{-1}). For C-PP, strain-hardening was observed

for all strain rates. The expansion ratio of the samples during the foaming process can be related to extensional viscosity. The comparison of the expansion ratios of the samples are as follow: C-PP (55) > LCB-PP (~27) > HMC-PP (~7) > L-PP (~5) (Xu et al., 2013). It should be mentioned that HMC-PP and L-PP, which had the lowest expansion ratios in comparison with the other two, did not show strain-hardening at high strain rates. The authors showed that, C-PP and LCB-PP, which had the highest expansion ratios, had a closed and uniform cell structure. The maximum and minimum cell densities were approximately 10^8 cells/cm^3 (C-PP) and $2x10^3$ cells/cm^3 (L-PP), while the maximum and minimum cell sizes were 175 μm (LCB-PP) and 20 μm (L-PP). Cells rupture can be seen in the L-PP samples, which is related to its lowest extensional viscosity among all the samples (Xu et al., 2013). Moreover, HMC-PP showed several open-cell and significant amount of cell rupture. HMC-PP showed strain-hardening behavior only at the lowest strain rate of 0.01 s^{-1}. Hence, it can be concluded that having strain-hardening at low shear rate had no significant effect on improving cell structure.

2.8 Effect of foaming conditions on the foaming behavior of PP

2.8.1 Effect of temperature

It is widely accepted that temperature is one of the most important parameters controlling the final properties of a foamed polymer. Moreover, it is known that increasing foaming temperature facilitates cell growth. On the other hand, decreasing foaming temperature results in lower cell diameter and increasing cell size distributions (Huang et al., 2008). This is because the reduction of the foaming temperature increases the melt viscosity and the strength of the matrix, which limits bubble growth (higher resistance).

In addition, linear PP has a very narrow foaming temperature window of around 2-4°C (Huang and Wang, 2007; Xu et al., 2007; Yu et al., 2011). This fact can be seen obviously from Figure 2.8. A comparison of Figure 2.8 (a,b-1) with (a,b-2) shows that increasing the foaming temperature by only 3°C made an obvious effect on cell sizes in PP nano-

composites. Controlling the temperature within this narrow range is a great challenge, especially for foaming systems with high volume or for continuous foaming processes (Xu et al., 2007).

Some researchers believe that the presence of nano-$CaCO_3$ enables performing the foaming process at a lower temperature in comparison with neat PP (Huang and Wang, 2007). Moreover, some investigations showed that PP composites, in comparison with neat polymers, are less sensitive to temperature (Ding et al., 2013; Nam et al., 2002; Zheng et al., 2010). It is reported that blending PP with HDPE (Huang et al., 2008) and PTFE (Wang et al., 2013) also decreased the temperature dependency of PP. Figure 2.13 shows a comparison between the effect of temperature on the foaming behavior of neat PP and PP nano-$CaCO_3$ composites, which was investigated in another study (Ding et al., 2013). It was found that cell size of foamed PP nano-$CaCO_3$ varied only slightly with increasing temperature, but neat PP was more sensitive to temperature changes.

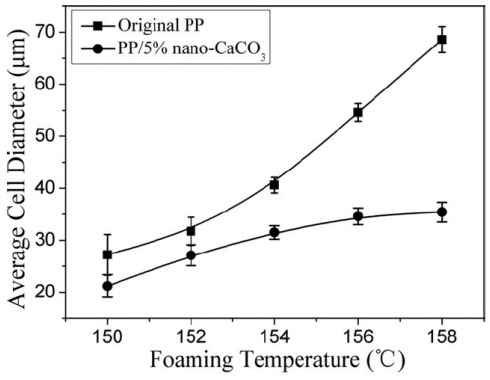

Figure 2.13. Average cell diameter of foamed PP and PP/5% nano-CaCO3 as a function of foaming temperature (saturation conditions of all samples: 25 MPa and 80 °C) (Ding et al., 2013).

The effect of temperature on the foaming behavior of PP can be discussed in two cases: high and low temperatures. At high temperature, increasing temperature has less effect on SC-CO_2 solubility (Ding et al., 2013). As a result, if temperature is high enough, it has less effect on the foaming behavior of polymer composites. On the other hand, at low temperature, some crystalline regions can still be present. It is known that the amorphous regions are much less

rigid than the crystalline regions. Hence, cells grow in crystalline regions with slower rates compared to amorphous regions and result in smaller cell sizes. In this case, non-uniform cell size structures are achieved. But, using nanoparticles as nucleating agents hindered PP chain segments mobility (Gilbert-Tremblay et al., 2012), and hence PP crystallinity decreased leading to less effect of crystallinity on the foaming behavior. Therefore, the presence of nanoparticles as nucleating agents leads to a more uniform cell structure and also less temperature sensitivity.

Xu et al. reported that in the batch process, simultaneous control of both foaming temperature and saturation pressure had more significant effect on PP foaming behavior (Xu et al., 2007). As illustrated by their results, lower foaming temperature and higher saturation pressure are more favorable to create uniform foam structures in comparison with higher foaming temperature and lower saturation pressure. Moreover, the narrow temperature window for PP was again clearly seen from the results (Xu et al., 2007).

2.8.2 Effect of foaming pressure and pressure drop rate

Park et al. (Park et al., 1995) found that both the magnitude of pressure drop and the pressure drop rate play important roles in cell nucleation during microcellular processing. The effect of pressure drop on cell nucleation can be estimated by the classical nucleation theory as the cell nucleation rate ($N_{nucl.}$) is given by (Colton and Suh, 1987; Park et al., 1995):

$$N_{nucl.} = f_0 C_0 exp\left(\frac{-\Delta G_{nucl.}}{kT}\right) \tag{2.9}$$

where $\Delta G_{nucl.}$ is the Gibbs free energy calculated by:

$$\Delta G_{nucl.} = \frac{16\,\pi\,\gamma_{bp}^3}{3\,\Delta P^2} \tag{2.10}$$

where ΔP is the pressure drop of the gas/polymer solution, f_0 is the frequency factor of gas molecules joining the nucleus, C_0 is the concentration of gas molecules, k is the Boltzmann's constant, T is the temperature, and γ_{bp} is surface energy of the polymer-bubble interface.

Equations (2.9-2.10) indicate that, by increasing pressure drop, the cell nucleation rate will increase. Hence, for a constant pressure drop with a sudden pressure drop rate, the cell density should be constant (Park et al., 1995). However, in reality, the pressure drop happens during a finite time period. Hence, the pressure drop rate will affect the nucleation time period and accordingly the nucleation rate (Park et al., 1995). Also, the pressure drop and pressure drop rate can be controlled by changing the geometry of the die channel (nozzle) and the mass flow rate in extrusion (Spitael and Macosko, 2004). Decreasing the nozzle diameter leads to a higher pressure drop rate, which increases the nucleation rate (Sauceau et al., 2011).

Wang et al. (Wang et al., 2013) examined the effect of the saturation pressure on the foaming behavior of PP/carbon fibers using SC-CO_2 as blowing agent. They studied three different saturation pressures and showed that at the lowest saturation pressure of 10 MPa, several large cells were created. It was believed that those large cells were formed in the amorphous regions, while small ones were in or around the crystalline regions (Wang et al., 2013). By increasing the saturation pressure to 15 and 20 MPa, more uniform cell size distribution was created. It was also reported that both the average cell diameter and cell density increased with increasing saturation pressure.

Xu et al. studied the effect of different pressure drop rates on the foaming behavior of PP using CO_2 as a blowing agent (Xu et al., 2007). They found that, at specific foaming temperature and saturation pressure, cell density increased with increasing pressure drop rate. They also showed that both cell size and volume expansion ratio first increased with increasing pressure drop rate from 1.5 to 5 MPa/s, then decreased at higher pressure drop rate.

2.9 Conclusion

Because of its outstanding characteristics, polypropylene is an interesting material in the foaming industry. However, its foaming behavior is limited by its low melt strength leading to poor cell nucleation and cell coalescence, thus limiting high expansion ratios.

Several investigations were devoted to modify the melt strength of conventional (linear) PP using different methods. The main results can be summarized as follow:

1- The four main methods used to improve the melt strength of PP are: adding particles as nucleating agent, introducing long chain branching, blending with a high melt strength polymer and crosslinking.
2- Using nanoparticles as nucleating agents hinders PP chain segments mobility and hence PP crystallinity decreases. As a result, the effect of crystallinity on the foaming behavior will also decrease.
3- The crystallinity of PP is reduced in the presence of nanoparticles, which results in a more uniform cell structure. Moreover, the presence of well-dispersed nucleating agents leads to higher melt viscosity and melt strength, which results in the formation of finer and more uniform cell structures.
4- The commonly used compatibilizer for better dispersion of particles in PP is PP-g-MA, which facilitates both cells nucleation and growth. The presence of PP-g-MA results in a more uniform cell structure as well as higher cell density and cell size.
5- Since cell growth stops when crystallization starts, the investigation of the effect of nucleating agents on PP crystallization is a useful method to predict its foaming behavior.
6- The effect of interfaces in immiscible polymer blends like PP-HDPE is effective for cell nucleation, but gradually vanishes with increasing nano-particles content.
7- The presence of low content (0.5% wt.) and well-dispersed particles (nucleating agents) were found to be the best methods to improve the foaming behavior of PP.
8- The introduction of even small amounts (10%) of branched PP results in strain-hardening enhancement. Hence, cell coalescence can be prevented, which improves the foaming behavior of PP. However, a very large number of branches per chain may decrease the strain at break of the polymer melt, which results in lower PP foamability.
9- Branched PP shows higher crystallization temperature than linear PP. By introducing branches, the crystallization temperature can increase by up to 30 °C. In other words, crystallization starts sooner for branched PP, in comparison with linear PP.
10- Melt shear viscosity ratio (VR) of the dispersed phase to continuous phase close to unity is more favorable to produce a lamellar and small size dispersed phase in polymer blends.

11- Blending HDPE with PP is a common method to improve the foaming behavior of PP. The creation of heterogeneous phases leads to an improvement of cell nucleation at the interface as a result of its lower energy barrier for cell nucleation.
12- By introducing a crosslinking structure, cell coalescence is efficiently decreased. Moreover, the open-cell content is reduced and cell distribution is more homogeneous.
13- Strain-hardening at low strain rate has no significant effect on cell structure improvement.
14- Linear PP is very sensitive to temperature and has a very narrow foaming temperature window (around 2-4 °C).
15- Blends of PP with other polymers, such as HDPE, in comparison with their corresponding neat polymer components, are less sensitive to temperature changes.
16- Both the magnitude of pressure drop and the pressure drop rate play important roles in cell nucleation during microcellular processing.
17- Generally, increasing pressure drop rate will increase cell density.

Acknowledgment

Financial support from the Natural Sciences and Engineering Research Council of Canada (NSERC) and Fonds Québécois de la Recherche sur la Nature et les Technologies (FRQNT) was received for this work.

Chapter 3

Literature review 2: Cellular polymer ferroelectret: A review on their development and their piezoelectric properties

Abolfazl Mohebbi, Frej Mighri, Abdellah Ajji, Denis Rodrigue, *Advances in Polymer Technology*, DOI 10.1002/adv.21686, 2016.

Résumé

En raison de leur capacité à montrer un comportement ferroélectret lorsqu'ils sont exposés à un champ électrique externe, les polymères cellulaires ont récemment été pris en considération pour les applications ferroélectrets. Ces films de polymère cellulaire peuvent être produits par étirage ou en moussant, mais en fonction de l'application et des conditions d'utilisation, différents polymères tels que le polypropylène, le poly(téréphtalate d'éthylène), le poly(naphtalate d'éthylène), le poly(tétrafluoro éthylène), le polypropylène réticulé et certaines cyclo-oléfines, ont été pris en compte. Néanmoins, le polypropylène cellulaire est le matériau le plus étudié en raison de ses propriétés exceptionnelles telles que son fort coefficient piézoélectrique d_{33}, sa flexibilité, sa bonne résistance à la fatigue, sa bonne capacité à piéger les charges et son faible coût. Dans cette revue, les progrès récents liés aux matériaux utilisés pour les applications de ferroélectret et leur traitement sont discutées. L'effet de différents paramètres tels que la pression, la résistance électrique de claquage de la phase gazeuse, la présence de charges et la température d'utilisation sur le coefficient d_{33} sont présentées et discutées.

Abstract

Because of their ability to show ferroelectret behavior when exposed to an external electric field, cellular polymers have been recently considered for ferroelectret applications. These cellular polymer films can be produced by stretching or foaming, but depending on the application and conditions, different polymers, such as polypropylene, poly(ethylene terephthalate), poly(ethylene naphthalate), poly(tetrafluoro ethylene), cross-linked polypropylene and some cyclo-olefines, have been considered. Nevertheless, cellular polypropylene was the most investigated material because of its outstanding properties such as high piezoelectric d_{33} coefficient, flexibility, good fatigue resistance, good charge trapping properties and low cost. In this review, recent advances related to the materials used for ferroelectret applications and their processing are discussed. The effect of different parameters such as pressure, electrical breakdown strength of the gas phase, presence of fillers, and service temperature on the d_{33} coefficient are presented and discussed.

3.1 Introduction

Cellular thermoplastic polymers or polymer foams are widely used in several applications due to their excellent properties such as lightweight, high strength to weight ratio, excellent acoustic and heat insulation (Colton and Suh, 1987; Klempner and Frisch, 1991), high specific mechanical properties (Collais and Baird, 1995), and high fatigue resistance (Seeler and Kumar, 1993). Recently, they have been considered as good candidates in piezoelectric applications because of other advantages such as low permittivity, low thermal conductivity, softness and flexibility. Furthermore, their impedance is much closer to that of air and water than compact/solid materials.

Cellular thermoplastic polymers can present piezoelectric-like behavior through internal charging by submitting the material to a high external electric field. Nowadays, cellular charged polymers are under investigation for new applications such as actuators, vibration control, ultrasonic transducers, tactile sensors, ferroelectret devices, energy conversion devices, speakers, microphones, keyboards, shock sensors, thermal and optical property measurement devices (Gerhard-Multhaupt, 2002; Lang and Muensit, 2006; Paajanen et al., 2000). Moreover, piezoelectric devices made from cellular polymer films are very interesting because of their low material cost, ease of processing and the possibility to produce very thin and flexible films with low density (Qaiss et al., 2012).

So the aim of this paper is to present a critical review of the recent developments associated to the piezoelectric behavior of cellular polymers. To start, the concepts of piezoelectricity, piezoelectric d_{33} coefficient, ferroelectric and ferroelectret will be discussed. Second, different methods to produce ferroelectret cellular polymers are presented. Then, the different methods to determine the d_{33} coefficient are discussed with their related equations and parameters. Finally, the parameters controlling the ferroelectret behavior of cellular polymers are reviewed based on the literature.

3.2 Piezoelectric properties

The word “piezoelectricity” is related to the relation between “electricity” and “pressure”, the latter being derived from the Greek word “piezo”, which means squeeze or pressure.

Piezoelectricity in materials was first discovered by Pierre and Jacque Curie in 1880 (Lin and Lin, 2012). Piezoelectric materials are able to convert electric or magnetic fields into mechanical displacement and vice versa. This reversible effect is the result of a direct relationship between the stress and the polarization density of the bulk material (Newnham, 2004). This property is measured via the so-called d_{33} coefficient (Mellinger, 2003). This coefficient is also associated with other names, such as piezoelectric d_{33} coefficient (Hillenbrand and Sessler, 2004; Hillenbrand et al., 2005; Qaiss et al., 2013; Wan et al., 2011; Zhang et al., 2004) or electromechanical d_{33} coefficient (Dansachmuller et al., 2005; Paajanen et al., 2001). The values are reported with units of pC/N.

Classical piezoelectric systems include crystals such as quartz, topaz, special ceramics, as well as natural materials such as silk, bone, collagen, and DNA (a nucleic acid carrying the genetic information in cells) (Qaiss et al., 2012). Piezoelectric materials can also be produced from polar polymers. Piezoelectricity in polymers was first discovered by Kawai in 1969 when polar polymer films were drawn and polarized by heating at 90°C and cooled while a static electric field was imposed though their thickness (Kawai, 1969). Poly(vinylidene fluoride) (PVDF), as a polar polymer, showed strong piezoelectric properties and was widely used (Destruel et al., 1984; Kawai, 1969; Ohigashi, 1976). This group of polar polymers is also categorized as piezoelectric materials and their behavior is named "ferroelectric".

About three decades ago, Kirjavainen and coworkers in Finland discovered a considerable piezoelectric d_{33} coefficient for charged cellular polypropylene (PP) films (Kirjavainen, 1987; Savolainen and Kirjavainen, 1989). They charged the voids of the cellular polymer by applying a high voltage to the structure, which generated internal dielectric barrier micro-discharges. As a result of this phenomenon, the deposited charges on the internal surface of the voids created piezoelectric-like properties and electrical dipoles were obtained.

Considering that cellular polymers show a ferroelectric-like behavior by imposing a high electrical field, a new group of piezoelectric materials was developed based on cellular polymers (Fang et al., 2008; Gilbert-Tremblay et al., 2012; Qaiss et al., 2012; Wegener, 2010; Wegener et al., 2005). During this treatment, positive and negative electrical charges are created on the opposite faces of each cell surfaces (Qiu et al., 2013). Since, they do not have

intrinsic molecular dipoles, their cavities can be internally charged with dielectric barrier discharges (DBD) (Lindner et al., 2002; Qiu et al., 2011). Cellular non-polar polymers, such as PP, as a result of the macroscopic similarity in their polarization behavior, in comparison with typical ferroelectric polymers (such as ferroelectric PVDF), are often so-called "piezoelectret" and their behavior is named "ferroelectret" (Lindner et al., 2004; Tuncer, 2005).

3.3 Comparison between ferroelectric and ferroelectret materials and their charging mechanism

PVDF, because of its strong molecular dipoles, exhibits good piezoelectric and mechanical properties, and is also chemically stable (Chang et al., 2010; Heywang et al., 2008; Holmes-Siedle et al., 1984). Three different crystalline phases of untreated PVDF are defined as: α, β, and γ. The β-phase can be obtained by mechanical stretching and electrical polarization, which is useful for generating piezoelectricity (Chang et al., 2010). Figure 3.1 shows the creation of dipoles in PVDF (a) as a piezoelectric material in comparison with PP (c), which is a piezoelectret material. Also, Figure 3.1 (b) presents the simplest piezoelectric model in ferroelectric materials: positively and negatively charged particles that are connected by springs having force constants of k_1 and k_2 (Chang et al., 2010). It is estimated that in cellular space-charged (piezoelectret) materials, such as PP, the point of symmetry is broken on a macroscopic order of about 10^5 μm^3 (or 10^{14} nm^3) (estimated cell dimensions: 100x100x10 μm^3), while for PVDF, as a piezoelectric material, it is on a nano-scale order of about 0.1 nm^3 (with unit cell dimensions 0.858x0.49x0.256 nm^3 for PVDF, β-phase) (Lindner et al., 2004). Hence, the cell volume for symmetry breakup in PP is about a factor of 10^{15} larger than for the unit cell volume of PVDF. Thus, the piezoelectric property for cellular non-polar polymers, such as PP, is more different compared to polar polymers such as PVDF. Accordingly, this behavior for PP is sometimes referred as quasi-piezo or ferroelectric behavior (Bauer et al., 2005; Lindner et al., 2004). Moreover, this behavior in ferroelectrets comes from the deformation of charged cells, whereas in polar piezoelectric materials, ion displacement in a lattice is the source of this behavior (Bauer et al., 2004).

Ferroelectric polymers show moderate electromechanical d_{33} coefficient ranging from 20 to 30 pC/N, whereas ferroelectrets show larger d_{33} with values well above 100 pC/N (Heywang et al., 2008; Kressmann, 2001).

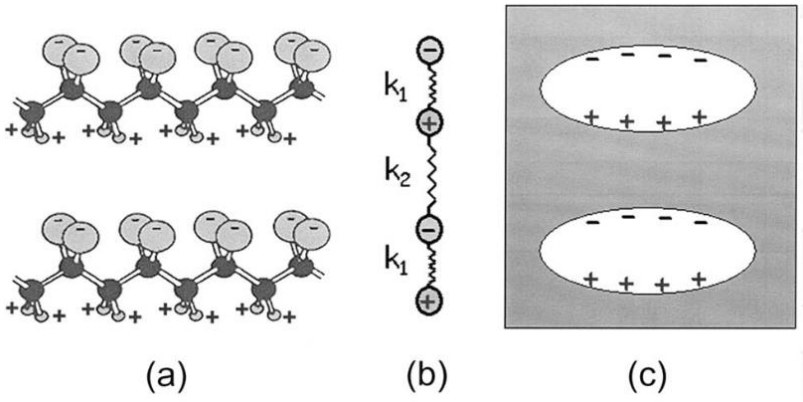

Figure 3.1. a) Ferroelectric PVDF, b) simple model for piezoelectricity in ferroelectric materials (positively and negatively charged particle that are connected by springs having force constants of k_1 and k_2), and c) ferroelectret PP (clear ellipsoidal areas are gas bubble and the dark area is the polymer matrix) (Lindner et al., 2004).

The charging process of cellular polymers takes place through charge transfer across the cells, which starts from the sample surface. In the case of using an AC-voltage supplier above the breaking threshold of the gas in the cells, as the AC-voltage creates periodic (cyclic) behavior, and breakdown occurs during each half cycle, while the direction of the microscopic dipoles switch from each half cycle to the next half cycle (Lindner et al., 2002; Lindner et al., 2004). This phenomenon is shown in Figure 3.2.

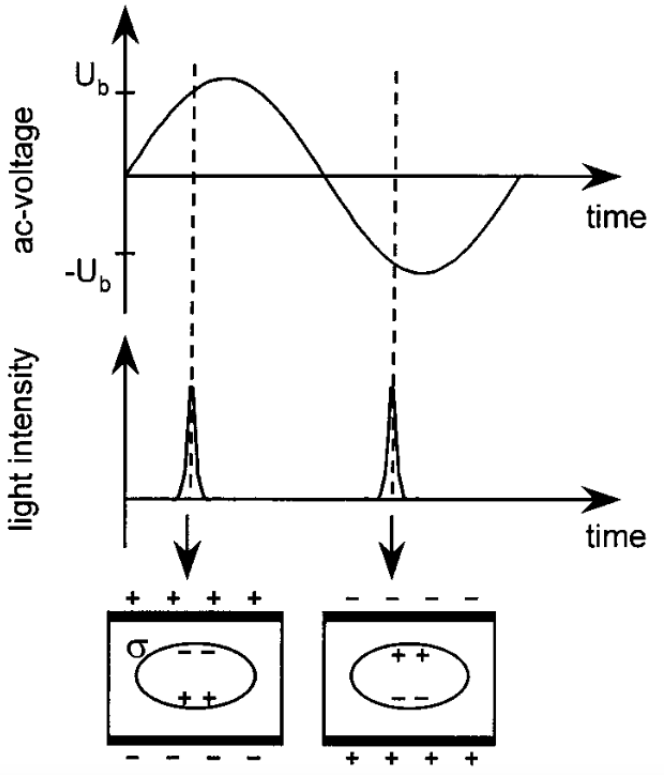

Figure 3.2. Dielectric barrier microdischarges through a cellular structure by an AC-voltage (Lindner et al., 2002).

Lindner et al. (Lindner et al., 2002) studied the mechanism for charging cellular polymers. They showed that a minimum voltage is required for charging a cellular polymer structure. As shown in Figure 3.3, a threshold voltage of 1.5 kV is required to start significant light emission. Moreover, for efficient charging, a 2 kV AC-voltage level is needed. Also, it can be shown that the breakdown switched every 500 μs, which is the time of a half cycle. The authors also found that one of the outstanding differences of ferroelectric and ferroelectret materials is their thermodynamic stability. Ferroelectric materials are thermodynamically stable, while ferroelectrets behave in a metastable way with increasing service temperature, but are stable for several years at room temperature (Lindner et al., 2002).

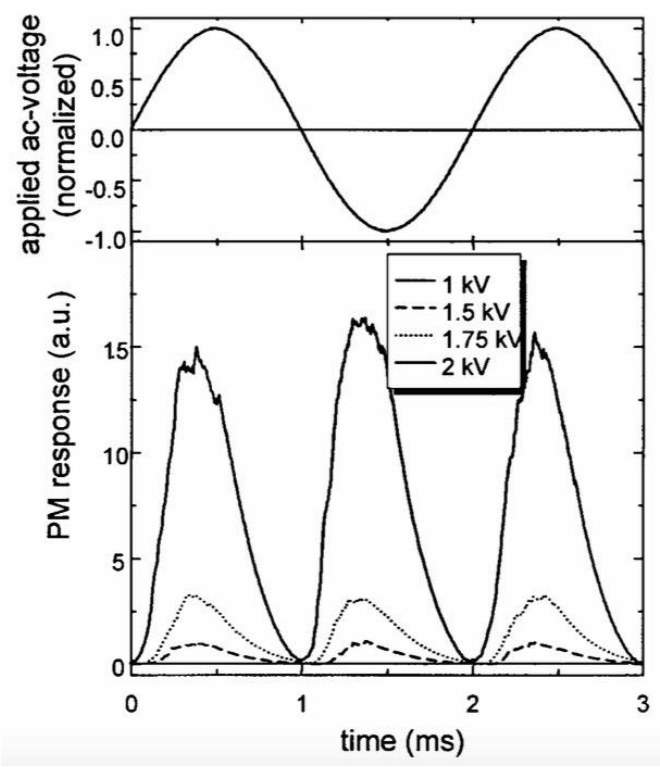

Figure 3.3. Transit light emission detected by photomultiplier (PM) recording (bottom curve) for the sinusoidal AC-voltage (top curve) at different voltage level (Lindner et al., 2002).

3.4 Calculation of threshold voltage

It is reported that, in the contact charging method, the electromechanical d_{33} coefficient presents three different trends related to the charging voltage V (Zhang et al., 2005):

- for $V_0 < V < 2V_0$, d_{33} increases with charging voltage,
- for $V \leq V_0$, d_{33} is equal to zero,
- for $V \geq 2V_0$, d_{33} is almost constant.

where V_0 is the theoretical threshold voltage, which is given by the following relation (Zhang et al., 2005):

$$V_0 = E_c \left(\frac{\varepsilon_{gr}}{\varepsilon_{pr}} S_1 + S_2 \right) \tag{3.1}$$

where, $E_c, \varepsilon_{pr}, \varepsilon_{gr}, S_1$, and S_2 are the critical breakdown electric field, the relative dielectric constant of the polymer and gas, and the equivalent thickness of the solid and void layers, respectively.

Paschen breakdown is known to be responsible for the internal charging of the cells in ferroelectret materials (Qiu et al., 2008; Sessler and Hillenbrand, 1999). Based on Paschen's law, the breakdown voltage between two electrodes in a gas (the voltage necessary to start a discharge) can be calculated. According to Townsend's model of Paschen breakdown, the critical breakdown value in a uniform electric field is a function of gas pressure (p) and the electrode spacing (S), as given by the following relation (Mellinger and Mellinger, 2011; Paajanen et al., 2001; Qiu et al., 2011; Qiu et al., 2008):

$$E_c = \frac{Ap}{B+ln(pS)} \tag{3.2}$$

where B is given by:

$$B = ln\left(\frac{C}{ln(1+1/\gamma)}\right) \tag{3.3}$$

and A, C and γ are constants. When the cells are filled by air, $A = 273.8$ V mPa^{-1}, $C = 11$ mPa^{-1} and $\gamma = 0.01$. The latter is the so-called second ionization coefficient (Qiu et al., 2011; Qiu et al., 2008). Ferroelectrets are almost ideal dielectrics with very low permittivity and high breakdown voltage (Döring et al., 2012).

3.5 Relation between the piezoelectric d_{33} coefficient and the elastic modulus c_{33}

The relation between the elastic modulus or elastic stiffness (c_{33}) in the surface normal direction (film thickness direction) and the electromechanical d_{33} coefficient can be calculated as (Dansachmuller et al., 2005; Hillenbrand et al., 2005; Sessler and Hillenbrand, 1999; Zhang et al., 2014):

$$d_{33} = \frac{\varepsilon\sigma}{c_{33}} \frac{S\,S_1}{(S_1+\varepsilon S_2)^2} \tag{3.4}$$

where ε is the permittivity of the solid material, σ is the charge density on the surface of the voids and *S* is the total thickness of the sample given by:

$$S = S_1 + S_2 \tag{3.5}$$

The simplified equation (3.4) is driven by a hypothesis as shown in Figure 3.4. It is assumed that the film is made up of layers of solid and void in which all the solid layers are charged to one polarity on their top surface and the other polarity on their bottom surface (Hillenbrand et al., 2005).

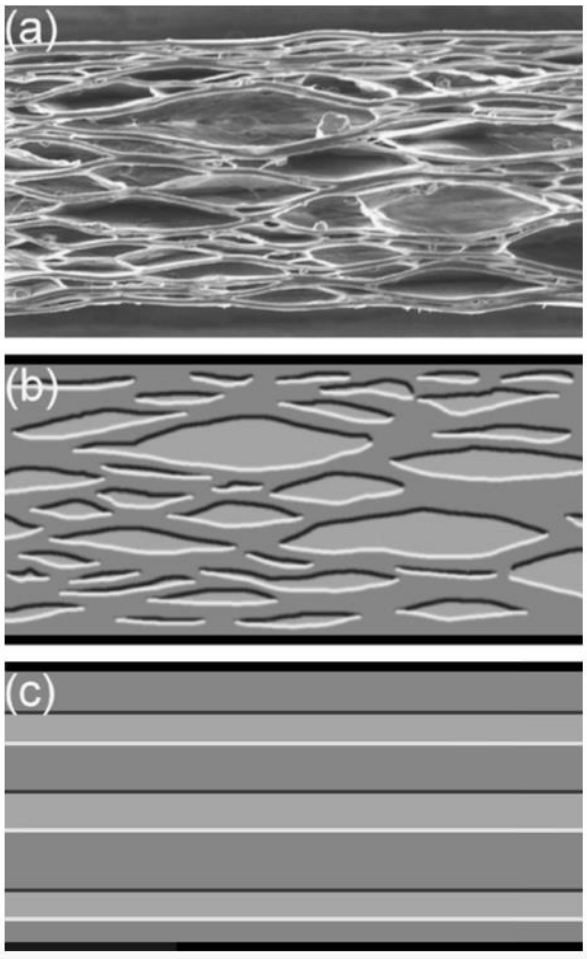

Figure 3.4. (a) SEM image of a cellular PP film, (b) schematic representation of this film, and (c) equivalent structure of parallel layers for modeling (Hillenbrand et al., 2005).

The compressive Young's modulus or elastic modulus (c_{33}) in the surface normal direction can be calculated as (the free boundary condition) (Mellinger, 2003; Neugschwandtner et al., 2000; Zhang et al., 2009):

$$c_{33} = 4f_a^2 S^2 \rho_s \tag{3.6}$$

where f_a and ρ_s are the anti-resonance frequency (which can be determined from the dielectric spectra) and the area density of the sample, respectively.

3.6 Methods to measure the piezoelectric d_{33} coefficient

Five common procedures are used to determine the d_{33} value of cellular electrets polymer films: the quasi-static (Hillenbrand and Sessler, 2004; Klimiec et al., 2015; Qiu et al., 2007; Zhang et al., 2004, 2007; Zhang et al., 2007; Zhang et al., 2014), dynamic (Hillenbrand and Sessler, 2004; Wegener et al., 2004; Zhang et al., 2014), interferometric (Hillenbrand and Sessler, 2004; Hillenbrand et al., 2005; Zhang et al., 2004; Zhang et al., 2007), resonance (Hillenbrand and Sessler, 2004) and acoustic (Hillenbrand and Sessler, 2004; Zhang et al., 2007) methods.

3.6.1 Resonance method

In the resonance method, using an impedance analyzer, the real and imaginary parts of the impedance (Z) are determined. From these experimental data, the complex capacitance (C) can be calculated as:

$$\mathrm{C} = {}^{1}\!/_{(2\pi f Z)i} \tag{3.7}$$

where f is frequency.

On the other hand, the electromechanical d_{33} coefficient, which is determined by the inverse piezoelectric effect, is given by (Jonscher, 1999; Meitzler et al., 1987; Zhang et al., 2009):

$$\tilde{C}(\omega) = \frac{\varepsilon_r^S \varepsilon_0 A}{S} \frac{1}{1 - k_t^2 \frac{tan\left(\frac{\omega}{4f_a}\right)}{\frac{\omega}{4f_a}}} - iC_{loss} \tag{3.8}$$

$$k_t = d_{33}\sqrt{\frac{c_{33}}{\varepsilon_r^S \varepsilon_0}} \tag{3.9}$$

where $\tilde{C}(\omega)$, ε_r^S, ε_0, A, k_t, and C_{loss} are respectively the complex capacitance, relative permittivity of the sample under constant stain, vacuum permittivity, electrode area, electromechanical coupling factor, and loss capacitance of the sample.

To determine the d_{33} coefficient, the real part of Equ. (3.8) is used to fit the real part of the capacitance experimental data (Equ. (3.7)) for the frequency range available using different fitting methods (nonlinear least squares) to get the parameters f_a and k_t (An et al., 2009). Then, by substitution of these values in Equ. (3.6) and Equ. (3.9), the c_{33} and d_{33} coefficients can be calculated.

3.6.2 Quasi-static method

The quasi-static method involves the generation of pressure by applying a force $F = mg$ (g is the gravity acceleration) to a known area of the sample by placing a mass 'm' on the sample or by removing it, which results in charge generation. A charge amplifier measures the generated charge and the output signal of the amplifier is recorded with an oscilloscope (Hillenbrand and Sessler, 2004). The d_{33} coefficient is then obtained by (Schwodiauer et al., 2000; Zhang et al., 2007; Zhang et al., 2014):

$$d_{33} = \frac{Q}{F} = \frac{\sigma}{p} \tag{3.10}$$

where Q is the charge generated on the electrodes and σ is the charge density generated upon applying a mechanical pressure p (= F/A) to the sample over part of its surface area A (σ = Q/A).

3.6.3 Dynamic method

In the dynamic method, a mass '*m*' is placed on the sample and a shaker accelerates this system sinusoidally (Hillenbrand and Sessler, 2004). Hence, the sample is subjected to two forces: a static force '*mg*' and a dynamic force '*ma*', the latter being measured by an accelerometer. Moreover, by measuring the generated charge and calculating the total force, including the static and dynamic forces, the d_{33} coefficient can be determined. Accordingly, by controlling the four effective parameters including the frequency and the amplitude of the input signal of the shaker, the mass '*m*' and the area of the sample, the d_{33} coefficient can be determined in a wide range of conditions.

3.6.4 Acoustic method

The d_{33} coefficient obtained through the acoustic method can be obtained by the determination of the sensitivity of a microphone built within the cellular film. The sensitivity *M* of a microphone is defined as (Zhang et al., 2007):

$$M = \frac{\tilde{V}}{\tilde{p}} = d_{33}\frac{S_1 + S_2}{\varepsilon\,\varepsilon_0} \tag{3.11}$$

where $\tilde{V}$ and $\tilde{p}$ are the open-circuit voltage and the sound pressure acting on the microphone diaphragm.

3.6.5 Interferometric method

The interferometric method measures the inverse d_{33} piezoelectric coefficient. By applying an AC voltage $\tilde{V}$ to the sample, the thickness variation $\tilde{S}$ is measured with a laser vibrometer (Hillenbrand and Sessler, 2004; Zhang et al., 2007). Then, the d_{33} coefficient is obtained as follows (Zhang et al., 2007):

$$d_{33} = \frac{\tilde{S}}{\tilde{V}} \tag{3.12}$$

When the d_{33} coefficient is determined by applying a force to the sample and measuring its voltage (or charge) variation, the resulted d_{33} coefficient is a direct coefficient. On the other

hand, the inverse d_{33} coefficient is obtained by applying a voltage to the sample and measuring its thickness variation. From Equ. (3.12), the d_{33} coefficient is determined by dividing the thickness variation by the applied voltage. This is why the obtained coefficient is the inverse d_{33} coefficient.

Depending on laser focusing and the diameter of the laser spot, thickness variation of a relatively small area of the sample is measured. Usually, the diameter of the laser spot is smaller than 100 μm. Hence, local variations of d_{33} can be measured within a specified area (Zhang et al., 2007).

3.6.6 Comparison of the methods

The quasi-static method is the simplest and most direct procedure to determine the d_{33} coefficient via the direct piezoelectric effect, but the calculated d_{33} coefficient from this method is generally overestimated (Altafim et al., 2006; Miao et al., 2014; Zhang et al., 2007). The dynamic method is also a direct method, whereas the interferometric, resonance, and acoustic methods are indirect ones, that is, the inverse d_{33} coefficient is obtained. Nevertheless, the interferometric method works on larger frequency range (up to several hundred kilohertz) in comparison with dynamic methods (typically up to 1 kHz) (Miao et al., 2014).

3.7 Ferroelectret materials

Among a variety of ferroelectret materials, cellular PP is the most investigated material as a result of its outstanding properties such as large d_{33} coefficient (about 20 to 40 times higher than that of PVDF), flexibility, as well as lightweight and low cost (Bauer et al., 2004; Neugschwandtner et al., 2001; Qiu et al., 2007; Wan et al., 2010; Zhang et al., 2014).

PP has a dielectric nature, so the charges are retained at the cell walls after the discharge. Moreover, it has good fatigue resistance, which is an important property for piezoelectric materials (Gilbert-Tremblay et al., 2012). It also has good stiffness as well as good charge trapping properties. Hence, the development of piezoelectric cellular polymers started with PP (Wegener, 2010). Recently, this knowledge was developed for cellular films made from

polyethylene (Braña et al., 2011), poly(ethylene terephthalate) (PET) (Wegener et al., 2005; Wirges et al., 2007), poly(ethylene naphthalate) (PEN) (Fang et al., 2007; Fang et al., 2008), poly(tetrafluoro ethylene) (PTFE) (Gerhard-Multhaupt et al., 2000; Xia et al., 1999; Zhang et al., 2007; Zhang et al., 2007), cross-linked polypropylene (XPP) (Wu et al., 2015; Zhang et al., 2007; Zhang et al., 2011; Zhang et al., 2009; Zhang et al., 2014) , as well as some cyclo-olefins polymers (COP) and copolymers (Montanari et al., 2007; Saarimaki et al., 2005; Saarimaki et al., 2006).

Thin cellular PP films (50-100 μm thick with cells having a length of 100 μm and a height up to 10 μm) are considered as useful materials for piezoelectric applications (Gilbert-Tremblay et al., 2012). Single films are shown to have a good piezoelectric d_{33} coefficient up to 1200 pC/N at low frequency (Bauer et al., 2004). This coefficient can increase up to 2010 pC/N for hybrid multilayer films (Qiu et al., 2007; Zhang et al., 2004). Moreover, the response of both single layer and hybrid multi-layer cellular PP films exhibit a linear relationship with the applied pressure (in direct piezoelectric mode) and also with the amplitude of the exciting voltage (in inverse piezoelectric mode) (Qiu et al., 2007). It was shown that the electromechanical d_{33} coefficient for biaxially stretched cellular polyethylene films can be up to five times higher than for uniaxially stretched ones (Braña et al., 2011).

Several models were introduced to predict the piezoelectric behavior of cellular polymers and these models can be found elsewhere (Anton et al., 2014; Bosse et al., 2012; Challagulla and Venkatesh, 2013; Harris and Mellinger, 2012; Hillenbrand and Sessler, 2000; Hillenbrand et al., 2005; Mellinger and Mellinger, 2011; Montanari et al., 2005; Paajanen et al., 2000; Paajanen et al., 2000; Qaiss et al., 2013; Sessler and Hillenbrand, 1999; Taylor and Fernandez, 2005; Xu et al., 2013; Zhang et al., 2005; Zhukov and Von Seggern, 2007). Nevertheless, several PP applications as ferroelectrets in microphones (Hillenbrand and Sessler, 2004; Kressmann, 2001; Zhang et al., 2007; Zhang et al., 2014), ultrasonic transducers (Döring et al., 2010; Döring et al., 2012; Ealo et al., 2009; Rupitsch et al., 2011; Sessler and Hillenbrand, 2009; Wegener et al., 2005), and accelerometers (Hillenbrand et al., 2010) have been investigated.

3.7.1 Methods to obtain ferroelectret materials

To achieve good piezoelectric properties, cellular polymer films can be generally produced by two common methods: stretching or foaming (see Figure 3.5). In the stretching method, a polymer composite film (filled with solid particles) is produced and then stretched to initiate cells around the solid particles by delamination/decohesion at their interface. In the foaming method, a cellular structure is created by the introduction of gases like in a foaming process. The foaming process and related concepts were extensively discussed in our previous review (Mohebbi et al., 2015). Nevertheless, cellular polymer films can be produced by other methods inside a closed mold (Zhang et al., 2006) or using thermoforming (Altafim et al., 2006).

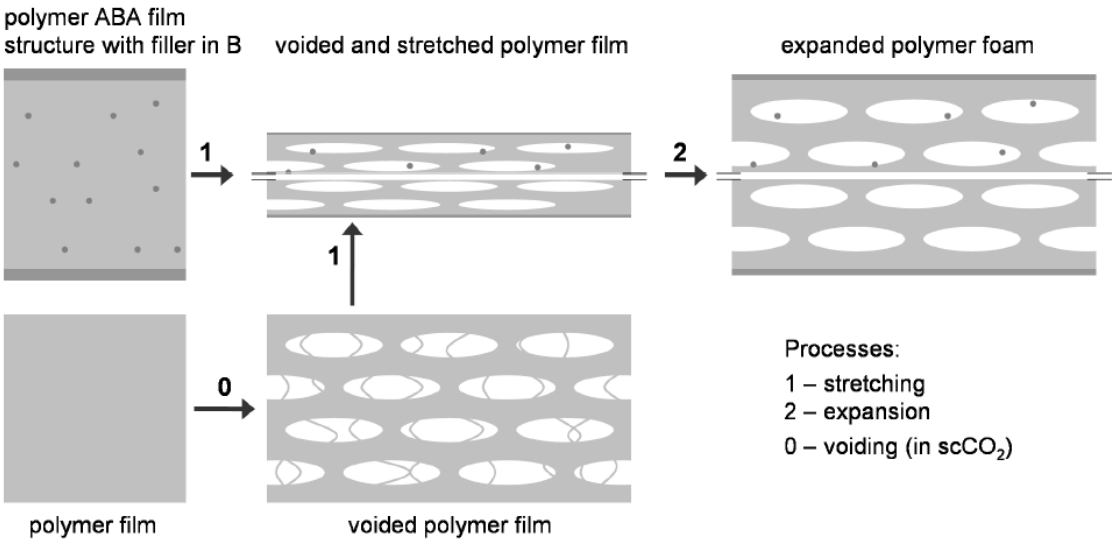

Figure 3.5. Film cellular structure produced by stretching a composite film (top) or by direct film foaming (bottom) (Wegener, 2010).

Piezoelectricity in the cellular morphology can be obtained by using a gas, such as N_2, into the closed-cell structure and its ionization with a high voltage external electric field, which can be produced using devices such as corona discharge (Qaiss et al., 2012; Wegener, 2010). This procedure is schematically presented in Figure 3.6.

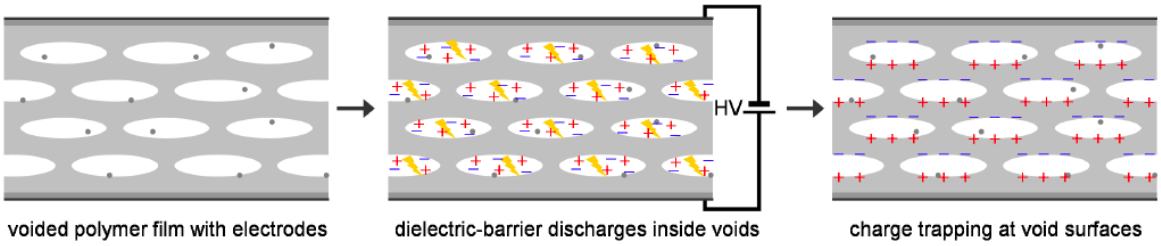

Figure 3.6. Procedure to charge a cellular polymer film (Wegener, 2010).

Charge deposition in the cells is based on the internal Paschen breakdown, which starts when the charging voltage is higher than the threshold voltage of the breakdown of the gas (air, N_2, etc.) in the cells (Harris et al., 2011; Qiu et al., 2007). In this method, the internal cell surfaces are charged by a series of DBD (Harris and Mellinger, 2014; Lindner et al., 2002; Qiu et al., 2007). Hence, during the DBD, opposite sign charges are separated and trapped on the internal top and bottom surfaces of the cells to create macroscopic dipoles. Charging ferroelectrets by DBD creates light emission, which can be photographed with a digital camera (An et al., 2012; Harris and Mellinger, 2014; Lindner et al., 2002; Qiu, et al., 2007).

Piezoelectric properties of PET film foam were investigated by Wegener et al. (Wegener et al., 2005). They used PET film foams with thicknesses of 160 ± 10 μm and densities in the range between 0.37 and 0.40 g/cm^3. They annealed the samples at temperatures between 70 and 160 °C for 16 h to decrease the void heights and the elastic modulus, as well as to increase the film density. Accordingly, the film thickness decreased by about 70 μm and the film density increased from about 0.4 to 0.66 g/cm^3. Then, the authors charged the samples in a pressure chamber under a N_2 atmosphere at a pressure of 6 bars and voltages between -27 and -60 kV for a charging time of 30 s. The charged samples were metallized on both film surfaces with 50 nm thick aluminum electrodes. The piezoelectric d_{33} coefficients were measured while the samples were kept at a constant temperature of around 110 °C in a gas stream. A maximum d_{33} coefficient of 23 pC/N was reported for a charged PET film having a density of 0.67 g/cm^3 (Wegener et al., 2005). Although this value is much lower than that for charged cellular PP films (about 500 pC/N (Wegener et al., 2004)), it is comparable to that of polar ferroelectric polymers such as PVDF (about 30 pC/N (Zhang et al., 2014)). Moreover, PET is more thermally stable than PP (Wegener et al., 2005).

In another investigation on the piezoelectric behavior of PET, the cellular structure was obtained through a foaming process via supercritical CO_2 (Wirges et al., 2007). Thereafter, the films were biaxially stretched at 230 °C up to 150 % followed by a N_2 inflation at 230 °C for 2 hours. To prepare the samples for piezoelectric measurements, they were charged with sulfur hexafluoride (SF_6) at a pressure of 3 bar with voltages ranging from -20 to -60 kV for a charging time of 60 s. The d_{33} coefficient was measured via the dynamic method by applying a static force of 3.0 N followed by a dynamic force with an amplitude of 1 N at a frequency of 2 Hz. In this case, the d_{33} values up to 500 pC/N were reported.

Zhang et al. (Zhang et al., 2014) studied the piezoelectric behavior of irradiated crosslinked PP (IXPP) films with a thickness of 1.5 mm and an area density of 0.0067 g/cm^2. It was shown that the average void diameter was 300 μm and the average wall thickness of the cells was about 2 μm. The samples were biaxially stretched under a thermal treatment and then charged via the corona method at a voltage of -25 kV for a charging time of 60 s. Afterward, the samples were metallized on both sides via aluminum evaporation. The d_{33} coefficient was measured via the dynamic method (direct piezoelectric effect). In this method, the samples were fixed using two outside jaws of a digital caliper to detect the length variation. A static force of 1.0 N followed by a dynamic sinusoidal force F_d with an amplitude of 0.5 N were applied and the induced charge Q was measured via a charge amplifier. The d_{33} coefficient was calculated by the ratio of Q/F_d (Zhang et al., 2014). The maximum d_{33} coefficient achieved was 100 pC/N for a sample of 260 μm in thickness. However, a higher d_{33} coefficient of about 400 pC/N for IXPP film was also reported (Zhang et al., 2009). The reported values for charged cellular IXPP films are lower than for charged cellular PP film (about 500 pC/N).

It was also observed that the dynamic values of the piezoelectric d_{33} coefficients of IXPP films are lower than the quasi-static d_{33} values (Zhang et al., 2009; Zhang et al., 2014). It is believed that the difference between the quasi-static and dynamic methods can be related to the increase of the Young's modulus of IXPP with increasing frequency due to its viscoelastic behavior (Zhang et al., 2009).

In another investigation, Zhang et al. (Zhang et al., 2011) used the same foamed IXPP films as in the previous study (Zhang et al., 2014), but the d_{33} coefficient was measured through the quasi-static method. They charged the treated samples via corona discharge at a voltage of -20 kV for a charging time of 60 s. Then, the samples were metallized on both sides via aluminum evaporation. The maximum d_{33} coefficient was 308 pC/N for a sample produced with an elongation ratio of 200 % and a Young's modulus of 0.54 MPa. The authors also performed a similar investigation for the same IXPP foamed films and reported a d_{33} coefficient of 400 pC/N using a different sample treatment (Zhang et al., 2007).

The ferroelectret behavior of PEN was studied by Fang et al. (Fang et al., 2007). They obtained cellular PEN films through foaming of a 100 μm PEN films via supercritical CO_2 in a two steps batch process. Then, they biaxially stretched the cellular films at a ratio of about 1.5. The samples were then inflated and charged with corona discharge either in air at atmospheric pressure and a voltage of −21 kV or in SF_6 at a pressure of 3 bars with a higher voltage of -50 kV and a charging time of 15 s. Afterward, the samples were metallized on both sides via aluminum evaporation. The d_{33} coefficient was measured through the dynamic method by applying a static force of 3.0 N followed by a dynamic sinusoidal force F_d with an amplitude of 1 N at a frequency of 2 Hz to get the electrical response (Fang et al., 2007). The conclusions from this study are as follow:

- A maximum d_{33} coefficient was obtained from PEN foamed films with an optimum density of 1.1 g/cm^3.
- Higher charging voltage resulted in higher piezoelectric d_{33} coefficient.
- Compared to the charged PP films, the piezoelectricity of charged PEN films is more stable at elevated temperatures (up to 80 °C). The piezoelectric behavior of PP ferroelectret is not stable above 60 °C.
- By increasing the temperature up to 100 °C, PEN ferroelectret showed a decrease of d_{33} by around 32 %, while above 120 °C the samples showed no piezoelectricity.

Quasi-static and dynamic piezoelectric behaviors of cellular PTFE were investigated by Zhang et al. (Zhang et al., 2014). They used commercial three-layered PTFE films composed of a central cellular PTFE film (100-250 μm in thickness) and two dense PTFE layers of

about 20 μm as skins. The samples were charged via the corona method at a voltage of -25 kV for a charging time of 60 s followed by metallization with thin aluminum layers on both skin sides. The quasi-static method was performed as follows: first, a quasi-static force F of 1.96 N was applied to the sample during a relatively long time. Then, the force was removed and the generated charge Q during 10 s was measured with an electrometer. The measurement was done while a static force of 0.25 N was permanently applied to the film to reduce the potential effect of film bending (Zhang et al., 2014).

The dynamic piezoelectric d_{33} coefficient was achieved via the microphone sensitivity. Hence, the pressure sensitivity M_p of the microphone was evaluated as the ratio between the output voltage (V) and the actual sound pressure (P) in front of the microphone after being placed in a sound field (Zhang et al., 2012). Accordingly, the dynamic piezoelectric d_{33} coefficient of the ferroelectret material was calculated as follows (Zhang et al., 2014):

$$d_{33} = M_p \frac{C_F}{A_F} \tag{3.13}$$

where C_F is the capacitance and A_F is the area of the ferroelectret sample. The results showed that the quasi-static piezoelectric d_{33} coefficients at a pressure of 3.2 kPa were in the range of 1000-2700 pC/N. Samples were also annealed to stabilize their ferroelectret behavior. After annealing for 25 hours at 90 and 120 °C, the piezoelectric d_{33} coefficients were respectively stabilized at about 1700 and 1000 pC/N. On the other hand, the dynamic piezoelectric d_{33} coefficients increased from 200 to 300 pC/N when the frequency was decreased from 10000 to 100 Hz.

Hillenbrand et al. (Hillenbrand et al., 2005) measured the piezoelectric d_{33} coefficient of cellular PP films (50 μm thick with an area density of 0.0029 g/cm^2). They obtained the cellular structure by the stretching method using $CaCO_3$ particles. Also, they inflated the sample with N_2 at a pressure of 20 bars at room temperature for a period of 3 h. They annealed the samples at a temperature of 80 °C for 2 h. Then, the samples were charged via the corona method at a voltage of 32 kV for a charging time of 60 s. Afterward, the samples were metallized on both sides via aluminum evaporation. The measurement of the d_{33} coefficient

was performed through the interferometric method (inverse piezoelectric effect). The maximum d_{33} coefficient was about 650 pC/N for a 58 μm thick sample.

In another study, Anton et al. (Anton et al., 2014) measured the piezoelectric d_{33} coefficient of cellular PP films of 85 μm in thickness. For the dynamic measurement of the d_{33} coefficient, three static forces obtained from masses of 100, 500, and 1000 g were applied. For each sample, three dynamic forces with the acceleration peak obtained from masses of 60.1, 60.3, and 60.5 g for a frequency range of 10 to 1000 Hz were applied and the electrical responses were measured. The results showed that an almost constant piezoelectric d_{33} coefficient of 175 pC/N through the entire frequency range for the PP cellular film was observed.

The piezoelectric behavior of multilayers of cellular PP films were also investigated and compared to single layer films (Qiu et al., 2007). The samples were charged by the corona method at a voltage of -20 kV for a charging time of 15 s. To obtain the multi-layer films, such as three-layered films, three single-layer cellular PP piezoelectric films were superposed to achieve a hybrid multilayer system in such a way that the surfaces with the positive and negative charges were attached to the surface with the same charge, as shown in Figure 3.7. The d_{33} coefficients were around 580 pC/N for the single layer, and around 1440-2010 pC/N for the three-layer and five-layer systems, respectively.

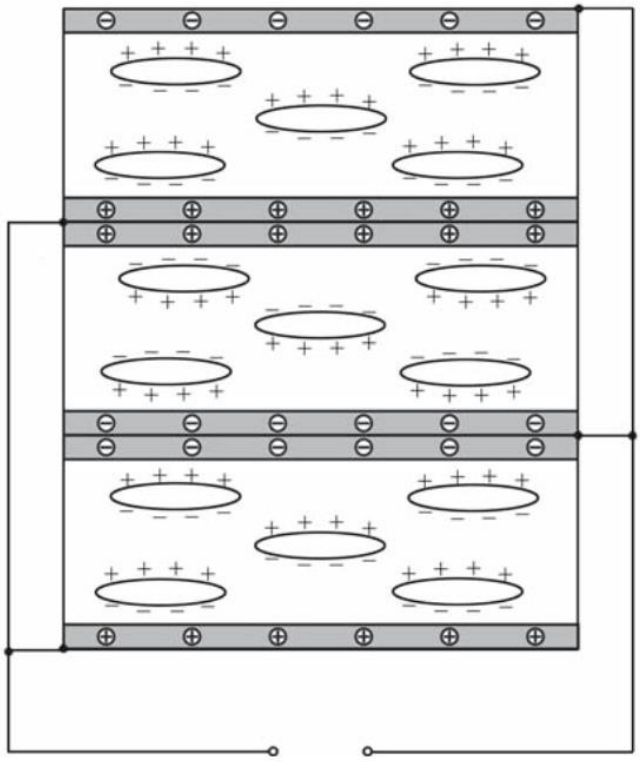

Figure 3.7. Example of a charged three-layer cellular PP system (Qiu et al., 2007).

3.7.2 Effect of ionizing gas type and inflation pressure on the d_{33} coefficient

It is reported that the applied inflation pressure is one of the most effective parameters to control the d_{33} coefficient of cellular ferroelectret films, because of its effect on the viscosity of the polymer matrix (Wan et al., 2011). It was reported that for cellular polymers, such as PTFE, ferroelectret films d_{33} coefficient is pressure dependent (Zhang et al., 2014).

More effective corona charging is possible with higher ambient gas pressure during charging or by using different gases with higher electrical breakdown strength (Paajanen et al., 2001; Qiu et al., 2005). Table 3.1 shows the relative breakdown strength of some commonly used gases in a uniform DC electric field at atmospheric pressure. It can be seen that SF_6 has the highest breakdown strength, which is three times higher than for air.

Table 3.1. Relative breakdown strength of some applicable gases in corona discharge (Paajanen et al., 2001).

Gas	Relative breakdown strength
SF_6	1.00
N_2O	0.44
N_2	0.36
Air	0.30
Ar	0.07

Paajanen et al. (Paajanen et al., 2001, 2001) found that by replacing air with nitrogen inside the cells of cellular PP films during a pressure treatment procedure, a d_{33} coefficient of about 790 pC/N was achieved. Moreover, it was found that a higher d_{33} coefficient could be achieved by corona charging in N_2 atmosphere at 100-450 kPa or in N_2O atmosphere at 100-140 kPa.

The effect of replacing air with SF_6 inside the cellular structure of PP film on its piezoelectric d_{33} coefficient was also investigated by Qiu et al. (Qiu et al., 2005). In this case, the pre-inflated samples were charged under a pressure of 400 kPa using SF_6 as the ionizing gas. The samples were charged via the corona method at a voltage of -60 kV for a charging time of 15 s. For comparison, the same samples were charged at atmospheric pressure via the corona method at a voltage of -32 kV for a charging time of 15 s, using air as the ionizing gas. The d_{33} coefficient of the samples was obtained through the dynamic mechanical excitation method. A static force of 1.0 N followed by a dynamic force with an amplitude of 1 N and a frequency of 2 Hz were applied to the samples. A significant enhancement of the electromechanical activity was reported for the cellular PP films saturated with SF_6 compared to the samples treated by a similar procedure in air. The electromechanical d_{33} coefficient of cellular PP films charged in air was about 215 pC/N whereas that of cellular PP films charged in SF_6 was about 350 pC/N. However, the d_{33} coefficient of the cellular PP films saturated

with SF_6 was much lower than that of cellular PP films saturated with N_2 (790 pC/N) (Paajanen et al., 2001).

By controlling the inflation pressure of the cells, the optimum electromechanical d_{33} coefficient for cellular PP films were investigated by Wegener et al. (Wegener et al., 2004). As shown in Figure 3.8, when the elastic modulus (c_{33}) exhibits a minimum, the electromechanical d_{33} coefficient shows a maximum, and generally, these two parameters present inverse trends. The same inverse trend was also observed by Sborikas and Wegener (Sborikas and Wegener, 2013). Two different gas diffusion expansion (GDE) regimes were studied to control the morphology of the cells. In the first GDE regime, the external pressure was reduced to the atmospheric pressure during an isothermal process at room temperature. As a result, the higher gas pressure inside the closed cells led to their inflation. In the second GDE regime, the external pressure was first increased and held at a constant value for a certain period. Hence, the gas diffused into the cells until the internal pressure of the cells became equal to the externally applied pressure. Then, the external pressure was reduced back to the atmospheric pressure, which resulted in cell inflation in a controlled manner. It was concluded that the inflation obtained from the second GDE regime was permanent, while the inflation from the first GDE regime was not (Wegener et al., 2004).

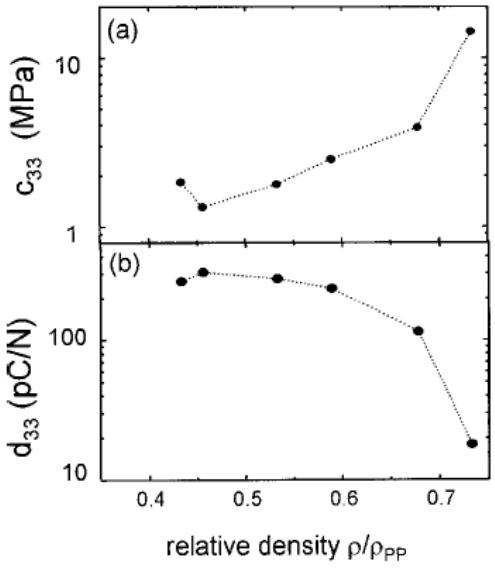

Figure 3.8. Typical values for: (a) elastic modulus and (b) electromechanical d_{33} coefficient for cellular PP films (Wegener et al., 2004).

Zhang et al. (Zhang et al., 2004) improved the piezoelectric behavior of cellular PP through a double inflation process. They used co-extruded PP films consisting of five-layer with a total thickness of 50 μm. This sample contained a cellular PP layer with a thickness of 37 μm in the middle and two thin covering layers of PP as well, with thicknesses of 0.5-7 μm on each side. The cellular structure was obtained by mixing the PP polymer with solid mineral particles during the film extrusion step then by biaxial stretching the filled PP film. The average cells length and height were 100 and 5 μm, respectively. Also, the cellular structure of the middle layer had an area density of 0.0029 g/cm^2. All samples were treated as follow:

- A pressure step using N_2 at 20 bars and room temperature for 3 hours in a pressure chamber. In this step, N_2 diffused into the cells.
- Annealing the samples at 80 or 100 °C for 2 hours.
- Pressure reduction to atmospheric pressure then gradual cooling. Cell inflation started as a result of higher internal cell pressure.
- Charging via the corona process at a voltage of 32 kV for a charging time of 60 s.
- Metallization of the samples on both sides.
- Application of a second expansion step at a pressure of 8 bars for 2 h at room temperature, then for another 2 h at 45°C.
- Pressure reduction to atmospheric pressure.

The authors observed a significant enhancement in the film thickness after the second inflation process. The d_{33} piezoelectric coefficient of the samples was measured through the quasi-static method and the results showed a 40 % increase in d_{33} for the two-step procedure compared to the single step. A d_{33} coefficient of 1400 pC/N at 0.01 Hz and about 500 pC/N at 25 kHz for the two-step process were obtained (Zhang et al., 2004a).

Qaiss et al. (Qaiss et al., 2012) investigated the piezoelectric properties of cellular PP-$CaCO_3$ composite films (10 % wt. of $CaCO_3$ of 10 μm) followed by a stretching step. They compared the piezoelectric behavior of the produced films inflated via two different procedures: constant or stepwise pressure increase. As shown in Figure 3.9, it was found that the stepwise

procedure allowed the N_2 gas to better diffuse into the cells resulting in a higher inflation level.

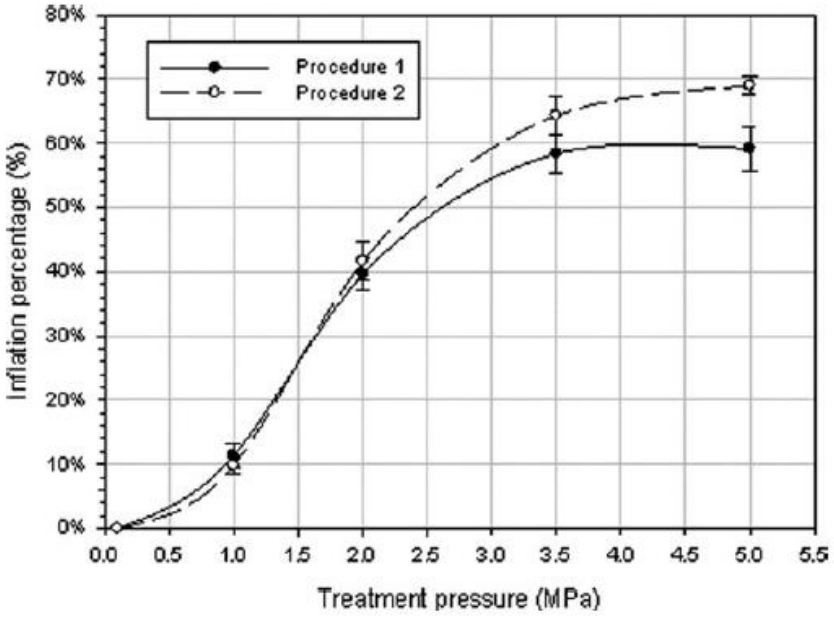

Figure 3.9. Inflation percentage immediately after removing the samples from the treatment chamber as a function of final treatment pressure in: procedure 1 (constant pressure) and procedure 2 (stepwise pressure increase) (Qaiss et al., 2012).

Fang et al. (Fang et al., 2007) investigated the piezoelectric effect of cellular PEN produced by a two-step process. First, they exposed the film to supercritical carbon dioxide for saturation, then the sample underwent a heat treatment for a specific time and temperature, well above the glass-transition temperature of PEN to create the cells and inflate them. Finally, they stretched the film biaxially and charged them via the corona discharge. As shown in Figure 3.10, the results show that the d_{33} coefficient of the samples increased with density up to a maximum and then decreased to zero. Also, the samples with small voids, which are related to the high sample density and its stiffer structures, showed lower piezoelectric behavior. Higher inflation results in more spherical voids and lower sample density. Also, a higher elastic stiffness was achieved with spherical voids. When stiffness increases, the d_{33} coefficient decreases (Equ. 3.4) and this is why a lower film density resulted in lower d_{33} coefficient. This behavior was also reported in other works (Wegener et al.,

2004; Wegener et al., 2005). It is believed that, since the density of PET (1.3 g/cm^3) is higher than that of PP (0.9 g/cm^3), untreated PET films are too stiff to be used for ferroelectret applications. Hence, to be a good piezoelectret, more inflation would be needed in comparison with PP films (Wegener et al., 2005).

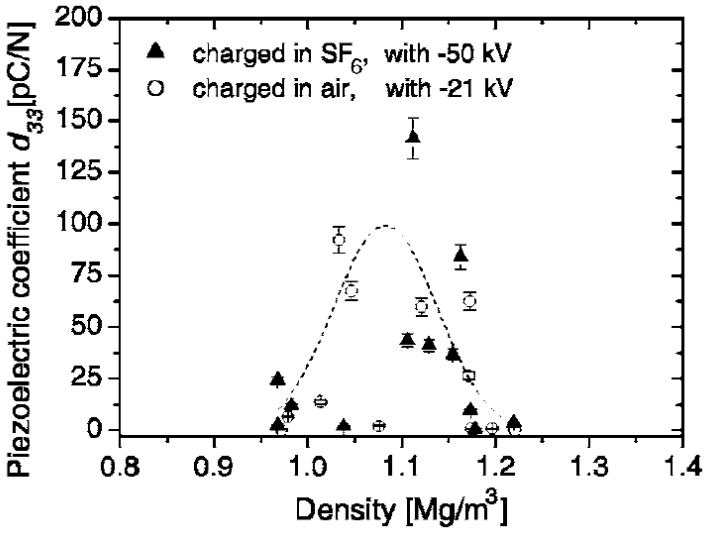

Figure 3.10. Variation of the d_{33} coefficient with density of PEN for two different ionizing gases and charging parameters (Fang et al., 2007).

3.7.3 Effect of cell size and cell shape on the piezoelectric d_{33} coefficient

Suitable cell geometry for piezoelectric applications must have a large surface area with a lens-shaped cross-section (Lindner et al., 2004; Tuncer, 2005; Xu et al., 2013). Moreover, to achieve a maximum piezoelectric signal, the cellular structure must be developed through the whole area of the samples. Cells with thinner walls can lead to lower Young's modulus, which is suitable for effective piezoelectric behavior. Wegener et al. (Wegener et al., 2004) reported that a lower Young's modulus results in a higher piezoelectric d_{33} coefficient. Moreover, Zhang et al. (Zhang et al., 2014) concluded that for ferroelectrets, the Young's modulus in the surface normal direction is 2 or 3 orders of magnitude smaller than that parallel to the surface, which results in a large piezoelectric coefficient. Moreover, it was

reported that the piezoelectric coefficient decreases with increasing film thickness and increases with increasing cell density (Qaiss et al., 2013).

Zhang et al. (Zhang et al., 2014) investigated the piezoelectric effect of cellular cross-linked polypropylene (IXPP) films produced by irradiation followed by compression molding. They used commercial foam sheets and biaxially stretched the samples at a temperature of 100 °C. Then, the samples were pressed at 70 °C under 7 MPa. They showed that, after the treatment, the cells coalesced in the extension direction and created "disk-like" cells. It was reported that such "disk-like" cell geometry increased the charging capacity and decreased the Young's modulus of the samples in the surface normal direction (Hillenbrand et al., 2005; Zhang et al., 2007; Zhang et al., 2011; Zhang et al., 2009; Zhang et al., 2014). Hence, the piezoelectric activity of the films increased. An example of disk-like cells is shown in Figure 3.11 (Zhang et al., 2007).

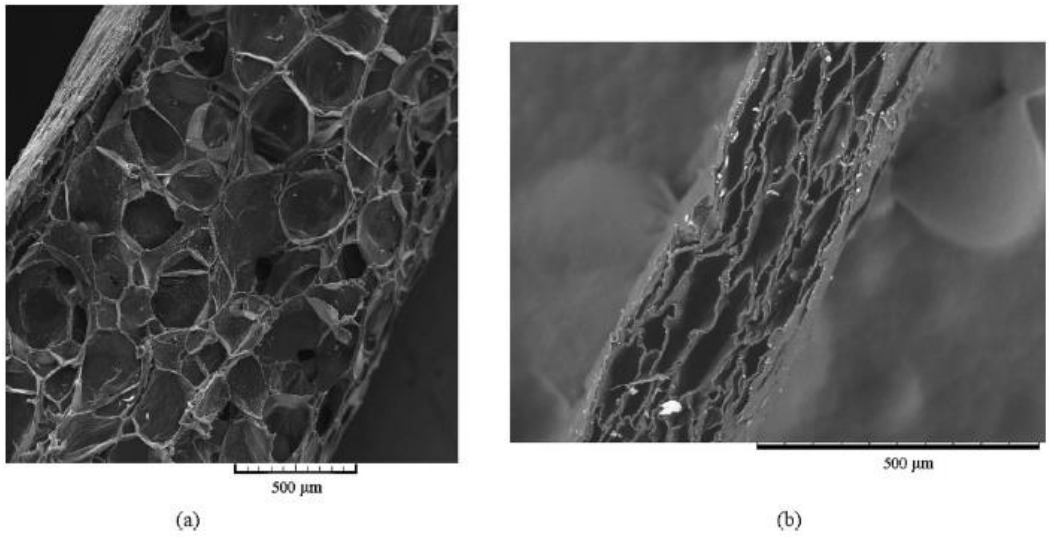

Figure 3.11. SEM images of irradiation cross-linked PP films: (a) before and (b) after treatment (Zhang et al., 2007).

As illustrated in Figure 3.12, ferroelectret materials show a so-called U-shaped behavior (Wegener et al., 2005). The elasticity of the foam depends on the size, the shape and the percentage of cells in the matrix (Wan et al., 2010). Different cross-sections of the cellular structure are shown at the top of Figure 3.12. As reported, samples with smaller cell

sizes produce stiffer materials, they show lower piezoelectricity. Small or flat cells are stiffer and reduce the electromagnetic response (Qaiss et al., 2012). Hence, cells size, aspect ratio (cell shape), and elastic behavior of the films are effective parameters for piezoelectric purposes. By expanding the cells during the inflation step, the cell wall thickness decreases resulting in more deformation through vibration because of their lower elastic stiffness. Moreover, based on Equ. (3.4), lower elastic stiffness (c_{33}) leads to higher d_{33} coefficients. The piezoelectric activity is increased until an optimum cellular structure is obtained and the piezoelectric activity shows a maximum. Then, more expansion will lead to more spherical voids and higher elastic stiffness resulting in lower piezoelectric activity.

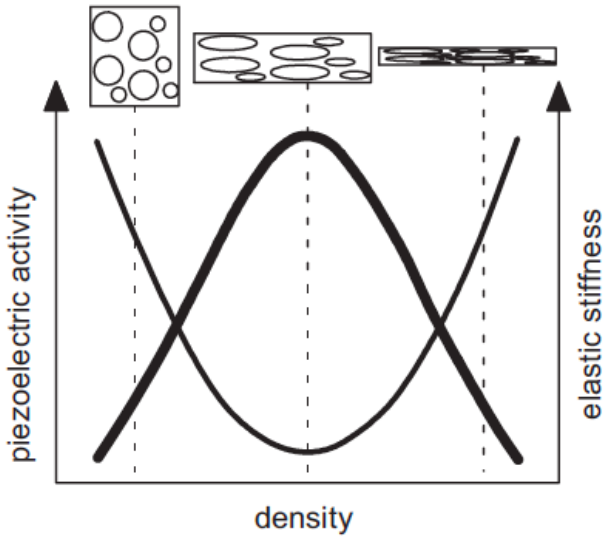

Figure 3.12. Typical variation of piezoelectric activity (thick line) and elastic stiffness (thin line) as a function of sample density (Wegener et al., 2005).

Tuncer simulated the elastic properties of cellular structures in ferroelectrets with two geometrical models: truss-like and eye-shaped (Tuncer, 2005). As illustrated in Figure 3.13, the solid cells consist of either straight or curved boundary structures. The marked rectangular regions $(0,0) \leq (x,y) \leq ({}^{a}/_{2}, {}^{b}/_{2})$ in the figures are used as unit cells (computational domain for modeling).

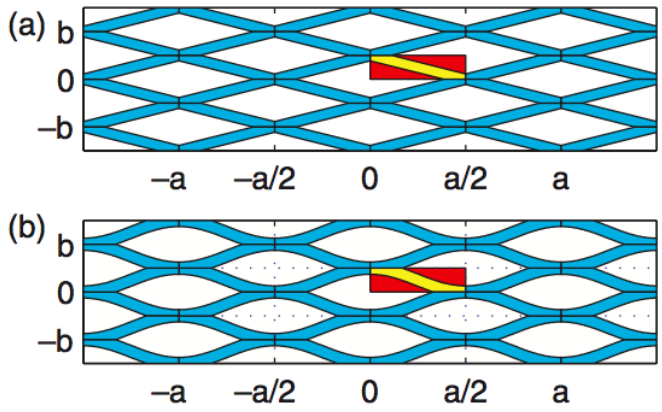

Figure 3.13. Schematic representation of: (a) truss-like and (b) eye-shaped geometrical structures (Tuncer, 2005).

The cell-wall thickness of the truss-like structure (t^t) is calculated as (Tuncer, 2005):

$$t^t(\mathrm{q},\mathrm{a},\mathrm{b}) = 2\sqrt{A}sin(2\alpha) \tag{3.14}$$

where a and b are the length and width of the unit-cell and q is the volume fraction of the solid part, which is defined as the ratio of the densities of the cellular material ρ^c to the bulk material ρ^b; $q = {\rho^c}/{\rho^b}$. Also:

$$A = \left(\frac{b}{2} - m\,tan\,\alpha\right)^2 + \left(\frac{a}{2} - m\right)^2 \tag{3.15}$$

$$m = \sqrt{\frac{1-qab}{4\tan\alpha}} \tag{3.16}$$

$$\alpha = tan^{-1}\left(\frac{b}{a}\right) \tag{3.17}$$

The cell-wall thickness of the eye-shaped structure (t^e) is calculated as (Tuncer, 2005):

$$l_i = \frac{b}{4}\left[1 + cos\left(\frac{2\pi x}{a}\right)\right] + (-1)^i\frac{t^e}{2} \qquad \mathrm{i} = 1, 2 \tag{3.18}$$

where l_1 and l_2 are the lower and upper lines of the assumed unit cells, respectively.

Gibson and Ashby (Gibson and Ashby, 1997) introduced the famous power-law relation between the effective Young's modulus (E_e) and the volume fraction of the bulk material (q) as:

$$E_e = \kappa q^n E_s \tag{3.19}$$

where κ and n are two parameters depending on film microstructure, and E_s is the Young's modulus of the solid material (Tuncer, 2005).

The authors verified the two models for three different aspect ratios (a/b) of 2, 4, and 8. The conclusions from this study were as follow:

- The normalized effective Young's modulus (E_e/E_s) of the structures decreased with increasing (a/b) ratio.
- For the range $0.15 < q < 0.85$, the variation of effective Young's modulus of the truss-like and eye-like structures is almost the same, but eye-like cells showed a lower elastic modulus than truss-like cells.
- For other volume fractions ($q < 0.15$ and $q > 0.85$), the eye-like cells showed a higher elastic modulus than truss-like cells.

For a constant cell wall thickness, both eye-like and trust-like structures have similar elastic modulus in the ranges $4 < a/b < 10$ and $q > 0.15$.

3.7.4 Effect of additives on the piezoelectric d_{33} coefficient

The improvement of the charge storage stability by using organic and/or inorganic additives with PP was also investigated (Behrendt et al., 2006; Klimiec et al., 2015; Mohmeyer et al., 2004). In order to facilitate the formation of cracks during film stretching, fillers having low compatibility with the matrix should be used. The most used polymer-based composite for cellular ferroelectric investigations is PP-$CaCO_3$. Moreover, $CaCO_3$ with a prism shape is a more suitable candidate for stress concentrations and consequently crack initiation (Gilbert-Tremblay et al., 2012).

PP and $CaCO_3$ have low interactions associated with low difference in their solubility parameters ($\delta_{pp}(8.2) - \delta_{CaCO_3}(7.5) = 0.7\ cal^{1/2}cm^{-3/2}$) (Qaiss et al., 2012). This means that during the mixing step, $CaCO_3$ will be dispersed inside the PP matrix in the form of small agglomerates having weak compatibility with the PP matrix. Actually, in this context, a good dispersion must be in balance with interfacial decohesion.

The crystallinity of the polymer is also an important factor for good piezoelectric behavior. It is believed that the interfaces between the amorphous and crystalline areas have the highest potential for electrical charges drift. Hence, samples with more interfacial area can retain charges and the piezoelectric effect for a longer period of time. However, so far, there is no method to determine exactly the amount of interfacial area between the amorphous and crystalline phases. Three main parameters can affect the crystallinity of the samples: particle size, particle concentration, and the cooling rate of the process (Mohmeyer et al., 2007).

Gilbert-Tremblay et al. (Gilbert-Tremblay et al., 2012) studied the effect of pressure, particle size (0.7, 3.2 and 12 μm), and particle concentration (5-20 wt.%) on the cellular structure of PP-$CaCO_3$ films for piezoelectric applications. They obtained cellular PP-$CaCO_3$ films by twin-screw extrusion and stretched them to create cells around the $CaCO_3$ particles. They reported that, because $CaCO_3$ particles act as nucleating agent, for low $CaCO_3$ loading, the crystallinity of the PP-$CaCO_3$ increases with increasing $CaCO_3$ content. However, at high $CaCO_3$ loading, these particles and their agglomeration prevented polymer chain mobility leading to a reduced crystallinity. Figure 3.14 shows SEM pictures of the stretched films with three different $CaCO_3$ sizes. It can be seen that $CaCO_3$ having the smallest size was not large enough to create cells during the stretching step. But for samples containing $CaCO_3$ with 3 μm particle size, cracks started to propagate around the particles. Also, Figure 3.14c shows that most of the largest $CaCO_3$ particles could generate cells. They were able to produce a cellular film with a density ratio of 0.8 and decrease the density ratio between 0.4 and 0.6 by adding a pressure treatment step (Figure 3.15).

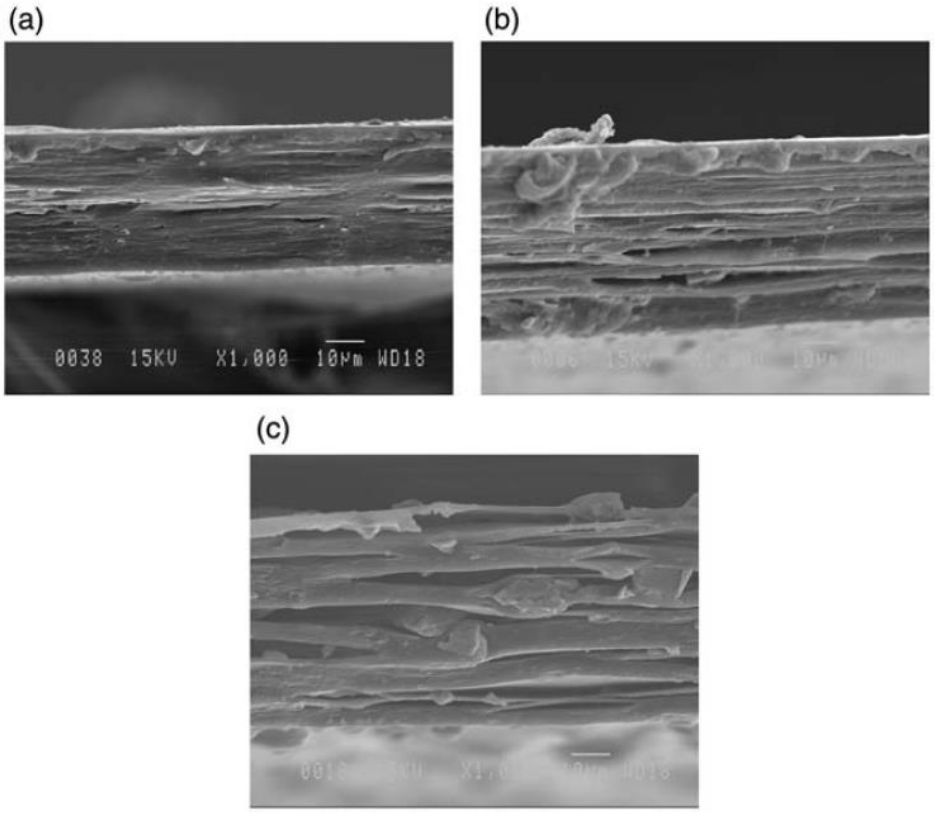

Figure 3.14. SEM images of the cross-section of stretched PP-$CaCO_3$ films with different $CaCO_3$ sizes: (a) 0.7 µm, (b) 3 µm, and (c) 12 µm (all images are 1000X) (Gilbert-Tremblay et al., 2012).

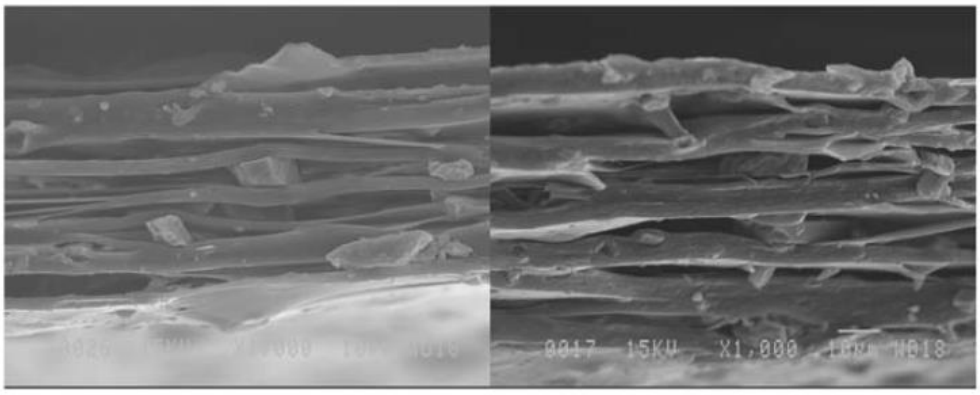

Figure 3.15. SEM images of the cross-section of a stretched film before (left) and after (right) pressure treatment (all images are 1000X) (Gilbert-Tremblay et al., 2012).

3.7.5 Effect of other parameters on the piezoelectric d_{33} coefficient

The effect of other parameters on the d_{33} coefficient, such as temperature (Fang et al., 2007; Zhang et al., 2009), frequency (Zhang et al., 2014) , and chemical modification of PP (An et al., 2006; An et al., 2009; Tang et al., 2007), were also investigated. Fang et al. (Fang et al., 2007) performed thermal stability tests for cellular PEN films. The samples were placed at different temperatures for 1 h and then the d_{33} coefficient was measured at room temperature (Fang et al., 2007). It was found that, at temperatures above 100 °C, the d_{33} coefficient significantly decreased. The effect of time on the d_{33} coefficient was also studied. The d_{33} coefficient, which was 23 pC/N when charged at -21 kV, decreased by about 50 % after one day at constant temperature (100 °C). Under the same conditions, but for samples charged at -50 kV, a reduction from 27 to 16 pC/N (about 60 %) was also observed.

In another investigation, IXPP was corona charged at room temperature and a piezoelectric d_{33} coefficient up to 400 pC/N was reported (Zhang et al., 2009). Then, d_{33} decreased to 30 % of its original value when the samples were exposed to 90 °C for one day, while under the same conditions for linear PP films, only 17 % of the piezoelectricity was preserved (Zhang et al., 2009).

An et al. (An et al., 2009) were able to improve the thermal stability of piezoelectric cellular PP by chemical modification, which was performed through chromic acid oxidation at 70-80 °C and then hydrofluoric acid treatment at room temperature. The d_{33} coefficient for the unmodified sample was about 125 pC/N, which increased to about 220 pC/N after chemical modification. The measurement of the d_{33} coefficient was performed through the quasi-static method. Based on the treatment method and the required electromechanical activity, the maximum service temperature of cellular PP films was reported to be in the range between 60 and 80 °C (Mellinger et al., 2006; Taylor and Fernandez, 2005).

As shown in Figure 3.16, Zhang et al. (Zhang et al., 2014) reported that the electromechanical d_{33} coefficient of IXPP is frequency independent in the range 2-100 Hz under different static strains. The same result was reported for the piezoelectric d_{33} coefficient of cellular PP films. Their dynamic d_{33} coefficient was frequency independent over a wide frequency range of 10-1000 Hz (Anton et al., 2014).

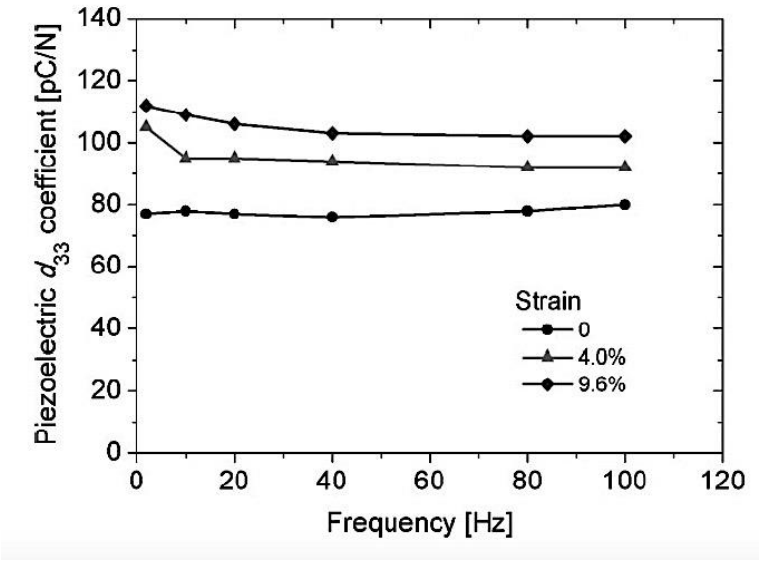

Figure 3.16. Variation of the piezoelectric d_{33} coefficient with frequency for IXPP at different static strain (Zhang et al., 2014).

3.8 Conclusions

In this review, recent advances related to the development and characterization of materials used for ferroelectric applications were reviewed. Considering that cellular thermoplastic polymers can be tailored to get a good piezoelectric-like behavior, which is the so-called ferroelectret behavior, they were the main subject of the current paper. Today, cellular space-charged polymers are under investigation for several applications such as actuators, vibration control, ultrasonic transducers, tactile sensors, ferroelectret devices, energy conversion devices, speakers, microphones, keyboards, shock sensors, as well as thermal and optical property measurement devices.

The main part of this review was devoted to PP-based cellular films and their characteristics for ferroelectric applications. Piezoelectricity in charged cellular polymers, such as PP, comes from the deformation of charged cells, in which positive and negative electrical charges are created on the opposite faces of each cell surfaces, whereas in polar piezoelectric materials, ion displacement in a lattice is the origin of this behavior. This property is achieved through internal charging by placing the material into an external high electric field. Moreover, the voltage of the electric field must be higher than the threshold voltage.

Furthermore, according to Townsend's model of Paschen breakdown, the critical breakdown electric field in a uniform electric field is a function of gas pressure and electrode spacing (pS factor). The quasi-static method is the simplest and most direct procedure to determine the d_{33} coefficient via the direct piezoelectric effect.

Also, the main methods used for the production of cellular polymers were discussed. Cellular polymer films are generally produced by two common methods: stretching and foaming. In the stretching method, solid particles such as $CaCO_3$ having low compatibility with the polymeric matrix are used to facilitate cell creation through decohesion at their interface. Cellular PP-based films are the most extensively investigated ferroelectret material as a result their large d_{33} coefficient.

Furthermore, the main parameters affecting the piezoelectric d_{33} coefficient were reviewed. Piezoelectric d_{33} coefficient has an inverse relation with the elastic (Young's) modulus, and therefore is directly related with the shape of the cells. Cells with disk-like cross-section and thin cell walls can lead to lower Young's modulus and is considered as the optimum structure for higher piezoelectric response. Pressure, electrical breakdown strength of the gas, additives, and service temperature are other parameters controlling the d_{33} coefficient of cellular ferroelectret films.

Based on the results of the different investigations reviewed in this work, several conclusions can be drawn to optimize and control d_{33} as follows:

- N_2 is mostly used as the ionizing gas both for the inflation process and corona charging of ferroelectret materials. Higher d_{33} coefficient is achieved using N_2 in comparison with air.
- Ferroelectret samples can be charged via corona charging at voltages ranging from -30 to -60 kV for a charging time of 30-60 s.
- A ferroelectret materials having a cellular structure containing eye-like cells with dimension aspect ratio $4 < a/b < 10$ and $q > 0.15$ (q is the volume fraction of the solid part) are optimum for piezoelectric purpose.

PP is the most used ferroelectret material. Single layer PP films have a d_{33} coefficient varying from 175 to 650 pC/N. This coefficient can be increased up to 2100 pC/N for a five-layer PP film.

For better comparison, the piezoelectric coefficients of frequently used ferroelectrets are reported in Table 3.2 with their respective processing method.

Table 3.2. Piezoelectric d_{33} coefficient of different polymer-based ferroelectret materials with their processing methods and characterization conditions.

Material	Maximum reported d_{33} coefficient (pC/N)	Method of production (cellular structure)	Piezoelectric measurement method	Charging conditions	Ref.
PET	23	Foaming	---	Corona charging at 6 bar of N_2, voltage between -27 and -60 kV for 30 s	(Wegener et al., 2005)
PET	500	Foaming with CO_2 followed by biaxial stretching	Dynamic	Corona charging at 3 bar of SF_6, voltage between -20 and -60 kV for 60 s	(Wirges et al., 2007)
PTFE	300	Cellular PTFE core and two compact PTFE skin layers	Dynamic	Corona charging at voltage of -25 kV for 60 s	(Zhang et al., 2014)

PTFE	1700	Cellular PTFE core and two compact PTFE skin layers	Quasi-static	Corona charging at voltage of -25 kV for 60 s	(Zhang et al., 2014)
PEN	140	Foaming with CO_2 followed by biaxial stretching	Dynamic	Corona charging in the presence of SF_6, at voltage of -50 kV for 15 s	(Fang et al., 2007)
IXPP	100	Foaming followed by biaxial stretching	Dynamic	Corona charging at voltage of -25 kV for 60 s	(Zhang et al., 2014)
IXPP	308	Foaming followed by 200% stretching	Quasi-static	Corona charging at voltage of -20 kV for 60 s	(Zhang et al., 2011)
IXPP	400	Foaming	Quasi-static	Corona charging at voltage of -32 kV for 60 s	(Zhang et al., 2007; Zhang et al., 2009)
PP	306	Stretching filler-loaded PP	Dynamic	---	(Wegener et al., 2004)
PP	130	Foaming	Dynamic	Corona charging at voltage up to 10 kV for 30 s	(Sborikas and

					Wegener, 2013)
PP	590	---	---	Corona charging at voltage up to -24 kV for 30 s	(Wegener et al., 2004)
PP	330	Foaming	Dynamic	---	(Wegener et al., 2004)
PP	300	Foaming	---	Corona charging	(Wegener, 2010)
PP	650	Stretching $CaCO_3$-loaded PP	Interferometric method	Corona charging at voltage of 32 kV for 60 s	(Hillenbrand et al., 2005)
PP	1400	Stretching filler-loaded PP followed by biaxial stretching: porous PP core and two compact PP skin layers	Quasi-static	Corona charging at voltage of 32 kV for 60 s	(Zhang et al., 2004)
PP	350	Cellular PP core and two compact PP skin layers	Dynamic	Corona charging at 400 kPa of SF_6, at voltage of -60 kV for 15 s	(Qiu et al., 2005)

PP	215	Cellular PP core and two compact PP skin layers	Dynamic	Corona charging at voltage of -32 kV for 15 s	(Qiu et al., 2005)
PP	580	Single layer of biaxial-stretched filler-loaded PP	Quasi-static	Corona charging in the presence of N_2, at voltage of -20 kV for 15 s	(Qiu et al., 2007)
PP	1440	Three-layer of stretched filler-loaded PP	Quasi-static	Corona charging in N_2, at voltage of -20 kV for 15 s	(Qiu et al., 2007)
PP	2100	Five layer of stretched filler-loaded PP	Quasi-static	Corona charging in N_2, at voltage of -20 kV for 15 s	(Qiu et al., 2007)
PP	175	Stretching filler-loaded PP followed by biaxial stretching	Dynamic	Corona charging	(Anton et al., 2014)

Acknowledgment

Financial support from the Natural Sciences and Engineering Research Council of Canada (NSERC) and Fonds Québécois de la Recherche sur la Nature et les Technologies (FRQNT) was received for this work.

Chapter 4

Effect of processing conditions on the cellular morphology of polypropylene foamed films for piezoelectric applications

Abolfazl Mohebbi, Frej Mighri, Abdellah Ajji, Denis Rodrigue, *Cellular Polymers*, **Accepted** (2016).

Résumé

Dans ce travail, l'extrusion-calandrage en continu a été utilisée pour produire des films moussés en polypropylène (PP) pour des applications piézoélectriques. La production est basée sur un moussage physique en utilisant de l'azote supercritique (SC-N2) et le carbonate de calcium ($CaCO_3$) comme agent de nucléation. En particulier, les paramètres d'extrusion (conception des vis, profil de température, concentration d'agent gonflant et de nucléation) et les conditions de post-extrusion (température de calandrage et de vitesse d'étirage) ont été optimisées pour obtenir une structure cellulaire spécifique (oculaire) avec une distribution uniforme de la taille des cellules. La morphologie dans les deux directions (machine et transversale), ainsi que les propriétés de traction ont été caractérisées. Les résultats montrent qu'une structure cellulaire ayant un rapport d'aspect supérieur pour les cellules mène à un module de Young inférieur, ce qui est approprié pour les films cellulaires piézoélectriques. En général, la morphologie de la mousse développée présente un fort potentiel pour la production de films ferroélectrets à base de PP pour une utilisation dans différentes applications piézoélectriques.

Abstract

In this work, continuous extrusion-calandering was used to produce polypropylene (PP) foam films for piezoelectric applications. The setup is based on physical foaming using supercritical nitrogen (SC-N_2) and calcium carbonate ($CaCO_3$) as nucleating agent. In particular, the extrusion parameters (screw design, temperature profile, blowing agent and nucleating agent content) and post-extrusion conditions (calendaring temperature and speed) were optimized to achieve a specific stretched eye-like cellular structure with uniform cell size distribution. The morphology in both machine and transverse directions, as well as tensile properties were characterized. The results show that a cellular structure with a higher cell aspect ratio has a lower Young's modulus, which is appropriate for piezoelectric cellular films. Generally, the developed foam morphology presents high potential for the production of ferroelectret PP films used in different piezoelectric applications.

4.1 Introduction

Thermoplastic foams are materials composed of a thermoplastic polymer matrix as the continuous phase and gas bubbles as the dispersed phase (Mohebbi et al., 2015). This cellular structure can be produced by using chemical or physical blowing agents. The latter, generally based on inert gases has several advantages such as chemical inertness, non-toxicity, and non-flammability (Eckert, 1996; Sauceau et al., 2007; Zirkel et al., 2009). Thermoplastic foams are widely used for food packaging, acoustic, automotive parts, and thermal insulation applications (Kumar, 1993; Nofar et al., 2012; Okolieocha et al., 2015; Suh et al., 2000). This wide range of applications are related to their lightweight, high strength to weight ratio, excellent insulation property (Colton and Suh, 1987; Klempner and Frisch, 1991), high impact strength and toughness (Collais and Baird, 1995), high fatigue life (Seeler and Kumar, 1993), low cost, and easy processing (Okolieocha et al., 2015). During the last decades, polymeric foams have been considered as good candidates for piezoelectric applications (Anton et al., 2014; Fang et al., 2007).

Piezoelectric materials are able to convert electric or magnetic field into a mechanical deformation and vice versa. After charging by an appropriate method such as corona discharge, cellular nonpolar polymers like polypropylene (PP), can exhibit piezoelectric-like behavior (Fang et al., 2008; Gilbert-Tremblay et al., 2012; Kirjavainen, 1987; Qaiss et al., 2012; Savolainen and Kirjavainen, 1989; Wegener, 2010; Wegener et al., 2005), often called "ferroelectret" (Lindner et al., 2004; Tuncer, 2005). During this process, positive and negative electrical charges are created on the opposite faces of each cell surface making them piezoelectric materials (Qiu et al., 2013). Ferroelectret materials are currently under investigation for several applications such as actuators, vibration control, ultrasonic transducers, tactile sensors, energy conversion devices, speakers, microphones, keyboards, shock sensors, as well as thermal and optical property measurement devices (Mohebbi et al., 2016). PP is known to have excellent properties such as low material cost, high service temperature (Antunes et al., 2010; Yu et al., 2011; Zhang et al., 2009), high tensile modulus as well as excellent chemical resistance (Vasile and Seymour, 1993). However, PP foaming was found to be limited because of its low melt strength (Burt, 1978; Park and Cheung, 1997; Yu et al., 2011; Zhai et al., 2010), poor cell nucleation behavior (Zhai et al., 2008), and very

narrow foaming temperature window (Huang and Wang, 2007; Xu et al., 2007; Yu et al., 2011). Most of the challenges and solutions related to PP foaming were extensively discussed in our previous work (Mohebbi et al., 2015).

For piezoelectric applications, in addition to cell density and cell size, cell shape and cell orientation are also important parameters (Li et al., 2012). To achieve good piezoelectric properties, it is important to produce a film having an eye-shaped cellular structure (Lindner et al., 2004; Tuncer, 2005; Xu et al., 2013). So far, different methods, such as stretching (Anton et al., 2014; Hillenbrand et al., 2005; Qiu et al., 2007; Zhang et al., 2004), closed mold (Zhang et al., 2006), and thermoforming (Altafim et al., 2006), have been used to produce such cellular structure. However, these methods are batch (discontinuous) and are not very efficient in terms of industrial production (low rates). So the main objective of this work is to produce, in a continuous form, an appropriate cellular structure inside a PP film. To achieve this goal, an extrusion-calendaring foaming process was developed. Depending on the cellular structure sought (uniform distribution of eye-like shape cells), an optimization of the processing conditions must be made (Gendron, 2004; Lee, 2000; Okolieocha et al., 2015).

4.2 Experimental investigation

4.2.1 Material used

For this work, polypropylene HP 3462 (Total Petrochemicals, USA) with a density of 0.905 g/cm^3 and a MFI of 4.1 g/10 min (230°C at 2.16 kg) was used as the matrix, while nitrogen (N_2) (purity of 99.999% from Praxair, Canada) was selected as the physical blowing agent. Nano-calcium carbonate ($CaCO_3$) Ultra-Pflex A-1-194-11 (Specialty Minerals Inc., USA) with an average particle size of 70 nm was added as a nucleating agent.

4.2.2 Foaming process

It is known that saturated polymers with inert gases in their supercritical state followed by a rapid pressure drop (rapid thermodynamic instability) results in the creation of a large number

of nuclei (nucleation), which can grow to produce microcellular foams (Mohebbi et al., 2011). Supercritical fluids (SCF), as a result of their low viscosity and negligible surface tension, have high mass transfer rates into polymers (Li et al., 2002). Carbon dioxide (CO_2) and nitrogen (N_2) are the most commonly used SFC. It is also known that heterogeneous nucleation is more effective than homogeneous (neat polymer) nucleation (Mohebbi et al., 2015). The presence of well dispersed nucleating sites using a suitable nucleating agent in the polymer matrix can substantially improve cell density and reduce cell size, leading to improved structure uniformity (Mohebbi et al., 2011).

Physical foaming was performed through continuous extrusion on a Leistritz ZSE18HP co-rotating twin-screw extruder (diameter = 18 mm and length/diameter = 40). A slit-die (15 cm in width and 0.5 mm in thickness) and a three-roll calendaring system (roll diameter and length are 15 cm and 20 cm, respectively) were used to produce the foamed PP films. Roll temperature was set at 40°C. The extruder used has nine temperature zones including the die and the optimum temperature profile from the feeding zone to the die was: 180, 180, 185, 185, 185, 180, 180, 180, and 167°C. The screw speed was set at 260 rpm and a constant flow rate of 1.14 kg/h was used. Supercritical conditions for N_2 are P_C = 3.4 MPa and T_C = 126 K (Zong and Yang, 2006). In this work, a stream of N_2 gas with a pressure of 7 MPa was injected in zone 2 of the extruder. A precise mass flow meter/controller model F-201CV-5K0-ABD-22-V (Hoskin Scientific Co., USA) with an accuracy of 1 ml/min was used to control the flow rate. The complete extrusion setup is presented in Figure 4.1.

To achieve cellular PP films having good eye-like cellular morphology, suitable for good piezoelectric properties (Lindner et al., 2004; Tuncer, 2005; Xu et al., 2013), the samples were uniaxially stretched between the die exit and the first roller of the calendar (distance of 10 cm). After some processing and composition optimization such as temperature profile, screw configuration, die temperature, SC-N_2 flow rate, and stretching speed, different foamed PP films with and without nucleating agent, were produced. Sample specifications are presented on Table 4.1.

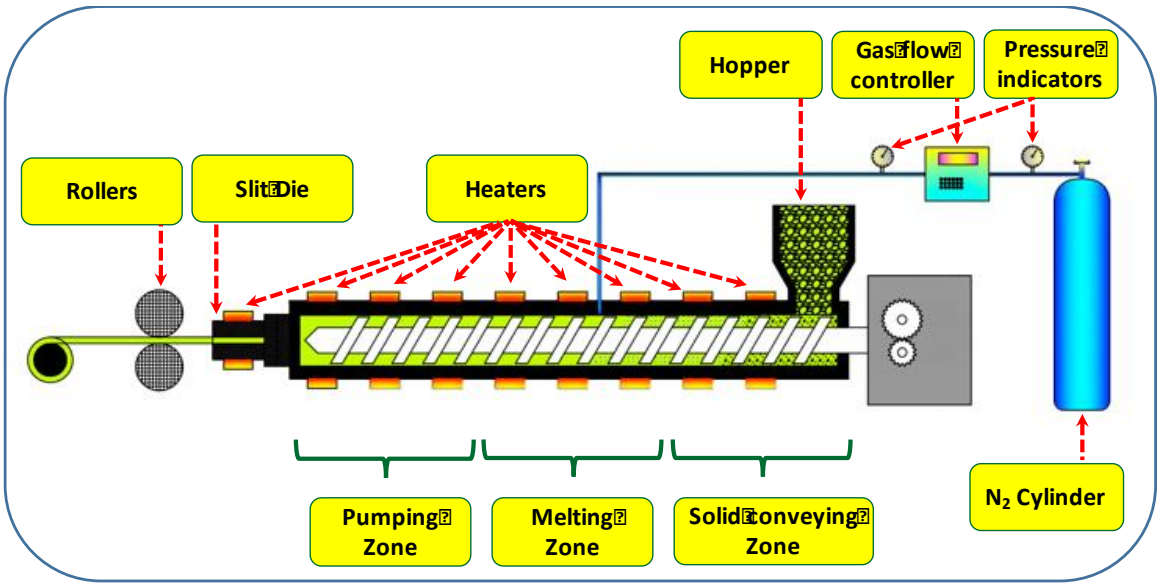

Figure 4.1. Foaming process setup used to produce thin PP foamed films.

Table 4.1. Specifications of the foamed PP films studied.

Sample code	Uniaxial stretching speed (cm/min)	Die temperature (°C)	Nucleating agent ($CaCO_3$) (% wt.)
PP-S1	30	167	0
PP-S2	45	167	0
PP-S3	60	167	0
PP-S4	45	160	0
PP-S5	45	174	0
PPn-S1	45	167	2
PPn-S2	45	167	4

4.3 Morphological characterization

For morphological analyses, a scanning electron microscopy (SEM) JEOL JSM 840A was used. The samples were first frozen in liquid nitrogen and broken in the machine (longitudinal, L) and transverse (T) directions, and then coated with Pd/Au. Based on the pictures obtained, cell shape, cell size, cell densities, and sample thickness were analyzed using the *ImageJ* (National Institute of Health, USA) software. Because of cell deformation from stretching, cell density was calculated as (Gosselin and Rodrigue, 2005):

$$N = N_1(N_2)^{1/2} \tag{4.1}$$

where N_1 and N_2 are cell densities in the machine and transverse directions, respectively, calculated as:

$$N_i = \frac{n}{A} \tag{4.2}$$

where n and A are the number of cells and area of the micrograph, respectively.

Density was measured by a Quantachrome Ultrapyc 1200e gas pycnometer (with nitrogen). The values reported on Table 4.2 are based on five samples.

4.4 Mechanical properties characterization

The tensile properties of the samples were characterized using an Instron universal testing machine, model 5565 (Instron, USA) with a 500 N load cell. The tests were performed at room temperature according to ASTM D882. A crosshead speed of 50 mm/min was used. The values reported for Young's modulus, tensile strength, and elongation at break are based on averaging at least five samples.

4.5 Thermal stability characterization

Thermogravimetric analysis (TGA) was used to investigate the thermal stability of the samples and also to confirm particle content for samples having nucleating agents. The tests were performed using a TGA Q5000 IR (TA Instruments, USA) in nitrogen at a heating rate of 10°C/min from 50 to 650°C.

4.6 Results and discussion

4.6.1 Effect of processing parameters on the quality of the foamed films

The production of thin-foamed PP films with a good eye-like cellular morphology, suitable for good piezoelectric properties (Lindner et al., 2004; Tuncer, 2005; Xu et al., 2013), has several challenges, briefly reviewed on Figure 4.2.

a) Unfoamed PP film: A uniform PP film was first produced through this setup and, as shown on Figure 4.2-a). The film was initially transparent.

b) Foamed PP film using N_2 under its supercritical state (Figure 4.2-b): When N_2 was introduced at low pressure (below its supercritical state), large and poorly distributed cells in the range of 2 to 3 mm were obtained. Since the film is expected to be thin (less than 500 μm), this was not suitable to produce a uniform cellular structure. Hence, pressure was increased to reach the supercritical state.

c) Foamed PP film using SC-N_2: As shown on Figure 4.2-c, high N_2 pressure led to the production of a better foamed PP film (opaque region) having smaller cell sizes. However, the foamed structure was not homogeneous mostly because of non-homogeneous N_2 saturation into the PP matrix. A proper screw configuration was designed to improve gas dispersion/distribution (Figure 4.3).

d) Foamed PP film using a proper saturation of SC-N_2: Since the thickness of the PP film is quite low, a very small variation in N_2 flow rate resulted in die pressure variation. As seen on Figure 4.2-d, this led to periodic bubble rupturing and an accumulation of melt after the die exit leading to samples having a non-uniform surface. This was avoided by a precise control of SC-N_2 flow rate using a mass flow meter/controller with an accuracy of 1 ml/min.

e) Foamed PP film using a proper saturation of SC-N_2 well above the optimum foaming temperature (Figure 4.2-e): The foaming temperature is known as one of the most important parameters affecting the final properties of foamed polymers. Increasing foaming temperature improves bubble growth (Mohebbi et al., 2011), but a too high temperature can lead to cell collapse (Huang and Wang, 2007; Xu et al., 2007). The presence of a narrow foaming temperature for PP, as reported by several researchers (Huang and Wang, 2007; Xu et al., 2007; Yu et al., 2011), was another important challenge in this work. As seen on Figure 4.2-e, increasing the foaming temperature from 167 to 177°C led to obvious collapse of the film. For our conditions, a very narrow temperature range leading to good cellular films was also observed: 167±4°C. This will be discussed extensively in the following section.

f) Foamed PP film using a proper saturation of SC-N_2 at the optimum foaming temperature (Figure 4.2-f): A uniform foamed PP film with a thickness of less than 500 μm can be produced using the optimum processing conditions (die temperature of 167°C).

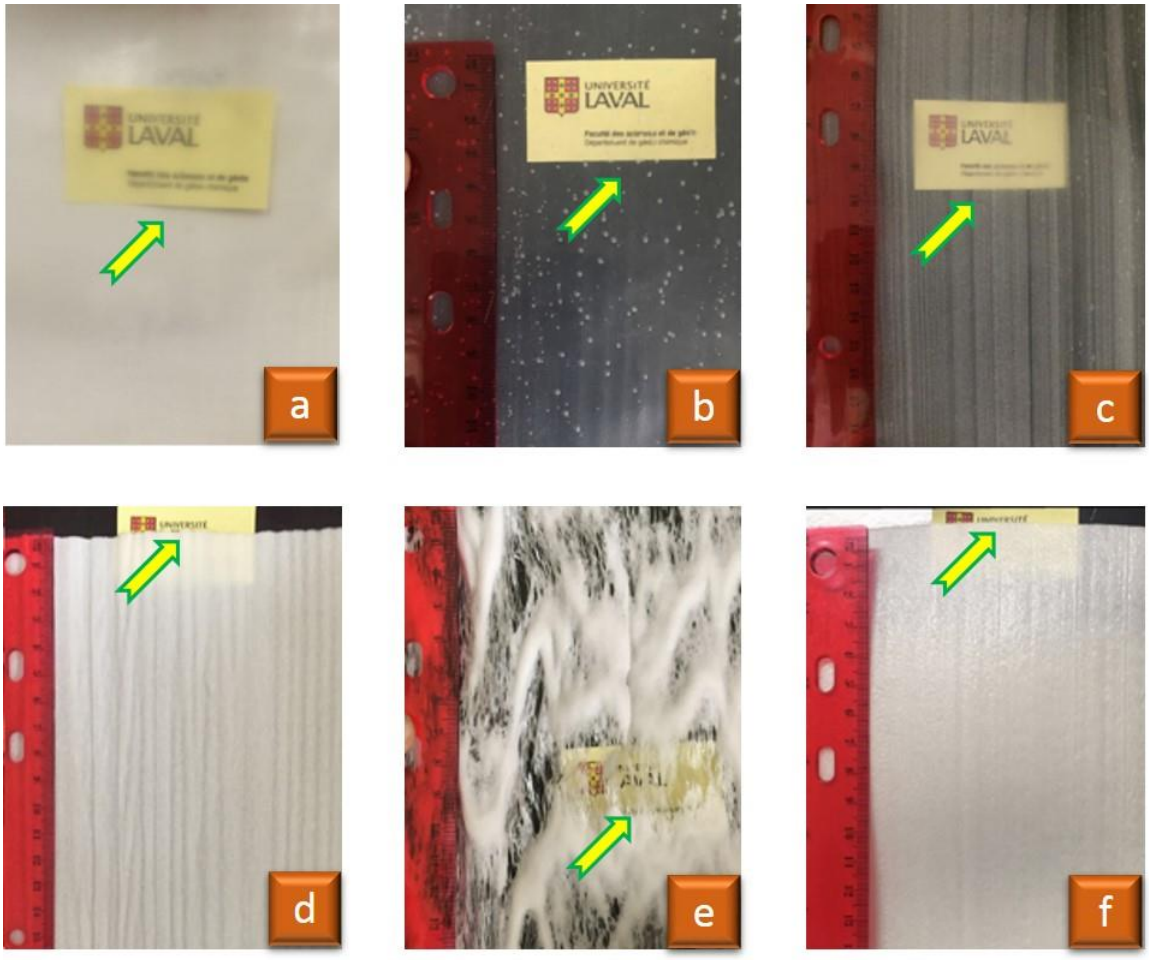

Figure 4.2. General overview of the foams through the optimization steps described: **a)** unfoamed PP film, **b)** foamed PP film using low N_2 (2 MPa), **c)** foamed PP film using SC-N_2 (7 MPa), **d)** foamed PP film using a proper saturation of SC-N_2 (7 MPa), **e)** foamed PP film using a proper saturation of SC-N_2 (7 MPa) with a die temperature of 177°C, and **f)** foamed PP film using a proper saturation of SC-N_2 (7 MPa) with a die temperature of 167°C.

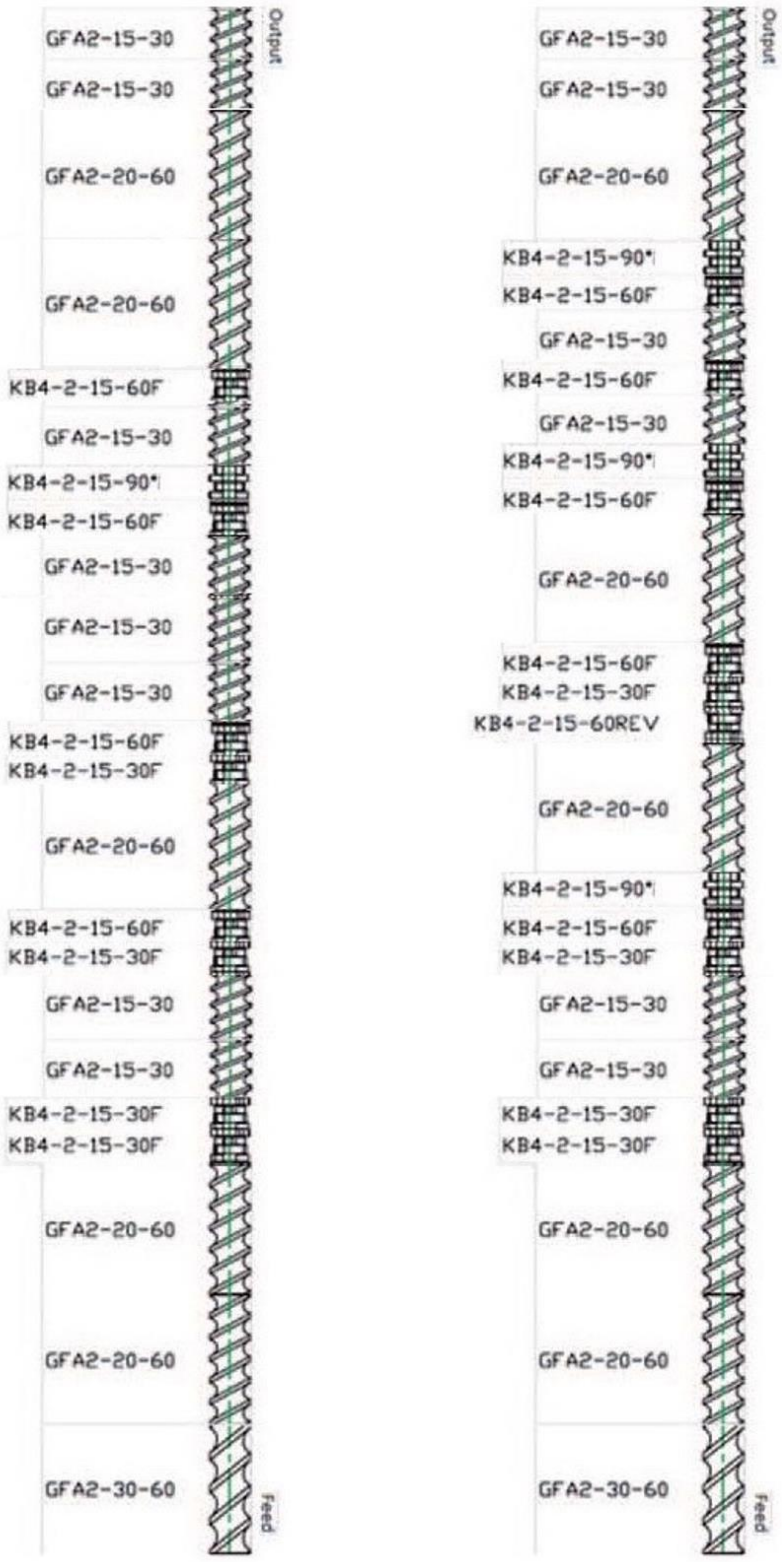

Figure 4.3. Schematic representation of the initial (left) and optimized (right) extruder screw configurations.

4.6.2 Optimization of the foaming process

As reported in the literature that a thin cellular film having eye-shaped cells with an aspect ratio (*AR*) above 4 ($4 < AR < 10$ [23]) is the best structure for good piezoelectric properties (Lindner et al., 2004; Tuncer, 2005; Xu et al., 2013). Here, the effect of processing parameters on the final properties of the foamed PP films is presented. The results of the morphological analyses for all the samples based on their typical SEM images (Figure 4.4, Figure 4.6 and Figure 4.8) are reported on Table 4.2. These results are systematically discussed, including mechanical properties, for the processing conditions described on Table 4.1.

Table 4.2. Morphological properties of the foamed PP films studied.

Sample code	Density (g/cm^3)	Film thickness (μm)	Cell aspect ratio (*AR*)	Cell size in L-direction (μm)		Cell size in T-direction (μm)		Cell density (10^5 cells/cm^3)
				Major	Minor	Major	Minor	
PP-S1	0.737 ± 0.012	657 ± 51	3.7 ± 1.4	147 ± 67	41 ± 15	53 ± 33	34 ± 21	4.7 ± 1.3
PP-S2	0.712 ± 0.007	586 ± 19	4.9 ± 1.5	161 ± 86	33 ± 15	55 ± 35	32 ± 16	4.2 ± 1.5
PP-S3	0.708 ± 0.005	531 ± 55	6.1 ± 2.4	163 ± 80	28 ± 12	55 ± 29	33 ± 15	3.9 ± 0.9
PP-S4	0.738 ± 0.015	526 ± 50	2.7 ± 0.7	81 ± 37	32 ± 14	52 ± 21	33 ± 13	4.1 ± 0.5
PP-S5	0.706 ± 0.004	602 ± 77	4.7 ± 2.0	157 ± 87	35 ± 19	54 ± 27	38 ± 20	3.1 ± 0.5
PPn-S1	0.707 ± 0.003	483 ± 13	5.4 ± 1.0	171 ± 55	31 ± 8	57 ± 23	37 ± 15	6.5 ± 0.8
PPn-S2	0.720 ± 0.009	540 ± 41	3.8 ± 1.3	158 ± 76	43 ± 21	84 ± 39	51 ± 24	2.9 ± 0.7

4.6.2.1 Effect of stretching speed

Typical SEM images in the machine (L) and transverse (T) directions for samples produced with different stretching speeds and a constant die temperature of 167ºC are presented on Figure 4.4. As shown, increasing the stretching speed from PP-S1 to PP-S3 led to a more elongated cellular structure with higher *AR* values. However, further increase in stretching speed for PP-S3 resulted in some defects and non-uniform cellular structure. Their corresponding Young's modulus, tensile strength, and elongation at break are presented on Figure 4.5 where they are also compared with unfoamed PP. *AR* values are also presented on Figure 4.5. Table 4.2 clearly indicates that the densities of these samples are much lower (up to 22%) than those of the unfoamed PP film (0.905 g/cm^3), which confirms that good foaming occurred.

When the stretching speed was 30 cm/min (PP-S1), the corresponding *AR* was below the target value. By increasing the stretching speed to 45 cm/min (PP-S2), and to 60 cm/min (PP-S3), the *AR* respectively increased up to about 4.9 and 6, respectively. However, as shown on Figure 4.4, some defects (highlighted by arrows) occurred as a result of high stretching. Besides, from a mechanical point of view, Figure 4.5 shows that increasing the stretching speed leads to a lower modulus, lower strength, and also lower elongation at break, associated to higher *AR* values. In particular, PP-S2 has an elongation at break of only 5.5%, 20% less than PP-S1 (about 7%). Although PP-S3 has a lower Young's modulus than PP-S2, associated to the presence of defects, this film is not suitable for piezoelectric cellular applications. Furthermore, it is clear that foaming (creation of a cellular structure) results in lower elongation at break. The unfoamed PP has an elongation at break above 400%, while all the foamed samples are below 7%. Nevertheless, PP films for piezoelectric applications are mainly used under small deformation and this is not a major limitation. But tensile modulus and tensile strength are also lower compared to the unfoamed PP.

It was reported in the literature that the charging capacity of eye-like cellular structures increases as *AR* increases, while Young's modulus decreases (Hillenbrand et al., 2005; Zhang et al., 2007; Zhang et al., 2011; Zhang et al., 2009; Zhang et al., 2014), whereas a circular cell shape (low *AR* value) would results in higher elastic stiffness, not suitable for piezoelectric films (Wegener, Wirges, et al., 2005). This concept has been extensively

discussed in our previous work (Mohebbi, et al., 2016). Based on the results obtained, a stretching speed of 45 cm/min (PP-S2) was selected to optimize the other processing conditions.

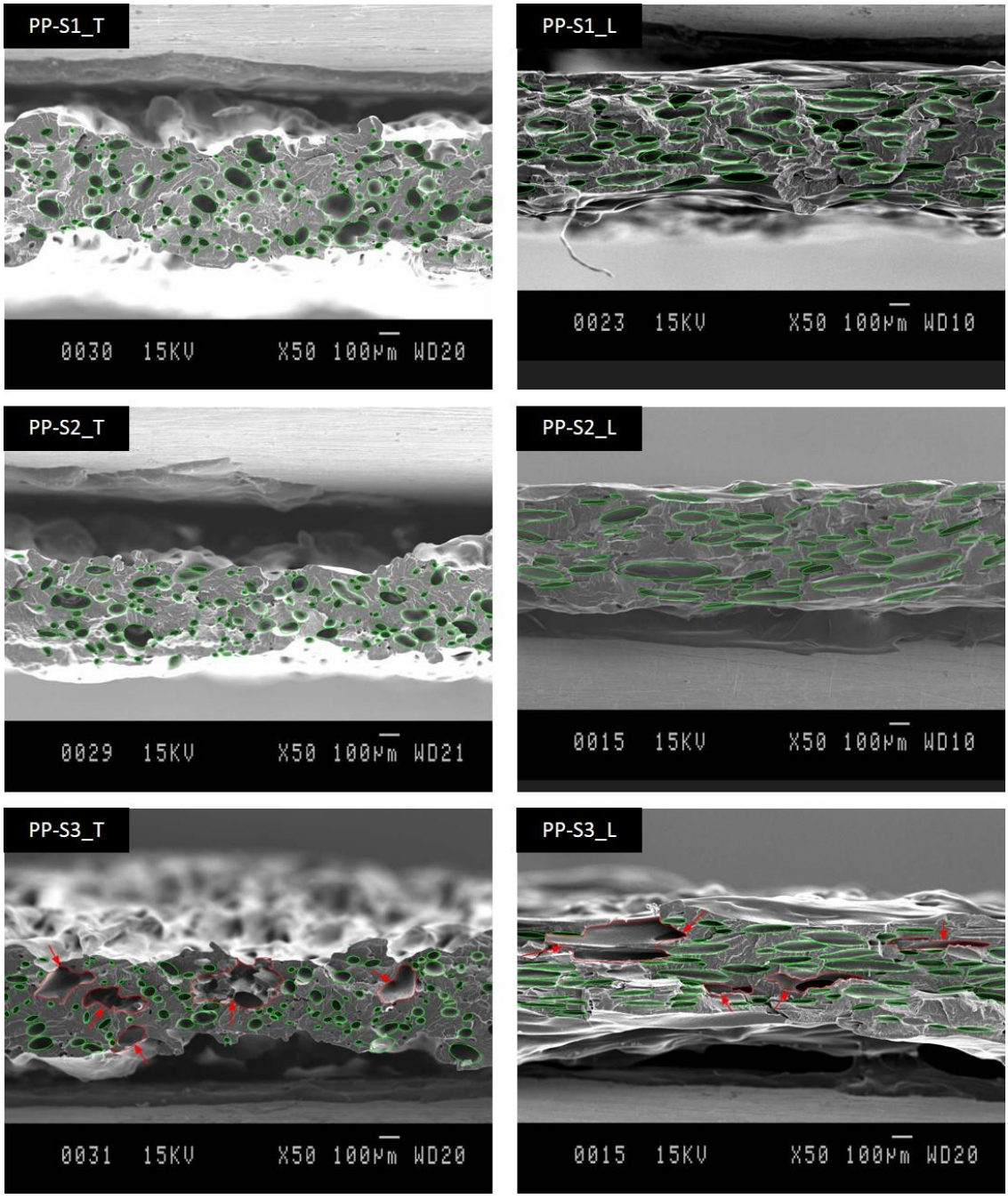

Figure 4.4. Typical SEM pictures of the foamed PP samples produced at different stretching speed: Machine (right column) and transverse (left column) directions.

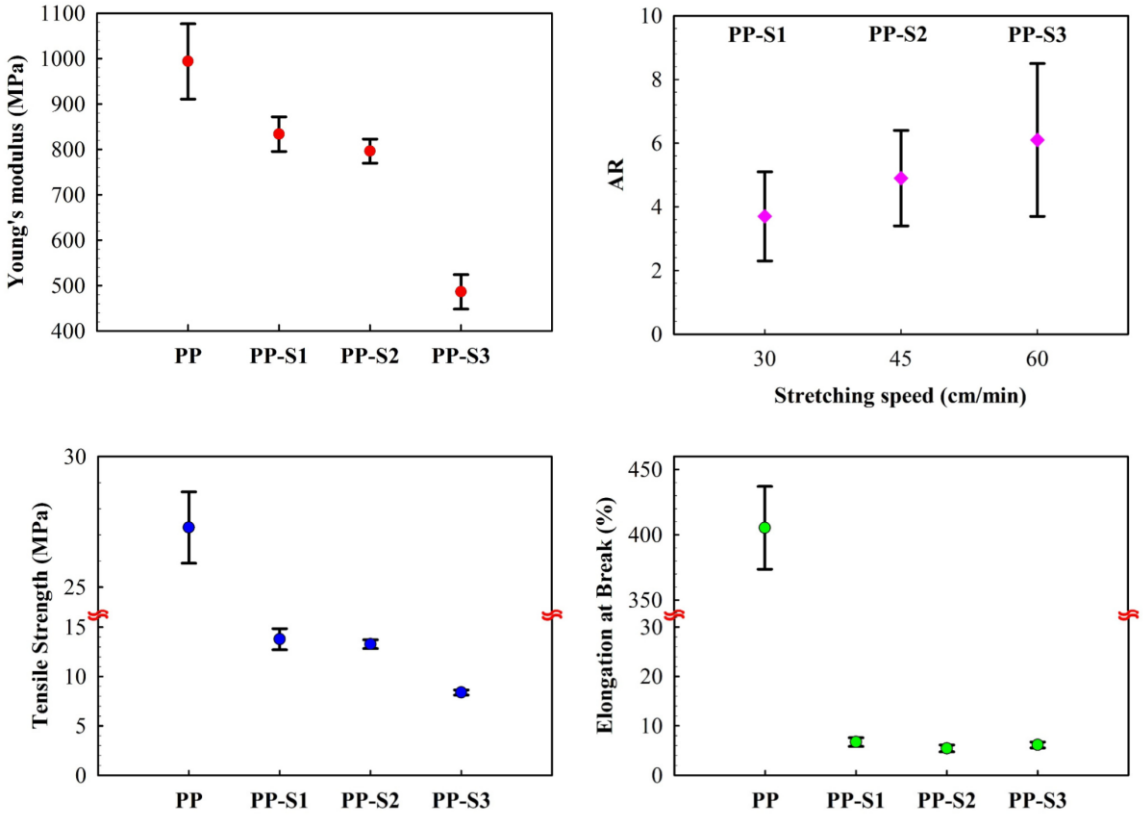

Figure 4.5. Young's modulus, tensile strength, elongation at break, and *AR* value (machine direction) of the samples produced with different stretching speed.

4.6.2.2 Effect of die temperature

Based on the results of the previous section, PP-S2 (stretching speed of 45 cm/min and die temperature of 167°C) was selected and compared with two other new samples (PP-S4 and PP-S5) produced at different die temperatures. As reported earlier, PP has a very narrow foaming temperature window of about 2 to 4°C (Huang and Wang, 2007; Xu et al., 2007; Yu et al., 2011). Hence, to determine the optimum die temperature, the temperature range to study becomes very narrow. But a variation of ±4°C from 167°C was found to produce similar results, and this is why the findings are not presented. So a variation of ±7°C: PP-S4 at 160°C and PP-S5 at 174°C was selected. Figure 4.6 presents typical SEM images of both samples in the machine (*L*) and transverse (*T*) directions. The corresponding tensile behavior including Young's modulus, tensile strength, and elongation at break are reported on Figure 4.7, together with their *AR* values.

For a die temperature of 160°C (PP-S4), the *AR* was 2.7, which is well below the target value for piezoelectric cellular films. Moreover, as reported on Table 4.2, the major cell size in the L-direction of PP-S4 is 81 μm, which is about 50% lower than that of PP-S2 (161 μm) produced with a die temperature of 167°C. This is expected since lower temperature leads to higher viscosity/melt strength making the materials more difficult to stretch and limiting cell growth (Huang et al., 2008). Another effect is the higher density of PP-S4 (0.738 g/cm^3) compared to that of PP-S2 (0.712 g/cm^3). But as seen on Figure 4.4 (for PP-S2) and Figure 4.6, increasing the die temperature from 167°C (PP-S2) to 174°C (PP-S5) resulted in a highly inhomogeneous open-cell structure with cell coalescence and collapse, as highlighted by arrows in the L and T directions. This effect is related to the low viscosity and melt strength at high temperature leading to poor bubble growth stabilization (Mohebbi et al., 2011). Hence, PP-S4 cannot be a good choice for piezoelectric cellular films.

On the other hand, form a mechanical point of view, increasing the die temperature resulted in associated properties to increase *AR* values. (Figure 4.7). From Figure 4.7, shows that the tensile properties of PP-S2 (*AR* = 4.9) are lower than PP-S4 (*AR* = 2.7). The results indicate that a cellular structure with a higher cell aspect ratio (PP-S2) has lower Young's modulus. Moreover, even PP-S5 (the same as PP-S3 in previous section, with high stretching rate) has a lower Young's modulus than PP-S2, but this is caused by the presence of defects in its structure. These failures led to a non-uniform cellular structure, which is not suitable for piezoelectric cellular films. Based on the results obtained, a stretching speed of 45 cm/min and a die temperature of 167°C were selected for further optimization.

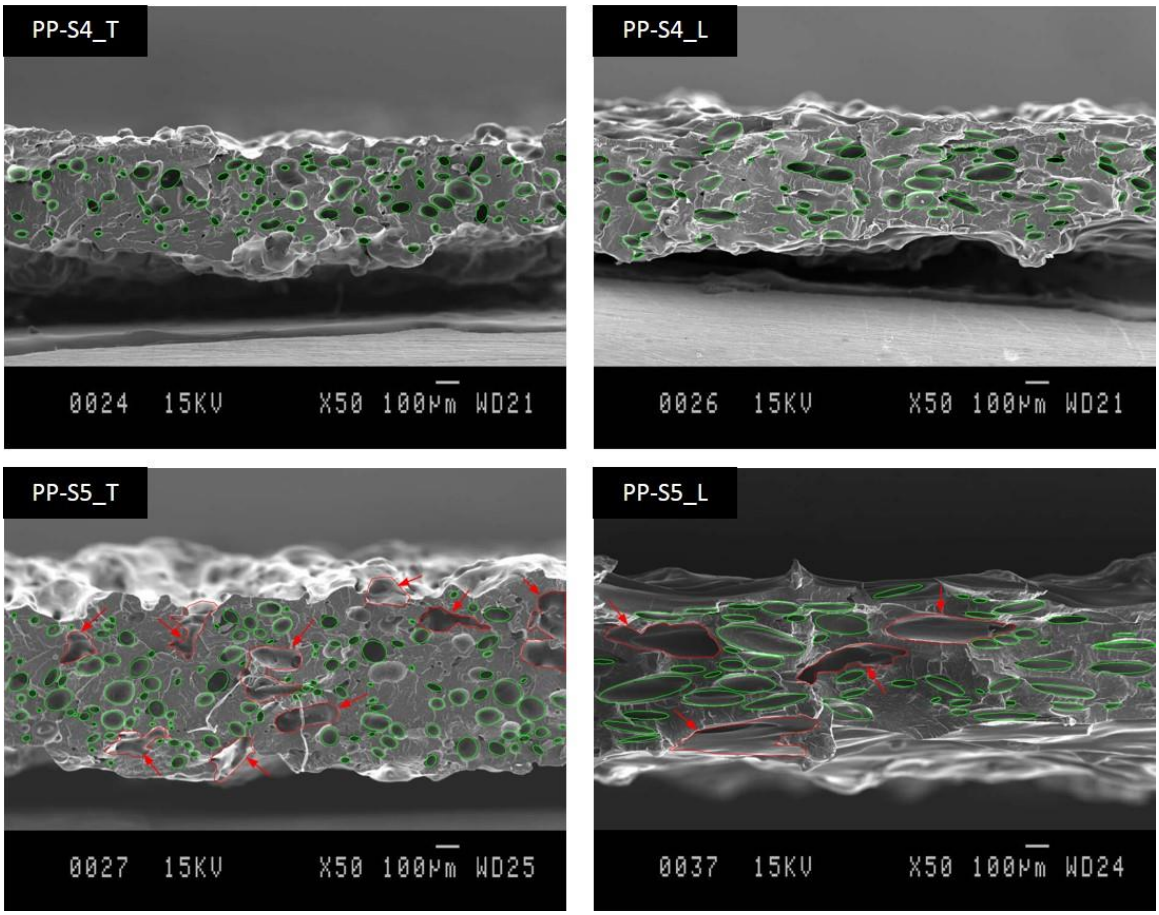

Figure 4.6. Typical SEM pictures of the foamed PP samples produced with different die temperature: Machine (right column) and transverse (left column) directions.

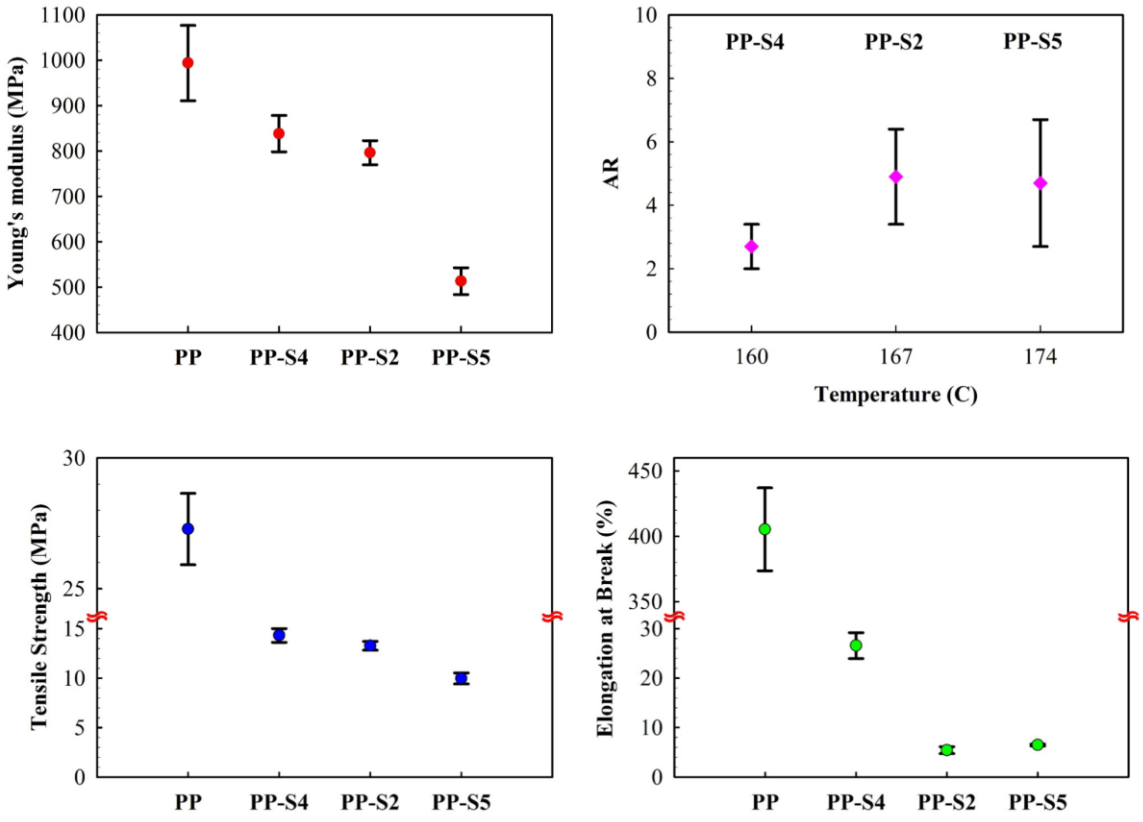

Figure 4.7. Young's modulus, tensile strength, elongation at break, and *AR* value (machine direction) of the samples produced at different die temperatures.

4.6.2.3 Effect of nucleating agent

In the previous sections, the optimum conditions for the stretching speed and die temperature were determined, and PP-S2 was selected as the best sample. Here, the sample morphology was improved using $CaCO_3$ as a nucleating agent. For this reason, two different weight concentrations of nano-$CaCO_3$ were used: 2% (PPn-S1) and 4% (PPn-S2). It should be mentioned that adding 1% nucleating agent was also performed, but the results were similar to 2%, so they are not presented.

Typical SEM images of PPn-S1 and PPn-S2 in both machine (*L*) and transverse (*T*) directions are presented on Figure 4.8, while their corresponding tensile behavior and *AR* values are presented on Figure 4.9.

As reported on Figure 4.4 (for PP-S2) and Figure 4.8, as well as on Table 4.2, the addition of 2% of nucleating agent (PPn-S1) not only increased the *AR* to 5.4, but also led to a more uniform cell size distribution (lower standard deviation). PPn-S1 has a major cell size in the L direction of 171 μm with a standard deviation of 55 μm, compared PP-S2 which has a major cell size in the L-direction of 161 μm and a SD of 86 μm. This indicates the effectiveness of the nucleating agent to improve the cell size distribution, but also to increase the cell density from 4.2 to $6.5x10^5$ cells/cm^3 (over 50% increase). So a better foam structure (in terms of homogeneity and values) was produced. As seen on Figure 4.8, increasing the nucleating agent content from 2% (PPn-S1) to 4% (PPn-S2) led to the creation of a non-uniform cell structure. Also, PPn-S2 has an *AR* value of 3.8, which is below the lowest *AR* value of 4 to achieve good piezoelectric properties. This is most probably the result of particle agglomeration at high nanoparticle concentration. Furthermore, as reported on Table 4.2, among all the samples, PPn-S1 has the lowest density (0.707 g/cm^3) indicating efficient foaming: as more cells are rapidly created, the blowing agent is consumed faster to produce the cellular structure with less gas losses.

From a mechanical point of view, Figure 4.9 shows that among all the samples, PSn-S1 has the lowest Young's modulus (600 MPa). Furthermore, PSn-S1 in comparison with the other samples, has the lowest strength (10 MPa) and elongation at break (5%).

The particle content of PPn-S1 and PPn-S2 were investigated by TGA. Figure 4.10 and Figure 4.11 show the results for these samples in contrast to PP. From TGA plots (Figure 4.10), it is clear that above 460°C PP is completely degraded while the curves of PPn-S1 and PPn-S2 decreased to close to 2% and 4%, respectively. This confirms that PPn-S1 and PPn-S2 contain respectively about 2% and 4% of nucleating agent ($CaCO_3$), which was the only inorganic material used in their production. Furthermore, T_{10} (the temperature for 10% mass loss) for PP, PPn-S1, and PPn-S2 is 388, 400, and 404°C, respectively. Therefore, the presence of nano-$CaCO_3$ not only improved the cell density and cell uniformity, but also the thermal stability of the films. In addition, from the derivative of the thermogravimetric curves (DTGA) (Figure 4.11), the maximum decomposition temperature ($T_{max.\,dec}$) was obtained; i.e. the temperature at which the rate of thermal decomposition is maximum. DTGA plots

indicate slight increases in $T_{max.\ dec}$ from 436°C for neat PP to 438°C for samples with nucleating agent.

Hence, the results show that to produce a thin (less than 500 μm) cellular PP film with eye-like cellular structure, a sample containing 2% nano-$CaCO_3$ foamed at a die temperature of 167°C and uniaxially stretched at 45 cm/min (PPn-S1) is more suitable and thermally stable for piezoelectric applications. However, PP-S2, the optimum sample using neat PP, can be used to compare the piezoelectric behavior with PPn-S1. Furthermore, PP-S1, with a lower *AR* value (3.7), but very close to the lowest *AR* value of 4 for piezoelectric applications, has a cell density similar to PP-S2 and could probably be used for piezoelectric cellular films.

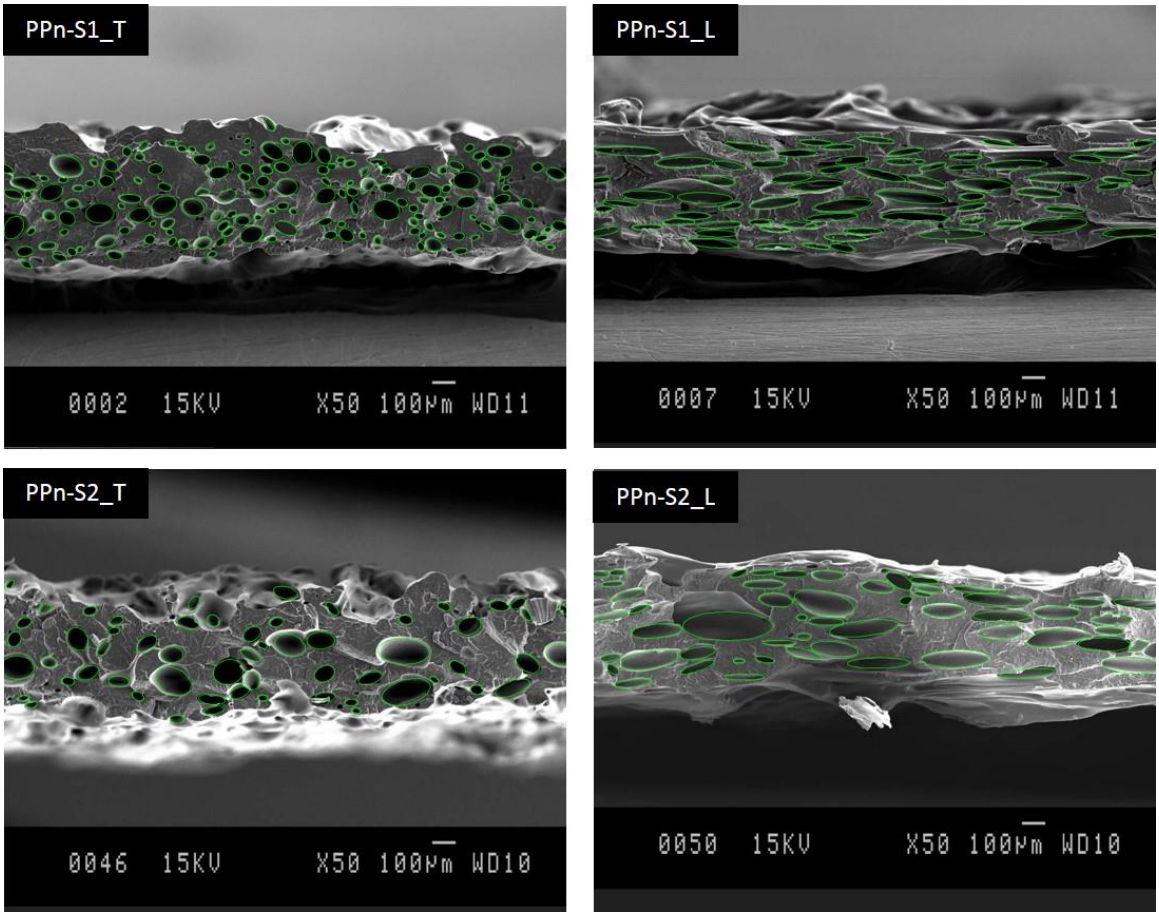

Figure 4.8. Typical SEM pictures of the foamed PP samples produced with different nucleating agent contents: Machine (right column) and transverse (right column) directions.

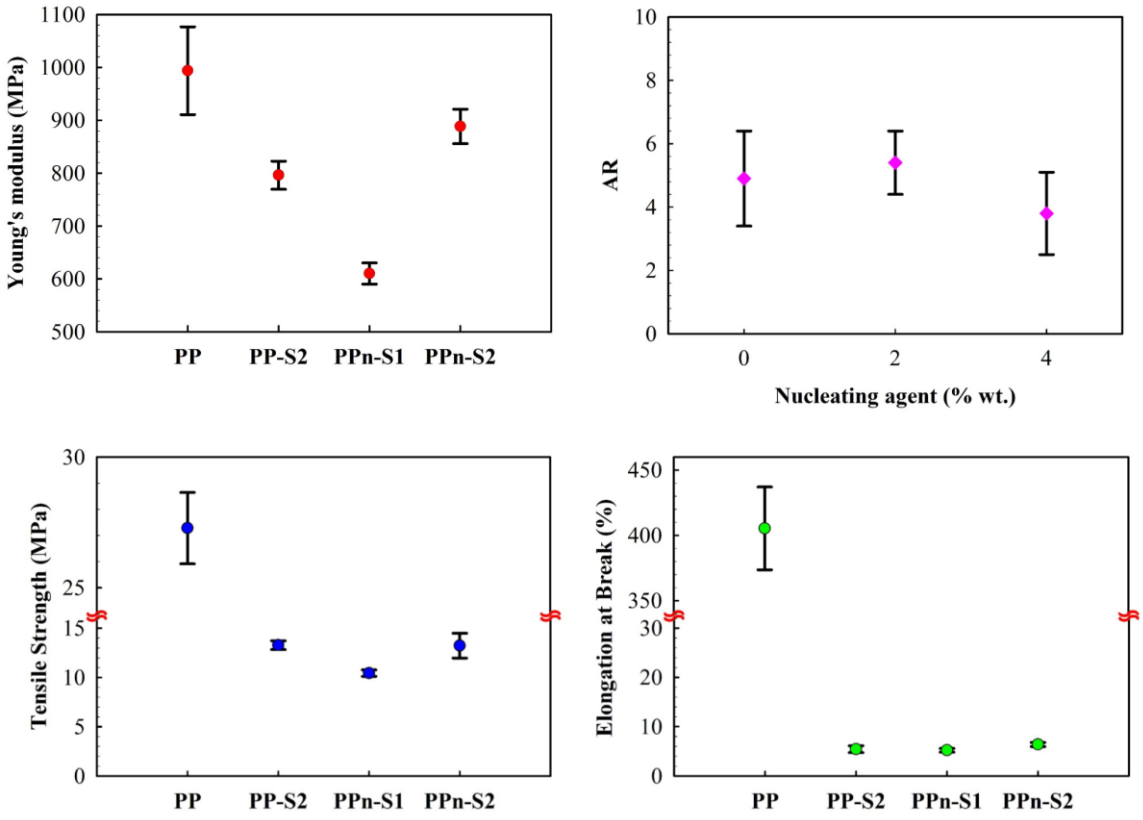

Figure 4.9. Young's modulus, tensile strength, elongation at break, and *AR* value (machine direction) of the samples produced with different nucleating agent content.

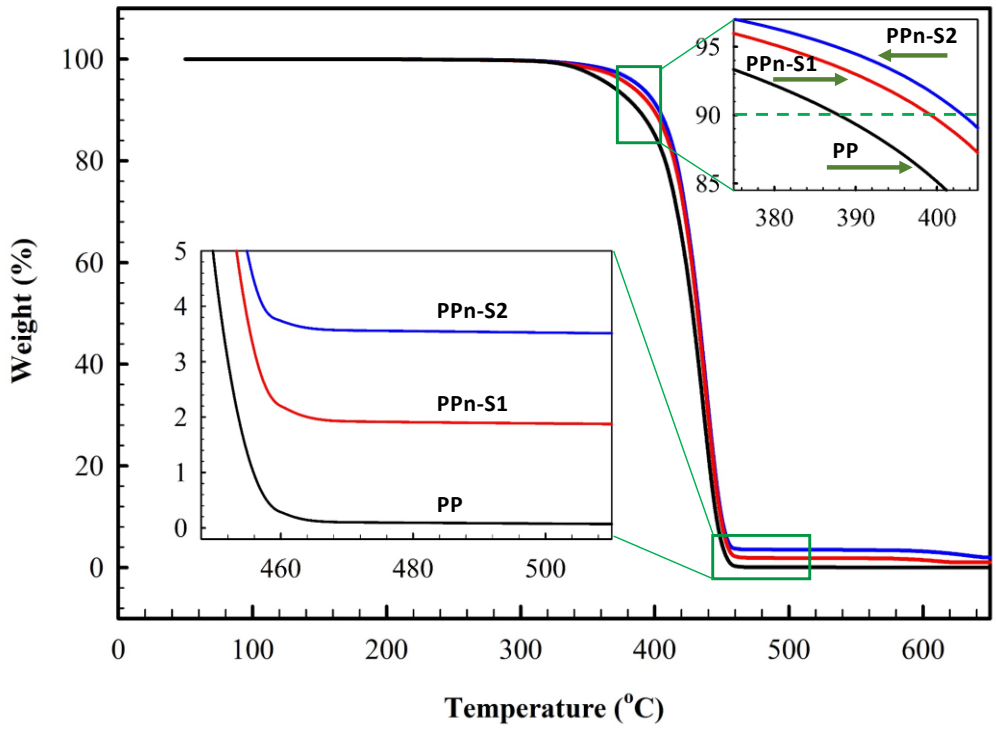

Figure 4.10. TGA plots of PPn-S1 and PPn-S2 compared to neat PP.

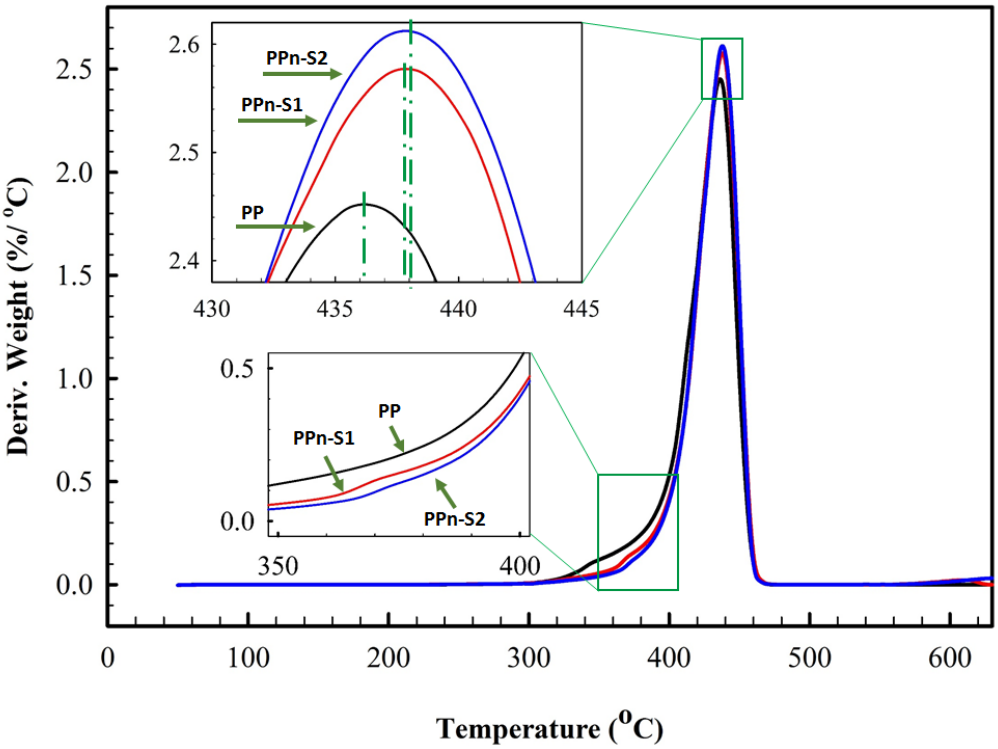

Figure 4.11. DTGA plots of PPn-S1 and PPn-S2 compared to neat PP.

4.7 Conclusion

Considering that cellular polypropylene films can be tailored to get a good morphological structure needed for piezoelectric films, this study investigated the processing conditions to produce a uniform eye-shaped cellular structure for PP film thickness lower than 500 μm. This was possible by using a low cost physical foaming agent (supercritical nitrogen) and extrusion-calendaring.

The results showed that PP has a very narrow foaming temperature window of 167±4°C. By increasing the die temperature outside this range, open-cells were formed and a non-uniform cell structure was obtained, while decreasing the foaming temperature below this optimum range resulted in limited bubble growth and stretching possibility. The presence of 2% nano-$CaCO_3$ as a nucleating agent resulted in a uniform eye-like cellular structure with a cell aspect ratio of 5.4, needed for cellular piezoelectric films. Thermal characterization of the corresponding films showed that the incorporation of $CaCO_3$ nanoparticles increased their thermal stability. Finally, a stretching velocity of 45 mm/min was found to be optimum since below this stretching condition, an aspect ratio above 4 was not obtained without any localized defects (cell collapse). For all the samples produced, tensile properties (modulus, strength, and elongation at break) were reported and related to the foam structure obtained.

Acknowledgements

Financial support from the Natural Sciences and Engineering Research Council of Canada (NSERC) and Fonds Québécois de la Recherche sur la Nature et les Technologies (FRQNT) were received for this work. The technical support of Mr. Yann Giroux was also highly appreciated.

Chapter 5

Polymer ferroelectret based on polypropylene foam: Piezoelectric properties prediction using dynamic mechanical analysis

Abolfazl Mohebbi, Frej Mighri, Abdellah Ajji, Denis Rodrigue, *Polymers for Advanced Technologies*, DOI: 10.1002/pat.3908 (2016).

Résumé

Des films minces de polypropylène (PP) moussés ont été produits par extrusion en continu avec de l'azote supercritique (N_2) et ensuite chargé par décharge corona. Les échantillons ont été caractérisés par une analyse mécanique dynamique (DMA) comme une méthode simple pour prédire les propriétés piézoélectriques du PP cellulaire obtenu. Ces résultats ont ensuite été liés à l'analyse morphologique basée sur la microscopie électronique à balayage (SEM) et les propriétés mécaniques en traction. Les résultats ont montré que la présence d'un agent de nucléation ($CaCO_3$) a amélioré sensiblement la morphologie (en termes de taille des cellules et la densité cellulaire) de la mousse produite. De plus, une optimisation des conditions d'extrusion (conception de la vis, profil de température, concentration d'agent gonflant et de nucléation) et de post-extrusion (température de calandrage et la vitesse d'étirage) a conduit au développement d'une structure cellulaire de forme étirée (oculaire) avec une distribution uniforme de la taille des cellules. Cette morphologie a produit des modules de perte et de stockage plus élevés dans la direction de la machine (longitudinale) que dans la direction transversale, ainsi que des propriétés piézoélectriques supérieures. Les résultats morphologiques et mécaniques ont montré que plus le rapport d'aspect des cellules est élevé, plus le module de Young est faible, ce qui est adapté pour obtenir des propriétés piézoélectriques supérieures. Enfin, le meilleur coefficient piézoélectrique quasi-statique d_{33} obtenu était de 550 pC/N pour un PP ferroélectret cellulaire ayant une structure cellulaire de forme oculaire uniforme en utilisant le N_2 comme gaz d'ionisation à l'intérieur des cellules, tandis que la valeur la plus élevée était seulement de 250 pC/N lorsque l'air a été utilisé. Par conséquent, la valeur de d_{33} peut être améliorée de plus de 100% simplement en remplaçant l'air par du N_2 comme gaz ionisant.

Abstract

Thin polypropylene (PP) foam films were produced by continuous extrusion using supercritical nitrogen (N_2) and then charged via corona discharge. The samples were characterized by dynamic mechanical analysis (DMA) as a simple method to predict the piezoelectric properties of the cellular PP obtained. The results were then related to morphological analysis based on scanning electron microscopy (SEM) and mechanical properties in tension. The results showed that the presence of a nucleating agent ($CaCO_3$) substantially improved the morphology (in terms of cell size and cell density) of the produced foam. Also, an optimization of the extrusion (screw design, temperature profile, blowing agent and nucleating agent content) and post-extrusion (calendaring temperature and speed) conditions led to the development of a stretched eye-like cellular structure with uniform cell size distribution. This morphology produced higher storage and loss moduli in the machine (longitudinal) direction than for the transverse direction, as well as higher piezoelectric properties. The morphological and mechanical results showed that higher cell aspect ratio led to lower Young's modulus, which is suitable to achieve higher piezoelectric properties. Finally, the best quasi-static piezoelectric d_{33} coefficient was 550 pC/N for a cellular PP ferroelectret having a uniform eye-like cellular structure using N_2 as the ionizing gas inside the cells, while the highest value was only 250 pC/N when air was used. Hence, the value of d_{33} can be improved by more than 100% just by replacing air with N_2 as the ionizing gas.

5.1 Introduction

Piezoelectric materials are able to convert electric fields into a mechanical displacement and vice versa. This property is resulting from a direct relationship between the stress and the polarization density of the bulk material (Newnham, 2004; Tajitsu, 2006). Piezoelectricity in materials was first discovered by Pierre and Jacque Curie in 1880 (Lin and Lin, 2012). Later on, cellular structures were introduced into polymers to produce piezoelectric materials (Kirjavainen, 1987; Savolainen and Kirjavainen, 1989). Piezoelectric devices made from cellular polymer films, in comparison with other piezoelectric materials based on crystals such as quartz, topaz, and special ceramics, have several advantages such as low material costs and the possibility to produce flexible films with low density (Belhora et al., 2015; Qaiss et al., 2012; Xie et al., 2011). Hence, these new materials are under study for several applications such as actuators, vibration control, energy conversion devices, speakers, microphones, shock sensors, etc. (Belhora et al., 2015; Gerhard-Multhaupt, 2002; Lang and Muensit, 2006; Paajanen et al., 2000).

So far, different methods such as stretching (Anton et al., 2014; Hillenbrand et al., 2005; Qiu et al., 2007; Zhang et al., 2004), closed mold (Zhang et al., 2006), thermoforming (Altafim et al., 2006), and foaming (Fang et al., 2007; Wegener, 2010; Wegener et al., 2005) have been used for the production of cellular structures and these methods have been extensively compared in our previous work (Mohebbi et al., 2016). Polymer foams are materials including a solid polymer matrix as the continuous phase and gas bubbles as the dispersed phase (Mohebbi et al., 2015). But a tailor-made cellular structure can be achieved by controlling the nucleation step (Mohebbi et al., 2011). Foams can be produced by using chemical or physical blowing agents. In comparison with chemical blowing agents, physical ones like inert gases have several advantages such as chemical inertness, non-toxicity, and non-flammability (Eckert, 1996; Sauceau et al., 2007; Zirkel et al., 2009). For piezoelectric applications, in addition to cell density and average cell size, cell shape and orientation are also important parameters (Li et al., 2012).

Among all polymers, polypropylene (PP), as a result of its excellent properties such as low cost, high flexibility, good fatigue resistance, high service temperature (Antunes et al., 2010; Yu et al., 2011; Zhang et al., 2009), high tensile modulus and good chemical resistance

(Vasile and Seymour, 1993), is a suitable matrix for foaming. Due to its industrial interest, most of the related challenges in PP foaming were resolved and extensively discussed in our previous work. Nevertheless, PP is a nonpolar polymer, and its cellular films can exhibit good piezoelectric-like properties after a proper charging process by imposing a high electrical field (Fang et al., 2008; Gilbert-Tremblay et al., 2012; Kirjavainen, 1987; Qaiss et al., 2012; Savolainen and Kirjavainen, 1989; Wegener, 2010; Wegener et al., 2005). This effect is generally referred to as the "piezoelectret effect" and the behavior is named "ferroelectret" (Lindner et al., 2004; Tuncer, 2005). In ferroelectret materials, the piezoelectric behavior comes from positive and negative electrical charges which are created on opposite faces of each cell surfaces (Qiu et al., 2013).

It is known that the morphology or cellular structure, which is strongly related to the processing conditions (Gendron, 2004; Lee, 2000; Okolieocha et al., 2015), has a direct effect on the mechanical and piezoelectric properties of foams. To produce tailor-made structures for piezoelectric applications, the relationships between mechanical and piezoelectric properties must be understood. To date, some investigations on the relationships between the tensile and piezoelectric properties of cellular structures have been published (Anton et al., 2014; Qiu et al., 2005; Wegener et al., 2004; Wu et al., 2015; Zhang et al., 2009; Zhang et al., 2014). But other mechanical characterizations such as dynamic mechanical analysis, impact resistance, and compression resistance have seldom been used to get a complete behavior of the materials produced.

One of the most interesting mechanical analyses for viscoelastic polymers is dynamic mechanical analysis (DMA), especially in the linear region. In this region, since the applied stresses are very low, small deformations are produced and the results can provide useful information about the microscopic structure. To the best of the authors' knowledge, no information can be found in the literature about the relationships between DMA and the piezoelectric properties of cellular structures. As the piezoelectric properties of cellular materials are related to their elasticity and deformation under different frequencies/applied forces, DMA was selected as a useful analysis to find relationships between these properties. Hence, the main objectives of this work is to determine the relationships between morphological and DMA properties of cellular PP films with respect to their final

piezoelectric behavior. To achieve this objective, a methodology was developed to produce very thin cellular PP films with controlled morphologies through continuous extrusion and physical foaming. Then, a comprehensive study was performed on the morphological (SEM) and mechanical properties (DMA) of the samples produced. Finally, the piezoelectric properties are related to the mechanical behavior of the films with different cellular morphologies.

5.2 Experimental

5.2.1 Material

Polypropylene (PP-3462) was purchased from Total Petrochemicals (USA). This PP is an extrusion grade homopolymer with a MFI of 4.1 g/10 min (230°C, 2.16 kg) and a density of 0.905 g/cm^3. As a physical blowing agent, nitrogen (N_2) with a purity of 99.999% (Praxair, Canada) was used in its supercritical state. Finally, nano-calcium carbonate ($CaCO_3$), Ultra-Pflex A-1-194-11 of spherical shape (Specialty Minerals Inc., USA), with an average particle size of 70 nm, was used as a nucleating agent.

5.2.2 Foaming process

PP foamed films were produced through physical foaming using supercritical N_2. Saturated polymers with an inert gas in its supercritical state followed by a rapid pressure drop is known to result in the creation of a large number of small cells which can grow to produce microcellular foams (Mohebbi et al., 2011). Supercritical fluids (SCF), because of their low viscosity and negligible surface tension, have high mass transfer rates into polymers (Huang and Xu, 2011; Li et al., 2002; Rao and Zhang, 2008), and this principle was used to produce microcellular foams. It is also known that the presence of a well dispersed nucleating agent in the polymer matrix substantially improves the nucleation rate creating a higher number of uniform nucleation sites (heterogeneous nucleation) in comparison with a neat polymer (homogeneous nucleation), thus leading to a more uniform cellular structure (Mohebbi et al., 2011).

Physical foaming was performed through continuous extrusion on a Leistritz ZSE18HP co-rotating twin-screw extruder (diameter = 18 mm and length/diameter = 40). A slit die with dimensions of 15 cm by 0.5 mm and a calendaring system including three rolls having a width of 20 cm and set at 40°C were used to produce the foamed PP films. The extruder has nine temperature zones including the die and the optimum temperature profile from the feeding zone to the die was found to be: 180, 180, 185, 185, 185, 180, 180, 180, and 167°C. The screw speed was set at 260 rpm and a constant flow rate of 1.14 kg/h was used. A high pressure nitrogen gas cylinder was used to obtain supercritical N_2. Supercritical conditions for N_2 are P_C = 3.4 MPa and T_C = 126 K (Zong and Yang, 2006). To ensure a maximum N_2 saturation, a stream of SC-N_2 with a pressure of 7 MPa and a flow rate of 5 ml/min was injected in zone 2 of the extruder, which was controlled by a mass flow meter/controller model F-201CV-5K0-ABD-22-V (Hoskin Scientific Co., USA). More information on the experimental setup can be found in our previous work (Mohebbi et al., 2016).

To achieve a good eye-like cellular morphology, which is suitable for good piezoelectric properties (Lindner et al., 2004; Tuncer, 2005; Xu et al., 2013), the samples were uniaxially stretched in the melt state between the die exit and the first roller of the calendar (distance of 10 cm). After some processing and composition optimization in terms of screw configuration, temperature profile, die temperature, stretching speed and nucleating agent (Mohebbi et al., 2016), different closed-cell foamed PP films, with and without nucleating agent, were produced. The specifications of the selected samples studied here are reported in Table 5.1.

Table 5.1. Specification of the foamed PP films studied.

Sample code	Uniaxial stretching speed (cm/min)	Nucleating agent ($CaCO_3$) (% wt.)
PP-S1	30	0
PP-S2	45	0
PPn-S1	45	2

5.2.3 Ferroelectret sample preparation

Following the foaming process, the samples were cut from the uniaxially stretched cellular films. Then, the samples were charged by a corona process using a discharge generator with a needle voltage of -21 kV. The needle was set at a distance of 4 cm from the samples and the charging time was set as 60 s. During corona charging, the gas inside the cells was ionized and positive/negative electrical charges were created on the opposite faces of each cell surface. Finally, the samples were metalized on both sides with an aluminum coating to create conductive surfaces for piezoelectric measurement.

To investigate the effect of the ionizing gas type, a series of samples were prepared by replacing air with nitrogen inside the cells during a pressure treatment procedure. In this procedure, the samples were placed in a one-liter cylindrical high-pressure vessel (Autoclave Engineers, USA) equipped with pressure indicators and connected to a N_2 cylinder. Then, the vessel was purged with N_2 to remove air. Afterward, the pressure was set at 5 MPa to produce a supercritical N_2 atmosphere and the samples were kept inside the pressurized vessel for 24 h at room temperature.

5.3 Morphological analysis

Scanning electron microscopy (SEM) was used to investigate the cellular structure of the foamed PP films. The samples were first frozen in liquid nitrogen and then broken in both machine (longitudinal) and transverse directions. Based on SEM pictures taken on a JEOL JSM-840A, a complete morphological characterization including cell shape, cell size, cell densities, and sample thickness was done using the *ImageJ* software (National Institute of Health, USA).

Sample density was obtained using a Quantachrome Ultrapyc 1200e gas (nitrogen) pycnometer. The reported values are based on the average of five samples.

5.4 Mechanical analysis

The tensile properties of the samples were obtained using an Instron model 5565 universal testing machine (Instron, USA) with a 500 N load cell. The tests were performed at room temperature according to ASTM D882. A crosshead speed of 50 mm/min was used and the values reported are based on the average of at least five samples.

The tensile mechanical behavior of the samples at room temperature was also studied using a dynamic mechanical analyzer (DMA) RSA3 (TA Instrument, USA). Rectangular samples (25 x 7.5 mm^2) were analyzed in the linear viscoelastic range of the materials. First, strain sweep tests were performed to determine the range of the linear viscoelastic region. Then, frequency sweeps (fixed strain amplitude of 0.05% which is inside the linear viscoelastic region) were performed to compare the dynamic behavior of the samples in the longitudinal (*L*) and transverse (*T*) processing directions. The frequency range of the test was 10^{-1} to 10^2 Hz and the reported data are the average of at least three measurements.

5.5 Piezoelectric analysis

The quasi-static method was used to measure the d_{33} coefficient from the direct piezoelectric effect (Zhang et al., 2014; Zhang et al., 2014). The d_{33} coefficient corresponds to the ratio of the induced charge Q to the applied force F perpendicular to the surface of the film as (Mohebbi et al., 2016):

$$d_{33} = {}^{Q}/_{F} = {}^{Q}/_{mg} \tag{5.1}$$

where *m* is the mass applied on the sample and *g* is the acceleration of gravity.

The induced charge was measured by a programmable electrometer (Keithley 6512, USA) as:

$$Q = \int_0^t I\, dt \tag{5.2}$$

where *t* and *I* are the duration time of the experiment and the electric current, respectively.

The measured charge was transferred to a computer using a data acquisition module NI USB-6211 (National Instruments, USA). In the experiment, a static force of 1.57 N was applied on the sample surface, and removed quickly. After 10 s, the produced charge Q was measured by the electrometer (Wu, et al., 2015). For each sample, this procedure was repeated three times and the average value of the induced charge (Q) was used to calculate the d_{33} coefficient.

5.6 Results and discussion

5.6.1 Morphological analysis

Typical SEM images of the three different samples are presented in Figure 5.1 and the corresponding morphological analyses are reported in Table 5.2. Due to cell deformation, the cell density was calculated as (Gosselin and Rodrigue, 2005):

$$N = N_1(N_2)^{1/2} \tag{5.3}$$

where N_1 and N_2 are the surface cell densities in the machine and transverse directions respectively, which are calculated as:

$$N_i = \frac{n}{A} \tag{5.4}$$

where n is the number of cells and A is the corresponding micrograph area.

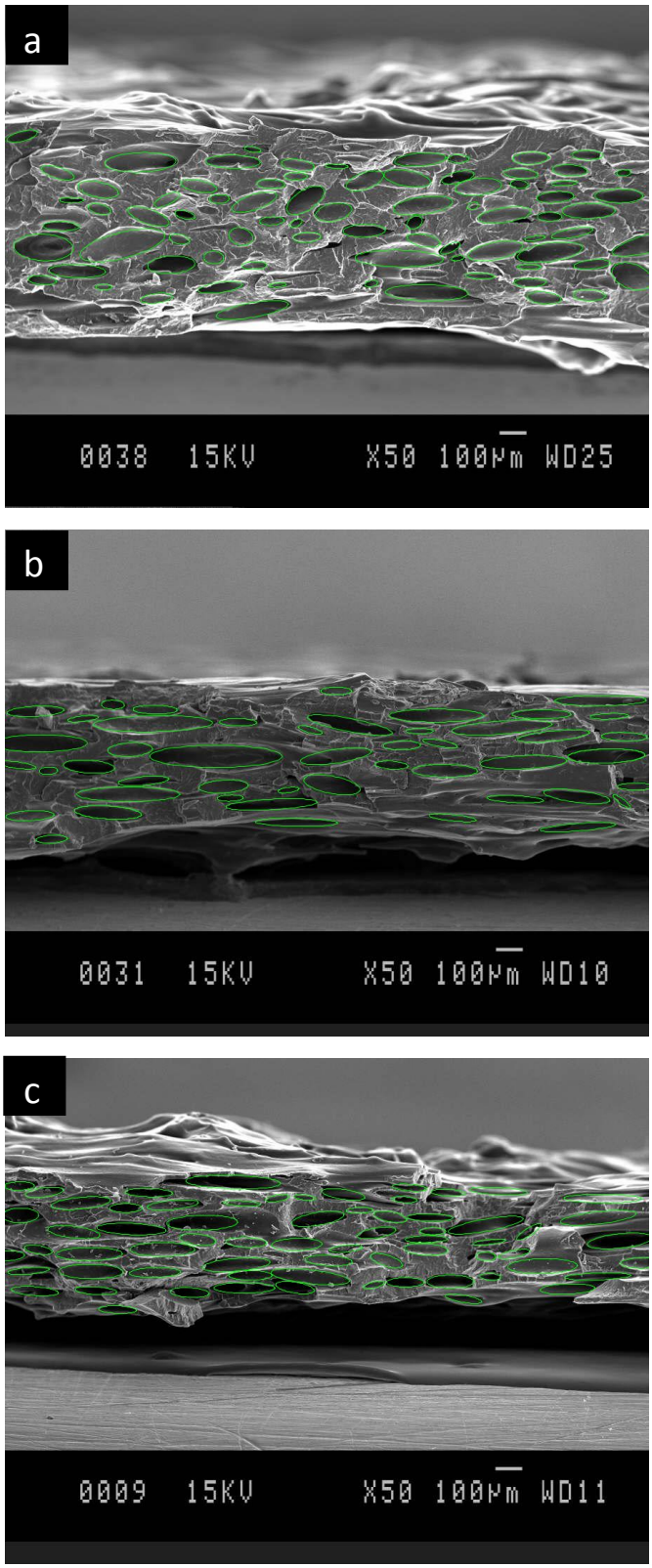

Figure 5.1. Typical SEM pictures of the foamed PP films in the machine direction: a) PP-S1, b) PP-S2, and c) PPn-S1.

Table 5.2. Morphological properties of the samples produced.

Sample code	Average density (g/cm^3)	Cell aspect ratio (*AR*)	Cell size L direction (μm)	Cell size T direction (μm)	Cell density (10^5 cells/cm^3)
PP-S1	0.737 ± 0.012	3.7 ± 1.4	147 ± 67	41 ± 15	4.7 ± 1.3
PP-S2	0.712 ± 0.007	4.9 ± 1.5	161 ± 86	33 ± 15	4.2 ± 1.5
PPn-S1	0.707 ± 0.003	5.4 ± 1.0	171 ± 55	31 ± 8	6.5 ± 0.8

It is obvious that the densities of these samples are much lower (up to 22%) than unfoamed PP films (0.905 g/cm^3), which confirms that good foaming occurred. Also, all the samples have an eye-shaped cell structure due to uniaxial stretching at the die exit. It has been reported that a cellular film having eye-shaped cells with an aspect ratio (*AR*) above 4 is the best structure for piezoelectric applications (Lindner et al., 2004; Tuncer, 2005; Xu et al., 2013). When the stretching ratio is low (PP-S1), *AR* is below the target value of 4. By increasing the stretching ratio (PP-S2), the *AR* increases up to about 4.9. However, the cell size distribution is not uniform for these samples as large and small cells are observed (wide cell size distribution). By adding a nucleating agent (PPn-S1) and under the same foaming conditions, not only the *AR* increased to about 5.4, but also a more uniform cell size distribution is obtained (lower standard deviation). PPn-S1 has an average cell length in the longitudinal direction of 171 μm with a standard deviation (SD) of 55 μm in comparison with PP-S2, which has a cell size of 161 μm and a SD of 86 μm. This indicates the effectiveness of the nucleating agent in improving cell density from 4.2 to $6.5x10^5$ cells/cm^3 (more than 50% increase) to get a better structure (in terms of homogeneity and value) for piezoelectric applications. The effect of these different cell morphologies on the mechanical and piezoelectric properties are reported and discussed in the next sections.

5.6.2 Mechanical analysis

The Young's modulus, tensile strength, and elongation at break of the three developed PP cellular films are compared with those of unfoamed PP film in Table 5.3 while Figure 5.2 presents typical stress-strain curves for these samples. Table 5.3 shows that PPn-S1 has the lowest strength and modulus, which can be associated to its higher AR (Table 5.2). This is in agreement with literature where it has been reported that for eye-like cellular structures, increasing the *AR* ratio increases the charging capacity of ferroelectret materials, while Young's modulus decreases (Hillenbrand et al., 2005; Zhang et al., 2007; Zhang et al., 2011; Zhang et al., 2009; Zhang et al., 2014). This behavior is related to the U-shape of the cellular structure (Wegener et al., 2005): i.e. increasing the *AR* ratio results in low elastic stiffness which is suitable for piezoelectric application. More information about the U-shape behavior is available in our previous work (Mohebbi et al., 2016). Wegener et al. (Wegener et al., 2004) also reported that lower Young's modulus leads to higher piezoelectric properties. Among the samples, PSn-S1 shows the lowest Young's modulus of about 600 MPa. Furthermore, PSn-S1, in comparison with the other samples, has the lowest strength and elongation at break of about 10 MPa and 5%, respectively. The SEM images (Figure 5.1) showed that this sample has an eye shaped cellular structure with a good cell size distribution and higher cell deformation (*AR*). Such structure confirms again the positive role of the nucleating agent in the production of a suitable structure for piezoelectric applications. This will be further discussed in the next section.

Table 5.3. Mechanical properties (machine direction) of the samples produced.

Sample code	Young's modulus (MPa)	Tensile strength (MPa)	Elongation at break (%)
PP	993.8 ± 83.2	27.3 ± 1.4	405.3 ± 31.7
PP-S1	833.4 ± 38.2	13.8 ± 1.1	6.7 ± 0.9
PP-S2	796.2 ± 26.6	13.3 ± 0.5	5.4 ± 0.7
PPn-S1	610.2 ± 20.1	10.4 ± 0.3	5.2 ± 0.4

As seen in SEM images (Figure 5.1), PP-S2 has a more stretched cellular structure (*AR* of 4.9) than PP-S1 (*AR* of 3.7), and this has a direct effect on their tensile properties. On the other hand, from Figure 5.2 and Table 5.3, the tensile properties of PP-S2 in terms of Young's modulus, elongation at break, and tensile strength are lower than PP-S1, especially PP-S2 has an elongation at break of about 5.5% which is 20% less than that PP-S1 (about 7%). Hence, it can be concluded that a more stretched cellular structure, which is appropriate for piezoelectric properties, results in lower tensile properties in terms of Young's modulus, elongation at break, and tensile strength. Furthermore, it is clear that foaming (creation of a cellular structure) results in lower elongation at break. As seen in Figure 5.2 and Table 5.3, the unfoamed PP film has an elongation at break above 400%, while the cellular films are below 7%. Also, Young's modulus and tensile strength decreased by replacing some of the matrix (polymer) by gas (cells) in foamed samples; i.e. introduction of a high number of voids.

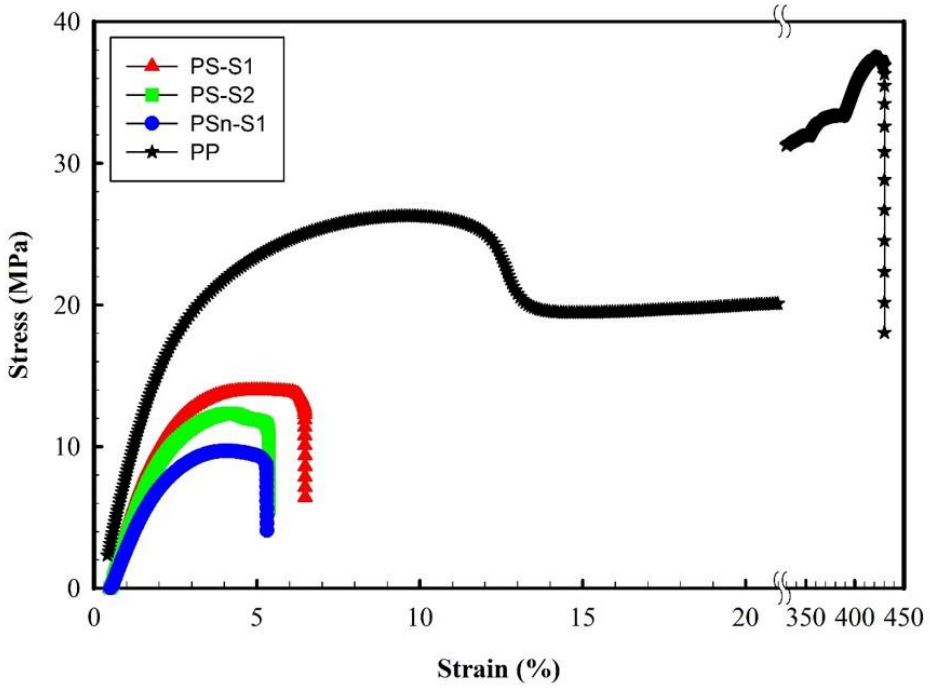

Figure 5.2. Stress-strain curves (machine direction) of the samples produced.

Figure 5.3 presents the sample preparation for DMA analysis and a picture of a film sample mounted in the grips of the DMA machine. As expected, two different morphologies are obtained depending on the direction analyzed: longitudinal (*L*) and transverse (*T*). The storage and loss moduli as a function of frequency (both directions) for the unfoamed and cellular PP films developed are presented in Figure 5.4 and Figure 5.5, respectively. It can be seen that for all the samples, the storage and loss moduli (*E′* and *E″*) in the *L* direction are higher compared to the *T* direction. This confirms that the cells are effectively deformed in the *L* direction. Also, PPn-S1 has the lowest storage and loss moduli as for Young's modulus (Table 5.3) because it has the most uniform cell size distribution, the highest AR, and the lowest density. Furthermore, Figure 5.4 and Figure 5.5 show that the unfoamed PP films have higher storage modulus (about 20% higher than the foamed samples) and loss modulus (about 50% higher than the foamed samples). This is another advantage of DMA where both the elastic and viscous properties of the materials can be analyzed separately.

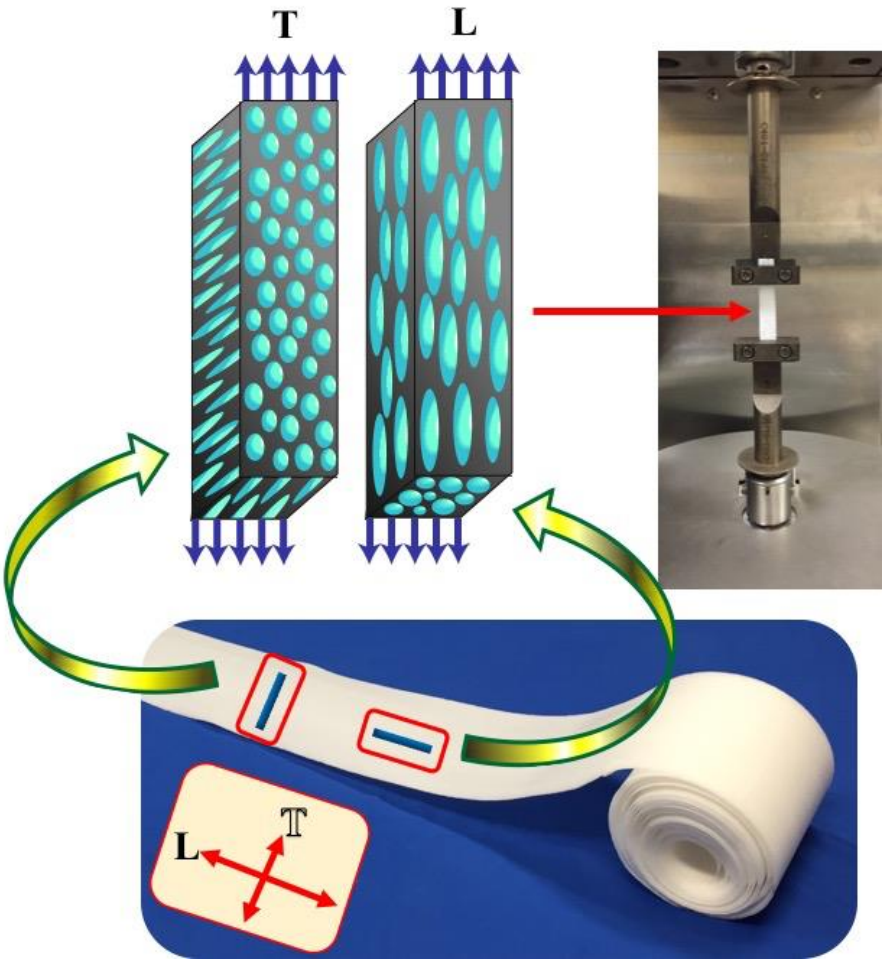

Figure 5.3. Typical foamed film morphologies in the machine and transverse directions and a picture of the DMA setup.

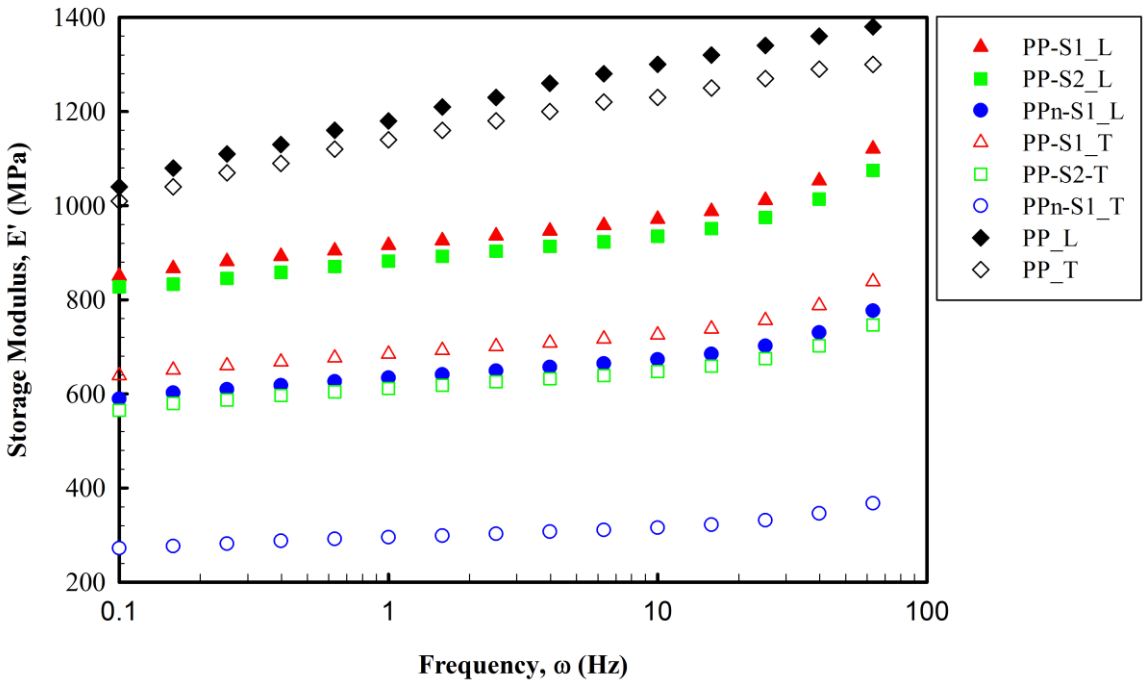

Figure 5.4. Storage modulus as a function of frequency for the samples produced.

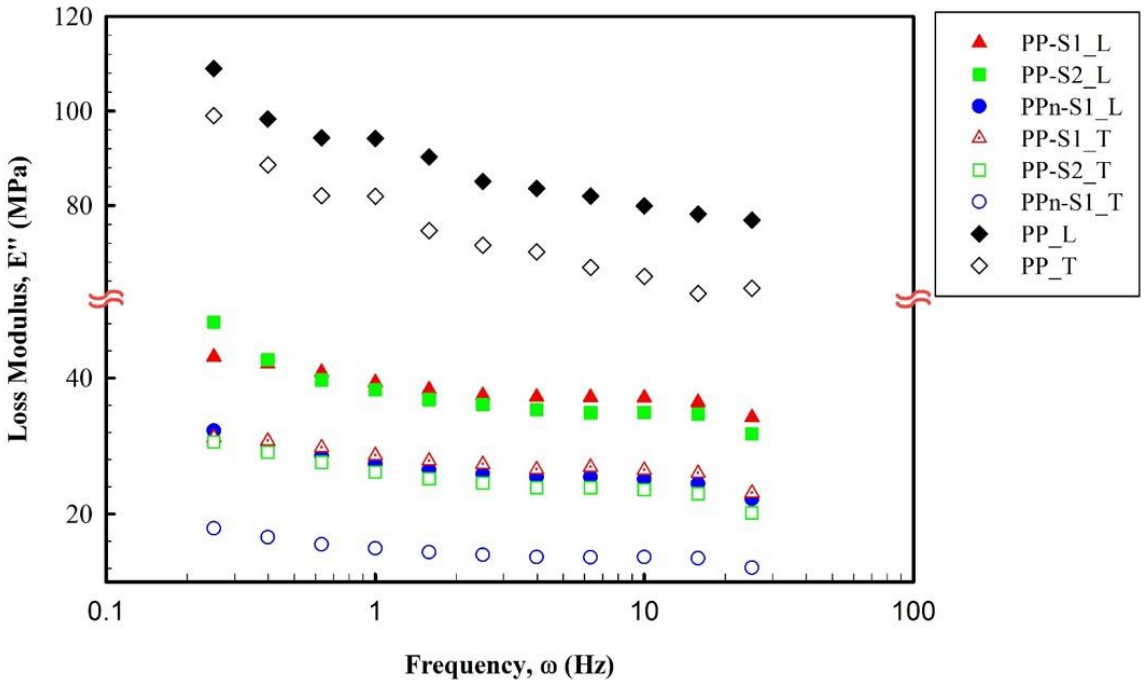

Figure 5.5. Loss modulus as a function of frequency for the samples produced.

As mentioned above, in order to get good piezoelectric properties, an eye-shaped cell structure with $AR > 4$ should be produced (Lindner et al., 2004; Tuncer, 2005; Xu et al., 2013). Such structures can be obtained via uniaxial stretching of the matrix since the cells are elongated along the stretching direction (longitudinal). This leads to different mechanical behavior in the longitudinal (L) and transverse (T) directions as reported in Figure 5.4 and Figure 5.5. Therefore, analyzing the mechanical response of the cellular PP films in both directions will provide useful information about the morphology of the sample. For this reason, the ratio $E'(L)/E'(T)$ and $E''(L)/E''(T)$ is presented in Figure 5.6 and Figure 5.7, respectively. It can be seen that for both modulus ratios, the highest values are obtained for PPn-S1, which has the highest AR value and the most uniform cell size distribution. It will be shown in the next section that this cellular film also shows the highest piezoelectric behavior. For the other two cellular films, PP-S2 has higher $E'(L)/E'(T)$ and $E''(L)/E''(T)$ values than PP-S1. Their SEM images (Figure 5.1) showed that PP-S2 has a more stretched cellular structure than PP-S1. This result indicates that both modulus ratios are very sensitive to the cellular structure. So these parameters can be used as a new criterion to qualify the cellular morphology needed for good piezoelectric properties; i.e. a simple DMA test can be performed to predict the piezoelectric behavior of the cellular structures without the need to perform a complete and time consuming morphological analysis such as SEM/image analysis.

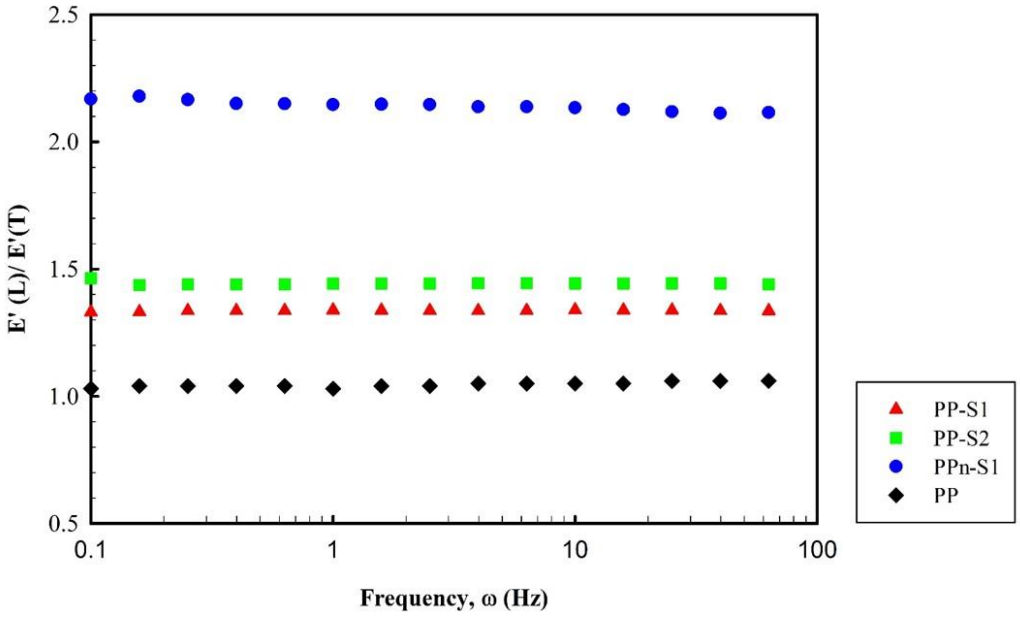

Figure 5.6. Ratio of the storage modulus in the longitudinal (*L*) over the transverse (*T*) directions as a function of frequency (AMR1).

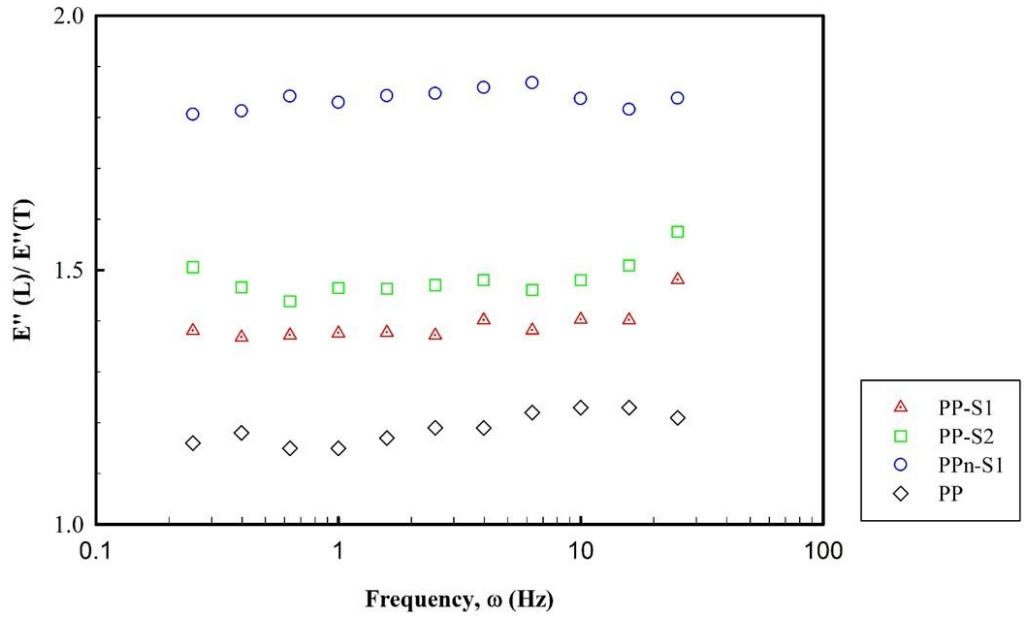

Figure 5.7. Ratio of the loss modulus in the longitudinal (*L*) over the transverse (*T*) directions as a function of frequency (AMR2).

Hence, it is proposed that a new parameter called AMR (anisotropic modulus ratio) can be used to quantify the film cellular structure. So, AMR1 and AMR2 are used for the ratios of *E′(L)/E′(T)* and *E″(L)/E″(T)*, respectively. Furthermore, as seen in Figure 5.6 and Figure 5.7, the unfoamed PP film, which has no cellular structure, shows AMR1 and AMR2 values close to unity. Nevertheless, values slightly above 1.0 are obtained which can be related to orientation of the PP molecules and spherulites in the stretching direction.

Based on the results obtained, it can be concluded that a ferroelectret film having a more elongated eye-like cellular structure (higher AR), shows a lower Young's modulus and a higher AMR values as well as a higher piezoelectric d_{33} coefficient, while a force F is applied perpendicular to the film sample (in thickness direction).

5.7 Charging voltage measurements

Although a higher charging voltage can result in higher piezoelectric properties (Zhang et al., 2005), it has been shown that very high charging voltage can lead to electrical sparking and therefore an optimum voltage should be used. As seen in Figure 5.8, electrical sparking led to local burning and the creation of holes in the films. Hence, this parameter is highly important to optimize the charging step. Also, the maximum charging voltage (before electrical sparking occurs) depends on the needle distance (distance between the needle tip and the sample surface). The samples were charged by a corona method in a nitrogen atmosphere of 50 and 100 kPa.

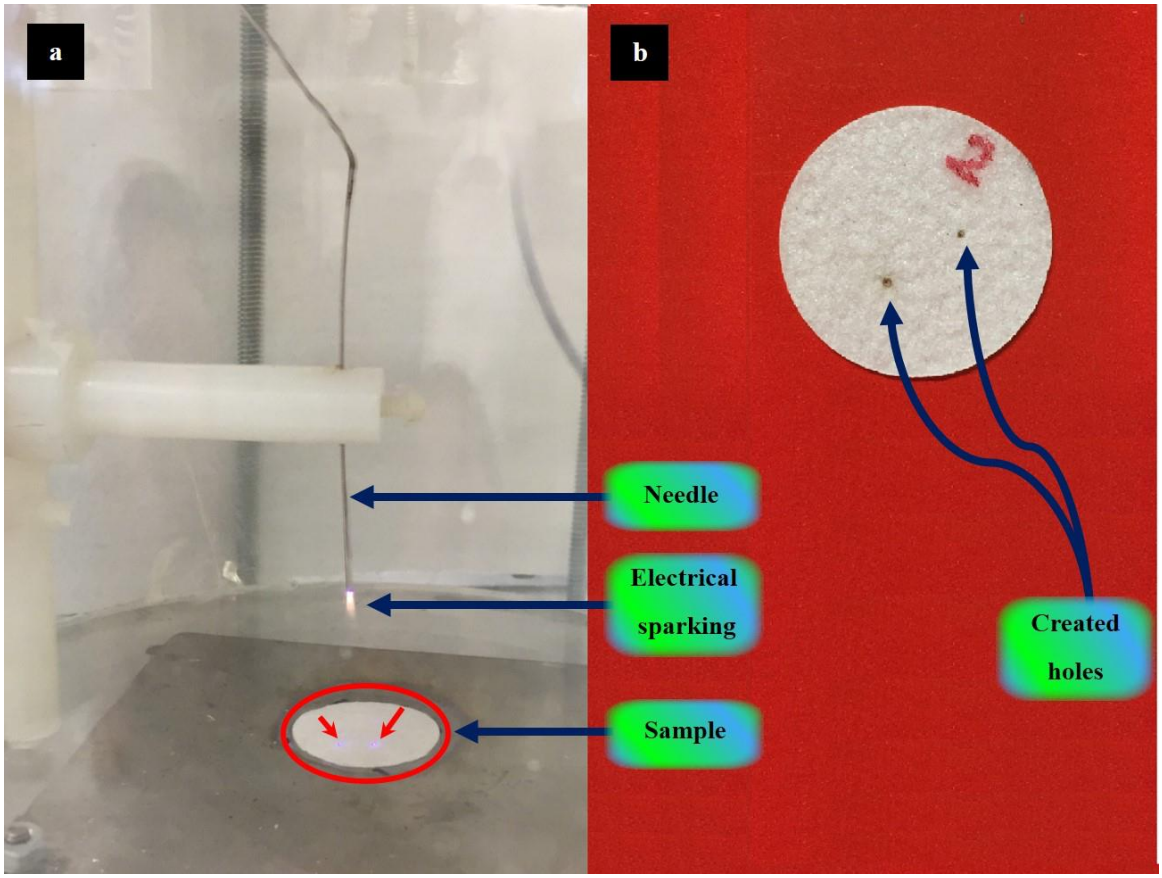

Figure 5.8. a) An example of electrical sparking during corona charging, and b) creation of holes in the samples due to electrical sparking.

As presented in Figure 5.9, the maximum charging voltage increases with increasing needle distance. Furthermore, higher charging voltage can be achieved at higher N_2 pressure. Nevertheless, shorter needle distance results in higher N_2 pressure sensitivity. As shown in Figure 5.9, the difference between the charging voltage is more important at a needle distance of 2 cm than at 5 cm. Finally, as reported by other studies (Mohebbi et al., 2016; Qiu et al., 2005), it can be concluded that more effective corona charging is possible at higher gas atmosphere pressure.

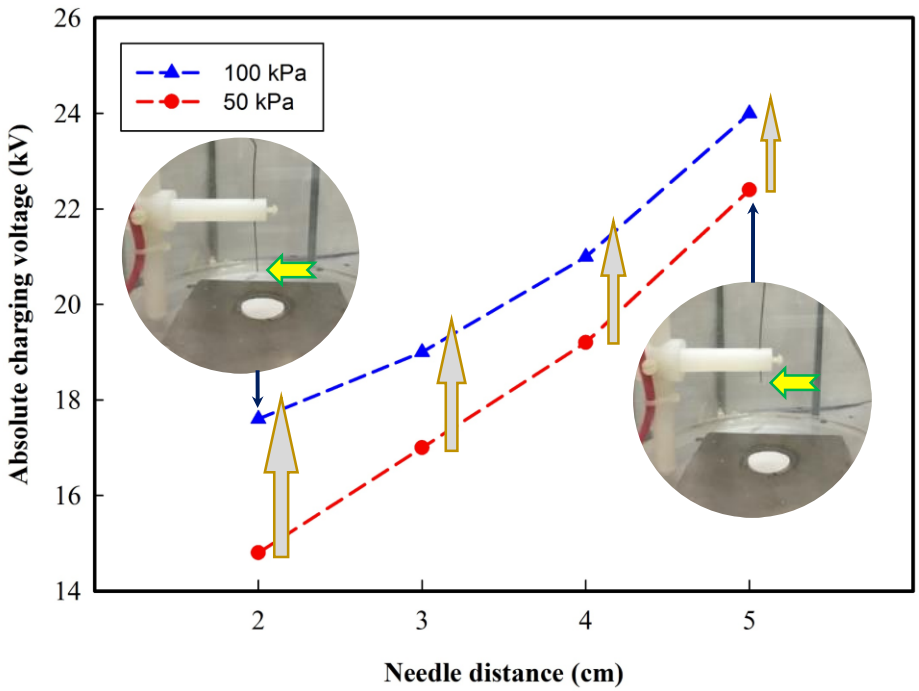

Figure 5.9. Maximum charging voltage as a function of needle distance in different N_2 atmospheres (50 and 100 kPa).

5.8 Piezoelectric properties

The piezoelectric d_{33} coefficient for the samples with different AMR1 values having air or N_2 as ionizing gas is reported in Figure 5.10. As seen from Figure 5.6, because AMR1 has a more stable trend (more precise measurement) over a wide frequency range, it is selected as the main parameter to study the variation of the piezoelectric d_{33} coefficient. PPn-S1, which has the most uniform eye-like cells structure and higher AMR1 value of about 2.14 in comparison with the other samples (1.34 for PP-S1 and 1.44 for PP-S2), also shows the highest piezoelectric d_{33} coefficients of about 250 pC/N when air is used as the ionizing gas. On the other hand, PP-S1 and PP-S2, which have lower ARM1 values, as well as higher Young's moduli, have much lower d_{33} piezoelectric coefficients (below 110 pC/N).

The results show that by replacing air with N_2 inside the cells, higher piezoelectric d_{33} coefficients were achieved. Other researchers reported similar result for ferroelectret PP

(Paajanen et al., 2001, 2001). The reason is that N_2 has higher breakdown strength than air resulting in more effective corona charging. For example, the relative breakdown strength of N_2 and air with respect to SF_6 are 0.36 and 0.30, respectively (Paajanen et al., 2001). Here, a maximum piezoelectric d_{33} coefficient of 550 pC/N was achieved for PPn-S1 when N_2 was used as the ionizing gas, which also has the highest AMR1 value. To the best of our knowledge, this value is much better than typical values reported in the literature: about 350 pC/N for PP (Zhang et al., 2014). The value can also be compared to 250 pC/N when charging was done in air. This indicates that the piezoelectric d_{33} coefficient was more than doubled just by replacing air with N_2 inside the cells as ionizing gas.

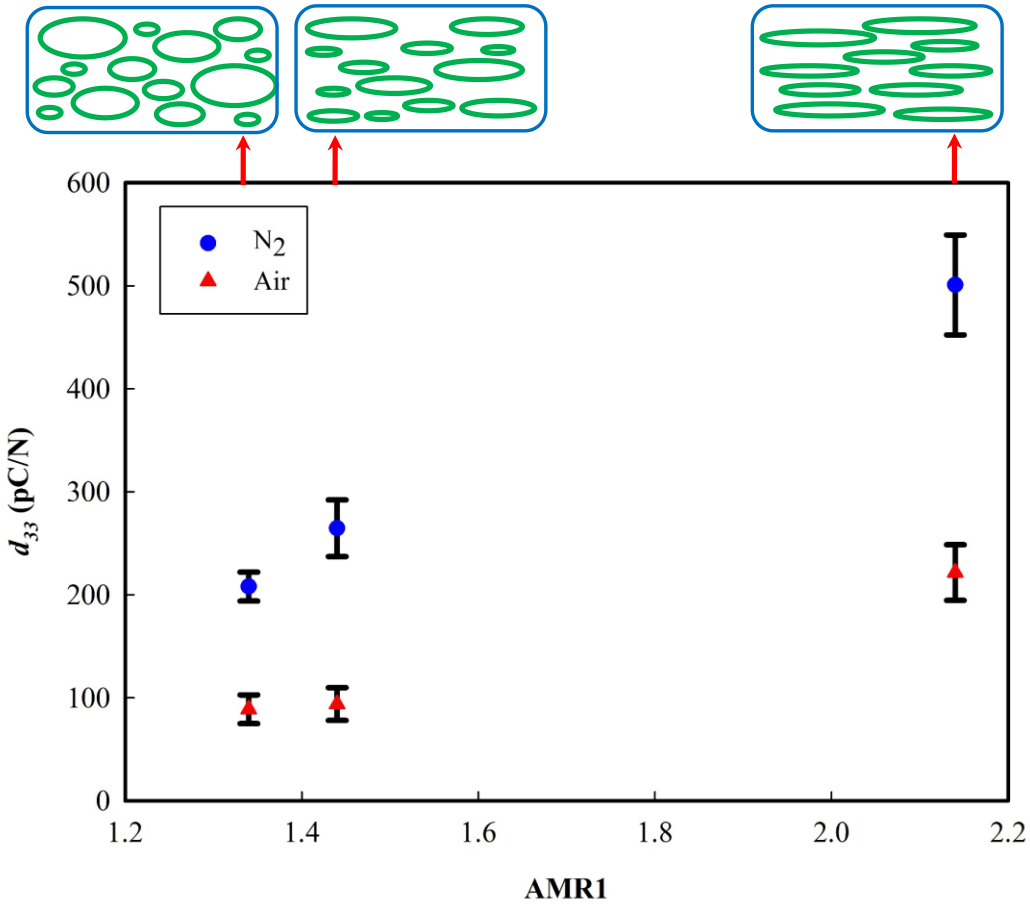

Figure 5.10. Piezoelectric d_{33} coefficient as a function of AMR1 for the samples using air or nitrogen as the ionizing gas.

Hence, based on the results obtained, it can be concluded that higher AMR values lead to higher piezoelectric d_{33} coefficient, but a minimum of around 1.7 (AR > 4) should be achieved based on the results for the system studied (Figure 5.6 and Figure 5.7). Nevertheless, more data are needed to confirm if these criteria hold for all materials.

Finally, the piezoelectric d_{33} coefficient was optimized as a function of needle distance using PPn-S1 since this sample has the highest piezoelectric properties. While charging filed is the most important parameter in the charging process through corona discharge method, the needle distance has a significant role to create a more effective charging field on the sample (Zhang et al., 2014). Furthermore, to produce a more uniform/effective charging field some works used a mesh grid instead of a single needle (Wu et al., 2015). Hence, in this work, it was tried to optimize the needled distance to have a more effective charging field in the setup used. As shown in Figure 5.11, the piezoelectric d_{33} coefficient increases with increasing needle distance up to 4 cm due to increasing charging voltage, resulting in more effective corona charging. However, for a needle distance above 4 cm, the piezoelectric d_{33} coefficient decreases due to the non-uniformity of the corona charging over the whole surface of the film.

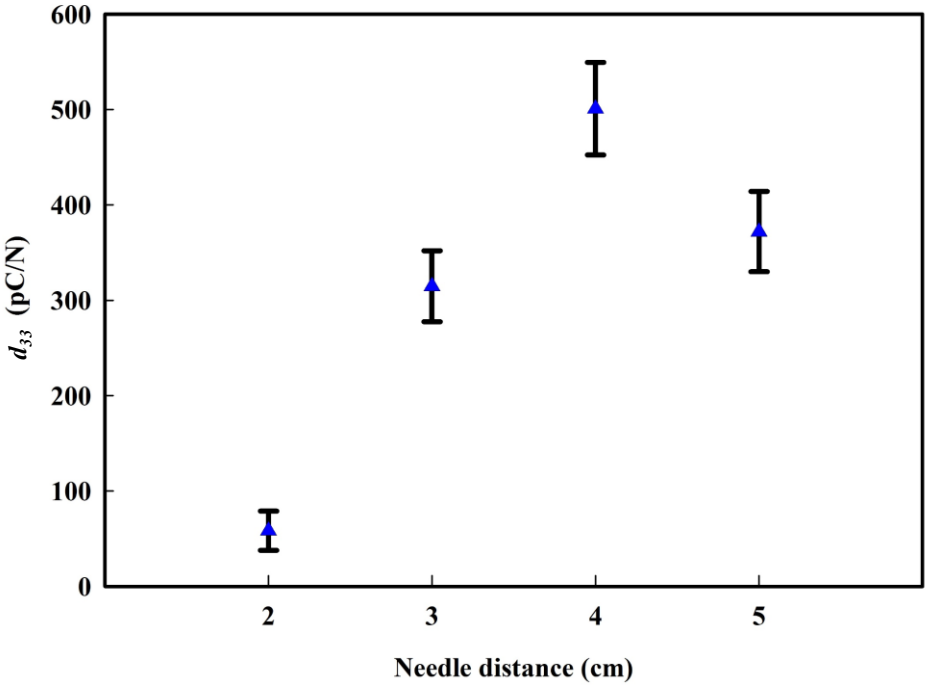

Figure 5.11. Piezoelectric d_{33} coefficient for PPn-S1 charged with different needle distance.

5.9 Conclusion

This work showed that a continuous foaming process based on flat film extrusion/calendaring with supercritical N_2 can be a suitable methodology to obtain very thin cellular PP films with controlled morphologies leading to good piezoelectric d_{33} coefficient. The presence of $CaCO_3$ as a nucleating agent resulted in a foamed film having a more uniform cellular morphology with a well-developed eye-like shape. This structure was shown to have the highest piezoelectric properties.

Also, the mechanical behavior of the samples showed that the foam morphology has a direct effect on the mechanical properties of the produced films; especially due to material stretching (anisotropy) at the extruder die exit. Samples having eye-like cellular structure with more uniform size distribution, had a lower Young's moduli. A simple DMA test was used to predict the piezoelectric behavior of the cellular structures without the need to perform a complete and time consuming morphological analysis such as SEM/image analysis. In this method, new parameters called AMR1 and AMR2 are proposed for the ratios of $E'(L)/E'(T)$ and $E''(L)/E''(T)$, respectively. This was used to quantify the cellular structure. The results showed that samples having uniform cellular structures with higher cell *AR* had higher AMR1 and AMR2 values. The variation of AMR1 with frequency showed a more stable trend over a wide frequency range. Hence, the variation of the piezoelectric d_{33} coefficient with respect to AMR1 was studied. It was shown that increasing AMR1 resulted in higher piezoelectric d_{33} coefficient.

From the results obtained, a quasi-static piezoelectric d_{33} coefficient of 550 pC/N was achieved for a cellular PP ferroelectret with AMR1 = 2.1 having N_2 as the ionizing gas inside the cells, while the same sample had only 250 pC/N when air was used. Hence, the piezoelectric d_{33} coefficient can be substantially increased by simply replacing air with N_2 inside the cells as ionizing gas.

Finally, based on the limited results obtained, it can be concluded that higher AMR values led to higher piezoelectric d_{33} coefficient, but a minimum of around 1.7 should be achieved

to get $AR > 4$. Nevertheless, more data are needed to confirm if these criteria hold for all materials.

Acknowledgement

Financial support from the Natural Sciences and Engineering Research Council of Canada (NSERC) and Fonds Québécois de la Recherche sur la Nature et les Technologies (FRQNT) was received for this work. The technical support of Professor Xiaoqing Zhang and Dr. Hojjat Mahi Hassanabadi, as well as Mr. Jean Côté, Mr. Yann Giroux, and Mr. André Ferland was also highly appreciated.

Chapter 6

Polymer ferroelectret based on polypropylene foam: Piezoelectric properties improvement using post-processing thermal-pressure treatment

Abolfazl Mohebbi, Frej Mighri, Abdellah Ajji, Denis Rodrigue, *Journal of Applied Polymer Science*, 134 (10) 44577 (2017).

Résumé

Dans ce travail, l'effet des paramètres de post-traitement (temps, température et pression) sur la morphologie, ainsi que les propriétés mécaniques et piézoélectriques de films de polypropylène (PP) moussé a été étudié. Deux méthodes de post-traitement différentes, en fonction de la saturation d'un film expansé avec de l'azote supercritique (N_2), ont été utilisées pour obtenir une structure cellulaire de forme oculaire optimisée avec un rapport d'aspect (RA) élevé des cellules. Les résultats ont montré que, lorsque l'échantillon était exposé à une augmentation progressive de la température et de la pression, une structure cellulaire appropriée avec une valeur élevée de RA (environ 6,6) était obtenue, ce qui conduit à un coefficient piézoélectrique quasi-statique d_{33} élevée de 800 pC/N (45% supérieur à celui des échantillons non-traités) indiquant l'importance du post-traitement sur le comportement piézoélectrique de ces films. D'autre part, lorsque le traitement était effectué par étapes, la morphologie cellulaire changeait d'une forme oculaire à une forme moins allongée, ce qui entraîne des valeurs inférieures de d_{33}. La caractérisation a montré qu'une plus grande élongation mène à un plus grand rapport d'aspect des cellules abaissant le module de Young, ce qui est nécessaire pour obtenir des propriétés piézoélectriques supérieures. Enfin, l'analyse mécanique dynamique (DMA) a été utilisée comme une méthode simple pour corréler les propriétés piézoélectriques de PP moussé. Ceci a été fait par le biais du rapport des modules de stockage dans la direction longitudinale à la valeur dans le sens transversal, qui est en relation directe avec l'anisotropie (valeur de RA) des films et donc du comportement piézoélectrique.

Abstract

In this work, the effect of post-processing parameters (time, temperature and pressure) on the morphology, as well as mechanical and piezoelectric properties of foamed polypropylene (PP) films was studied. Two different post-processing methods, based on the saturation of a foamed film with supercritical nitrogen (N_2), were used to obtain an optimized eye-like cellular structure with a high cell aspect ratio (*AR*). The results showed that, when the sample was exposed to a gradual temperature and pressure increase, an appropriate cellular structure with high *AR* value (about 6.6) was obtained, leading to a high quasi-static piezoelectric d_{33} coefficient of 800 pC/N (45% higher than for the untreated samples) indicating the importance of the post-processing treatment on the piezoelectric behavior of these films. On the other hand, when the treatment was done by steps, cell morphology changed from an eye-like to a less elongated shape, resulting in lower d_{33} values. The tensile characterization showed that higher cell aspect ratio led to lower Young's modulus, which is suitable to achieve higher piezoelectric properties. Finally, dynamic mechanical analysis (DMA) was used as a simple method to correlate with the piezoelectric properties of cellular PP. This was done via the ratio of the storage moduli in the longitudinal to the value in the transverse directions, which is directly related film anisotropy (*AR* value) and thus to the piezoelectric behavior.

6.1 Introduction

Ferroelectrets, as a special group of piezoelectric materials, are cellular nonpolar polymer films usually charged via high electrical fields (Mohebbi et al., 2016). As the piezoelectric behavior is related to the ability of materials to convert electric or magnetic fields into a mechanical displacement and vice versa, there is a direct relation between the stress and the polarization density of the bulk material (Newnham, 2004). Piezoelectricity in ferroelectret materials is resulting from positive and negative electrical charges created on the opposite faces of each cell surface during a charging process, such as corona charging (Lindner et al., 2004; Qiu et al., 2013; Tuncer, 2005; Zhang et al., 2015). This effect was first introduced by Pierre and Jacque Curie in 1880 (Lin and Lin, 2012), and then developed based on cellular polymer films (Kirjavainen, 1987; Savolainen and Kirjavainen, 1989). These new piezoelectric materials, as a result of their low material and processing costs, are currently under study for several applications such as actuators, vibration control, energy conversion devices, speakers, microphones, sensors, etc. (Gerhard-Multhaupt, 2002; Lang and Muensit, 2006; Paajanen et al., 2000; Qaiss et al., 2012; Wen et al., 2013; Zhang et al., 2011). More information on processing and related issues is available in our previous works (Mohebbi et al., 2015; Mohebbi et al., 2016).

Among the nonpolar polymers, cellular PP films can exhibit good piezoelectric-like properties after a proper charging process by imposing a high electrical field (Fang et al., 2008; Gilbert-Tremblay et al., 2012; Kirjavainen, 1987; Qaiss et al., 2012; Savolainen and Kirjavainen, 1989; Wegener, 2010; Wegener et al., 2005). Today, the popularity of PP is related to its excellent properties, such as low cost, high flexibility, good fatigue resistance (Antunes et al., 2010; Yu et al., 2011; Zhang et al., 2009), high tensile modulus and good chemical resistance (Vasile and Seymour, 1993).

It is well known that the morphology or cellular structure, which is strongly related to the processing conditions (Gendron, 2004; Lee, 2000; Okolieocha et al., 2015), has a direct effect on the mechanical and piezoelectric properties of foamed films. Furthermore, in addition to cell density and average cell size, cell shape and orientation are also important parameters for piezoelectric applications (Li et al., 2012). It has been reported that an eye-like cellular

structure with a cell *AR* (ratio between cell length and height) above 4 is suitable to obtain ferroelectret materials with good piezoelectric properties (Lindner et al., 2004; Tuncer, 2005; Xu et al., 2013). In our previous work, different types of eye-like cellular structures with good cellular homogeneity were successfully produced through continuous physical foaming using supercritical N_2 and after process and composition optimization (screw configuration, temperature profile, die temperature, stretching speed, flow rate, nucleating and blowing agent content), (Mohebbi et al., 2016). To achieve an eye-like cell shape structure it was observed that there is an optimum uniaxial stretching ratio at the die exit. As extensively discussed in this study, stretching above this optimum stretching ratio resulted in film failure and collapse/break-up of the cellular structure. Hence, to improve films cellular morphology (in terms of cell deformation), post-processing treatment was applied. The idea was to internally stretch the cells by a driving force based on supercritical N_2 molecules diffusing into the cellular structure and controlling the deformation to mainly occur in the longitudinal direction (machine direction). To achieve this objective, two different thermal-pressure treatments were applied and their effect on the morphological, mechanical, thermal and piezoelectric property of the resulting samples was studied.

To date, some investigations on the relationships between the tensile and piezoelectric properties of cellular structures have been published (Anton et al., 2014; Qiu et al., 2005; Wegener et al., 2004; Wu et al., 2015; Zhang et al., 2009; Zhang et al., 2014). However, other mechanical characterizations, such as DMA, compression strength and impact resistance have seldom been used to relate the mechanical properties of cellular materials to their piezoelectric behavior. Since the piezoelectric properties of cellular materials are related to their elasticity and deformation under different frequencies/applied forces, DMA was selected as an accurate tool to investigate these relationships. Hence, another objective of this study is to use DMA as a simple and powerful method, especially in the linear region, to determine the effect of the cellular structure on film piezoelectric behavior after post-processing treatment. Since in the linear region, the applied stresses are very low, small deformations are produced and the results can provide useful and accurate information about the microscopic structure of the cellular films. To the best of the authors' knowledge, no information can be found in the literature about the relationships between DMA and the piezoelectric properties of cellular structures. So, a comprehensive study was performed to

determine the effect of post-processing conditions on the morphological (SEM), mechanical (DMA) and thermal (DSC) properties of the samples produced and to relate this information with their piezoelectric behavior.

6.2 Experimental

6.2.1 Materials

The material used in this study was a uniaxially stretched foamed PP film with an eye-like cellular morphology. The film has a thickness of around 500 μm and a density of 0.707 g/cm^3. This sample was produced through a designed continuous physical foaming process using supercritical N_2 by optimization of the processing conditions and film composition. More details can be found in our previous work (Mohebbi et al., 2016). The properties of the initial film, coded PPn-S1, are presented in Table 6.1.

6.2.2 Thermal-pressure treatment

To achieve an eye-like cellular structure PP film with a high cell aspect ratio (*AR*), which is suitable for good piezoelectric properties (Lindner et al., 2004; Tuncer, 2005; Xu et al., 2013), two different post-processing treatments in terms of temperature and pressure (TPT) were applied using a one-liter cylindrical high-pressure vessel (Autoclave Engineers, USA) connected to a N_2 (Praxair, Canada) cylinder. In these TPT, the samples were placed in the high-pressure vessel. Then, the vessel was purged with N_2 to remove air. To achieve a high N_2 diffusion into the samples, the pressure was selected from atmospheric up to 5 MPa, which is well above the critical pressure of nitrogen (P_C = 3.4 MPa and T_C = 126 K) (Mohebbi et al., 2015). Moreover, as the melting temperature (T_m) of the PP used is 165°C and its glass transition temperature (T_g) is about 0°C, the temperature range was selected from room temperature up to 105°C. This range was chosen to be well above T_g so the polymer chains have some mobility to facilitate N_2 diffusion, but at the same time well below T_m to prevent film deformation during the treatment.

In the first post-processing treatment (R1), a stepwise TPT procedure was applied to the sample. As shown in Figure 6.1a, the pressure and temperature in each step were increased by 1 MPa and 20°C, respectively. Furthermore, 20°C increase in temperature was performed over a 2 min period and the system was kept for 3 min to stabilize at each conditions. Hence, each step represents a period of 5 min. In this case, the temperature increase started when the samples were first kept at a pressure of 1 MPa for a period of 5 min. Then, a stepwise TPT was applied: pressure up to 5 MPa (which is above the supercritical pressure of N_2) and temperature up to 105°C. Afterward, the samples were kept for about 10 min under these conditions and the system was cooled to room temperature while the pressure kept at 5 MPa. To keep the final cell structure produced, the pressure was kept constant until complete cooling, which took about 2 h. Finally, the vessel was depressurized and the samples were removed for analysis. The specifications of the sample obtained under this treatment are presented in Table 6.1 and the sample is coded as PPn-S1-R1.

As shown in Figure 6.1b, in the second post-processing treatment (R2), the temperature was first increased up to 105°C in one step, while the pressure was kept at 1 MPa, which took about 10 min. Like for R1, in this TPT the temperature increase also started when the samples were first kept at 1 MPa for a period of 5 min. Afterward, a stepwise pressure increase from 1 to 5 MPa was performed at a constant temperature of 105°C. In each step, the system was kept for 5 min to stabilize. Then, similar to R1, the samples were kept for about 10 min in the final conditions and the system was cooled down to room temperature (2 h) while the pressure was kept at 5 MPa. Finally, the vessel was depressurized and the samples were removed for analysis. The sample from this procedure was coded as PPn-S1-R2 and its specifications are presented in Table 6.1. Although other thermal-pressure treatments are possible, they were investigated and did not produced the cellular morphology sought. This is why they are not presented here.

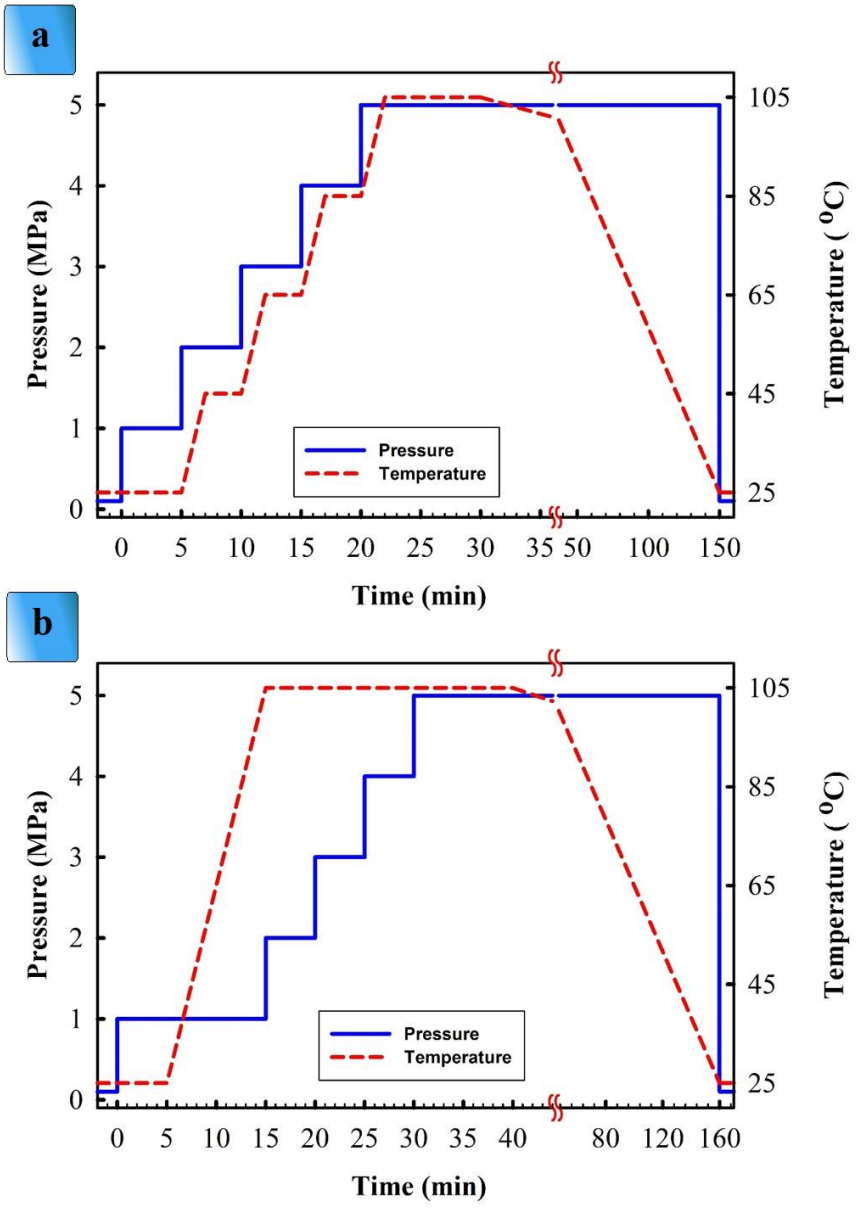

Figure 6.1. Schematic diagrams for the two TPT studied: a) R1 and b) R2.

6.2.3 Ferroelectret sample preparation

To achieve an effective corona charging, the air inside the cells was replaced by N_2 before charging. The reason is that N_2 has a higher breakdown strength than air (Paajanen et al., 2001). For this reason, the samples were placed in a one-liter cylindrical high-pressure vessel (Autoclave Engineers, USA) connected to a N_2 cylinder. The vessel was first purged with N_2

to remove air. Then, the pressure was set at 5 MPa to achieve supercritical N_2 conditions inside the vessel and the samples were left for 24 h at room temperature.

Afterward, the samples were charged by a corona process using a discharge generator (Static charge generator, Simco, USA) with a needle voltage of -21 kV and a charging time of 60 s. The charging needle was set at a distance of 4 cm from the samples. As shown in Figure 6.2, the gas inside the cells was ionized through corona charging and positive/negative electrical charges were created on the opposite faces of each cell surface. Afterward, the external surfaces were metalized with an aluminum coating to be conductive for piezoelectric measurements.

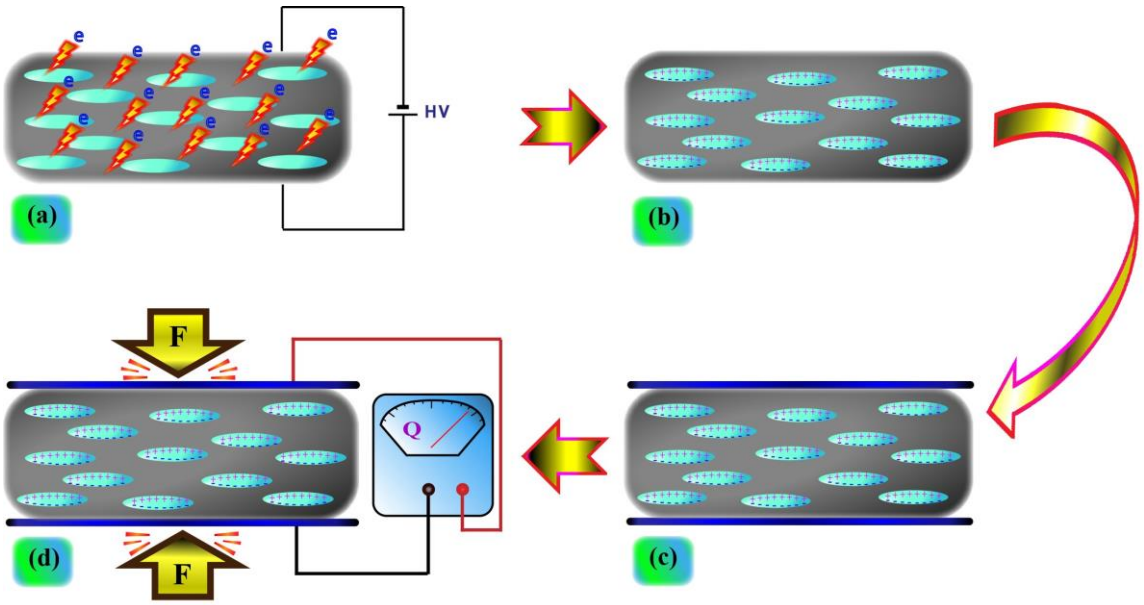

Figure 6.2. Schematic diagrams for: a) corona charging, b) charged sample having positive/negative electrical charges on the opposite faces of cell surfaces, c) charged sample with aluminum coating on both sides, and d) piezoelectric measurement.

6.2.4 Morphological analysis

The morphology of the foamed PP films was studied using scanning electron microscopy (SEM) with a JEOL JSM-840A (JEOL, Japan). The samples were first frozen in liquid nitrogen to have a clean fractured surface and were broken in both machine (longitudinal) and transverse directions. Afterward, the samples were coated with a Pd/Au layer and a

complete morphological characterization including cell shape, cell size, cell densities, and sample thickness using the *ImageJ* software (National Institute of Health, USA), was done based on SEM pictures taken at different magnifications.

6.2.5 Thermal analysis

Thermal analysis was performed to determine the crystallinity of the samples using differential scanning calorimetry (DSC) on a Perkin Elmer DSC7 (USA). Each sample was heated from 50°C to 250°C at a rate of 10°C/min.

The degree of crystallinity (X_C) was evaluated as (Kuboki, 2013):

$$X_C = \frac{\Delta H_{exp}}{\Delta H^*} \times \frac{1}{W_f} \tag{6.1}$$

where ΔH_{exp} is the experimental heat of fusion calculated from DSC curves, ΔH^* is the heat of fusion of the fully crystalline PP (210 J/g (Kuboki, 2013)), and W_f is the weight fraction of PP in the foamed samples.

6.2.6 Mechanical characterization

The tensile properties of the samples were characterized using an Instron model 5565 universal testing machine (Instron, USA) with a 500 N load cell according to ASTM D882. Rectangular samples (100 x 10 mm^2) were characterized at room temperature with a crosshead speed of 50 mm/min. At least five samples were tested to get an average and standard deviation for tensile modulus, tensile strength, and elongation at break.

The tensile behavior of the samples was also investigated using a dynamic mechanical analyzer (DMA) RSA3 (TA Instrument, USA). Rectangular samples (25 x 7.5 mm^2) were characterized in the linear viscoelastic range of the materials at room temperature. First, strain sweep tests were performed to determine the limits of the linear viscoelastic region of the samples. Then, frequency sweeps between 10^{-1} and 10^2 Hz (strain amplitude of 0.05%, which is inside the linear viscoelastic region) were done in both the longitudinal (L) and transverse

(*T*) processing directions. The reported values for storage and loss modulus are the average of at least three measurements.

6.2.7 Piezoelectric characterization

The d_{33} coefficient of the ferroelectret samples was measured from the quasi-static method, which is a direct method to measure piezoelectric properties (Mohebbi et al., 2016; Zhang et al., 2014; Zhang et al., 2014). The d_{33} coefficient corresponds to the ratio of the induced charge Q to the force F applied perpendicular to the film surface as (Mohebbi et al., 2016):

$$d_{33} = {}^{Q}/_{F} = {}^{Q}/_{mg} \tag{6.2}$$

where m is the mass applied on the sample and g is the acceleration of gravity.

The induced charge was detected by a programmable electrometer (Keithley 6512, USA) as:

$$Q = \int_0^t I \, dt \tag{6.3}$$

where t and I are the duration of the experiment and the electric current, respectively.

A data acquisition module NI USB-6211 (National Instruments, USA) was used to transfer the experimental data to a computer for further analysis. In this procedure, a static force of 1.57 N was applied on the ferroelectret sample, and removed quickly. After 10 s, the produced charge Q was measured by the electrometer (Wu et al., 2015). For each sample, this procedure was repeated three times and the average value of the induced charge was used to calculate the d_{33} coefficient.

6.3 Results and discussion

6.3.1 Morphological characterization

Typical SEM images of the original sample (PPn-S1) and the treated samples (PPn-S1-R1 and PPn-S1-R2) in both longitudinal (*L*) and transverse (*T*) directions are presented in Figure 6.3. Their corresponding *AR*, cell size (in both L and T directions), and cell density, are

reported in Table 6.1. Due to cell deformation and different morphology in both *L* and *T* directions, the cell density (cells/cm^3) was calculated as (Gosselin and Rodrigue, 2005):

$$N = N_1(N_2)^{1/2} \tag{6.4}$$

where N_1 (cells/cm^2) and N_2 (cells/cm^2) are the surface cell densities in the longitudinal and transverse directions respectively, which are calculated as:

$$N_i = \frac{n}{A} \tag{6.5}$$

where *n* is the number of cells and *A* is the corresponding micrograph area.

As shown by SEM pictures of Figure 6.3, all the samples have an eye-shaped cell structure due to the uniaxial stretching at the die exit. It has been reported that a cellular film having eye-shaped cells with an *AR* above 4 is the best structure for piezoelectric applications (Lindner et al., 2004; Tuncer, 2005; Xu et al., 2013). As presented in Table 6.1, the original sample (PPn-S1) has an average *AR* of 5.4. As seen from Figure 6.3, for sample PPn-S1-R1, the cells are larger in size and more elongated in the *L* direction leading to a 20% increase in *AR* (6.6). Hence, the thermal-pressure treatment TPT-1, which corresponds to a stepwise increase of both temperature and pressure, was very effective to produce a structure with more stretched eye-like cells. Because of cell expansion, cell density of PPn-S1-R1, in comparison with PPn-S1, decreased from 6.5x10^5 to 5.2x10^5 cells/cm^3.

Figure 6.3 shows that the cells of PPn-S1-R2, in comparison with PPn-S1(original sample), are also more expanded. However, TPT-2 led to a cell shape change from eye-like to a less elongated shape and a decrease in the *AR* (around 5.1). Hence, TPT-2, which is based on a stepwise increase in temperature, is not an appropriate procedure to get the desired structure. Furthermore, it can be seen from Figure 6.3 that cell combination/coalescence occurred in both *L* and *T* directions. Hence, cell density in PPn-S1-R2 also decreased to become even lower than PPn-S1-R1 (6.5x10^5 to 4.4x10^5 cells/cm^3).

Table 6.1. Morphological properties of the samples produced compared to the original sample (PPn-S1) (Mohebbi et al., 2016).

Sample code	Cell aspect ratio (*AR*)	Cell size *L*-direction (μm)	Cell size *T*-direction (μm)	Cell density (10^5 cells/cm^3)
PPn-S1	5.4 ± 1.0	171 ± 55	31 ± 8	6.5 ± 0.8
PPn-S1-R1	6.6 ± 1.5	199 ± 100	33 ± 12	5.2 ± 0.5
PPn-S1-R2	5.1 ± 1.9	205 ± 117	43 ± 23	4.4 ± 0.6

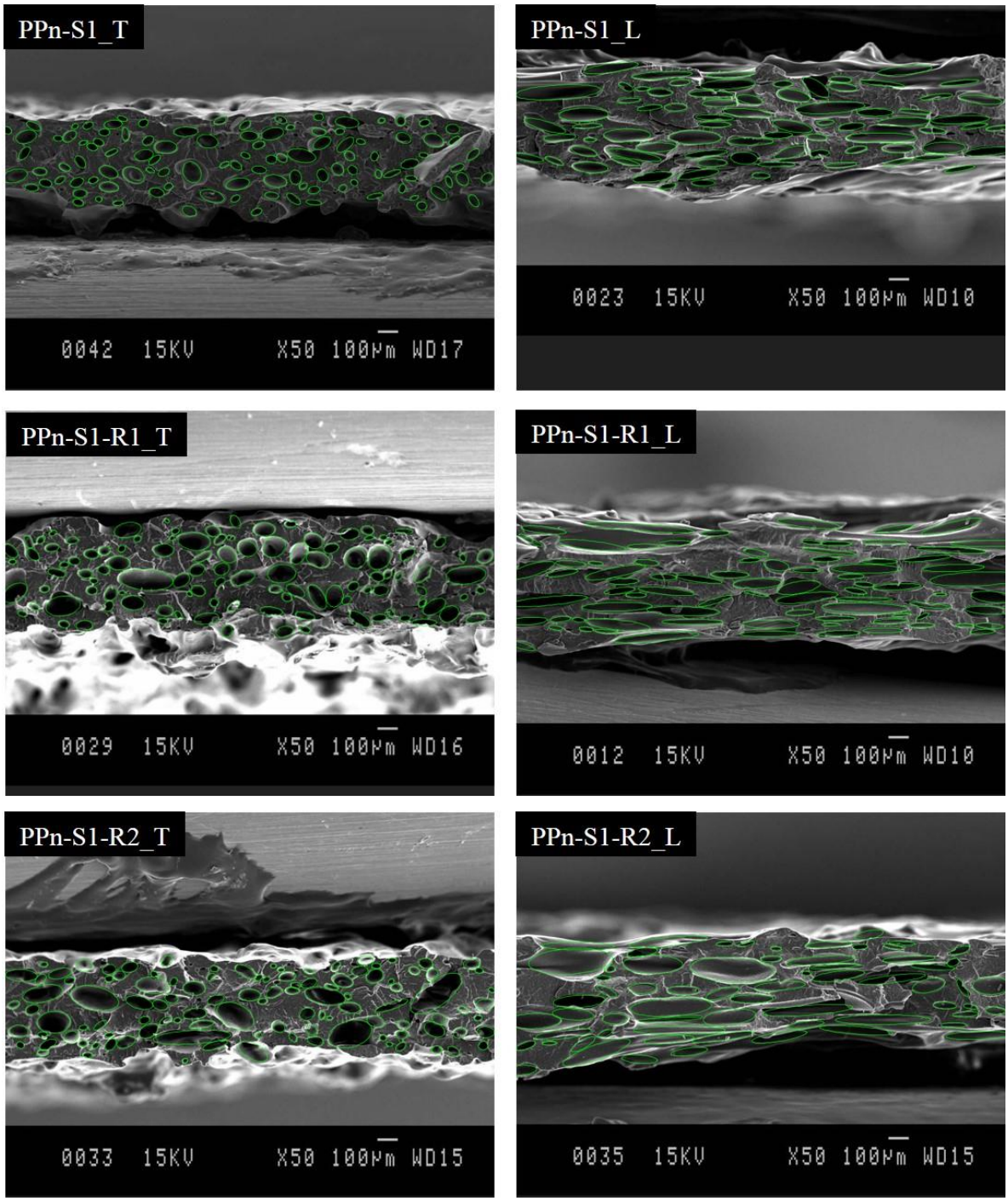

Figure 6.3. Typical SEM pictures of the foamed PP films in the longitudinal (*L*) and transverse (*T*) directions.

6.3.2 Mechanical and thermal properties

Young's modulus, tensile strength, and elongation at break of the samples are reported in Figure 6.4 together with a sketch of the cellular structure of both original and treated cellular films. As shown in Figure 6.4b, PPn-S1-R1 has the lowest Young modulus of about 580 MPa, which can be associated to its higher AR (Table 6.1). This behavior can be interpreted by the U-shape behavior of the cellular structure (Wegener et al., 2005): i.e. increasing the *AR* of cellular structure results in lower elastic stiffness leading to films having higher piezoelectric properties. More information about the U-shape behavior is available in our previous work (Mohebbi et al., 2016a). On the other hand, Figure 6.4b shows that PPn-S1-R2, which has a cellular structure with less elongated cell shape (lower *AR* of about 5.1), has a higher Young's modulus of about 630 MPa. Furthermore, as seen in Figure 6.4c and Figure 6.4d, the samples showed similar tensile strength, but the elongations at break for both treated samples, PSn-S1-R1 and PSn-S1-R2, are slightly higher than the original sample (PSn-S1). This can be explained by crystallinity differences between the original and treated samples. As reported in Table 6.2 the crystallinity of PPn-S1 decreased from 42% to a value below 40% for PPn-S1-R1 and PPn-S1-R2 (5% decrease in crystallinity degree). Generally, lower crystallinity produces higher elongation at break (Kundu et al., 2003; Müller et al., 2009). Also, lower crystallinity can be the result of an increased free volume fraction during the thermal-pressure treatment. It has been reported that gas pressure has a significant effect on the free volume hole sizes, and the amount of dissolved gas can influence the size of these free volumes (Andersson et al., 2010). Furthermore, it has been shown that supercritical fluids (SCF), as a result of their low viscosity and negligible surface tension, have high mass transfer rates into polymers (Li et al., 2002). The change of free volume and crystalline areas of the treated samples is schematically shown in Figure 6.5: the diffusion of SC-N_2 molecules into the samples and between the molecules leads to a decrease in the crystalline area of the samples. In this figure, the crystalline areas of the original sample before TPT are shown with arrows, which for the samples after the TPT regimes (PPn-S1-R1 and PPn-S1-R2) are decreased to smaller areas. This resulted in the reduction of crystallinity and accordingly an increase of the elongation at break of the treated samples.

It should be mentioned that the mechanical properties of unfoamed PP are much higher than foamed PP. This is mainly related to the replacement of a substantial amount of the PP matrix, which is responsible for the mechanical performance (elongation at break, Young's modulus, tensile strength) by cells (filled with gas).

Table 6.2. DSC results of the samples produced.

Sample code	Volume fraction of PP (W_f)	ΔH (J/g)	Crystallinity, X (%)
PPn-S1	0.98	86.5	42.0
PPn-S1-R1	0.98	81.9	39.8
PPn-S1-R2	0.98	82.7	40.2

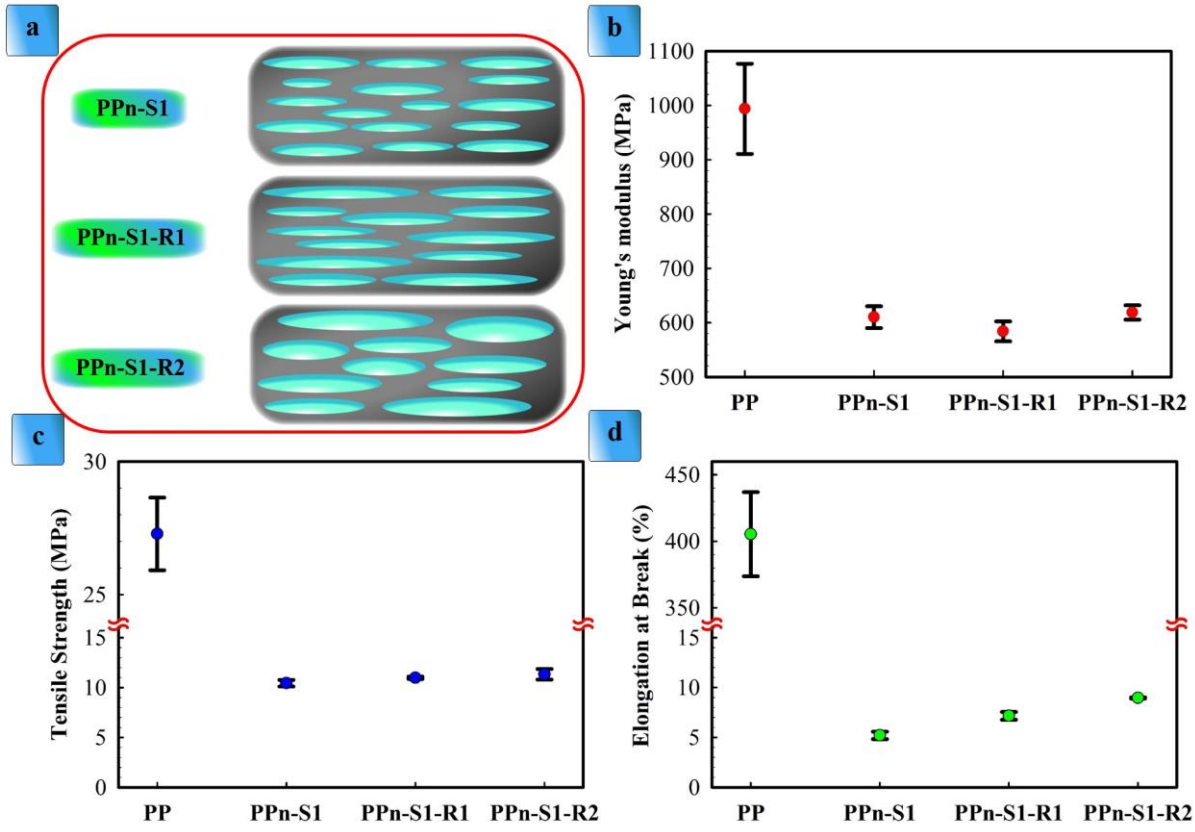

Figure 6.4. a) Schematic representation of the cellular structure, b) Young's modulus, c) tensile strength, and d) elongation at break in the machine (L) direction of the samples.

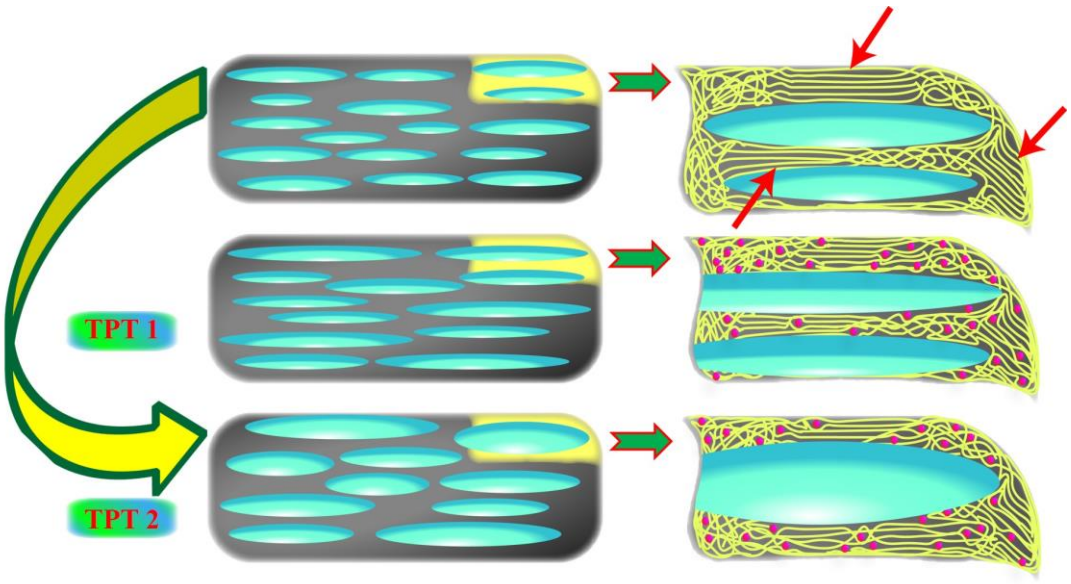

Figure 6.5. Schematic representation of the proposed structures of PPn-S1 by imposing the TPT and the effect of N_2 molecules diffusion into their crystalline areas leading to the structure of PPn-S1-R1 and PPn-S1-R2.

Based on SEM results (Figure 6.3), two different morphologies in the longitudinal (*L*) and transverse (*T*) directions are obtained. The DMA results in terms of storage (*E'*) and loss (*E''*) moduli as a function of frequency in both *L* and *T* directions for the unfoamed and cellular PP films are shown in Figure 6.6. The results show that the storage and loss moduli of all samples in the *L* direction are higher compared to those in the *T* direction, which confirms the effective cell deformation in the *L* direction. As for Young's modulus (Figure 6.4b) PPn-S1-R1 also has the lowest storage and loss moduli due to its highest *AR* value (Table 6.1). Furthermore, Figure 6.6 shows that the unfoamed PP film has higher storage modulus (about 75% higher than that of the foamed samples) and loss modulus (about 350% higher than that of the foamed samples). This is another advantage of DMA where both the elastic (related to *E'*) and viscous (related to *E''*) properties of the materials can be analyzed separately.

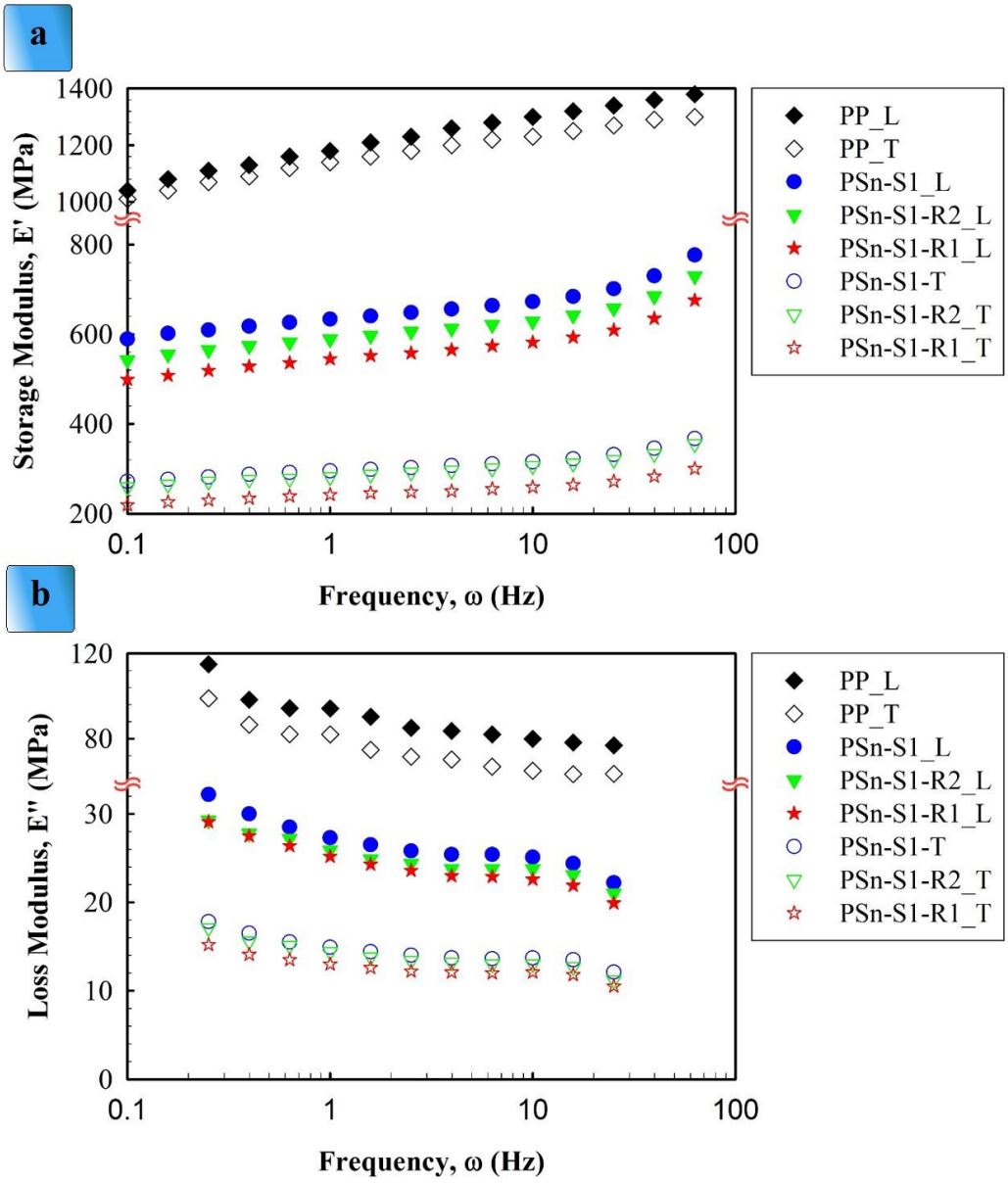

Figure 6.6. a) Storage and b) loss moduli, as a function of frequency for the samples produced.

Two parameters can be proposed as:

$$AMR1 = E'(L)/E'(T) \quad (6.6)$$

and

$$AMR2 = E''(L)/E''(T) \quad (6.7)$$

Both parameters are function of frequency and their corresponding curves are presented in Figure 6.7. For both moduli ratios, the highest values for AMR1 and AMR2 are obtained for PPn-S1-R1, which has the highest *AR* value (Table 6.1). On the other hand, the lowest values for AMR1 and AMR2 are obtained for PPn-S1-R2, which has the lowest *AR* value (about 5.1). Hence, it can be concluded that both ratios, which are obtained through DMA analysis, are very sensitive to the morphology of the cellular structure: an *AR* variation from 5.1 to 6.6 led to a 10% increase of AMR1 and 14% of AMR2. So a simple DMA test can be performed to determine if the morphology of a cellular film can be appropriate for piezoelectric applications without the need to perform a complete and time consuming morphological characterization of the cellular structure of the films such as SEM/image analysis.

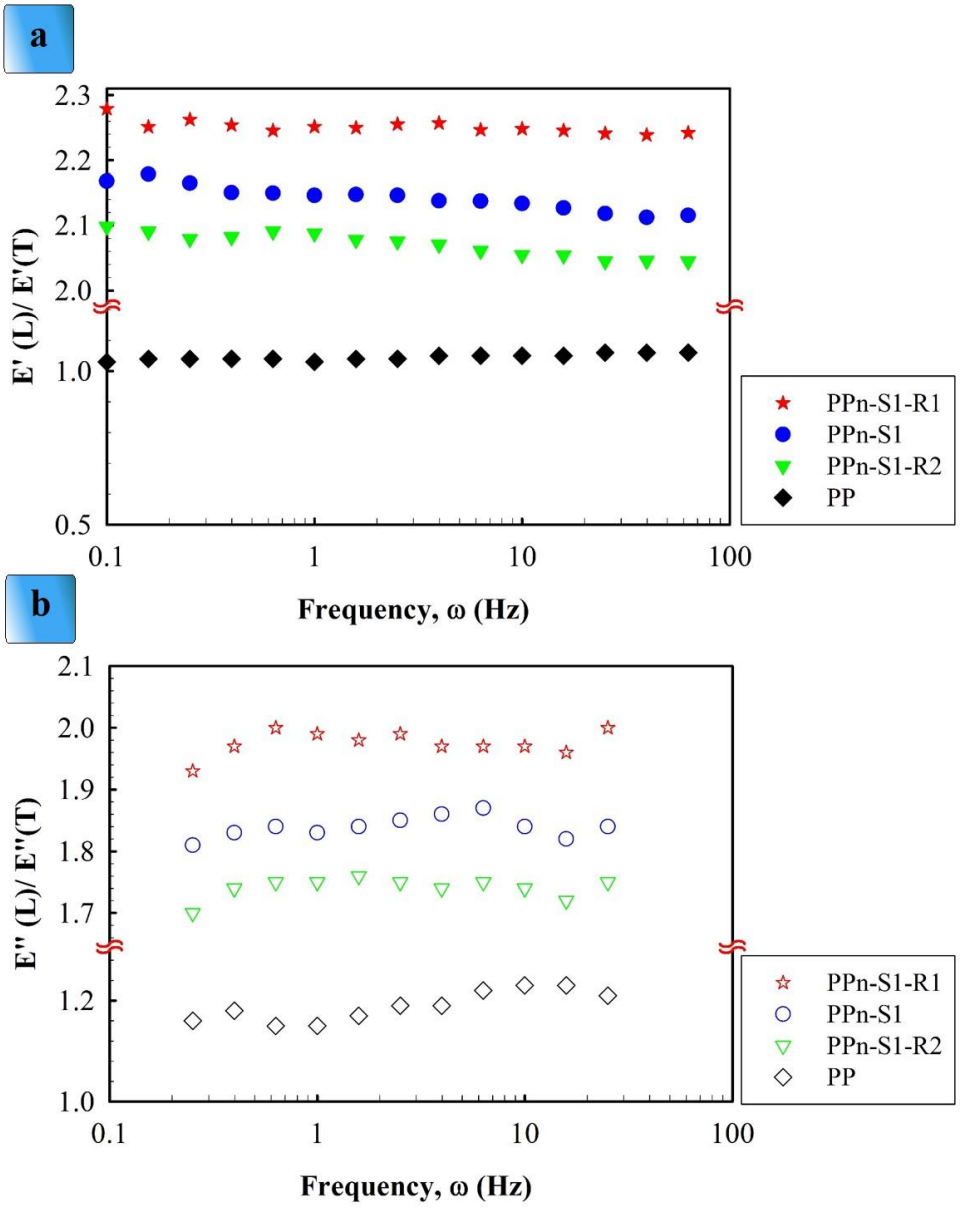

Figure 6.7. Storage and loss moduli ratios as a function of frequency for the longitudinal (*L*) over the transverse (*T*) direction: (a) AMR1 and (b) AMR2.

6.3.3 Piezoelectric properties of the developed cellular films

The output charge diagrams for the samples having N_2 as the ionizing gas are presented in Figure 6.8. Furthermore, the piezoelectric d_{33} coefficient of the ferroelectret films is presented in Figure 6.9, as a function of AMR1, together with their respective Young's

modulus and *AR* value. Actually, the importance of AMR1 as a useful and sensitive parameter to predict the piezoelectric d_{33} coefficient is confirmed by the trends observed for the Young's moduli (mechanical parameter) and *AR* value (morphological parameter). Both parameters have been already used in literature to understand the piezoelectric behavior of ferroelectret films (charged cellular structure) (Hillenbrand et al., 2005; Wegener et al., 2004; Zhang et al., 2007; Zhang et al., 2011; Zhang et al., 2009; Zhang et al., 2014). As seen from Figure 6.7, because AMR1 has a more stable trend (more precise measurement in the solid state) over a wide frequency range, it is selected as the main parameter to study the variation of the piezoelectric d_{33} coefficient. The results show that PPn-S1-R1, which has an eye-like cell structure with the highest AMR1 value of about 2.30 in comparison with the other samples (2.14 for PPn-S1 and 2.07 for PPn-S1-R2), shows the highest average output charge of 1300 pC (Figure 6.8) and a piezoelectric d_{33} coefficient above 800 pC/N (Figure 6.9). Moreover, this sample has the highest *AR* value of 6.6 (Table 6.1) and the lowest Young's modulus of 580 MPa (Figure 6.4). On the other hand, PPn-S1-R2, which has a less elongated cell shape and the lowest *AR* value, as well as the highest Young's modulus, shows the lowest AMR1 value as well as the lowest output charge of 700 pC (Figure 6.8) with a piezoelectric d_{33} coefficient of only 450 pC/N (Figure 6.9).

Therefore, based on the results obtained, higher AMR1 can be associated to a cellular structure having a higher *AR* value and a lower Young's modulus, resulting in a higher piezoelectric d_{33} coefficient. On the other hand, a lower AMR1 is an indication that the cellular structure has a less elongated shape (lower *AR* value) and consequently a higher Young's modulus, leading to a lower piezoelectric d_{33} coefficient.

To the best of our knowledge, the piezoelectric d_{33} coefficient obtained for the original ferroelectret PP sample (550 pC/N for PPn-S1) is much better than typical piezoelectric d_{33} values of about 350 pC/N reported in literature (Zhang et al., 2014). Moreover, this piezoelectric d_{33} value increased by about 45% for PPn-S1-R1 (800 pC/N) through effective post-processing treatment. So the stepwise TPT procedure was very effective to increase the *AR* value and the piezoelectric d_{33} coefficient. On the other hand, the one-step temperature increase TPT led to less elongated cells with lower *AR* as well as lower AMR1 and piezoelectric d_{33} coefficient.

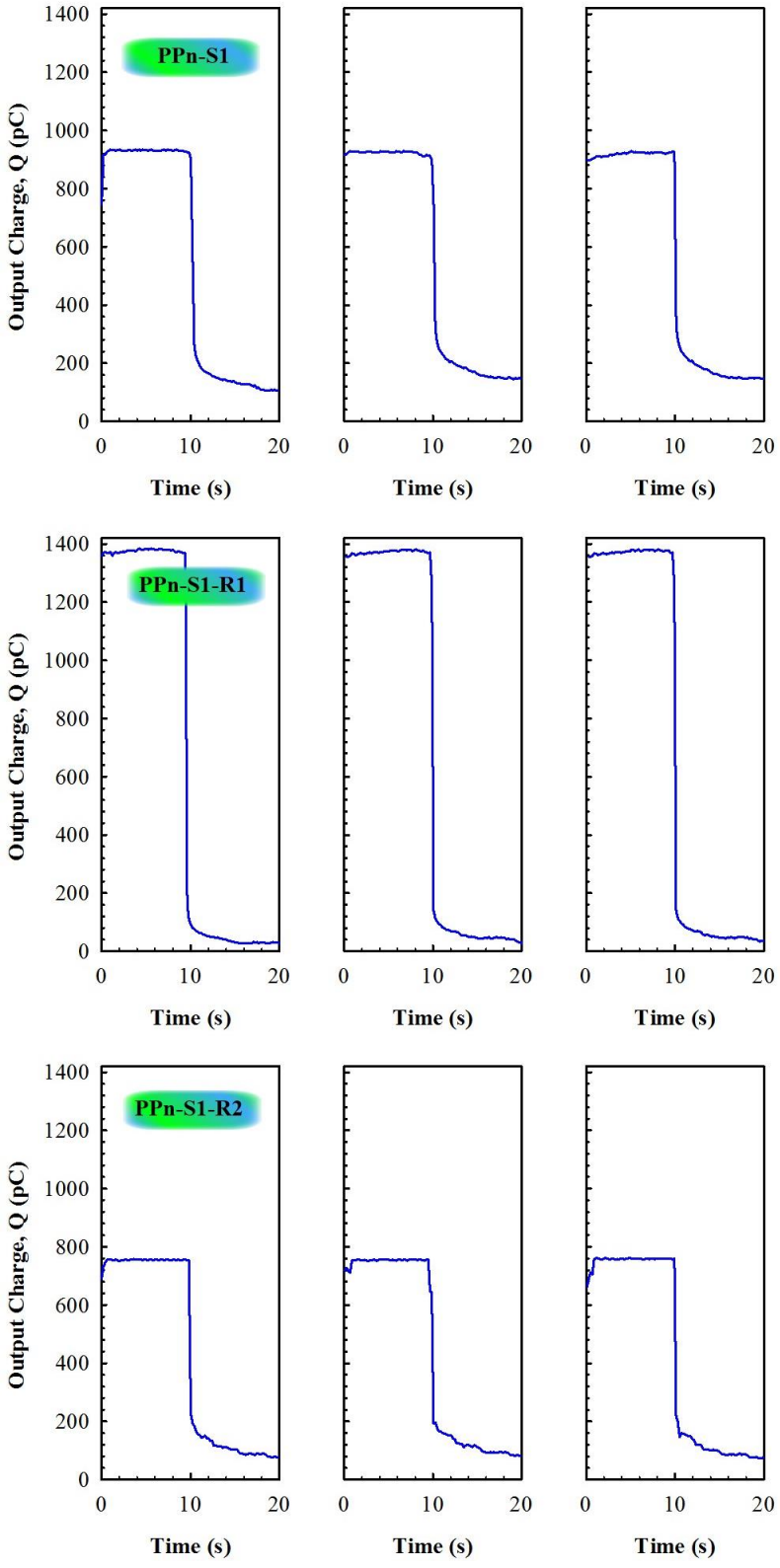

Figure 6.8. Output charge diagrams for the ferroelectret films produced (three repetitions for each sample to show repeatability).

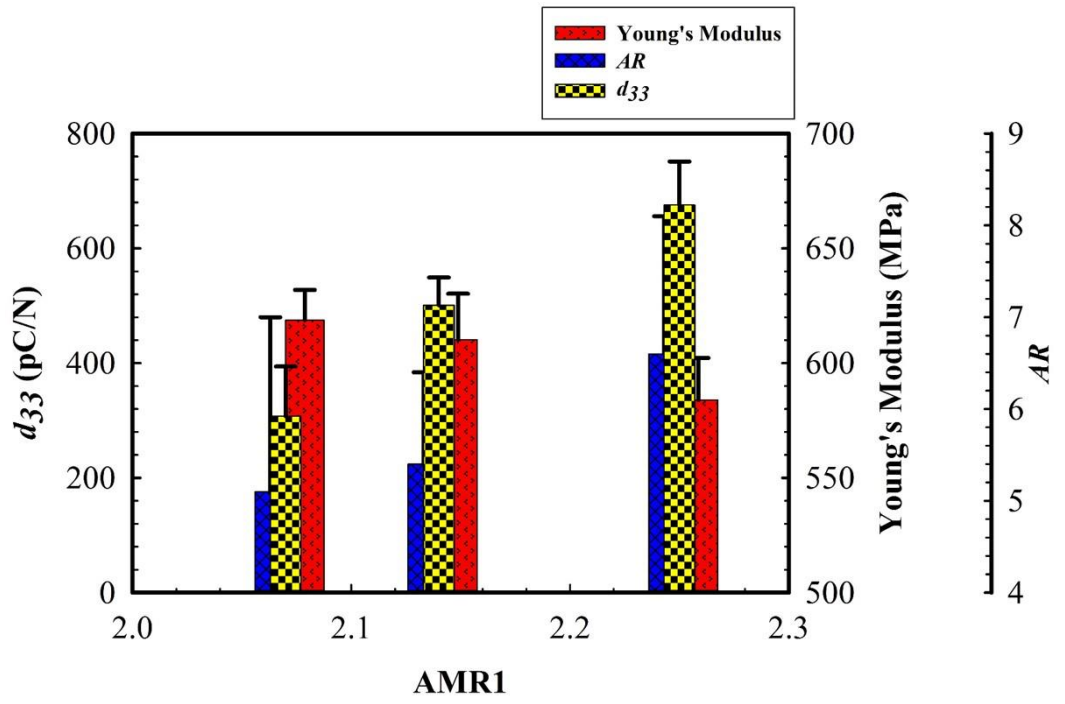

Figure 6.9. Piezoelectric d_{33} coefficient, Young's modulus and *AR* value as a function of AMR1 for the ferroelectret films.

The resulting structure from both TPT can be interpreted as follow. It is known in materials that crack propagation normally takes place from sharp corners (having low tip radius), which are stress concentration points (Persson et al., 2005). In TPT-1, when the sample is placed into a stepwise temperature and pressure increase (Figure 6.10), as the two tips of the cells in comparison with the other parts of the cells have more tendency to propagate/stretch (because they have lower radius of curvature; stress concentration points Figure 6.10a), N_2 molecules seem to accumulate more in those tips. Hence, a higher driving force resulting from the accumulated N_2 molecules in both extremities led to more cells expansion/stretching in the longitudinal (*L*) direction in comparison with the transverse (*T*) direction (Figure 6.10b). By its propagation, the tips radius are more decreased and their tendency to propagation as well as accumulation of N_2 molecules is further increased, finally leading to a more stretched eye-like shape cell with a higher *AR* value in comparison with the initial state. On the other hand, for TPT-2, as it is a rapid process in terms of temperature increase, the N_2 molecules do not have enough time to accumulate in both extremities which are

pushed apart of the cell surfaces similarly. Here, by its propagation, the cells are only expanding and both tip radii increase so decreasing their tendency to propagate as well as accumulate N_2 molecules leading to a less elongated cell shape with a lower *AR* value in comparison with the initial state (Figure 6.10b). Nevertheless, more investigations would be needed to fully understand the relation between all the properties investigated; i.e. between post-treatment conditions and final morphology.

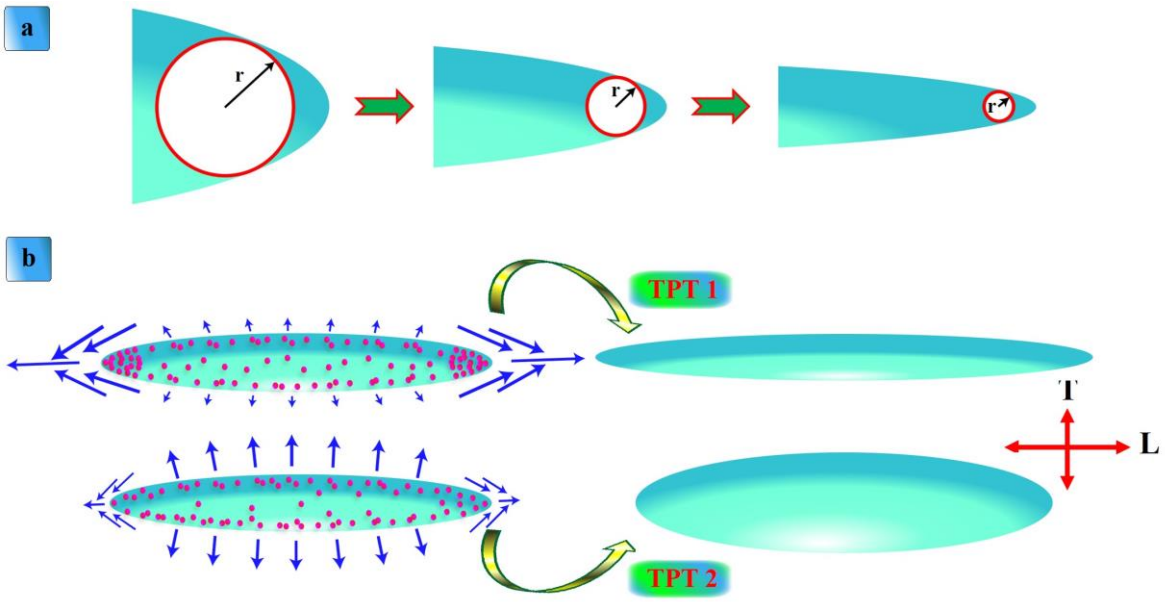

Figure 6.10. Schematic representation of a) decrease in tip-radius as a result of stretching in the *L* direction, and b) cell expansion by imposing different TPT and their respective resulting structure.

6.4 Conclusion

This work showed that through a successful gradual post-processing thermal-pressure treatment, the cells of foamed PP films were internally stretched by diffusing supercritical N_2 molecules into the cellular structure. Hence, a ferroelectret material based foamed PP film having an eye-like cellular structure with a high aspect ratio (*AR*) value of 6.6 was obtained. The piezoelectric d_{33} coefficient of this treated ferroelectret PP film was improved by 45% (800 pC/N) in comparison with the untreated sample (550 pC/N). Furthermore, the mechanical characterization of the foamed PP films showed that the cell morphology has a

direct effect on the mechanical properties of the films as samples having higher *AR* values had lower Young's moduli. Finally, it was shown that a simple DMA characterization can be used as a rapid analysis to predict the piezoelectric behavior of the cellular structures. So a cellular structure of higher *AR* values had higher AMR1 (*E′(L)/E′(T)*) and AMR2 (*E″(L)/E″(T)*), leading to higher piezoelectric d_{33} coefficients.

Acknowledgements

Financial support from the Natural Sciences and Engineering Research Council of Canada (NSERC) and Fonds Québécois de la Recherche sur la Nature et les Technologies (FRQNT) was received for this work. The technical support of Mr. Jean Côté, Mr. Yann Giroux, and Mr. André Ferland is also highly appreciated.

Chapter 7

Conclusions and recommendations

7.1 General conclusions

Today, cellular polymers are under investigation for several piezoelectric applications such as actuators, vibration control, ultrasonic transducers, sensors, energy conversion devices, speakers, microphones, keyboards, shock sensors, as well as thermal and optical property measurement devices.

The first part of this work showed that the developed continuous foaming process based on flat film extrusion-calendaring with supercritical nitrogen (SC-N_2) is a suitable and low cost method to obtain very thin (less than 500 μm) polypropylene (PP) films having uniform and well-developed eye-like cellular structure leading to a good quasi-static piezoelectric d_{33} coefficient. The results showed that the selected PP has a very narrow foaming temperature window of 167±4ºC. By increasing the die temperature outside this range, open-cells were formed and a non-uniform cellular structure was obtained, while decreasing the foaming temperature below this optimum range resulted in limited bubble growth and stretching possibility. The presence of 2% nano-$CaCO_3$ as a nucleating agent had an effective role in the production of a uniform well-developed eye-like cellular structure needed for ferroelectret films. Moreover, the mechanical results showed that the foam morphology has a direct effect on the mechanical properties of the produced films. This is related to material stretching (anisotropy) at the extruder die exit. Samples having eye-like cellular structure with more uniform cell size distribution were shown to have lower Young's moduli.

In the second part of the study, it was shown that charging of the obtained eye-like cellular structure PP films using corona discharge followed by metallization resulted in ferroelectret films having a good piezoelectric d_{33} coefficient. Piezoelectricity in charged cellular polymers, such as PP, was created by the deformation of charged cells in which positive and negative electrical charges were created on the opposite faces of each cell surfaces. These electrical charges were obtained by ionizing the gas inside the cells through corona discharge. The results showed that the piezoelectric d_{33} coefficient can be substantially increased (more than double) by simply replacing air with N_2 inside the cells as the ionizing gas. Moreover, a simple dynamic mechanical analysis (DMA) test was proposed as a rapid analysis to predict the piezoelectric behavior of the cellular structure produced. DMA was performed in both

machine/longitudinal (L) and transverse (T) directions of the produced cellular PP films. In this context, two new parameters, called AMR1 and AMR2 (anisotropic modulus ratio), were proposed as the ratios $E'(L)/E'(T)$ and $E''(L)/E''(T)$, respectively. The results showed that samples having uniform cellular structures with higher cell aspect ratio (AR) had higher AMR1 and AMR2 values. The variation of the piezoelectric d_{33} coefficient with respect to AMR1, which had a more stable trend over a wide frequency range, was also studied. It was shown that increasing AMR1 from 1.44 to 2.14 resulted in about 200% increase in piezoelectric d_{33} coefficient (from 280 to 550 pC/N). However, a minimum AMR1 of around 1.7 is needed to achieve $AR > 4$, which is necessary to get good piezoelectric properties.

Finally, a more developed eye-like cellular PP film with a higher AR value of 6.6 was produced through a successful gradual temperature and pressure post-processing treatment. During this process, the cells inside the foamed PP films were internally stretched by diffusing supercritical N_2 molecules into the cellular structure. The piezoelectric d_{33} coefficient of this treated ferroelectret PP film was improved by 45% (800 pC/N) in comparison with the untreated sample (550 pC/N).

7.2 Recommendations for future work

- In this work, a special continuous extrusion-calendering method was developed to produce a low cost thin cellular PP film having a uniform eye-like structure leading to a good quasi-static piezoelectric d_{33} coefficient. As a next step, the optimization of the processing conditions could be done using high melt strength PP (alone or blended). This could improve the foaming and stretching steps to get a more elongated cellular structure to improve the piezoelectric properties of the final films.
- Applying biaxial stretching on the produced foamed films could improve the cellular structure in both machine and transverse directions. This could result in higher piezoelectric sensitivity. In fact, through this method, it would be possible to increase each cell surface area for higher charge accumulation.
- In the first part of the study, the eye-like structure of the PP films was improved using $CaCO_3$ as nucleating agent. It would be interesting to study various nucleating agents with different sizes and geometries such as nano-clay (platelet) and nano-glass fibre

(cylinders) to study their effect of the final properties of the PP films. But it should be mentioned that conductive nucleating agents such as carbon fibres, carbon nanotubes, and graphene cannot be used to produce materials for ferroelectret applications. The reason is that a non-conductive cellular structure is needed to keep the charges inside the cells and work as capacitances.

- Piezoelectric measurements based on other methods, as discussed in chapter 3 like resonance and dynamic methods, would be interesting to compare with the quasi-static results of this work.
- In the charging process used in this study, only N_2 was invetigated as an ionizing gas inside the cells to replace air. It would be interesting to study other gases with higher breakdown strength, such as SF_6, to further optimize the charging parameters.
- In this study, two parameters were proposed to predict the piezoelectric behavior of the samples using DMA. Moreover, it was shown that these parameteres were sensitive, simple and used as new parameteres to develop/design ferroelectret materials. Modeling of the relationships between AMR1, AR and d_{33} can open the door to tailor-made and better design of new ferroelectret materials. This can be very useful in the future to produce more sensitive structures, especially for sensors.
- Finally, modelling of the relationships between the piezoelectric d_{33} coefficient with the applied force would be another important complementary investigation. This would be of interest as the relationship between this coefficient and the applied force is highly non-linear. Hence, understanding this dependence would be a critical step towards the development and optimization of ferroelectret PP film design for specific applications. In this context, an analysis of the maximum force that the samples can sustain under different conditions would determine a reasonable working range for a produced material.

References

Alemán, J., Chadwick, A. V., He, J., Hess, M., Horie, K., Jones, R. G., Kratochvíl, P., Meisel, I., Mita, I., and Moad, G. (2007). Definitions of terms relating to the structure and processing of sols, gels, networks, and inorganic-organic hybrid materials (IUPAC Recommendations 2007). *Pure and Applied Chemistry*, 79(10), 1801-1829.

Altafim, R., Basso, H., Altafim, R., Lima, L., de Aquino, C., Neto, L. G., and Gerhard-Multhaupt, R. (2006). Piezoelectrets from thermo-formed bubble structures of fluoropolymer-electret films. *Dielectrics and Electrical Insulation, IEEE Transactions on, 13*(5), 979-985.

An, Z., Mao, M., Cang, J., Zhang, Y., and Zheng, F. (2012). Significantly improved piezoelectric thermal stability of cellular polypropylene films by high pressure fluorination and post-treatments. *Journal of Applied Physics, 111*(2), 024111.

An, Z., Tang, M., Xia, Z., Zheng, X., and Zhang, X. (2006). Chemical surface treatment and charge stability of polypropylene cellular electret film. *Acta Physica Sinica, 55*(2), 803-810.

An, Z., Zhao, M., Yao, J., Zhang, Y., and Xia, Z. (2009). Improved piezoelectric properties of cellular polypropylene ferroelectrets by chemical modification. *Applied Physics A, 95*(3), 801-806.

Andersson, A., Zhai, W., Yu, J., He, J., and Maurer, F. H. (2010). Free volume and crystallinity of poly (ethylene naphthalate) treated in pressurized carbon dioxide. *Polymer, 51*(1), 146-152.

Anton, S., Farinholt, K., and Erturk, A. (2014). Piezoelectret foam–based vibration energy harvesting. *Journal of Intelligent Material Systems and Structures*, *25*, 1681

Antunes, M., Gedler, G., and Velasco, J. I. (2013). Multifunctional nanocomposite foams based on polypropylene with carbon nanofillers. *Journal of Cellular Plastics, 49*(3), 259-279.

Antunes, M., Realinho, V., and Velasco, J. I. (2010). Study of the influence of the pressure drop rate on the foaming behavior and dynamic-mechanical properties of CO2 dissolution microcellular polypropylene foams. *Journal of Cellular Plastics, 46*(6), 551-571.

Bao, D., Liao, X., He, T., Yang, Q., and Li, G. (2013). Preparation of nanocellular foams from polycarbonate/poly (lactic acid) blend by using supercritical carbon dioxide. *Journal of Polymer Research, 20*(11), 1-10.

Bauer, S., Bauer-Gogonea, S., Camacho-Gonzales, F., Dansachmuller, M., Graz, I., Kaltenbrunner, M., Leonhartsberger, J. G., and Schwodiauer, R. (2005). Ferroelectrets: polymer-foam space-charge electrets with ferroelectric-like behaviour. In *IEEE 12th International Symposium on Electrets 2005*, pp. 24–27.

Bauer, S., Gerhard-Multhaupt, R., and Sessler, G. M. (2004). Ferroelectrets: Soft electroactive foams for transducers. *Physics Today, 57*(2), 37-43.

Behrendt, N., Altstadt, V., Schmidt, H.-W., Zhang, X., and Sessler, G. M. (2006). Development of porous polypropylene blends with NA11 particles and glass hollow spheres by biaxial stretching for electret applications. *Dielectrics and Electrical Insulation, IEEE Transactions on, 13*(5), 992-1000.

Belhora, F., Hajjaji, A., Fatnani, E., Zahra, F., Rjafallah, A., and Guyomar, D. (2015). Energy harvesting using hybridization of dielectric nanocomposites and electrets. *Polymers for Advanced Technologies, 26*(6), 569-573.

Bosse, P. W., Challagulla, K. S., and Venkatesh, T. (2012). Effects of foam shape and porosity aspect ratio on the electromechanical properties of 3-3 piezoelectric foams. *Acta Materialia, 60*(19), 6464-6475.

Braña, G. O., Segovia, P. L., Magraner, F., and Quijano, A. (2011). Influence of corona charging in cellular polyethylene film. *Journal of Physics: Conference Series,* 301, 012054.

Burt, J. G. (1978). The elements of expansion of thermoplastics Part II. *Journal of Cellular Plastics, 14*(6), 341-345.

Cantat, I., Cohen-Addad, S., Elias, F., Graner, F., Höhler, R., and Pitois, O. (2013). *Foams: structure and dynamics*: Oxford University Press, Oxford.

Challagulla, K., and Venkatesh, T. (2013). Computational Modeling of Piezoelectric Foams. *JOM, 65*(2), 256-266.

Chang, C., Tran, V. H., Wang, J., Fuh, Y.-K., and Lin, L. (2010). Direct-write piezoelectric polymeric nanogenerator with high energy conversion efficiency. *Nano Letters, 10*(2), 726-731.

Collais, D. I., and Baird, D. G. (1995). Tesile toughness of microcellular foams of polystyrene, styrene-acrylonitrile copolymer, and polycarbonate, and the effect of dissolved gas on the tensile toughness of the same polymer matrices and microcellular foams. *Polymer Engineering and Science, 35*(14), 1167-1177.

Colton, J. (1989). The nucleation of microcellular foams in semi crystalline thermoplastics. *Material and Manufacturing Process, 4*(2), 253-262.

Colton, J. S., and Suh, N. P. (1987). Nucleation of microcellular foam: theory and practice. *Polymer Engineering and Science, 27*(7), 500-503.

Colton, J. S., and Suh, N. P. (1987). The nucleation of microcellular thermoplastic foam with additives: Part I: Theoretical considerations. *Polymer Engineering and Science, 27*(7), 485-492.

Colton, J. S., and Suh, N. P. (1992). *Microcellular foams of semi-crystaline polymeric materials*, US Patents 5,160,674.

Dansachmuller, M., Schwodiauer, R., Bauer-Gogonea, S., Bauer, S., Paajanen, M., and Raukola, J. (2005). Elastic and electromechanical properties of polypropylene foam ferroelectrets. *Applied Physics Letters, 86*(3), 031910-031913.

Dealy, J., and Larson, R. (2006). *Structure and Rheology of Molten Polymers: From Structure to Flow Behavior and Back Again*: Hanser, Munich.

Dealy, J. M., and Wissbrun, K. F. (1990). *Melt rheology and its role in plastics processing*: Springer, New York.

DeNicola, A. J., Galambos, A. F., and Wolkowicz, M. D. (1992). Radiation treatment of polypropylene. *Polymeric Materials: Science and Engineering(PMSE). 67*, 106-108.

Destruel, P., Rojas, F. S., and Tougne, D. (1984). Pressure and temperature dependence of the electromechanical properties of polarized polyvinylidene fluoride films. *Journal of Applied Physics, 56*(11), 3298-3303.

Dey, S., Natarajan, P., Xanthos, M., and Braathen, M. (1996). Use of inert gases in extruded medium density polypropylene foams. *Journal of Vinyl and Additive Technology, 2*(4), 339-344.

Ding, J., Shangguan, J., Ma, W., and Zhong, Q. (2013). Foaming behavior of microcellular foam polypropylene/modified nano calcium carbonate composites. *Journal of Applied Polymer Science, 128*(6), 3639-3651.

Doi, M. (1987). Molecular Theory for the Nonlinear Viscoelasticity of Polymeric Liquids Crystals *Theory and Applications of Liquid Crystals*: Springer, New York.

Doi, M., and Edwards, S. (1986). *The theory of polymer dynamics*: Claredon, Oxford.

Döring, J., Bovtun, V., Bartusch, J., Erhard, A., Kreutzbruck, M., and Yakymenko, Y. (2010). Nonlinear electromechanical response of the ferroelectret ultrasonic transducers. *Applied Physics A, 100*(2), 479-485.

Döring, J., Bovtun, V., Gaal, M., Bartusch, J., Erhard, A., Kreutzbruck, M., and Yakymenko, Y. (2012). Piezoelectric and electrostrictive effects in ferroelectret ultrasonic transducers. *Journal of Applied Physics, 112*(8), 084505.

Doroudiani, S., Park, C. B., and Kortschot, M. T. (1996). Effect of the crystallinity and morphology on the microcellular foam structure of semicrystalline polymers. *Polymer Engineering and Science, 36*(21), 2645-2662.

Doroudiani, S., Park, C. B., and Kortschot, M. T. (1998). Processing and characterization of microcellular foamed high- density polythylene/isotactic polypropylene blends. *Polymer Engineering and Science, 38*(7), 1205-1215.

Ealo, J. L., Camacho, J. J., and Fritsch, C. (2009). Airborne ultrasonic phased arrays using ferroelectrets: a new fabrication approach. *Ultrasonics, Ferroelectrics, and Frequency Control, IEEE Transactions on, 56*(4), 848-858.

Eckert, C. A. (1996). Supercritical fluids as solvents for chemical and materials processing. *Nature, 383*, 313-318.

Exerowa, D., and Kruglyakov, P. M. (1997). *Foam and foam films: theory, experiment, application* (Vol. 5): Elsevier, Amsterdam.

Fang, P., Wegener, M., Wirges, W., Gerhard, R., and Zirkel, L. (2007). Cellular polyethylene-naphthalate ferroelectrets: Foaming in supercritical carbon dioxide, structural and electrical preparation, and resulting piezoelectricity. *Applied Physics Letters, 90*(19), 192908.

Fang, P., Wirges, W., Wegener, M., Zirkel, L., and Gerhard, R. (2008). Cellular polyethylene-naphthalate films for ferroelectret applications: foaming, inflation and stretching, assessment of electromechanically relevant structural features. *e-Polymers, 8*(1), 487-495.

Ferrigno, T. H. (1967). *Rigid plastics foams*: Reinhold, New York.

Fujimoto, Y., Ray, S. S., Okamoto, M., Ogami, A., Yamada, K., and Ueda, K. (2003). Well-Controlled Biodegradable Nanocomposite Foams: From Microcellular to Nanocellular. *Macromolecular Rapid Communications, 24*(7), 457-461.

Gaylord, N. G., Katz, L., and Park, J. J. (1992). *Polypropylene foam sheets*, US Patents 5,116,881.

Gendron, R. (2004). *Thermoplastic foam processing: principles and development* (Vol. 2): CRC press.

Gerhard-Multhaupt, R. (2002). Less can be more. Holes in polymers lead to a new paradigm of piezoelectric materials for electret transducers. *Dielectrics and Electrical Insulation, IEEE Transactions on, 9*(5), 850-859.

Gerhard-Multhaupt, R., Kunstler, W., Gome, T., Pucher, A., Weinhold, T., Seiß, M., Z., Xia, A., Wedel, and Danz, R. (2000). Porous PTFE space-charge electrets for piezoelectric applications. *Dielectrics and Electrical Insulation, IEEE Transactions on, 7*(4), 480-488.

Gibbs, J. W. (1961). *The scientific papers of JW Gibbs* (vol. 1): Dover, New York.

Gibson, L. J., and Ashby, M. F. (1997). *Cellular solids: structure and properties*: Cambridge university press.

Gilbert-Tremblay, H., Mighri, F., and Rodrigue, D. (2012). Morphology development of polypropylene cellular films for piezoelectric applications. *Journal of Cellular Plastics, 48*(4), 341-354.

Gosselin, R., and Rodrigue, D. (2005). Cell morphology analysis of high density polymer foams. *Polymer Testing, 24*(8), 1027-1035.

Gotsis, A., Zeevenhoven, B., and Hogt, A. (2004). The effect of long chain branching on the processability of polypropylene in thermoforming. *Polymer Engineering and Science, 44*(5), 973-982.

Gunkel, F., Spörrer, A., Lim, G., Bangarusampath, D., and Altstädt, V. (2008). Understanding melt rheology and foamability of polypropylene-based TPO blends. *Journal of Cellular Plastics, 44*(4), 307-325.

Gupta, N., Pinisetty, D., and Shunmugasamy, V. C. (2013). *Reinforced polymer matrix syntactic foams: effect of nano and micro-scale reinforcement*: Springer, New York.

Han, D. H., Jang, J. H., Kim, H. Y., Kim, B. N., and Shin, B. Y. (2006). Manufacturing and foaming of high melt viscosity of polypropylene by using electron beam radiation technology. *Polymer Engineering and Science, 46*(4), 431-437.

Han, X., Shen, J., Huang, H., Tomasko, D. L., and Lee, L. J. (2007). CO_2 foaming based on polystyrene/poly (methyl methacrylate) blend and nanoclay. *Polymer Engineering and Science, 47*(2), 103-111.

Harris, S., and Mellinger, A. (2012). Pressure dependence of space charge deposition in piezoelectric polymer foams: simulations and experimental verification. *Applied Physics A, 107*(3), 553-558.

Harris, S., and Mellinger, A. (2014). Towards a better understanding of dielectric barrier discharges in ferroelectrets: Paschen breakdown fields in micrometer sized voids. *Journal of Applied Physics, 115*(16), 163302.

Harris, S., Mellinger, O., and Mellinger, A. (2011). Simulation of space charge deposition by barrier discharges in piezoelectric polymer foams. In *IEEE 2011 14th International Symposium on Electrets*, pp. 83–84.

Heywang, W., Lubitz, K., and Wersing, W. (2008). *Piezoelectricity: evolution and future of a technology*: Springer Science & Business Media, Heidelberg, Berlin.

Hillenbrand, J., Kodejska, M., Garcin, Y., Seggern, H., and Sessler, G. (2010). High-sensitivity piezoelectret-film accelerometers. *Dielectrics and Electrical Insulation, IEEE Transactions on, 17*(4), 1021-1027.

Hillenbrand, J., and Sessler, G. (2000). Piezoelectricity in cellular electret films. *Dielectrics and Electrical Insulation, IEEE Transactions on, 7*(4), 537-542.

Hillenbrand, J., and Sessler, G. (2004). Quasistatic and dynamic piezoelectric coefficients of polymer foams and polymer film systems. *Dielectrics and Electrical Insulation, IEEE Transactions on, 11*(1), 72-79.

Hillenbrand, J., and Sessler, G. M. (2004). High-sensitivity piezoelectric microphones based on stacked cellular polymer films (L). *The Journal of the Acoustical Society of America, 116*(6), 3267-3270.

Hillenbrand, J., Sessler, G. M., and Zhang, X. (2005). Verification of a model for the piezoelectric d33 coefficient of cellular electret films. *Journal of Applied Physics, 98*(6), 064105.

Holmes-Siedle, A., Wilson, P., and Verrall, A. (1984). PVdF: An electronically-active polymer for industry. *Materials and Design, 4*(6), 910-918.

Huang, H.-X. (2005). HDPE/PA-6 blends: Influence of screw shear intensity and HDPE melt viscosity on phase morphology development. *Journal of Materials Science, 40*(7), 1777-1779.

Huang, H.-X., Jiang, G., and Mao, S.-Q. (2005). Effect of Flow Fields on Morphology of PP/Nano/CaCO3 Composite and Its Rheological Behavior. In *ASME 2005 International Mechanical Engineering Congress and Exposition, American Society of Mechanical Engineers*.

Huang, H.-X., Jiang, G., and Mao, S.-Q. (2006). Microstructure and on-line shear viscosity of PP/nano-CaCO 3 composites prepared by twin-screw extruder. *Journal of Materials Science, 41*(15), 4985-4988.

Huang, H.-X., Wang, J.-K., and Sun, X.-H. (2008). Improving of cell structure of microcellular foams based on polypropylene/high-density polyethylene blends. *Journal of Cellular Plastics, 44*(1), 69-85.

Huang, H. X., Huang, Y. F., and Yang, S. L. (2005). Developing laminar morphology in higher- viscosity- ratio polyblends by controlling flow fields in a single- screw extruder. *Polymer International, 54*(1), 65-69.

Huang, H. X., and Wang, J. K. (2007). Improving polypropylene microcellular foaming through blending and the addition of nano- calcium carbonate. *Journal of Applied Polymer Science, 106*(1), 505-513.

Huang, H. X., and Xu, H. F. (2011). Preparation of microcellular polypropylene/polystyrene blend foams with tunable cell structure. *Polymers for Advanced Technologies, 22*(6), 822-829.

Imeokparia, D. D., Shmidt, C. D., and Suh, K. W. (1997). *Extruded, open-cell microcellular alkenylaromatic polymer foams and process for making*: US Patents 5,674,916.

Jiang, X.-L., Bao, J.-B., Liu, T., Zhao, L., Xu, Z.-M., and Yuan, W.-K. (2009). Microcellular foaming of polypropylene/clay nanocomposites with supercritical carbon dioxide. *Journal of Cellular Plastics, 45*(6), 515-538.

Jiang, X.-L., Liu, T., Xu, Z.-M., Zhao, L., Hu, G.-H., and Yuan, W.-K. (2009). Effects of crystal structure on the foaming of isotactic polypropylene using supercritical carbon dioxide as a foaming agent. *The Journal of Supercritical Fluids, 48*(2), 167-175.

Jonscher, A. K. (1999). Dielectric relaxation in solids. *Journal of Physics D: Applied Physics, 32*(14), R57.

Karami, A., and Balke, S. T. (2000). Polymer blend de- mixing and morphology development of immiscible polymer blends during tube flow. *Polymer Engineering and Science, 40*(11), 2342-2355.

Kawai, H. (1969). The piezoelectricity of poly (vinylidene fluoride). *Japanese Journal of Applied Physics, 8*(7), 975.

Kirjavainen, K. (1987). *Electromechanical film and procedure for manufacturing same*: US Patents 4,654,546.

Klempner, D., and Frisch, K. C. (1991). *Handbook of polymeric foams and foam technology*: Hanser, Munich.

Klempner, D., and Sendijarevic, V. (2004). *Polymeric foams and foam technology* (2nd ed.): Hanser Verlag, Munich.

Klimiec, E., Królikowski, B., Machnik, M., Zaraska, W., and Dzwonkowski, J. (2015). Increase of Piezoelectric Constant and Thermal Durability of Polypropylene Electret by Introducing SiO2 and Kaolin Filler and Creating a Cellular Structure. *Journal of Electronic Materials*, 1-9.

Krause, B., Diekmann, K., Van der Vegt, N., and Wessling, M. (2002). Open nanoporous morphologies from polymeric blends by carbon dioxide foaming. *Macromolecules, 35*(5), 1738-1745.

Kressmann, R. (2001). Linear and nonlinear piezoelectric response of charged cellular polypropylene. *Journal of Applied Physics, 90*(7), 3489-3496.

Kressmann, R. (2001). New piezoelectric polymer for air-borne and water-borne sound transducers. *The Journal of the Acoustical Society of America, 109*(4), 1412-1416.

Kuboki, T. (2013). Foaming behavior of cellulose fiber-reinforced polypropylene composites in extrusion. *Journal of Cellular Plastics*, doi: 10.1177/0021955X13504775.

Kuboki, T. (2013). Mechanical properties and foaming behavior of injection molded cellulose fiber reinforced polypropylene composite foams. *Journal of Cellular Plastics*, doi: 10.1177/0021955X13504776

Kumar, V. (1993). Microcellular polymers: novel materials for the 21st century. *Cellular Polymers, 12*(3), 207-223.

Kundu, P. P., Biswas, J., Kim, H., and Choe, S. (2003). Influence of film preparation procedures on the crystallinity, morphology and mechanical properties of LLDPE films. *European Polymer Journal, 39*(8), 1585-1593.

Lang, S., and Muensit, S. (2006). Review of some lesser-known applications of piezoelectric and pyroelectric polymers. *Applied Physics A, 85*(2), 125-134.

Larson, R. G. (1999). *The structure and rheology of complex fluids* (Vol. 4): Oxford university press, New York.

Lee, L. J., Zeng, C., Cao, X., Han, X., Shen, J., and Xu, G. (2005). Polymer nanocomposite foams. *Composites Science and Technology, 65*(15), 2344-2363.

Lee, S. (2000). Foam Extrusion: Theory and Practice. *Technomic Publications Inc., Lancaster, PA, 17608*, 75-77.

Lee, S.-T. (2002). *Foam extrusion: principles and practice*: CRC press, Boca Raton.

Lee, S.-T., Park, C. B., and Ramesh, N. S. (2006). *Polymeric foams: science and technology*: CRC Press, Boca Raton.

Lee, S.-T., and Ramesh, N. S. (2004). *Polymeric foams: mechanisms and materials*: CRC press, boca Raton.

Lee, S.-T., and Scholz, D. P. K. (2008). *Polymeric Foams: Technology and Developments in Regulation, Process, and Products*: CRC Press, Boca Raton.

Lee, Y. H., Park, C. B., Wang, K. H., and Lee, M. H. (2005). HDPE-clay nanocomposite foams blown with supercritical CO2. *Journal of Cellular Plastics, 41*(5), 487-502.

Leung, S. N., Wong, A., Guo, Q., Park, C. B., and Zong, J. H. (2009). Change in the critical nucleation radius and its impact on cell stability during polymeric foaming processes. *Chemical Engineering Science, 64*(23), 4899-4907.

Li, D., Liu, Z., Han, B., Song, L., Yang, G., and Jiang, T. (2002). Preparation of nanometer dispersed polypropylene/polystyrene interpenetrating network using supercritical CO_2 as a swelling agent. *Polymer, 43*(19), 5363-5367.

Li, L., Yokoyama, H., Nemoto, T., and Sugiyama, K. (2004). Facile fabrication of nanocellular block copolymer thin films using supercritical carbon dioxide. *Advanced Materials, 16*(14), 1226-1229.

Li, S., Xiao, M., Guan, Y., Wei, D., Xiao, H., and Zheng, A. (2012). A novel strategy for the preparation of long chain branching polypropylene and the investigation on foamability and rheology. *European Polymer Journal, 48*(2), 362-371.

Liao, R., Yu, W., and Zhou, C. (2010). Rheological control in foaming polymeric materials: II. Semi-crystalline polymers. *Polymer, 51*(26), 6334-6345.

Lin, C.-J., and Lin, P.-T. (2012). Tracking control of a biaxial piezo-actuated positioning stage using generalized Duhem model. *Computers and Mathematics with Applications, 64*(5), 766-787.

Lindner, M., Bauer-Gogonea, S., Bauer, S., Paajanen, M., and Raukola, J. (2002). Dielectric barrier microdischarges: Mechanism for the charging of cellular piezoelectric polymers. *Journal of Applied Physics, 91*(8), 5283-5287.

Lindner, M., Hoislbauer, H., Schwodiauer, R., Bauer-Gogonea, S., and Bauer, S. (2004). Charged cellular polymers with" ferroelectretic" behavior. *Dielectrics and Electrical Insulation, IEEE Transactions on, 11*(2), 255-263.

Liu, C., Wei, D., Zheng, A., Li, Y., and Xiao, H. (2006). Improving foamability of polypropylene by grafting modification. *Journal of Applied Polymer Science, 101*(6), 4114-4123.

Mahi Hassanabadi, H. (2013). *Relations between microstructural development and rheological properties in polymer nanocomposites.* Ph.D. thesis, Université Laval, 167 p.

Malone, B. A., and Park, C. P. (1996). *Extruded closed-cell polypropylene foam*: US Patents 5,527,573.

Marrucci, G., and Ianniruberto, G. (2004). Interchain pressure effect in extensional flows of entangled polymer melts. *Macromolecules, 37*(10), 3934-3942.

Martini, J. E. (1981). *The production and analysis of microcellular foam.* Ph.D. thesis, Massachusetts Institute of Technology.

Meitzler, A., Tiersten, H., Warner, A., Berlincourt, D., Couqin, G., and Welsh III, F. (1987). *IEEE standard on piezoelectricity*: IEEE Press, New York.

Mellinger, A. (2003). Dielectric resonance spectroscopy: a versatile tool in the quest for better piezoelectric polymers. *Dielectrics and Electrical Insulation, IEEE Transactions on, 10*(5), 842-861.

Mellinger, A., and Mellinger, O. (2011). Breakdown threshold of dielectric barrier discharges in ferroelectrets: where Paschen's law fails. *Dielectrics and Electrical Insulation, IEEE Transactions on, 18*(1), 43-48.

Mellinger, A., Wegener, M., Wirges, W., Mallepally, R. R., and Gerhard-Multhaupt, R. (2006). Thermal and temporal stability of ferroelectret films made from cellular polypropylene/air composites. *Ferroelectrics, 331*(1), 189-199.

Miao, H., Sun, Y., Zhou, X., Li, Y., and Li, F. (2014). Piezoelectricity and ferroelectricity of cellular polypropylene electrets films characterized by piezoresponse force microscopy. *Journal of Applied Physics, 116*(6), 066820.

Min, K., White, J. L., and Fellers, J. F. (1984). Development of phase morphology in incompatible polymer blends during mixing and its variation in extrusion. *Polymer Engineering and Science, 24*(17), 1327-1336.

Mittal, V. (2013). *Polymer Nanocomposite Foams*: CRC Press, Boca Raton.

Mohebbi, A., Mehrabani-Zeinabad, A., and Navid-Famili, M. (2011). Dynamic behavior of nucleation in supercritical N_2 foaming of polystyrene-aluminum oxide nanocomposite. *Polymer Science Series A, 53*(11), 1076-1085.

Mohebbi, A., Mighri, F., Ajji, A., and Rodrigue, D. (2015). Current issues and challenges in polypropylene foaming: A Review. *Cellular Polymers, 34*(6), 281-320.

Mohebbi, A., Mighri, F., Ajji, A., and Rodrigue, D. (2016). Cellular Polymer Ferroelectret: A Review on Their Development and Their Piezoelectric Properties. *Advances in Polymer Technology*, doi: 10.1002/adv.21686

Mohebbi, A., Mighri, F., Ajji, A., and Rodrigue, D. (2016). Effect of processing conditions on the cellular morphology of polypropylene foamed films for piezoelectric applications. *Cellular Polymers, Accepted*.

Mohebbi, A., Mighri, F., Ajji, A., and Rodrigue, D. (2016). Polymer ferroelectret based on polypropylene foam: Piezoelectric properties prediction using dynamic mechanical analysis. *Polymers for Advanced Technologies,* doi: 10.1002/pat.3908.

Mohmeyer, N., Behrendt, N., Zhang, X., Smith, P., Altstädt, V., Sessler, G. M., and Schmidt, H.-W. (2007). Additives to improve the electret properties of isotactic polypropylene. *Polymer, 48*(6), 1612-1619.

Mohmeyer, N., Müller, B., Behrendt, N., Hillenbrand, J., Klaiber, M., Zhang, X., Smith, P., Altstädt, V., Sessler, G. M., and Schmidt, H.-W. (2004). Nucleation of isotactic polypropylene by triphenylamine-based trisamide derivatives and their influence on charge-storage properties. *Polymer, 45*(19), 6655-6663.

Montanari, G., Fabiani, D., Ciani, F., Motori, A., Paajanen, M., Gerhard-Multhaupt, R., and Wegener, M. (2007). Charging properties and time-temperature stability of innovative polymeric cellular ferroelectrets. *Dielectrics and Electrical Insulation, IEEE Transactions on, 14*(1), 238-248.

Montanari, G. C., Mazzanti, G., Ciani, F., and Paajanen, M. (2005). Comparison and electrical modeling of new polymeric cellular electrets. *Ultrasonics, Ferroelectrics, and Frequency Control, IEEE Transactions on, 52*(11), 2088-2095.

Müller, C. M., Laurindo, J. B., and Yamashita, F. (2009). Effect of cellulose fibers on the crystallinity and mechanical properties of starch-based films at different relative humidity values. *Carbohydrate Polymers, 77*(2), 293-299.

Naguib, H. E., Park, C. B., and Lee, P. C. (2003). Effect of talc content on the volume expansion ratio of extruded PP foams. *Journal of Cellular Plastics, 39*(6), 499-511.

Naguib, H. E., Park, C. B., Lee, P. C., and Xu, D. (2006). A study on the foaming behaviors of PP resins with talc as nucleating agent. *Journal of Polymer Engineering, 26*(6), 565-588.

Naguib, H. E., Park, C. B., Panzer, U., and Reichelt, N. (2002). Strategies for achieving ultra low- density polypropylene foams. *Polymer Engineering and Science, 42*(7), 1481-1492.

Naguib, H. E., Park, C. B., and Reichelt, N. (2004). Fundamental foaming mechanisms governing the volume expansion of extruded polypropylene foams. *Journal of Applied Polymer Science, 91*(4), 2661-2668.

Naguib, H. E., Park, C. B., and Song, S.-W. (2005). Effect of supercritical gas on crystallization of linear and branched polypropylene resins with foaming additives. *Industrial and Engineering Chemistry Research, 44*(17), 6685-6691.

Naguib, H. E., Song, S. W., Park, C. B., and Byon, Y. J. (2000). Effect of Supercritical Carbon Dioxide and Nitrogen on Crystallization of Linear and Branched Propylene Resins Filled with Foaming Agents. *SPE, ANTEC Technical Papers, 46*, 1867-1873.

Nalawade, S. P., Picchioni, F., and Janssen, L. (2006). Supercritical carbon dioxide as a green solvent for processing polymer melts: Processing aspects and applications. *Progress in Polymer Science, 31*(1), 19-43.

Nam, G., Yoo, J., and Lee, J. (2005). Effect of long- chain branches of polypropylene on rheological properties and foam- extrusion performances. *Journal of Applied Polymer Science, 96*(5), 1793-1800.

Nam, P. H., Maiti, P., Okamoto, M., Kotaka, T., Nakayama, T., Takada, M., Ohshima, M., Usuki, A., Hasegawa, N., and Okamoto, H. (2002). Foam processing and cellular structure of polypropylene/clay nanocomposites. *Polymer Engineering and Science, 42*(9), 1907-1918.

Neugschwandtner, G., Schwödiauer, R., Vieytes, M., Bauer-Gogonea, S., Bauer, S., Hillenbrand, J., Kressmann, R., Sessler, G. M., Paajanen, M., and Lekkala, J. (2000). Large and broadband piezoelectricity in smart polymer-foam space-charge electrets. *Applied Physics Letters, 77*(23), 3827-3829.

Neugschwandtner, G. S., Schwodiauer, R., Bauer-Gogonea, S., Bauer, S., Paajanen, M., and Lekkala, J. (2001). Piezo-and pyroelectricity of a polymer-foam space-charge electret. *Journal of Applied Physics, 89*(8), 4503-4511.

Neway, B., Westberg, Å., Mattozzi, A., Hedenqvist, M. S., Baschetti, M. G., Mathot, V., and Gedde, U. W. (2004). Free volume and transport properties of homogeneous poly (ethylene-co-octene). *Polymer, 45*(11), 3913-3922.

Newnham, R. E. (2004). *Properties of Materials: Anisotropy, Symmetry, Structure: Anisotropy, Symmetry, Structure*: Oxford University Press, Oxford, UK.

Nofar, M., Majithiya, K., Kuboki, T., and Park, C. B. (2012). The foamability of low-melt-strength linear polypropylene with nanoclay and coupling agent. *Journal of Cellular Plastics, 48*(3), 271-287.

Ohigashi, H. (1976). Electromechanical properties of polarized polyvinylidene fluoride films as studied by the piezoelectric resonance method. *Journal of Applied Physics, 47*(3), 949-955.

Okamoto, K. T. (2003). *Microcellular processing*: Hanser, Munich.

Okamoto, M., Nam, P. H., Maiti, P., Kotaka, T., Nakayama, T., Takada, M., and Okamoto, H. (2001). Biaxial flow-induced alignment of silicate layers in polypropylene/clay nanocomposite foam. *Nano Letters, 1*(9), 503-505.

Okolieocha, C., Köppl, T., Kerling, S., Tölle, F. J., Fathi, A., Mülhaupt, R., and Altstädt, V. (2015). Influence of graphene on the cell morphology and mechanical properties of extruded polystyrene foam. *Journal of Cellular Plastics*, *51*(4), 413-426

Paajanen, M., Lekkala, J., and Kirjavainen, K. (2000). ElectroMechanical Film (EMFi)-a new multipurpose electret material. *Sensors and Actuators A: Physical, 84*(1), 95-102.

Paajanen, M., Välimäki, H., and Lekkala, J. (2000). Modelling the electromechanical film (EMFi). *Journal of Electrostatics, 48*(3), 193-204.

Paajanen, M., Wegener, M., and Gerhard-Multhaupt, R. (2001). Charging of cellular space-charge electret films in various gas atmospheres. In *IEEE Conference on Annual Report Electrical Insulation and Dielectric Phenomena*, pp. 24-27.

Paajanen, M., Wegener, M., and Gerhard-Multhaupt, R. (2001). Understanding the role of the gas in the voids during corona charging of cellular electret films-a way to enhance their piezoelectricity. *Journal of Physics D: Applied Physics, 34*(16), 2482.

Park, C., Baldwin, D., and Suh, N., Kumar, V., (1994). Cellular and microcellular materials. *The American Society of Mechanical Engineers*, *53*, 109-124.

Park, C. B., Baldwin, D. F., and Suh, N. P. (1995). Effect of the pressure drop rate on cell nucleation in continuous processing of microcellular polymers. *Polymer Engineering and Science, 35*(5), 432-440.

Park, C. B., Behravesh, A. H., and Venter, R. D. (1998). Low density microcellular foam processing in extrusion using CO2. *Polymer Engineering and Science, 38*(11), 1812-1823.

Park, C. B., and Cheung, L. K. (1997). A study of cell nucleation in the extrusion of polypropylene foams. *Polymer Engineering and Science, 37*(1), 1-10.

Persson, B., Albohr, O., Heinrich, G., and Ueba, H. (2005). Crack propagation in rubber-like materials. *Journal of Physics: Condensed Matter, 17*(44), R1071.

Porter, D. A., and Easterling, K. E. (1992). *Phase Transformations in Metals and Alloys*: CRC press, Boca Raton.

Potente, H., Krawinkel, S., Bastian, M., Stephan, M., and Pötschke, P. (2001). Investigation of the melting behavior and morphology development of polymer blends in the melting zone of twin- screw extruders. *Journal of Applied Polymer Science, 82*(8), 1986-2002.

Qaiss, A., Saidi, H., Fassi- Fehri, O., and Bousmina, M. (2012). Cellular polypropylene-based piezoelectric films. *Polymer Engineering and Science, 52*(12), 2637-2644.

Qaiss, A., Saidi, H., Fassi- Fehri, O., and Bousmina, M. (2013). Theoretical modeling and experiments on the piezoelectric coefficient in cellular polymer films. *Polymer Engineering and Science, 53*(1), 105-111.

Qiu, X., Gerhard, R., and Mellinger, A. (2011). Turning polymer foams or polymer-film systems into ferroelectrets: dielectric barrier discharges in voids. *Dielectrics and Electrical Insulation, IEEE Transactions on, 18*(1), 34-42.

Qiu, X., Mellinger, A., and Gerhard, R. (2008). Influence of gas pressure in the voids during charging on the piezoelectricity of ferroelectrets. *Applied Physics Letters, 92*(5), 052901.

Qiu, X., Mellinger, A., Wegener, M., Wirges, W., and Gerhard, R. (2007). Barrier discharges in cellular polypropylene ferroelectrets: How do they influence the electromechanical properties? *Journal of Applied Physics, 101*(10), 104112.

Qiu, X., Mellinger, A., Wirges, W., and Gerhard, R. (2007). Spectroscopic study of dielectric barrier discharges in cellular polypropylene ferroelectrets. *Applied Physics Letters, 91*(13), 132905.

Qiu, X., Sborikas, M., Wirges, W., and Gerhard, R. (2013). Fatigue and recovery of cellular-polypropylene piezoelectrets during and after dielectric-barrier discharges. In *IEEE Conference on Electrical Insulation and Dielectric Phenomena (CEIDP)*, pp. 591.

Qiu, X., Wegener, M., Wirges, W., Zhang, X., Hillenbrand, J., Xia, Z., Gerhard-Multhaupt, R., and Sessler, G. M. (2005). Penetration of sulfur hexafluoride into cellular polypropylene films and its effect on the electric charging and electromechanical response of ferroelectrets. *Journal of Physics D: Applied Physics, 38*(4), 649.

Qiu, X., Xia, Z., and Wang, F. (2007). Piezoelectricity of single-and multi-layer cellular polypropylene film electrets. *Frontiers of Materials Science in China, 1*(1), 72-75.

Rachtanapun, P., Selke, S., and Matuana, L. (2003). Microcellular foam of polymer blends of HDPE/PP and their composites with wood fiber. *Journal of Applied Polymer Science, 88*(12), 2842-2850.

Rachtanapun, P., Selke, S., and Matuana, L. (2004). Effect of the high- density polyethylene melt index on the microcellular foaming of high- density polyethylene/polypropylene blends. *Journal of Applied Polymer Science, 93*(1), 364-371.

Rachtanapun, P., Selke, S. E., and Matuana, L. M. (2004). Relationship between cell morphology and impact strength of microcellular foamed high- density polyethylene/polypropylene blends. *Polymer Engineering and Science, 44*(8), 1551-1560.

Rao, H., and Zhang, Z. (2008). Graft copolymerization of maleic anhydride/styrene onto isotactic polypropylene using supercritical CO_2. *Polymers for Advanced Technologies, 19*(7), 770-774.

Rolón-Garrido, V. H., and Wagner, M. H. (2007). The MSF model: relation of nonlinear parameters to molecular structure of long-chain branched polymer melts. *Rheologica Acta, 46*(5), 583-593.

Rupitsch, S. J., Lerch, R., Strobel, J., and Streicher, A. (2011). Ultrasound transducers based on ferroelectret materials. *Dielectrics and Electrical Insulation, IEEE Transactions on, 18*(1), 69-80.

Saarimaki, E., Paajanen, M., Savijarvi, A.-M., and Minkkinen, H. (2005). Novel heat durable electromechanical film processing: Preparations for electromechanical and electret applications. In *IEEE 2005 12th International Symposium on Electrets*, pp. 220-223.

Saarimaki, E., Paajanen, M., Savijarvi, A.-M., Minkkinen, H., Wegener, M., Voronina, O., Schulze, R., Wirges, W., and Gerhard-Multhaupt, R. (2006). Novel heat durable electromechanical film: processing for electromechanical and electret applications. *Dielectrics and Electrical Insulation, IEEE Transactions on, 13*(5), 963-972.

Sauceau, M., Fages, J., Common, A., Nikitine, C., and Rodier, E. (2011). New challenges in polymer foaming: A review of extrusion processes assisted by supercritical carbon dioxide. *Progress in Polymer Science, 36*(6), 749-766.

Sauceau, M., Nikitine, C., Rodier, E., and Fages, J. (2007). Effect of supercritical carbon dioxide on polystyrene extrusion. *The Journal of Supercritical Fluids, 43*(2), 367-373.

Savolainen, A., and Kirjavainen, K. (1989). Electrothermomechanical film. Part I. Design and characteristics. *Journal of Macromolecular Science-Chemistry, 26*(2-3), 583-591.

Sborikas, M., and Wegener, M. (2013). Cellular-foam polypropylene ferroelectrets with increased film thickness and reduced resonance frequency. *Applied Physics Letters, 103*(25), 252901.

Schramm, L. L. (1994). *Foams: fundamentals and applications in the petroleum industry* (Vol. 242): American Chemical Society Washington, DC.

Schwodiauer, R., Neugschwandtner, G., Schrattbauer, K., Lindner, M., Vieytes, M., Bauer-Gogonea, S., and Bauer, S. (2000). Preparation and characterization of novel piezoelectric and pyroelectric polymer electrets. *Dielectrics and Electrical Insulation, IEEE Transactions on, 7*(4), 578-586.

Seeler, K. A., and Kumar, V. (1993). Tension-tension fatigue of microcellular polycarbonate: initial results. *Journal of Reinforced Plastics and Composites, 12*(3), 359-376.

Sessler, G., and Hillenbrand, J. (1999). Electromechanical response of cellular electret films. *Applied physics letters, 75*(21), 3405-3407.

Sessler, G., and Hillenbrand, J. (2009). Broadband ferroelectret transducers. In *IEEE International Ultrasonics Symposium (IUS)*, pp. 393–397.

Spitael, P., and Macosko, C. W. (2004). Strain hardening in polypropylenes and its role in extrusion foaming. *Polymer Engineering and Science, 44*(11), 2090-2100.

Stange, J., and Münstedt, H. (2006). Rheological properties and foaming behavior of polypropylenes with different molecular structures. *Journal of Rheology, 50*(6), 907-923.

Stevenson, P. (2012). *Foam engineering: fundamentals and applications*: John Wiley and Sons, Chichester.

Suh, K. W., Park, C. P., Maurer, M., Tusim, M. H., Genova, R. D., Broos, R., and Sophiea, D. P. (2000). Lightweight cellular plastics. *Advanced Materials, 12*(23), 1779-1789.

Tajitsu, Y. (2006). Development of electric control catheter and tweezers for thrombosis sample in blood vessels using piezoelectric polymeric fibers. *Polymers for Advanced Technologies, 17*(11- 12), 907-913.

Taki, K., Yanagimoto, T., Funami, E., Okamoto, M., and Ohshima, M. (2004). Visual observation of CO2 foaming of polypropylene- clay nanocomposites. *Polymer Engineering and Science, 44*(6), 1004-1011.

Tang, M., An, Z., Xia, Z., and Zhang, X. (2007). Electret properties and chemical modification of cellular polypropylene films. *Journal of Electrostatics, 65*(4), 203-208.

Taylor, D., and Fernandez, O. (2005). Thermal instability of electromechanical films of cellular polypropylene. *Dielectrics and Electrical Insulation, IEEE Transactions on, 12*(4), 768-778.

Throne, J. L. (2004). *Thermoplastic foam extrusion: an introduction*: Hanser Verlag, Munich.

Tuncer, E. (2005). Numerical calculations of effective elastic properties of two cellular structures. *Journal of Physics D: Applied Physics, 38*(3), 497.

Vasile, C., and Seymour, R. B. (1993). *Handbook of Polyolefins*: Marcel Dekker, New York.

Wagner, M., Yamaguchi, M., and Takahashi, M. (2003). Quantitative assessment of strain hardening of low-density polyethylene melts by the molecular stress function model. *Journal of Rheology, 47*(3), 779-793.

Wagner, M. H., Kheirandish, S., Stange, J., and Münstedt, H. (2006). Modeling elongational viscosity of blends of linear and long-chain branched polypropylenes. *Rheologica Acta, 46*(2), 211-221.

Wagner, M. H., and Rolón-Garrido, V. H. (2008). Verification of branch point withdrawal in elongational flow of pom-pom polystyrene melt. *Journal of Rheology, 52*(5), 1049-1068.

Wan, Y., Xie, L., Zhang, X., and Zhong, Z. (2011). Time dependence of piezoelectric d 33 coefficient of cellular ferroelectret polypropylene film. *Applied Physics Letters, 98*(12), 122902-122903.

Wan, Y., Xie, L., and Zhong, Z. (2010). Micromechanical prediction of the effective electromechanical properties of cellular ferroelectrets. *Journal of Applied Physics, 108*(5), 054101.

Wang, C., Ying, S., and Xiao, Z. (2013). Preparation of short carbon fiber/polypropylene fine-celled foams in supercritical CO_2. *Journal of Cellular Plastics, 49*(1), 65-82.

Wang, K., Lee, Y., and Park, C. (2004). Optimum content of clay for microcellular ldpe/clay nanocomposite foams blown with CO_2. In *SPE ANTEC conference proceedings*, Paper 879.

Wang, K., Wu, F., Zhai, W., and Zheng, W. (2013). Effect of polytetrafluoroethylene on the foaming behaviors of linear polypropylene in continuous extrusion. *Journal of Applied Polymer Science, 129*(4), 2253-2260.

Wang, X., Tzoganakis, C., and Rempel, G. L. (1996). Chemical modification of polypropylene with peroxide/pentaerythritol triacrylate by reactive extrusion. *Journal of Applied Polymer Science, 61*(8), 1395-1404.

Wegener, M. (2010). *Piezoelectric polymer foams: Transducer mechanism and preparation as well as touch-sensor and ultrasonic-transducer properties.* In *Proceedings of SPIE, 7644, 76441A*, pp. 1-9.

Wegener, M., Bergweiler, S., Wirges, W., Pucher, A., Tuncer, E., and Gerhard-Multhaupt, R. (2005). Piezoelectric two-layer stacks of cellular polypropylene ferroelectrets: Transducer response at audio and ultrasound frequencies. *Ultrasonics, Ferroelectrics, and Frequency Control, IEEE Transactions on, 52*(9), 1601-1607.

Wegener, M., Tuncer, E., Wirges, W., Gerhard-Multhaupt, R., Dansachmüller, M., Bauer-Gogonea, S., Schwödiauer, R. , and Bauer, S. (2004). Ferroelectrets: Highly anisotropic electrically charged polymer foams for electromechanical transducer applications. In *Proceedings of the IEEE Ultrasonics Symposium*, pp. 1138-1141.

Wegener, M., Wirges, W., Fohlmeister, J., Tiersch, B., and Gerhard-Multhaupt, R. (2004). Two-step inflation of cellular polypropylene films: void-thickness increase and enhanced electromechanical properties. *Journal of Physics D: Applied Physics, 37*(4), 623.

Wegener, M., Wirges, W., Gerhard-Multhaupt, R., Dansachmüller, M., Schwödiauer, R., Bauer-Gogonea, S., Bauer, S., Paajanen, M., Minkkinen, H., and Raukola, J. (2004). Controlled inflation of voids in cellular polymer ferroelectrets: Optimizing electromechanical transducer properties. *Applied Physics Letters, 84*(3), 392-394.

Wegener, M., Wirges, W., and Gerhard- Multhaupt, R. (2005). Piezoelectric Polyethylene Terephthalate (PETP) foams–specifically designed and prepared ferroelectret films. *Advanced Engineering Materials, 7*(12), 1128-1131.

Wen, X., Wu, W., Ding, Y., and Wang, Z. L. (2013). Piezotronic Effect in Flexible Thin-film Based Devices. *Advanced Materials, 25*(24), 3371-3379.

Wirges, W., Wegener, M., Voronina, O., Zirkel, L., and Gerhard- Multhaupt, R. (2007). Optimized preparation of elastically soft, highly piezoelectric, cellular ferroelectrets from nonvoided poly (ethylene terephthalate) films. *Advanced Functional Materials, 17*(2), 324-329.

Wu, L., Zhang, X., and Zhang, X. (2015). Mechanical and piezoelectric performance of cross-linked polypropylene films treated with extending. *Ceramics International*, *41*, S218.

Wu, L., Zhang, X., and Zhang, X. (2015). Mechanical and piezoelectric performance of cross-linked polypropylene films treated with extending. *Ceramics International, 41*, S218-S222.

Xia, Z., Gerhard-Multhaupt, R., Künstler, W., Wedel, A., and Danz, R. (1999). High surface-charge stability of porous polytetrafluoroethylene electret films at room and elevated temperatures. *Journal of Physics D: Applied Physics, 32*(17), L83.

Xie, X., Gu, A., Liu, P., Liang, G., and Yuan, L. (2011). Preparation of high performance foams with excellent dielectric property based on toughened bismaleimide resin. *Polymers for Advanced Technologies, 22*(12), 1731-1737.

Xin, Z. X., Zhang, Z. X., Pal, K., Kim, K.-J., Kang, D. J., Kim, J. K., and Bang, D.-S. (2009). Microcellular Structure of PP/Waste Rubber Powder Blends with Supercritical CO2 by Foam Extrusion Process. *Journal of Cellular Plastics, 45*(6), 499-514.

Xu, B.-X., von Seggern, H., Zhukov, S., and Gross, D. (2013). Continuum modeling of charging process and piezoelectricity of ferroelectrets. *Journal of Applied Physics, 114*(9), 094103.

Xu, J. (2011). Microcellular injection molding (Vol. 9): John Wiley and Sons, Hoboken.

Xu, Z., Zhang, Z., Guan, Y., Wei, D., and Zheng, A. (2013). Investigation of extensional rheological behaviors of polypropylene for foaming. *Journal of Cellular Plastics, 49*(4), 317-334.

Xu, Z.-M., Jiang, X.-L., Liu, T., Hu, G.-H., Zhao, L., Zhu, Z.-N., and Yuan, W.-K. (2007). Foaming of polypropylene with supercritical carbon dioxide. *The Journal of Supercritical Fluids, 41*(2), 299-310.

Yang, K., Lee, S. H., and Oh, J. M. (1999). Effects of viscosity ratio and compatibilizers on the morphology and mechanical properties of polycarbonate/acrylonitrile- butadiene-styrene blends. *Polymer Engineering and Science, 39*(9), 1667-1677.

Yu, C., Wang, Y., Wu, B., Xie, Y., Yu, C., Chen, S., and Li, W. (2011). Evaluating the foamability of polypropylene with nitrogen as the blowing agent. *Polymer Testing, 30*(8), 887-892.

Zhai, W., Kuboki, T., Wang, L., Park, C. B., Lee, E. K., and Naguib, H. E. (2010). Cell structure evolution and the crystallization behavior of polypropylene/clay nanocomposites foams blown in continuous extrusion. *Industrial and Engineering Chemistry Research, 49*(20), 9834-9845.

Zhai, W., Leung, S. N., Wang, L., Naguib, H. E., and Park, C. B. (2010). Preparation of microcellular poly (ethylene- co- octene) rubber foam with supercritical carbon dioxide. *Journal of Applied Polymer Science, 116*(4), 1994-2004.

Zhai, W., and Park, C. B. (2011). Effect of nanoclay addition on the foaming behavior of linear polypropylene- based soft thermoplastic polyolefin foam blown in continuous extrusion. *Polymer Engineering and Science, 51*(12), 2387-2397.

Zhai, W., Wang, H., Yu, J., Dong, J., and He, J. (2008). Cell coalescence suppressed by crosslinking structure in polypropylene microcellular foaming. *Polymer Engineering and Science, 48*(7), 1312-1321.

Zhai, W., Wang, H., Yu, J., Dong, J., and He, J. (2008). Foaming behavior of polypropylene/polystyrene blends enhanced by improved interfacial compatibility. *Journal of Polymer Science Part B: Polymer Physics, 46*(16), 1641-1651.

Zhai, W., Wang, H., Yu, J., Dong, J.-Y., and He, J. (2008). Foaming behavior of isotactic polypropylene in supercritical CO_2 influenced by phase morphology via chain grafting. *Polymer, 49*(13), 3146-3156.

Zhang, P., Wang, X. J., Yang, Y., and Zhou, N. (2009). Effect of dynamic shear on the microcellular foaming of polypropylene/high- density polyethylene blends. *Journal of Applied Polymer Science, 114*(2), 1320-1328.

Zhang, P., Xia, Z., Qiu, X., Wang, F., and Wu, X. (2005). Influence of charging parameters on piezoelectricity for cellular polypropylene film electrets. In *IEEE 12th International Symposium on Electrets 2005*, pp. 39–42.

Zhang, X., Hillenbrand, J., and Sessler, G. (2004). Improvement of piezoelectric activity of cellular polymers using a double-expansion process. *Journal of Physics D: Applied Physics, 37*(15), 2146.

Zhang, X., Hillenbrand, J., and Sessler, G. (2004). Piezoelectric d_{33} coefficient of cellular polypropylene subjected to expansion by pressure treatment. *Applied Physics Letters, 85*(7), 1226-1228.

Zhang, X., Hillenbrand, J., and Sessler, G. (2006). Thermally stable fluorocarbon ferroelectrets with high piezoelectric coefficient. *Applied Physics A, 84*(1-2), 139-142.

Zhang, X., Hillenbrand, J., and Sessler, G. (2007). Ferroelectrets with improved thermal stability made from fused fluorocarbon layers. *Journal of Applied Physics, 101*(5), 054114.

Zhang, X., Hillenbrand, J., Sessler, G., Haberzettl, S., and Lou, K. (2012). Fluoroethylenepropylene ferroelectrets with patterned microstructure and high, thermally stable piezoelectricity. *Applied Physics A, 107*(3), 621-629.

Zhang, X., Huang, J., Chen, J., Wan, Z., Wang, S., and Xia, Z. (2007). Piezoelectric properties of irradiation-crosslinked polypropylene ferroelectrets. *Applied Physics Letters, 91*(18), 182901-182903.

Zhang, X., Huang, J., and Xia, Z. (2007). Piezoelectric activity and thermal stability of cellular fluorocarbon films. *Physica Scripta, 2007*(T129), 274.

Zhang, X., Pan, D., Wang, X., Cao, G., Sun, Z., and Xia, Z. (2011). Piezoelectric coefficients of cross-linked polypropylene films stretched at elevated temperatures. *Journal of Electrostatics, 69*(6), 554-558.

Zhang, X., Sessler, G. M., and Wang, Y. (2014). Fluoroethylenepropylene ferroelectret films with cross-tunnel structure for piezoelectric transducers and micro energy harvesters. *Journal of Applied Physics, 116*(7), 074109.

Zhang, X., Wang, X., Huang, J., and Xia, Z. (2009). Quasi-static and dynamic piezoelectric d 33 coefficients of irradiation cross-linked polypropylene ferroelectrets. *Journal of Materials Science, 44*(10), 2459-2465.

Zhang, X., Wu, L., and Sessler, G. M. (2015). Energy harvesting from vibration with cross-linked polypropylene piezoelectrets. *AIP Advances, 5*(7), 077185.

Zhang, X., Zhang, X., Sessler, G. M., and Gong, X. (2014). Quasi-static and dynamic piezoelectric responses of layered polytetrafluoroethylene ferroelectrets. *Journal of Physics D: Applied Physics, 47*(1), 015501.

Zhang, X., Zhang, X., You, Q., and Sessler, G. M. (2014). Low- Cost, Large- Area, Stretchable Piezoelectric Films Based on Irradiation- Crosslinked Poly (propylene). *Macromolecular Materials and Engineering, 299*(3), 290-295.

Zhang, Y., Liu, Y., and Wang, Z. L. (2011). Fundamental theory of piezotronics. *Advanced Materials, 23*(27), 3004-3013.

Zheng, W., Lee, Y., and Park, C. (2010). Use of nanoparticles for improving the foaming behaviors of linear PP. *Journal of Applied Polymer Science, 117*(5), 2972-2979.

Zhukov, S., and Von Seggern, H. (2007). Polarization hysteresis and piezoelectricity in open-porous fluoropolymer sandwiches. *Journal of Applied Physics, 102*(4), 044109.

Zirkel, L., Jakob, M., and Münstedt, H. (2009). Foaming of thin films of a fluorinated ethylene propylene copolymer using supercritical carbon dioxide. *The Journal of Supercritical Fluids, 49*(1), 103-110.

Zong, N., and Yang, V. (2006). Cryogenic fluid jets and mixing layers in transcritical and supercritical environments. *Combustion Science and Technology, 178*(1-3), 193-227.

Appendix A: Equipment Conditions

A1 Extruder

The extruder was equipped with a flat die as a continuous method to produce foamed PP films. The aim was to create a homogenous distribution of nucleating agent into the PP matrix. Moreover, through an appropriate screw design, the physical blowing agent (N_2) was

dispersed into the PP matrix as well. In this study, a Leistritz ZSE18HP co-rotating twin-screw extruder (diameter = 18 mm and length/diameter = 40) was used. The processing conditions are as follow:

Screw speed (rpm) 260

Feeding rate (kg/h) 1.14

Temperature profile

The extruder has nine temperature zones including the die. The optimum temperature profile from the feeding zone to the die for PP was found to be:

Zone	1	2	3	4	5	6	7	8	Die
Temperature (°C)	180	180	185	185	185	180	180	180	167

A2 Slit-die

A slit-die was installed on the extruder to produce the foamed PP films. Its specifications are as follow:

Width (cm) 15

Opening (mm) 0.5

A3 Calendaring system

A calendaring system including three-roll was used to apply uniaxial stretching on the produced foamed PP films to produce an eye-like cellular structure which was require for piezoelectric applications. The specifications related to the calendaring system are as follow:

Roll diameter (cm) 15

Roll width (cm) 20

Roll temperature (°C)	40

A4 Gas controller system

Nitrogen was used as a physical blowing agent in the foaming process. The N_2 was purchased from Praxair Canada with a purity of 99.999%. As the developed foaming process was based on N_2 in its supercritical state, an accurate controller system was needed. Hence, a precise mass flow meter/controller model F-201CV-5K0-ABD-22-V from Hoskin Scientific Co. USA was purchased. The specifications of the mass flow meter/controller are as follow:

Based gas designed	N_2
Gas pressure (MPa)	7
Gas temperature (°C)	25 (Room temperature)
Gas flow rate (ml/min)	1 - 2
Gas injection point	Zone 2 of the extruder

It should be mentioned that the supercritical conditions for N_2 are P_C = 3.4 MPa and T_C = 126 K. Hence, at room condition, N_2 is above its supercritical temperature. So, to create supercritical conditions for N_2, it is only needed to increase the pressure above its supercritical pressure.

Appendix B: Graphical Abstracts

B1 Graphical Abstract of Chapter 5

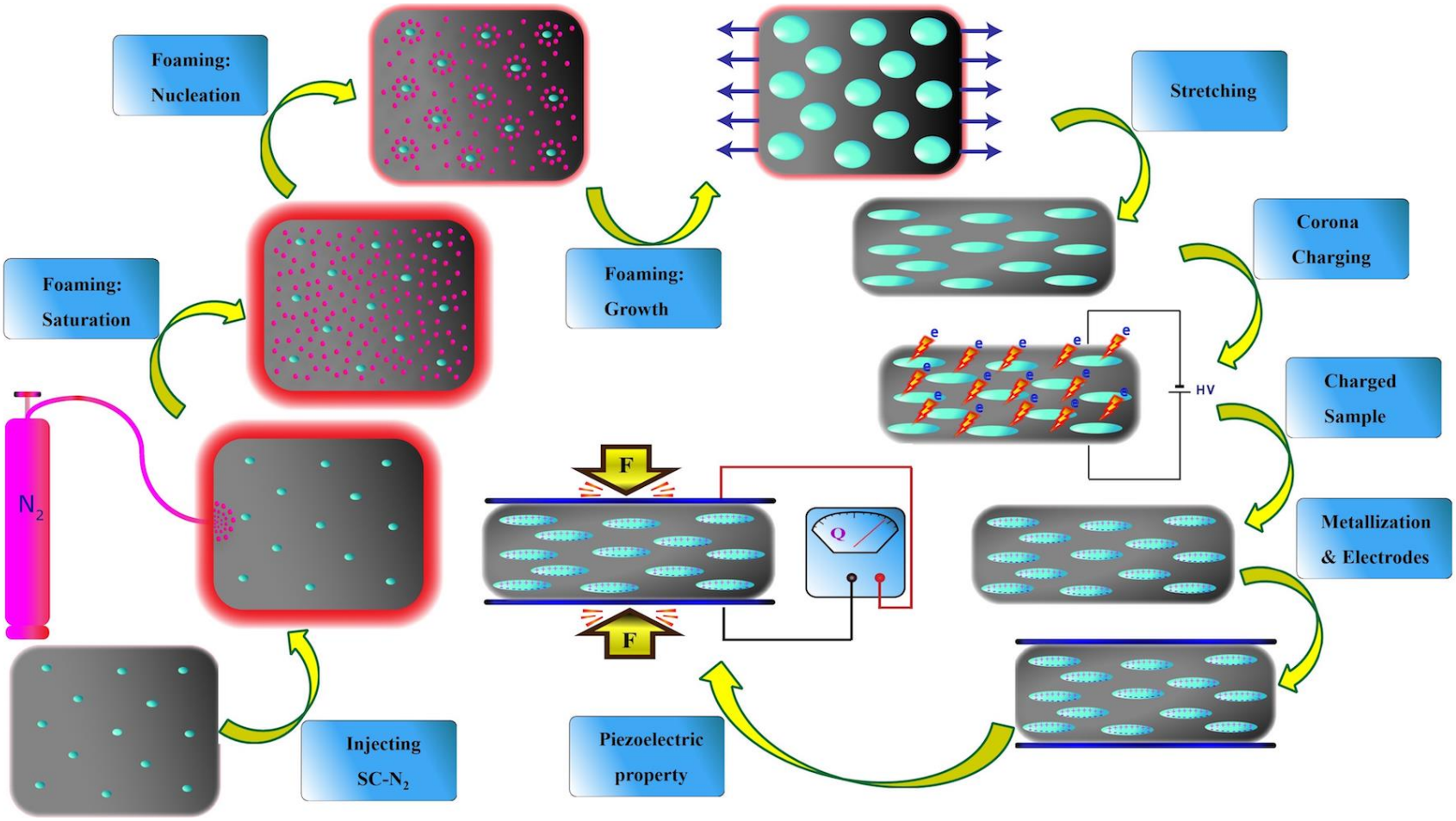

B2 Graphical Abstract of Chapter 6